

# Insights into Mechanisms of Secondary Organic Aerosol Formation: Approaching Atmospherically Relevant Conditions in an Atmospheric Reaction Chamber

Yarê Baker

Energie & Umwelt / Energy & Environment

Band / Volume 639

ISBN 978-3-95806-776-9





Forschungszentrum Jülich GmbH  
Institute of Climate and Energy Systems (ICE)  
Troposphäre (ICE-3)

# **Insights into Mechanisms of Secondary Organic Aerosol Formation: Approaching Atmospherically Relevant Conditions in an Atmospheric Reaction Chamber**

Yarê Baker

Schriften des Forschungszentrums Jülich  
Reihe Energie & Umwelt / Energy & Environment

Band / Volume 639

---

ISSN 1866-1793

ISBN 978-3-95806-776-9

Bibliografische Information der Deutschen Nationalbibliothek.  
Die Deutsche Nationalbibliothek verzeichnet diese Publikation in der  
Deutschen Nationalbibliografie; detaillierte Bibliografische Daten  
sind im Internet über <http://dnb.d-nb.de> abrufbar.

Herausgeber und Vertrieb: Forschungszentrum Jülich GmbH  
Zentralbibliothek, Verlag  
52425 Jülich  
Tel.: +49 2461 61-5368  
Fax: +49 2461 61-6103  
zb-publikation@fz-juelich.de  
[www.fz-juelich.de/zb](http://www.fz-juelich.de/zb)

Umschlaggestaltung: Grafische Medien, Forschungszentrum Jülich GmbH

Druck: Grafische Medien, Forschungszentrum Jülich GmbH

Copyright: Forschungszentrum Jülich 2024

Copyright Coverbild: Dr. Sören Zorn

Schriften des Forschungszentrums Jülich  
Reihe Energie & Umwelt / Energy & Environment, Band / Volume 639

D 468 (Diss. Wuppertal University, 2024)

ISSN 1866-1793  
ISBN 978-3-95806-776-9

Vollständig frei verfügbar über das Publikationsportal des Forschungszentrums Jülich (JuSER)  
unter [www.fz-juelich.de/zb/openaccess](http://www.fz-juelich.de/zb/openaccess).



This is an Open Access publication distributed under the terms of the [Creative Commons Attribution License 4.0](https://creativecommons.org/licenses/by/4.0/), which permits unrestricted use, distribution, and reproduction in any medium, provided the original work is properly cited.

## Statement

I declare that I have authored this thesis independently, that I used no other than the declared sources / resources, and that I have explicitly marked all material which has been quoted either literally or by content from the utilized sources. The thesis has not been submitted to any examination body in this, or similar, form.

Parts of this work have already been published in Baker et al. (2023). The publication encompasses the results regarding the system dominated by HO<sub>2</sub> (**Chapter 4.1**). Parts of the Introduction and Objective chapter (**Sections 1.1, 1.2, 2.1, 2.1.1, 2.1.3**), as well as the Methods chapter (**Sections 3.1.2, 3.1.4, 3.1.5 and Section 3.2** and its subsections) have also been utilized in the publication.

---

Place, Date

Signature



---

## Abstract

Secondary organic aerosol (SOA) is an important contributor to atmospheric aerosol, affecting radiative forcing, climate, and human health. A crucial process in the SOA formation mechanism is the production of highly oxygenated molecules (HOMs) by atmospheric oxidation of volatile organic compounds. These HOMs are of low enough volatility to condense or nucleate and thus contribute to SOA. HOMs are formed by autoxidation of organic peroxy radicals ( $\text{RO}_2$ ), wherein an intramolecular H-shift to the peroxy group is followed by  $\text{O}_2$  addition regenerating the peroxy functionality. Autoxidation steps can repeat several times continuing the radical chain, or the highly oxygenated peroxy radicals ( $\text{HOM-RO}_2$ ) can terminate to closed-shell products. HOMs have been detected in the atmosphere and in recent years their formation has been extensively studied in laboratory experiments. Yet HOM formation under atmospheric conditions and their role in SOA formation are not fully understood.

In laboratory studies, the experimental requirements often result in high concentrations of  $\text{RO}_2$ , including  $\text{HOM-RO}_2$ , which leads to an overemphasis of  $\text{RO}_2$  cross reactions. These conditions can increase the SOA formation yield, by formation of accretion products from  $\text{RO}_2+\text{RO}_2$  cross reactions and due to missing competition for HOM formation pathways. In comparison, the atmosphere is a complex mixture of reactants, where  $\text{HOM-RO}_2$  often predominantly react with the hydroperoxyl radical ( $\text{HO}_2$ ) or nitric oxide ( $\text{NO}$ ).

In this work, we studied the formation of HOM in the  $\alpha$ -pinene photooxidation system under various conditions approaching atmospheric relevance and investigated the system's SOA formation potential. We utilized experiments in the atmospheric reaction chamber SAPHIR-STAR, a continuously stirred tank reactor, which we operated as a steady-state chamber. The chemical reaction regime was shifted from  $\text{RO}_2$  dominated conditions to atmospherically more relevant conditions by increasing the concentrations of  $\text{HO}_2$  and  $\text{NO}$  -separately and in mixture. At the same time, in a newly developed experimental procedure, we ensured that the primary  $\alpha$ -pinene oxidation conditions were kept constant in the different regimes. We furthermore added ammonium sulfate seed particles in all chemical regimes to directly observe the condensation behavior of the HOM gas-phase products. This targeted seeding provides direct insight into the volatility of the HOM product distribution.

Our analysis showed that both high  $\text{HO}_2$  and  $\text{NO}$  result in a decrease in SOA formation potential. One important aspect is the suppression of accretion product formation from  $\text{HOM-RO}_2+\text{RO}_2$  due to competing  $\text{RO}_2+\text{HO}_2$  and  $\text{RO}_2+\text{NO}$  reactions. The system dominated by  $\text{RO}_2+\text{HO}_2$  showed an overall decrease in HOM product formation, which we attribute to the suppression of alkoxy radical formation by cross reactions of  $\text{RO}_2$ , which is crucial for an important HOM formation pathway in  $\alpha$ -pinene photooxidation, the formation of  $\text{C}_{10}\text{H}_{15}\text{O}_x\text{-HOM-RO}_2$ . As expected, the importance of

hydroperoxide termination products ( $\text{RO}_2+\text{HO}_2$ ) compared to carbonyl termination products ( $\text{RO}_2+\text{RO}_2$ ) significantly increased.

In the system with high NO (dominated by  $\text{RO}_2+\text{NO}$ ), overall HOM formation decreased when the fast reaction with NO interfered in the autoxidation chain, whereas at lower NO reaction rates, no overall reduction in the detected HOM gas-phase products was observed. The presence of NO clearly shifted the HOM product distribution: The reaction of HOM- $\text{RO}_2$  with NO formed organic nitrates as termination products and the fast alkoxy radical formation by  $\text{RO}_2+\text{NO}$  increased the importance of fragmentation products with carbon numbers smaller than 10.

In the mixed system with both high importance of  $\text{HO}_2$  and NO, an overlap of the effects of the individual reactants was observed.  $\text{HO}_2$  still suppressed the formation of  $\text{C}_{10}\text{H}_{15}\text{O}_x\text{-HOM-RO}_2$ , while NO facilitated the formation of organic nitrates and increased the contribution of fragments to the HOM product distribution. In the mixed system, termination reactions by  $\text{HO}_2$  and NO were fast enough to compete with the autoxidation, which reduced overall HOM formation.

The decrease in HOM products decreased the SOA formation potential and SOA yield. The SOA formation potential decreased additionally, due to the reduced accretion product formation from HOM- $\text{RO}_2$  with lower oxidized  $\text{RO}_2$ . The targeted seeding also revealed that HOMs containing organic nitrate groups and fragmentation products have higher volatility, decreasing the SOA formation potential further. These findings from the gas phase were corroborated by particle-phase measurements.

The atmospheric fate of HOM- $\text{RO}_2$  is defined by the importance of reactions with  $\text{RO}_2$ ,  $\text{HO}_2$  and NO and the overall reactivity of their surroundings. In this study, we present a set of experiments that systematically varied these parameters. Our results show that laboratory experiments with dominance of  $\text{RO}_2+\text{RO}_2$  cross reactions lead to overestimations of the SOA formation when the according SOA yield is directly transferred to the atmosphere. By mechanistic considerations, we were able to understand how the HOM product distribution depends on the  $\text{HO}_2$  and NO concentrations and to explain the reduced SOA formation by changes in the HOM products and their volatility.

# Table of Contents

<b>1. Introduction</b> .....	<b>1</b>
1.1 Atmospheric oxidation of volatile organic compounds and secondary organic aerosol formation .....	1
1.2 Objective.....	3
<b>2. Theoretical Background</b> .....	<b>7</b>
2.1 Generic $\alpha$ -pinene HOM peroxy radical chemistry .....	7
2.1.1 Reaction pathways of HOM-RO <sub>2</sub> with RO <sub>2</sub> and HO <sub>2</sub> .....	9
2.1.2 Reaction pathways of HOM-RO <sub>2</sub> with NO <sub>x</sub> .....	11
2.1.3 Reaction pathways of HOM alkoxy radicals.....	12
2.2 Oxidation product gas-to-particle partitioning .....	13
<b>3. Methods and Experiments</b> .....	<b>15</b>
3.1 Chemical Ionization Mass Spectrometry .....	15
3.1.1 Atmospheric Pressure Interface Time of Flight Mass Spectrometer .....	15
3.1.2 Multi-scheme chemical ionization inlet .....	16
3.1.3 General procedure for data analysis .....	18
3.1.4 Determination of oxidized compounds and HO <sub>2</sub> with MION-CIMS.....	20
3.1.5 Derivation of condensable HOM mass proxy in the gas-phase from CIMS-measurement ..	21
3.2 Atmospheric reaction chamber SAPHIR-STAR.....	22
3.2.1 Instrumentation .....	24
3.2.2 OH concentration and $\alpha$ -pinene OH turnover .....	25
3.2.3 Experimental conditions .....	27
3.2.4 Experimental procedure .....	28
3.2.5 Box model calculations for RO <sub>2</sub> sink estimation .....	30
<b>4. Results and Discussion</b> .....	<b>33</b>
4.1 Impact of high HO <sub>2</sub> .....	33
4.1.1 Impact of HO <sub>2</sub> on overall HOM formation .....	35
4.1.2 Impact of HO <sub>2</sub> on the HOM-RO <sub>2</sub> concentration .....	37
4.1.3 C <sub>10</sub> -HOM-RO <sub>2</sub> chemistry: Importance of C <sub>10</sub> H <sub>15</sub> O <sub>x</sub> and C <sub>10</sub> H <sub>17</sub> O <sub>x</sub> families.....	39
4.1.4 Impact of HO <sub>2</sub> on HOM alkoxy radical formation.....	40
4.1.5 Impact on carbonyl and hydroperoxide formation .....	43
4.1.6 Impact of HO <sub>2</sub> on condensable organic mass .....	45
4.1.7 Summary: Impact of HO <sub>2</sub> .....	48
4.2 Impact of NO .....	50
4.2.1 Impact on overall HOM formation .....	51
4.2.2 Impact of NO on the HOM-RO <sub>2</sub> concentration.....	52
4.2.3 C <sub>10</sub> -HOM-RO <sub>2</sub> chemistry: Importance of C <sub>10</sub> H <sub>15</sub> O <sub>x</sub> and C <sub>10</sub> H <sub>17</sub> O <sub>x</sub> families.....	54
4.2.4 Importance of HOM alkoxy chemistry in the system with NO .....	58
4.2.5 Formation of HOM organic nitrates.....	60

## VIII | Table of Contents

---

4.2.6	<i>Impact of NO on condensable organic mass</i> .....	63
4.2.7	<i>Summary: Impact of NO</i> .....	68
4.3	Combination of NO and high HO <sub>2</sub> .....	69
4.3.1	<i>Reduction of HOM formation in the system with NO and high HO<sub>2</sub></i> .....	70
4.3.2	<i>Impact of NO and high HO<sub>2</sub> on the HOM-RO<sub>2</sub> concentration</i> .....	72
4.3.3	<i>C<sub>10</sub>-HOM-RO<sub>2</sub> chemistry: Importance of C<sub>10</sub>H<sub>15</sub>O<sub>x</sub> and C<sub>10</sub>H<sub>17</sub>O<sub>x</sub> families</i> .....	73
4.3.4	<i>Competition for termination group formation in the system with NO and high HO<sub>2</sub></i> .....	75
4.3.5	<i>Changes in HOM alkoxy radical chemistry in the system with NO and high HO<sub>2</sub></i> .....	79
4.3.6	<i>Impact of combined NO and high HO<sub>2</sub> on condensable organic mass</i> .....	82
4.3.7	<i>Summary: Impact of NO and high HO<sub>2</sub> in combination</i> .....	87
<b>5.</b>	<b>Summary and conclusion</b> .....	<b>89</b>
5.1	Impact of HO <sub>2</sub> and NO on HOM formation chemistry .....	90
5.2	Impact of changed HOM formation chemistry on SOA formation .....	91
<b>6.</b>	<b>References</b> .....	<b>93</b>
<b>A.</b>	<b>Appendix</b> .....	<b>101</b>
A.1	Exemplary RO <sub>2</sub> sink distributions in the atmosphere .....	101
A.2	Voltage and flow settings of MION-API-TOF .....	102
A.3	Overview of experimental OH concentrations and $\alpha$ -pinene OH turnover .....	104
A.4	Modeling of experiments .....	105
A.4.1	<i>Box model input parameters: Wall loss and OH background reactivity</i> .....	105
A.4.2	<i>Box model results: HO<sub>2</sub>, RO<sub>2</sub>, NO and pinonaldehyde</i> .....	107
A.5	Error propagation.....	108
A.6	Peaklists .....	109
A.6.1	<i><math>\alpha</math>-Pinene + OH in the base and high HO<sub>2</sub> case</i> .....	109
A.6.2	<i><math>\alpha</math>-Pinene + OH at low and high HO<sub>2</sub> with NO in the system</i> .....	110
A.7	Exemplary reported HO <sub>2</sub> /RO <sub>2</sub> ratios from field studies.....	112
A.8	Estimation of change in peroxy radical steady state concentration between different chemical regimes .....	113
A.8.1	<i>Estimation for high HO<sub>2</sub> case in comparison to base case</i> .....	113
A.8.2	<i>Estimation for system with NO in comparison to base case</i> .....	113
A.9	Particular phase measurements and wall loss corrected SOA yield .....	114
A.10	Supplemental information for experiments with NO addition .....	115
A.10.1	<i>C<sub>10</sub>-HOM-RO<sub>2</sub> family observations in experiments with NO addition</i> .....	115
A.10.2	<i>Relative changes in the HOM-Mon families in experiments with NO addition</i> .....	116
A.10.3	<i>Contributions in the HOM-Frag product class in experiments with NO addition</i> .....	116
A.10.4	<i>Investigation of oxidation degree in experiments with NO addition</i> .....	117
A.10.5	<i>Information about additional “low NO” steady state</i> .....	118
A.10.6	<i>Gas-phase fraction remaining in presence of seed for the middle NO case</i> .....	119
A.11	Supplemental information for experiments with NO and HO <sub>2</sub> addition.....	120

---

A.11.1	Overview of contributions of product classes, groups, and families in the high NO, high HO <sub>2</sub> case .....	120
A.11.2	Information about additional “in-between NO” steady state .....	120
A.11.3	C <sub>10</sub> H <sub>16</sub> O <sub>2</sub> (formula composition of pinonaldehyde) signal in the system with NO and HO <sub>2</sub> in comparison to the base case .....	121
A.11.4	Investigation of oxidation degree in experiments with NO and HO <sub>2</sub> addition.....	121
A.11.5	Relative change in HOM-Frag groups compared to base case for middle NO, high HO <sub>2</sub> and high NO, high HO <sub>2</sub> system .....	122
A.11.6	Fraction remaining with seed in ON and non-ON product classes in system with just NO in comparison to system with NO and high HO <sub>2</sub> .....	122

## List of Illustrations

<b>Figure 1</b> Triangle plot with exemplary RO <sub>2</sub> fate only including the reactions with HO <sub>2</sub> , NO or RO <sub>2</sub> .....	3
<b>Figure 2</b> Simple autoxidation step scheme.....	7
<b>Figure 3</b> Internal RO <sub>2</sub> termination scheme with carbonyl formation and OH loss from a hydroperoxide group.....	8
<b>Figure 4</b> Overview of termination pathways for $\alpha$ -pinene RO <sub>2</sub> .....	8
<b>Figure 5</b> Reaction scheme of alkoxy-peroxy step.....	12
<b>Figure 6</b> 2D volatility basis set showing saturation mass concentration ( $c^0$ ) ranges of the volatility classes.....	14
<b>Figure 7</b> Scheme of the API-TOF (Junninen et al., 2010).....	15
<b>Figure 8</b> Scheme of the gas flows and ion paths in the MION inlet.....	17
<b>Figure 9</b> Modeled HO <sub>2</sub> concentration vs. normalized HO <sub>2</sub> signal.....	21
<b>Figure 10</b> Atmospheric reaction chamber SAPHIR-STAR with schematic flow set-up.....	23
<b>Figure 11</b> Exemplary timeseries of high HO <sub>2</sub> experiment.....	29
<b>Figure 12</b> Classification of the chemical regimes for the system with high HO <sub>2</sub> .....	34
<b>Figure 13</b> Overview of average, relative change in product classes detected in NO <sub>3</sub> -CIMS between high HO <sub>2</sub> case and base case.....	35
<b>Figure 14</b> Average contribution of the closed shell product classes to overall HOM product signal in the RO <sub>2</sub> +RO <sub>2</sub> dominated base case and the high HO <sub>2</sub> case.....	36
<b>Figure 15</b> Overview of average, relative change in monomer families detected in NO <sub>3</sub> -CIMS between high HO <sub>2</sub> case and base case.....	36
<b>Figure 16</b> Average contribution of the C <sub>20</sub> H <sub>30</sub> O <sub>z</sub> , C <sub>20</sub> H <sub>32</sub> O <sub>z</sub> , and C <sub>20</sub> H <sub>34</sub> O <sub>z</sub> family to the C <sub>20</sub> HOM-Acc group signal in the base case and high HO <sub>2</sub> case.....	40
<b>Figure 17</b> Average contribution of O <sub>odd</sub> and O <sub>even</sub> to the HOM-RO <sub>2</sub> families C <sub>10</sub> H <sub>15</sub> O <sub>x</sub> (left) and C <sub>10</sub> H <sub>17</sub> O <sub>x</sub> (right) signal in the base case and high HO <sub>2</sub> case.....	41
<b>Figure 18</b> Overview of average, relative change in C <sub>5</sub> , C <sub>7</sub> , C <sub>8</sub> , C <sub>9</sub> fragment groups detected in NO <sub>3</sub> -CIMS between high HO <sub>2</sub> case and base case.....	42
<b>Figure 19</b> Average contribution of the individual compounds to the C <sub>10</sub> H <sub>18</sub> O <sub>z</sub> family signal in the base case and high HO <sub>2</sub> case.....	43
<b>Figure 20</b> Average contribution of the C <sub>10</sub> H <sub>14</sub> O <sub>z</sub> , C <sub>10</sub> H <sub>16</sub> O <sub>z</sub> , and C <sub>10</sub> H <sub>18</sub> O <sub>z</sub> family to the HOM-Mon class in the base case and high HO <sub>2</sub> case.....	44
<b>Figure 21</b> Overview of average, relative change in product class signals between unseeded and seeded system.....	45
<b>Figure 22</b> Gas-phase fraction remaining in presence of seed for the base case (blue) and high HO <sub>2</sub> case (red).....	46
<b>Figure 23</b> Overview of the average, relative change in organic mass observed in the AMS (left y-axis, seeded experiments) and the mass weighted HOM signal that is supposed to condense as observed by NO <sub>3</sub> -CIMS (right y-axis, unseeded experiments) between the high HO <sub>2</sub> and base case.....	48
<b>Figure 24</b> Classification of the chemical regimes for the system with NO addition.....	50

<b>Figure 25</b> Overview of relative change in product classes detected in $\text{NO}_3$ -CIMS at the two NO levels compared to base case in unseeded system.....	51
<b>Figure 26</b> Contribution of the closed shell product classes to overall HOM-product signal in the base case and at the two NO levels.....	52
<b>Figure 27</b> Peak assignment of $\text{C}_{10}\text{H}_{15}\text{O}_9$ between organic nitrate compounds at middle NO level. ....	54
<b>Figure 28</b> Contribution of the $\text{C}_{10}\text{H}_{14}\text{O}_2$ , $\text{C}_{10}\text{H}_{16}\text{O}_2$ and $\text{C}_{10}\text{H}_{18}\text{O}_2$ families to the non-ON HOM-Mon in the base case and at the two NO levels.....	54
<b>Figure 29</b> Contribution of the $\text{C}_{20}\text{H}_{30}\text{O}_2$ , $\text{C}_{20}\text{H}_{23}\text{O}_2$ and $\text{C}_{20}\text{H}_{34}\text{O}_2$ families to the $\text{C}_{20}$ -HOM-Acc in the base case and at the two NO levels.....	55
<b>Figure 30</b> Behavior of clearly assignable HOM-Mon products from $\text{C}_{10}\text{H}_{15}\text{O}_x$ and $\text{C}_{10}\text{H}_{17}\text{O}_x$ in the base case and at the two NO levels.....	56
<b>Figure 31</b> Behavior of HOM-Frag groups in system with NO.....	58
<b>Figure 32</b> Formation of $\text{C}_7\text{H}_{11}\text{O}_3$ peroxy radical and acetone via menthene pathway.....	59
<b>Figure 33</b> Contribution of ON products to product sum as a function of measured steady-state NO concentration.....	62
<b>Figure 34</b> Contribution of measured ON product sum to overall product sum as a function of the calculated $\text{RO}_2+\text{NO}$ contribution to the $\text{RO}_2$ chemical sink.....	63
<b>Figure 35</b> Overview of relative change in signal in product classes between seeded and unseeded system.....	64
<b>Figure 36</b> Overview of relative change of ON product classes signal between seeded and unseeded system.....	64
<b>Figure 37</b> Gas-phase fraction remaining in presence of seed for the high NO case.....	66
<b>Figure 38</b> Overview of the relative change in organic mass observed in the AMS (left y-axis, seeded experiments) and the mass weighted HOM signal that is supposed to condense as observed by $\text{NO}_3$ -CIMS (right y-axis, unseeded experiments) between the $\text{NO}_x$ -free base case and the two NO levels.....	68
<b>Figure 39</b> Classification of the chemical regimes for the experiments with NO and $\text{HO}_2$ .....	69
<b>Figure 40</b> Overview of relative change in product classes for the two NO, high $\text{HO}_2$ cases compared to the base case.....	70
<b>Figure 41</b> Contribution of the closed-shell product classes to overall HOM product signal in the middle NO, high $\text{HO}_2$ case (top row) in comparison to the low $\text{HO}_2$ , $\text{NO}_x$ -free base case, the high $\text{HO}_2$ case and the middle NO, low $\text{HO}_2$ case (bottom row).....	71
<b>Figure 42</b> Contribution of the $\text{C}_{20}\text{H}_{30}\text{O}_2$ , $\text{C}_{20}\text{H}_{32}\text{O}_2$ , and $\text{C}_{20}\text{H}_{34}\text{O}_2$ family to the $\text{C}_{20}$ -HOM-Acc signal in the middle NO, high $\text{HO}_2$ case (top row) in comparison to the low $\text{HO}_2$ , $\text{NO}_x$ -free base case, the high $\text{HO}_2$ case and the middle NO, low $\text{HO}_2$ case (bottom row).....	74
<b>Figure 43</b> Contribution of measured ON-HOM to the overall product sum as a function of the $\text{RO}_2+\text{NO}$ contribution to the $\text{RO}_2$ chemical sink.....	76
<b>Figure 44</b> Contribution of the $\text{C}_{10}\text{H}_{14}\text{O}_2$ , $\text{C}_{10}\text{H}_{16}\text{O}_2$ , and $\text{C}_{10}\text{H}_{18}\text{O}_2$ family to the non-ON HOM-Mon signal in the middle NO, high $\text{HO}_2$ case (top row) in comparison to the low $\text{HO}_2$ , $\text{NO}_x$ -free base case, the high $\text{HO}_2$ case and the middle NO, low $\text{HO}_2$ case (bottom row).....	77
<b>Figure 45</b> Contribution of $\text{C}_{10}\text{H}_{18}\text{O}_2$ sum to clear $\text{C}_{10}\text{H}_{17}\text{O}_x$ product sum ( $\text{C}_{10}\text{H}_{18}\text{O}_2 + \text{C}_{10}\text{H}_{17}\text{NO}_2$ ) as a function of the calculated $\text{RO}_2+\text{HO}_2$ contribution to the $\text{RO}_2$ chemical sink.....	78

---

<b>Figure 46</b> Overview of relative change in HOM-Frag groups detected in $\text{NO}_3$ -CIMS in the high $\text{HO}_2$ system (lefthand bars), the middle NO, low $\text{HO}_2$ system (center bars) and the middle NO, high $\text{HO}_2$ system, (righthand bars), all in comparison to the low $\text{HO}_2$ , $\text{NO}_x$ free base case .....	80
<b>Figure 47</b> Contribution of the $\text{C}_5$ - to $\text{C}_9$ -HOM Frag groups to the HOM-Frag signal in the middle NO, high $\text{HO}_2$ case (top row) in comparison to the low $\text{HO}_2$ , $\text{NO}_x$ -free base case, the high $\text{HO}_2$ case and the middle NO, low $\text{HO}_2$ case (bottom row) .....	81
<b>Figure 48</b> Overview of relative change in signal in product classes between unseeded and seeded case in the middle NO, high $\text{HO}_2$ system. ....	82
<b>Figure 49</b> Gas-phase fraction remaining in presence of seed for the middle NO, high $\text{HO}_2$ case .....	83
<b>Figure 50</b> Gas-phase fraction remaining in presence of seed for the high NO, high $\text{HO}_2$ case .....	85
<b>Figure A1</b> Contribution of $\text{C}_{10}\text{H}_{15}\text{O}_x$ and $\text{C}_{10}\text{H}_{17}\text{O}_x$ to $\text{C}_{10}$ -HOM- $\text{RO}_2$ sum in base, middle NO and high NO case .....	115
<b>Figure A2</b> Contribution of $\text{O}_{\text{odd}}$ and $\text{O}_{\text{even}}$ to the HOM- $\text{RO}_2$ families $\text{C}_{10}\text{H}_{15}\text{O}_x$ (left) and $\text{C}_{10}\text{H}_{17}\text{O}_x$ (right) signal in the base case (from apinCO_2 experiment) and at the two NO levels .....	115
<b>Figure A3</b> Overview of relative change in monomer families detected in $\text{NO}_3$ -CIMS at the two NO levels compared to base case in unseeded system .....	116
<b>Figure A4</b> Contribution of the $\text{C}_5$ to $\text{C}_9$ HOM-Frag groups to overall HOM-Frag signal in the NO free case (experiment apinCO_2) and at the two NO levels in the pure NO cases .....	116
<b>Figure A5</b> Contribution of the different families to the $\text{C}_7$ -HOM-Frag group in the base case (experiment apinCO_2) and at the two NO levels in the pure NO cases .....	117
<b>Figure A6</b> Gas-phase fraction remaining in presence of seed for the middle NO case. ....	119
<b>Figure A7</b> Overview of relative change in HOM-fragment groups detected in $\text{NO}_3$ -CIMS in the middle NO, high $\text{HO}_2$ system (lefthand bars) and the high NO, high $\text{HO}_2$ case (righthand bars), both in comparison to the low $\text{HO}_2$ , $\text{NO}_x$ free base case .....	122

## List of Tables

<b>Table 1</b> Overview of experimental conditions with corresponding experiments .....	27
<b>Table 2</b> Overview of the relative change in organic mass observed in the AMS (seeded experiments) and the mass weighted HOM signal that is supposed to condense as observed by NO <sub>3</sub> -CIMS (unseeded experiments) for the system with NO and HO <sub>2</sub> in comparison to the base case .....	86
<b>Table A1</b> Concentrations RO <sub>2</sub> , HO <sub>2</sub> , NO in exemplary atmospheric conditions .....	101
<b>Table A2</b> Overview of utilized bulk reaction rate coefficients .....	101
<b>Table A3</b> Applied TOF power supply (TPS) settings (optimized) .....	102
<b>Table A4</b> OH concentration and $\alpha$ -pinene OH turnover in all experiments. ....	104
<b>Table A5</b> Calculated diffusion coefficients of an exemplary HOM-Mon, exemplary HOM-Acc and HO <sub>2</sub> .....	106
<b>Table A6</b> Box model HO <sub>2</sub> /RO <sub>2</sub> ratio results at varying RO <sub>2</sub> and HO <sub>2</sub> wall loss at low HO <sub>2</sub> /RO <sub>2</sub> (left) and high HO <sub>2</sub> /RO <sub>2</sub> (right) in the apinCO_1 experiment .....	106
<b>Table A7</b> Modeling results for HO <sub>2</sub> , RO <sub>2</sub> sum, NO and pinonaldehyde .....	107
<b>Table A8</b> Peaklist NO <sub>3</sub> -MION-CIMS for base and high HO <sub>2</sub> cases .....	109
<b>Table A9</b> Peaklist NO <sub>3</sub> -MION-CIMS for cases with NO (Fragments) .....	110
<b>Table A10</b> Peaklist NO <sub>3</sub> -MION-CIMS for cases with NO (Monomers and Accretion products) .....	111
<b>Table A11</b> Measured HO <sub>2</sub> and RO <sub>2</sub> concentrations from field studies under different atmospheric conditions. ....	112
<b>Table A12</b> Overview of important particle phase parameters. ....	114
<b>Table A13</b> Contribution weighted O/C ratio of the HOM-Mon families and HOM-Acc class in the base case and at the two NO levels .....	117
<b>Table A14</b> Important experimental parameters for the additional "low NO" steady state .....	118
<b>Table A15</b> Contributions of product classes, groups and families in the high NO, high HO <sub>2</sub> case. ....	120
<b>Table A16</b> Important experimental parameters for the additional "in-between NO, high HO <sub>2</sub> " steady state .....	120
<b>Table A17</b> Overview of change in C <sub>10</sub> H <sub>16</sub> O <sub>2</sub> (sum formula of pinonaldehyde) in amine-CIMS measurements compared to the no NO <sub>x</sub> , low HO <sub>2</sub> base case .....	121
<b>Table A18</b> Contribution weighted O/C ratio of the HOM-Mon families and HOM-Acc class in the base case and at the two NO levels at high HO <sub>2</sub> .....	121
<b>Table A19</b> Comparison of fraction of signal remaining in the presence of seed for system just with NO and system with NO and high HO <sub>2</sub> .....	122



## List of Abbreviations

AMS	<i>Aerosol mass spectrometer</i>
API	<i>Atmospheric pressure ionization</i>
APi	<i>Atmospheric pressure interface</i>
CI	<i>Chemical ionization</i>
CIMS	<i>Chemical ionization mass spectrometry</i>
CPC	<i>Condensation Particle Counter</i>
ELVOC	<i>Extra-low volatility organic compound</i>
FWHM	<i>Full width at half maximum</i>
HOM	<i>Highly oxygenated molecule</i>
HOM-Frag	<i>HOM Fragmentation product (carbon number 5 to 9)</i>
HOM-Mon	<i>HOM Monomer product (carbon number 10)</i>
HOM-Acc	<i>HOM Accretion product (carbon number 11 to 20)</i>
HR	<i>High resolution</i>
IVOC	<i>Intermediate-volatility organic compounds</i>
JPAC	<i>Jülich plant atmosphere chamber</i>
LVOC	<i>Low volatility organic compound</i>
MION	<i>Multi-scheme chemical ionization</i>
MS	<i>Mass spectrometer</i>
<i>m/Q</i>	<i>Mass-to-charge</i>
ON	<i>Organic nitrate</i>
PAN	<i>Peroxyacetyl nitrate</i>
PFA	<i>Perfluoroalkoxy</i>
PTR-MS	<i>Proton transfer reaction mass spectrometry</i>
SAPHIR	<i>Simulation of atmospheric photochemistry in a large reaction chamber</i>
SOA	<i>Secondary organic aerosol</i>
SMPS	<i>Scanning Mobility Particle Sizer</i>
STR	<i>Stirred tank reactor</i>
SVOC	<i>Semi-volatile organic compound</i>
TIC	<i>Total ion count</i>
TOF	<i>Time of flight</i>
VBS	<i>Volatility Basis Set</i>
VOC	<i>Volatile organic compound</i>



## Acknowledgement

There are many people without whom this work would have not been possible and that I want to thank. I want to thank Prof. Dr. Thorsten Benter for accepting the supervision of this work and making this thesis possible. Many thanks also to the IEK-8 and Prof. Dr. Andreas Wahner and Prof. Dr. Astrid Kiendler-Scharr for supporting my work and believing in this project.

There are no words to accurately describe my gratitude towards Dr. Thomas Mentel. I could have not asked for a better supervisor and mentor. No one taught me more about the scientific mindset (and of course HOMs!). Thank you for your guidance and help!

I also want to thank Dr. Sören Zorn: Not only because without him there would be no SAPHIR-STAR chamber to experiment in, but also for the things he taught me. Many thanks also to my colleagues Dr. Rongrong Wu and Dr. Hui Wang, for their input in all things regarding CIMS and data analysis. Furthermore, I need to thank the whole SAPHIR-STAR team. Thank you for the great work!

My sincere thanks also to Prof. Dr. Mattias Hallquist, Prof. Dr. Gordon McFiggans, their teams, and all people involved in the Manchester, Göteborg, Jülich cooperation -for many fruitful discussions and for the help in shaping this project. A special thanks to Dr. Sungah Kang for the laughs we could share even during stressful times and her unyielding support. Another special thanks to Veronica Geretti, for sharing the burdens of PhD and campaign life. We are a great team!

Last, but definitely not least, I want to thank my fiancée. For always being my greatest supporter. For being patient and understanding and for getting more interested in CIMS communication issues and atmospheric reaction chamber experiments than you probably ever expected. Thank you.



# 1. Introduction

## 1.1 Atmospheric oxidation of volatile organic compounds and secondary organic aerosol formation

In the atmosphere, highly oxidized products from the oxidation of biogenic or anthropogenic volatile organic compounds (VOCs) are an important source of secondary organic aerosol (SOA) (Ehn et al., 2014; Roldin et al., 2019; Mohr et al., 2019). SOA is an important contributor to the overall ambient aerosol and of interest because of its impact on climate, visibility, and human health (Hallquist et al., 2009).

Recently, many studies (Ehn et al., 2012; Ehn et al., 2014; Mentel et al., 2015; Berndt et al., 2016; Bianchi et al., 2017; Pullinen et al., 2020; Kang, 2021) have focused on understanding the oxidation pathways of VOCs that yield highly oxygenated molecules (HOMs), as these are expected to be of low enough volatility to condense into the particle phase. A key process for HOM formation is autoxidation (Ehn et al., 2014; Crouse et al., 2013). In the autoxidation process, oxygen is quickly added to an initial peroxy radical (RO<sub>2</sub>) via a series of intramolecular H-shifts and subsequent O<sub>2</sub> additions. The major termination pathway expected for autoxidation are bimolecular reactions (for a more detailed explanation see **Section 2.1**).

An important VOC for HOM formation through autoxidation is  $\alpha$ -pinene.  $\alpha$ -Pinene is the most abundant monoterpene in the atmosphere with emission rates estimated of around 32 Tg yr<sup>-1</sup> (Sindelarova et al., 2014). The sources of  $\alpha$ -pinene are mainly biogenic, specifically trees, though  $\alpha$ -pinene is also used in consumer products, which can be an important source in urban environments (McDonald et al., 2018). The oxidation of  $\alpha$ -pinene with OH (photooxidation) is therefore an important contributor to SOA formation during daytime and the reaction mechanisms of  $\alpha$ -pinene oxidation have been investigated in numerous studies (see McVay et al. (2016) and sources therein).

Experiments in atmospheric simulation chambers are an important tool for the investigation of VOC degradation and SOA formation (Kiendler-Scharr et al., 2023; Hidy, 2019) and such experiments helped to develop a basic mechanistic understanding of the ongoing chemistry (Saunders et al., 2003). However, many uncertainties remain since simulation experiments cannot cover the variability of the atmosphere and are often limited by the accessible experimental conditions, for example required VOC concentration and available reaction partners (McFiggans et al., 2019).

Chamber studies often work with only a singular compound and have to operate at higher precursor concentrations than those observed in the atmosphere for experimental reasons (e. g. detection limits). Such experiments cannot represent the complex mixture of VOCs and oxidized VOCs present in the

## 2 | Introduction

---

atmosphere (McFiggans et al., 2019). Higher precursor concentrations can lead per se to higher SOA yields than observed in the atmosphere (Henry et al., 2012; Shilling et al., 2009) and to a general preference of higher order processes which may not be important in the atmosphere.

One group of key intermediate species in the atmospheric VOC oxidation are peroxy radicals ( $\text{RO}_2$ ) in general, and HOM- $\text{RO}_2$  specifically for SOA formation. In typical laboratory settings, reactions of HOM- $\text{RO}_2$  with other organic peroxy radicals terminate the autoxidation chain. In the atmosphere, depending on the atmospheric conditions, termination by  $\text{HO}_2$  or  $\text{NO}$  is more likely leading to different closed-shell products (Schervish and Donahue, 2021).

The HOM product distribution and concentration, which subsequently define the SOA formation potential of the system, are therefore dependent on the contribution of the different  $\text{RO}_2$  reaction pathways. In this context, an important distinction is between reactions that sustain the  $\text{RO}_2$  functionality and termination reactions that form closed-shell products.

Reactions terminating the  $\text{RO}_2$  functionality and thus competing with the autoxidation will reduce the production of HOM, if they are sufficiently fast to intervene before a high oxidation degree is reached. In this case, oxidation degree and the SOA formation potential decrease. Thus, concentrations of the reaction partners for  $\text{RO}_2$  and their rate coefficients for the bimolecular termination reactions are important due to their competition to the autoxidation.

A way to visualize the contribution of the three main reaction partners  $\text{RO}_2$ ,  $\text{HO}_2$  and  $\text{NO}$  is a triangle plot, as shown in **Figure 1**, where each axis represents the contribution of one reaction partner. Herein, we treat the pool of all  $\text{RO}_2$  radicals like a single species with an average rate coefficient (compare Peng et al. (2019)). **Figure 1** shows different atmospheric examples for pristine, forested, and urban conditions. The examples show that compared to the laboratory setting (which we treat as the “base” case) in most atmospheric situations the reactions with  $\text{HO}_2$  and/or  $\text{NO}$  dominate, highlighting the importance of understanding the impact of these reaction partners individually and in mixture.

The aim of this work is to shift the reaction regimes in a chamber study from a typical laboratory regime ( $\text{RO}_2$ -dominated, base) towards atmospherically more relevant regimes. We will investigate different reaction conditions (reaction pool size and composition) to demonstrate their impact on the HOM product distribution and SOA formation potential on the example of  $\alpha$ -pinene photooxidation.

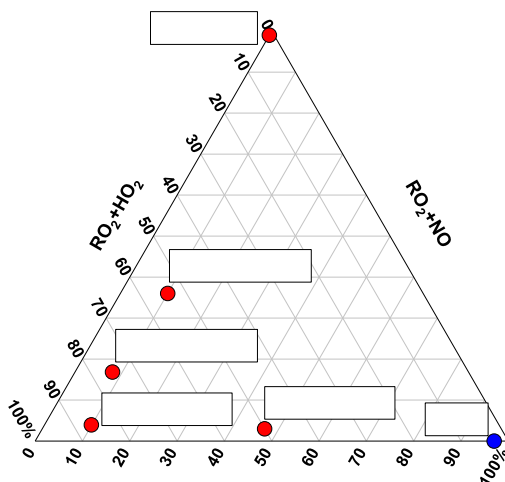


**Figure 1** Triangle plot with exemplary RO<sub>2</sub> fate only including the reactions with HO<sub>2</sub>, NO or RO<sub>2</sub>. Which grid lines correspond to which axes is indicated by the inclination of the axes' labels. Points show different ambient cases adapted from Peng et al. (2019) with the bulk reaction rate coefficients assumed in this work, further information in Appendix Section A.1.

## 1.2 Objective

Schervish and Donahue (2021) raised awareness that chamber studies could overestimate the SOA formation potential from the oxidation of terpenes such as  $\alpha$ -pinene compared to the atmosphere, due to the dominance of RO<sub>2</sub> cross reactions in absence of NO and small organic molecules that generate HO<sub>2</sub> radicals during their photooxidation. The thesis addresses this hypothesis and the objective is to methodically move from typical laboratory settings, i.e. “RO<sub>2</sub> dominance”, towards more atmospherically relevant conditions in the study of the photooxidation of  $\alpha$ -pinene. To achieve more atmospherically relevant conditions, we consider that the atmosphere is mixed, and that the chemical regime is characterized by the balance of RO<sub>2</sub>, HO<sub>2</sub> and NO.

To simulate different chemical regimes, experiments were performed in a thermo-stabilized glass chamber (SAPHIR-STAR, for details see Section 3.2) with varying HO<sub>2</sub> and NO sources (separately and simultaneously). SAPHIR-STAR is a continuously stirred tank reactor, which was laid out for high stability and reproducibility of the boundary conditions, and an objective of this work was to develop an optimal performance protocol. In this context, a novelty and an important step in the experimental design was the consequent adjustment of OH concentration and  $\alpha$ -pinene OH turnover to be as similar as possible in each of the different chemical regimes. Thus, effects of oxidant scavenging, i.e. changes due to different OH availability to  $\alpha$ -pinene and deviating oxidation conditions, were excluded (McFiggans et al., 2019).

## 4 | Introduction

---

The experiments address:

- a) Modification of formation pathways and product distribution of HOMs by the availability of  $\text{RO}_2$ ,  $\text{HO}_2$  and  $\text{NO}$ .
- b) The impact of the changes in the HOM product distribution on SOA formation by direct observation of the loss of the HOMs from the gas phase by condensation onto ammonium sulfate seed aerosol.

The consequent targeted seeding described in b) is part of the method development. Seed aerosol was added for each evolved chemical regime, allowing independent determination of the formed SOA mass and direct comparisons between the seeded and unseeded systems.

The goal of the study is characterization of the HOM product distributions in relation to the changes in the different chemical regimes. The key change is the different contributions to the reactions of  $\text{HOM-RO}_2$  with other  $\text{RO}_2$ ,  $\text{HO}_2$ , and  $\text{NO}$ . Here, two different mechanistic aspects will be addressed that are of importance for understanding SOA formation:

- a) The relative importance of the different termination reactions at the end of the autoxidation chain, which finally determine the volatility and the SOA formation potential of the HOM product distribution. A focus here is the formation of accretion products between  $\text{HOM-RO}_2$  and lower oxidized  $\text{RO}_2$ , as this process increases the SOA yield.
- b) The impact of  $\text{RO}_2$ ,  $\text{HO}_2$ , and  $\text{NO}$  on the autoxidation chain itself. If the termination reaction rate can compete with the autoxidation rate, a lower oxidation degree, earlier termination and higher volatility is expected. Fast termination will reduce the overall amount of observed HOM compounds and SOA.

A factor for both a) and b) is the elucidation of the role of alkoxy radical formation as they, as well, can increase the volatility by forming fragmentation products or continue and enhance the autoxidation chain by intramolecular H-shifts.

For the mechanistic interpretation, a generic framework is adapted to get an estimation of the relative importance of reactions of  $\text{RO}_2$ ,  $\text{HO}_2$  and  $\text{NO}$  with  $\text{HOM-RO}_2$  to describe their “expected contribution” to the  $\text{HOM-RO}_2$  reactions (see **Section 2.1**), including autoxidation and wall loss. Modeling of the standard gas-phase chemistry is used (see **Section 3.2.5**) to estimate required radical concentrations that cannot be measured and guides the interpretation. It is the “expected contribution” by  $\text{RO}_2$ ,  $\text{HO}_2$  and  $\text{NO}$  (as shown in **Figure 1**) that defines the chemical regime of a single experimental setting.

We begin the analysis with the system shifted towards termination via  $\text{RO}_2+\text{HO}_2$ . The  $\text{HO}_2$  dominated case is chosen as a starting point since  $\text{HO}_2$  will form the same product classes as the simple laboratory case dominated by  $\text{RO}_2+\text{RO}_2$  reactions. The main differences are expected in the formed

autoxidation termination products. Then the influence of NO on the  $\alpha$ -pinene OH system is discussed. In the system with NO, the new product class of organic nitrates emerges and, due to alkoxy radical formation with NO, a stronger impact on the HOM-RO<sub>2</sub> themselves is expected. Finally, both HO<sub>2</sub> and NO are considered in a mixed system, to see not only their competition, but also the effect on the autoxidation chain and HOM-RO<sub>2</sub> formation in this highly competitive chemical regime.

In each section, first the observed changes in the gas-phase HOM-product distribution are described and compared to the expectations from our generic understanding of the  $\alpha$ -pinene HOM formation chemistry. Then the changes in observed SOA formation are presented and it is discussed whether the observations are explained by our knowledge of the gas-phase changes.



## 2. Theoretical Background

### 2.1 Generic $\alpha$ -pinene HOM peroxy radical chemistry

The  $\alpha$ -pinene photooxidation starts with the attack of the OH radical on the  $\alpha$ -pinene molecule. OH addition is the main expected reaction pathway described in literature (Berndt, 2021; Berndt et al., 2016; Xu et al., 2019; Jenkin et al., 1997; Saunders et al., 2003). The addition of OH leads to the formation of a carbon centered radical that quickly adds  $O_2$  forming the peroxy radical  $C_{10}H_{17}O_3$  (MCM v3.3.1 (Jenkin et al., 1997; Saunders et al., 2003)).

However, some studies have reported the importance of  $C_{10}H_{15}O_x$  peroxy radical species for  $\alpha$ -pinene photooxidation HOM chemistry (Kang, 2021; Shen et al., 2022). The  $C_{10}H_{15}O_x$  species are well known from  $\alpha$ -pinene ozonolysis, where  $C_{10}H_{15}O_4$  can be directly formed via the so-called vinyl hydroperoxide path (Johnson and Marston, 2008; Iyer et al., 2021). In the reactions with OH, an important source of  $C_{10}H_{15}O_x$  is the H-abstraction from first-generation oxidation products such as pinonaldehyde ( $C_{10}H_{16}O_2$ ) (MCM v3.3.1 (Jenkin et al., 1997; Saunders et al., 2003; Fantechi et al., 2002)). Additionally, a recent study suggests a direct production pathway from  $\alpha$ -pinene: An  $C_{10}H_{15}O_2$  peroxy radical is formed by H-abstraction and  $O_2$  addition (Shen et al., 2022).

The first products and key species in the  $\alpha$ -pinene photooxidation are thus peroxy radicals with the composition of  $C_{10}H_{17}O_x$  and  $C_{10}H_{15}O_x$ . These peroxy radicals can undergo a rapid oxidation process called autoxidation. Autoxidation adds oxygen to the molecule via an intramolecular H-shift to the peroxy group, forming a hydroperoxide group and an alkyl radical, to which  $O_2$  immediately adds, reestablishing the peroxy functionality (Ehn et al., 2014; Crouse et al., 2013). An exemplary autoxidation step is shown in **Figure 2**. This process can be repeated multiple times yielding almost instantaneously highly oxygenated peroxy radicals (HOM-RO<sub>2</sub>).

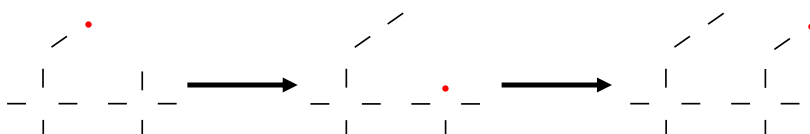


**Figure 2** Simple autoxidation step scheme

The autoxidation process is rapid with H-shift rates of about  $0.01 - 0.1 \text{ s}^{-1}$  and faster (Piletic and Kleindienst, 2022; Berndt, 2021; Xu et al., 2019; Vereecken et al., 2007). The autoxidation chain will run, quickly adding more oxygen to the molecule, until all available H-shift rates are slow enough for the termination reactions to compete. The rate of an H-shift is determined by the hydrogen's position in relation to the peroxy radical and the functional groups near the hydrogen and peroxy radical (Otkjaer et al., 2018; Vereecken and Nozière, 2020). The peroxy radicals have three major bimolecular

termination channels: the reaction with another RO<sub>2</sub>, with HO<sub>2</sub> or with NO. Acyl peroxy radicals can also react with NO<sub>2</sub>. Another important pathway is internal termination. A possible internal termination pathway resulting in the formation of a carbonyl and the loss of OH from the molecule is shown in **Figure 3** and was discussed for cyclohexene by Rissanen et al. (2014).

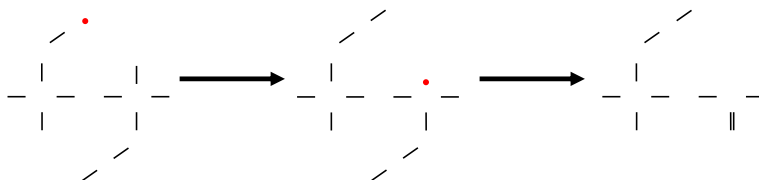


**Figure 3** Internal RO<sub>2</sub> termination scheme with carbonyl formation and OH loss from a hydroperoxide group.

As introduced above in traditional laboratory settings RO<sub>2</sub>+RO<sub>2</sub> reactions are often dominant, while in the atmosphere the reactions with HO<sub>2</sub> or NO are normally more important.

Based on these considerations, we apply a simplified generic reaction scheme to analyze our observations. We begin our discussion with the competing reactions of RO<sub>2</sub> and HO<sub>2</sub> (i.e. a “pristine” atmosphere, without influence of NO), before highlighting the importance of NO in **Section 2.1.2**.

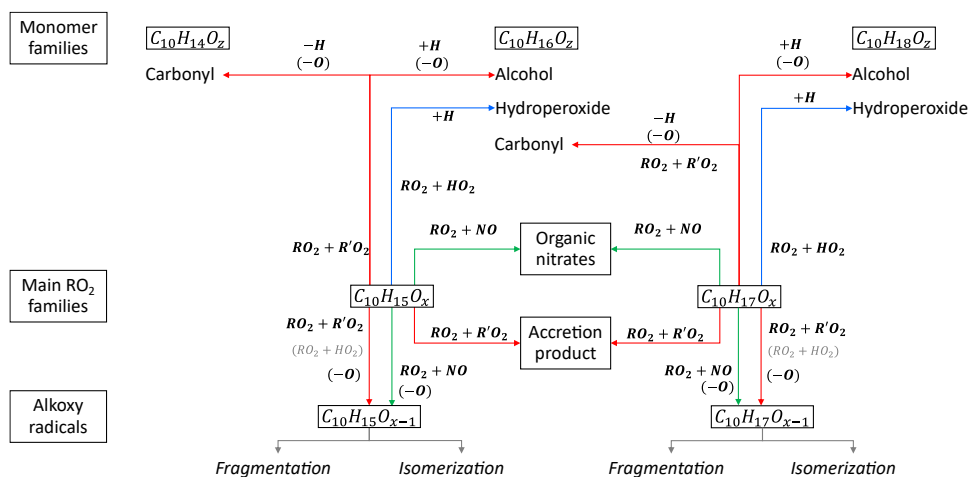


**Figure 4** Overview of termination pathways for  $\alpha$ -pinene RO<sub>2</sub>. RO<sub>2</sub>+RO<sub>2</sub> reactions are indicated by red arrows, RO<sub>2</sub>+HO<sub>2</sub> reactions by blue arrows and RO<sub>2</sub>+NO reactions by green arrows. Notation of functional groups refer to the functionality formed in the termination reaction.

**Figure 4** shows an overview of the reaction pathways for the main peroxy radical families in the  $\alpha$ -pinene photooxidation and the resulting product groups and families. The compounds can be separated into four classes: peroxy radicals (HOM-RO<sub>2</sub>), monomers (HOM-Mon), accretion products (HOM-Acc) and fragments (HOM-Frag). The HOM-RO<sub>2</sub> class consists of all detected HOM-RO<sub>2</sub>, however, we will focus on the analysis of the C<sub>10</sub>-HOM-RO<sub>2</sub> families. The HOM-Mon class contains the closed-shell C<sub>10</sub>-HOM products. The compounds in the fragment class contain less than ten carbon

atoms (C<sub>5</sub> to C<sub>9</sub>), while all HOM-Acc compounds contain more than ten carbon atoms. The compound classes are further divided into groups and families. Here, the term group is used for compounds with the same carbon number, while a family contains all compounds with the same carbon and hydrogen number but a varying oxygen number.

### 2.1.1 Reaction pathways of HOM-RO<sub>2</sub> with RO<sub>2</sub> and HO<sub>2</sub>

The notation “hydroperoxides”, “carbonyls”, “alcohols” etc. in **Figure 4** and in the following relates to the functionality of the group formed by the termination reaction. The termination of RO<sub>2</sub> with HO<sub>2</sub> will lead to hydroperoxide formation:



In the case of C<sub>10</sub>H<sub>15</sub>O<sub>x</sub>, reaction (R2-1) will lead to multifunctional C<sub>10</sub>H<sub>16</sub>O<sub>z</sub> hydroperoxides. For C<sub>10</sub>H<sub>17</sub>O<sub>x</sub>, it will lead to the formation of C<sub>10</sub>H<sub>18</sub>O<sub>z</sub> hydroperoxides. The termination via RO<sub>2</sub>+R'O<sub>2</sub> can either result in the formation of accretion products or in the formation of carbonyls and alcohols. For the accretion product formation, it is assumed that the two RO<sub>2</sub> chemically bond eliminating O<sub>2</sub> from the molecule:



Recombination reactions of the main peroxy radical families C<sub>10</sub>H<sub>15</sub>O<sub>x</sub> and C<sub>10</sub>H<sub>17</sub>O<sub>x</sub> lead to the product families C<sub>20</sub>H<sub>30</sub>O<sub>z</sub> (combination of two C<sub>10</sub>H<sub>15</sub>O<sub>x</sub>), C<sub>20</sub>H<sub>32</sub>O<sub>z</sub> (combination of C<sub>10</sub>H<sub>15</sub>O<sub>x</sub> and C<sub>10</sub>H<sub>17</sub>O<sub>x</sub>), and C<sub>20</sub>H<sub>34</sub>O<sub>z</sub> (combination of two C<sub>10</sub>H<sub>17</sub>O<sub>x</sub>).

However, due to reactions with smaller peroxy radicals, HOM-Acc families with smaller carbon and hydrogen numbers are also observed. Indeed, one reason why the RO<sub>2</sub>+R'O<sub>2</sub> termination is expected to affect the SOA formation potential is the formation of accretion products by scavenging of less oxidized and smaller RO<sub>2</sub> by HOM-RO<sub>2</sub>. Thus, the smaller RO<sub>2</sub> will also contribute to the SOA mass which would otherwise not be the case. For the HOM-RO<sub>2</sub> itself, it is expected that they contribute to SOA formation independently of the termination pathway, due to the low volatility of its expected termination products (Pullinen et al., 2020; McFiggans et al., 2019).

The second RO<sub>2</sub>+R'O<sub>2</sub> termination pathway is the formation of a carbonyl and alcohol compound:



In this reaction, both radicals lose an oxygen atom, and a hydrogen atom is transferred to the RO<sub>2</sub> forming the alcohol termination group. Preferences of RO<sub>2</sub> to form an alcohol or carbonyl compound are possible for individual reactions, but statistically carbonyl and alcohols should be formed with the

same fractions. Since mass spectrometry can only determine formula compositions, we cannot distinguish alcohols and hydroperoxides, which arise from RO<sub>2</sub> differing by one O atom. Moreover, carbonyl compounds are also formed by the internal termination (**Figure 3**). Therefore, the balance of alcohol and carbonyl formation of an individual HOM-RO<sub>2</sub> cannot be checked.

However, the formula composition can help to distinguish certain formation pathways. The C<sub>10</sub>H<sub>14</sub>O<sub>z</sub> family contains only carbonyl formed from a C<sub>10</sub>H<sub>15</sub>O<sub>x</sub>-RO<sub>2</sub> while the alcohol will be part of the C<sub>10</sub>H<sub>16</sub>O<sub>z</sub> family. The C<sub>10</sub>H<sub>16</sub>O<sub>z</sub> family also contains the carbonyl produced from the RO<sub>2</sub>+R'O<sub>2</sub> monomer termination of C<sub>10</sub>H<sub>17</sub>O<sub>x</sub>, while the alcohol from this RO<sub>2</sub> family will be found in the C<sub>10</sub>H<sub>18</sub>O<sub>z</sub> family. So, from a diagnostic point of view, C<sub>10</sub>H<sub>14</sub>O<sub>z</sub> as well as C<sub>10</sub>H<sub>18</sub>O<sub>z</sub> are uniquely related to one precursor radical family.

Besides closed-shell products, HOM-RO<sub>2</sub> can also form alkoxy radicals (HOM-RO). In general, alkoxy radicals are important intermediates in the oxidation scheme of organics and are formed via (**R2-4**) and probably also via (**R2-5**) for specific RO<sub>2</sub> (Jenkin et al., 2019):

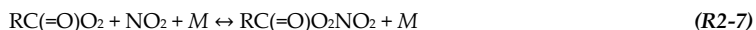


In reaction (**R2-5**) OH will be formed. The importance of reaction (**R2-5**) compared to reaction (**R2-4**) is still unclear in the literature, but functionalization of the RO<sub>2</sub> close to the peroxy group possibly enables this reaction (Iyer et al., 2018; Eddingsaas et al., 2012; Hasson et al., 2005; Jenkin et al., 2019). If reaction (**R2-5**) is of negligible importance, the reaction scheme will simplify and the effect of increased HO<sub>2</sub> is easier to diagnose.

Alkoxy radical formation is of importance as alkoxy radicals tend to fragment, leading to the formation of products with less carbon atoms, "fragments", (Vereecken et al., 2007). In the context of SOA formation, these fragments are less likely to contribute to SOA mass because of their lower molar mass and thus higher volatility. Reactions of alkoxy radicals will be discussed in **Section 2.1.3**.

### 2.1.2 Reaction pathways of HOM-RO<sub>2</sub> with NO<sub>x</sub>

NO and NO<sub>2</sub> are very important reaction partners of peroxy radicals in the atmosphere and because of their fast interconversion in the sunlit atmosphere, NO and NO<sub>2</sub> are often referred to together as NO<sub>x</sub>. In contrast to HO<sub>2</sub>, the reaction of RO<sub>2</sub> with NO and NO<sub>2</sub> creates a new product class: organic nitrates (ON).



The reactions forming ON are shown in (R2-6) and (R2-7). (R2-6) represents the reaction with NO, that every RO<sub>2</sub> can undergo. Reaction (R2-7) represents the special case of acyl peroxy radicals which can react with NO<sub>2</sub> forming so called peroxyacetyl nitrates (PAN-like organic compounds). However, PAN-like compounds tend to be thermally unstable and decompose back to their reactants. The thermal decomposition rate is highly temperature dependent (Seinfeld and Pandis, 2016). Noziere and Barnes (1998) reported dissociation rates for PAN compounds derived from  $\alpha$ -pinene oxidation similar to the dissociation rate of PAN itself.

In the formation of ON, no oxygen is lost and the oxygen from NO is added. Thus, the termination with NO will lead to products of higher mass and O/C ratio in comparison to termination with RO<sub>2</sub> or HO<sub>2</sub>. In reaction (R2-6) C<sub>10</sub>H<sub>15</sub>O<sub>x</sub> will form a C<sub>10</sub>H<sub>15</sub>NO<sub>z</sub> while C<sub>10</sub>H<sub>17</sub>O<sub>x</sub> will form a C<sub>10</sub>H<sub>17</sub>NO<sub>z</sub>. These two ON product families are therefore uniquely related to one precursor radical family.

Besides ON formation, the major reaction of RO<sub>2</sub> with NO is the formation of alkoxy radicals via (R2-8). Therefore, NO can directly interfere in the oxidation chain. HO<sub>2</sub> in comparison, is mainly expected to influence the termination pathway and only is expected to facilitate alkoxy radical formation in special cases, as described in Section 2.1.1. The reactions of alkoxy radicals are described in Section 2.1.3. If sufficient NO is available, its reaction with RO<sub>2</sub> is the main source of alkoxy radicals.



The branching ratio between formation of alkoxy radicals and closed-shell ON products in the reaction of RO<sub>2</sub>+NO depends on the temperature, pressure and the size and substitution of the RO<sub>2</sub> involved. However, it is generally expected that the alkoxy radical formation is the major reaction pathway (Ziemann and Atkinson, 2012). The “master chemical mechanism” (MCM v3.3.1) published by Jenkin et al. (1997) and Saunders et al. (2003) adopted a branching ratio into alkoxy radicals of about 0.7 for  $\alpha$ -pinene derived RO<sub>2</sub>. Details and trends of the branching ratio for RO<sub>2</sub> into RO can be found in Jenkin et al. (2019) and Ziemann and Atkinson (2012).

In the context of our photooxidation experiments, one should note that  $\text{NO}_x$  interacts with the  $\text{HO}_x$  cycle ( $\text{OH} + \text{HO}_2$ ) due to reactions (R2-9) and (R2-10) (Seinfeld and Pandis, 2016).  $\text{NO}$  reacts with  $\text{HO}_2$  to produce  $\text{OH}$ , thus representing a sink for  $\text{HO}_2$  and a source for  $\text{OH}$ . However, due to reaction (R2-10)  $\text{NO}_x$  represents a sink for  $\text{OH}$  at high  $\text{NO}_2$ .



Overall, the influence of  $\text{NO}_x$  on HOM formation are nonlinear as the interactions of  $\text{RO}_2$  with  $\text{NO}$  are complex and also depend on the ratio of  $\text{NO}$  to  $\text{NO}_2$  (Nie et al., 2023).

### 2.1.3 Reaction pathways of HOM alkoxy radicals

Alkoxy radicals ( $\text{RO}$ ) are the second important radical species in HOM formation. They are highly reactive and, once formed, have three general reaction pathways: The first possibility is reaction with  $\text{O}_2$  forming  $\text{HO}_2$  and a carbonyl function from the alkoxy radical. This reaction is mainly important for small, less functionalized alkoxy radicals as its reaction rate cannot compete with the other reaction channels of  $\text{HOM-RO}$ .

The second reaction channel is  $\alpha$ -bond scission (“fragmentation”) leading to an alkyl radical in one molecule and a carbonyl group in the other. This pathway is a source of  $\text{HOM-Frag}$  products as it can lead to  $\text{HOM-RO}_2$  with less than 10 carbon atoms. These  $\text{HOM-RO}_2$  may also continue the autoxidation chain.

The third possibility is isomerization via an intramolecular H-shift. This reaction channel can lead to formation of a new  $\text{RO}_2$  radical via an alkoxy-peroxy step (see Figure 5) (Vereecken and Peeters, 2010).

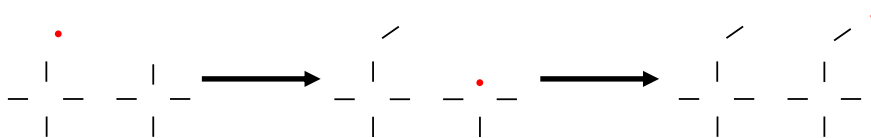


**Figure 5** Reaction scheme of alkoxy-peroxy step. Intramolecular H-shift generating an alcohol functional group and an alkyl radical, followed by  $\text{O}_2$  addition reforming the peroxy functionality.

H-Shifts retaining the carbon backbone become more likely with increasing functionalization (Vereecken et al., 2007), which for  $\alpha$ -pinene will lead to a next generation of  $\text{C}_{10}$ - $\text{HOM-RO}_2$ . The resulting peroxy radical can continue the autoxidation chain (Nie et al., 2023; Mentel et al., 2015). Furthermore, Kang (2021) studied alkoxy formation in the system with  $\text{NO}$  and proposed that  $\text{RO}$  formation can lead to an increase of oxidation degree in  $\text{HOM}$ -compounds in general by extending the length of the autoxidation chain. The reason would be the high efficiency of the intramolecular H-shift in  $\text{HOM-RO}$ . If the H-shift creates an alkyl radical, the subsequently formed  $\text{RO}_2$  will contain one

additional oxygen compared to the precursor RO<sub>2</sub>. Another possibility is the H-shift from an already existing hydroperoxide group, in that case, a peroxy radical is directly formed by the intramolecular H-shift and the newly formed RO<sub>2</sub> has one oxygen less compared to the precursor RO<sub>2</sub>.

Alkoxy radicals are too unstable to be detected directly, but we can make use of two diagnostic tools to assess the importance of HOM-RO: Firstly, the abundance of HOM-Frag products, as bond scission is one main reaction pathway for HOM-RO. Secondly, by coupling of an alkoxy and a peroxy step, the parity of the number of oxygen atoms in the HOM-RO<sub>2</sub> changes, while in pure autoxidation steps the oxygen parity remains the same as an even number of oxygen (2 per step) are added. For C<sub>10</sub>H<sub>17</sub>O<sub>x</sub> the expected starting parity is odd (C<sub>10</sub>H<sub>17</sub>O<sub>3</sub>), while for C<sub>10</sub>H<sub>15</sub>O<sub>x</sub> an even parity is expected (C<sub>10</sub>H<sub>15</sub>O<sub>2</sub> or C<sub>10</sub>H<sub>15</sub>O<sub>4</sub>). If an alkoxy-peroxy step occurs within the autoxidation chain, the H-shift forms an alcohol group and O<sub>2</sub> is added (**Figure 5**), leading to an uneven increase in oxygen number. Therefore, a parity change of the oxygen number can be used as an indication of alkoxy step abundance (Kang, 2021).

Based on the simplified generic mechanism presented in this chapter, we will use the changes in contribution and relative signal of the different families and classes to assess the impact of shifting the chemical regime on the  $\alpha$ -pinene photooxidation pathways.

## 2.2 Oxidation product gas-to-particle partitioning

Our study aims at understanding the SOA formation potential of the  $\alpha$ -pinene photooxidation system under varying conditions. Thus, an important property of the observed HOM products is their volatility and consequently their ability to partition into the particle phase.

In the literature, atmospheric oxidation products are commonly grouped into classes based on their volatility. Typical classes next to VOCs are intermediate-volatility organic compounds (IVOC), semi-volatile organic compounds (SVOC), low volatility organic compounds (LVOC) and extra low volatility organic compounds (ELVOC). Each class covers a certain vapor pressure range. The lumping of compounds into decadic "bins" was developed to handle the large variety of organic compounds in the atmosphere and is called the volatility basis set (VBS) (Donahue et al., 2011; Donahue et al., 2006). Applying the VBS allows to model the gas-to-particle partitioning of organic aerosols in the atmosphere in regional and global models.

The VBS is based on absorptive partitioning theory (Pankow, 1994). It uses mass based Raoult's law and the saturation mass concentration  $c^0$  to create a relationship between the mass concentration of a compound in the gas and particle phase. Saturation mass concentration is used as an equivalent to saturation vapor pressure. To assign compounds with unknown saturation mass concentration into the bins, the classes are also often related to oxidation degree resulting in the 2D-VBS shown in **Figure 6**.

The expected saturation mass concentration can be estimated with parametrizations from a compound's formula composition. This is a helpful tool, but it should be kept in mind that the actual volatility depends on the specific molecular structure. The fraction of the compound expected in the particle phase is defined by the effective saturation mass concentration and the available absorptive mass. Higher absorptive mass concentrations will lead to higher fractions in the particle phase and the condensation of more volatile compounds (Stolzenburg et al., 2022).

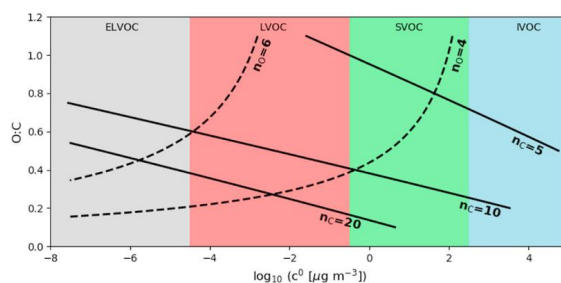


**Figure 6** 2D volatility basis set showing saturation mass concentration ( $c^0$ ) ranges of the volatility classes. The dependency on oxidation degree is shown by isopleths of constant carbon number with varying oxygen number (solid lines), and constant oxygen number with varying carbon number (dashed lines). (Stolzenburg et al., 2022)

The HOM products in this study are primarily expected to be in the LVOC and ELVOC volatility range, with some more volatile compounds in the SVOC range. HOM-Acc are commonly expected to be ELVOC. ELVOCs will condense on even very small pre-existing particles and may participate in new particle formation. LVOCs are expected to condense on sufficiently large particles (Bianchi et al., 2019).

## 3. Methods and Experiments

### 3.1 Chemical Ionization Mass Spectrometry

The main analytical instrument used for investigating the product distribution in the different chemical regimes is chemical ionization mass spectrometry (CIMS). CIMS is a powerful tool to study organic molecules. The defining feature of CIMS is the soft ionization by gas phase ion molecule reactions. Since no or only small amounts of analyte fragmentation occur, CIMS allows direct sum formula determination, which is crucial for the understanding of formation pathways of the HOM oxidation products. One big advantage of CIMS is its applicability to many analyte types, due to the many different possible reagent ions (Gross, 2011; Harrison, 1992).

In this work, negative-ion chemical ionization was applied, utilizing nitrate ( $\text{NO}_3^-$ ) and bromide ( $\text{Br}^-$ ) as the reagent ions. The use of two reagent ions in one instrument is possible due to the use of the multi-scheme ionization (MION) inlet (see Section 3.1.2).

CIMS techniques can be classified by the pressure at which the ionization occurs, as well as by the mass analyzer it is paired with. We used atmospheric pressure ionization (API) in combination with a time of flight (TOF) analyzer. The instrument set-up is briefly described in the following Section 3.1.1.

#### 3.1.1 Atmospheric Pressure Interface Time of Flight Mass Spectrometer

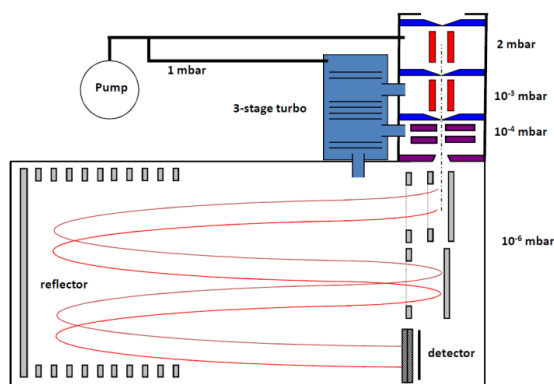


**Figure 7** Scheme of the APi-TOF (Junninen et al., 2010)

A schematic of the Atmospheric Pressure Inlet Time-Of-Flight mass spectrometer (API-TOF) used in this work is shown in Figure 7. The atmospheric pressure interface (APi) connects the

inlet (in our case the MION), where the analytes are ionized at atmospheric pressure to the mass analyzer (here a TOF analyzer) with  $10^{-6}$  mbar of pressure. The APi uses differential pumping to remove the gas in multiple pressure stages, while at the same time guiding the sampled ions. The flow rate into the interface is limited by a critical orifice. Thereafter, three differentially pumped chambers are utilized of which the first two contain quadrupoles as ion guides (shown in red in **Figure 7**). In the third chamber, the ion beam is focused and guided into the extraction region of the TOF via an ion lens assembly (shown in purple in **Figure 7**) (Junninen et al., 2010).

**Figure 7** also shows the schematic set-up of the TOF analyzer, where ions with different  $m/Q$  ratio are separated due to their velocities. The ions are extracted from the continuous ion beam and pulsed into the TOF by an acceleration voltage orthogonal to the ion beam. This ensures a simultaneous start of the ions.

In the TOF analyzer, all accelerated ions in on package drift along a field-free path. Owing to their different  $m/Q$  ratios the ions disperse during their flight, as ions with smaller  $m/Q$  ratio have higher velocities and reach the detector earlier than ions with larger  $m/Q$  ratio. TOF analyzers generally have a high sensitivity due to their high ion transmission. The resolving power of a TOF analyzer is defined by the length of the ion flight time and the resolving power can be increased using ion reflectors (reflectron) to elongate the flight time (Gross, 2011; Junninen et al., 2010). **Figure 7** shows a so called “W mode” utilizing two reflectors.

In our instrument, we employ the so called “long TOF” (LTOF) from the company Tofwerk (Tofwerk AG) operated in V-mode with only one ion reflection. A resolving power of around 8500 was reached for peaks at  $>200$   $m/Q$  in all experiments. This results in a mass resolution of 0.0235  $m/Q$  for peaks at 200  $m/Q$ . The detailed voltage settings for the TOF as well as for the inlet can be found in Appendix **Section A.2**.

### **3.1.2 Multi-scheme chemical ionization inlet**

The MION inlet (Karsa Oy) is an atmospheric pressure ionization inlet that allows the utilization of multiple reagent ion chemistries in quick succession within one instrument. The inlet consists of a flow tube with (in our case) two attached ion sources. The reagent ions are produced by enriching a nitrogen stream through a saturator with the reagent. The precursors are then ionized in the ion sources via soft x-ray radiation (Hamamatsu, type: PhotoIonBar L12535). A schematic overview of the flow paths (blue arrows) and the ion trajectory (pink arrows) can be found in **Figure 8**. Only the reagent ions are injected into the sample gas stream, while the excess reagent gas is led to the exhaust.

The reagent ions are accelerated and focused into the sample flow through a 5 mm orifice by applying an accelerator and deflector voltage (Rissanen et al., 2019).

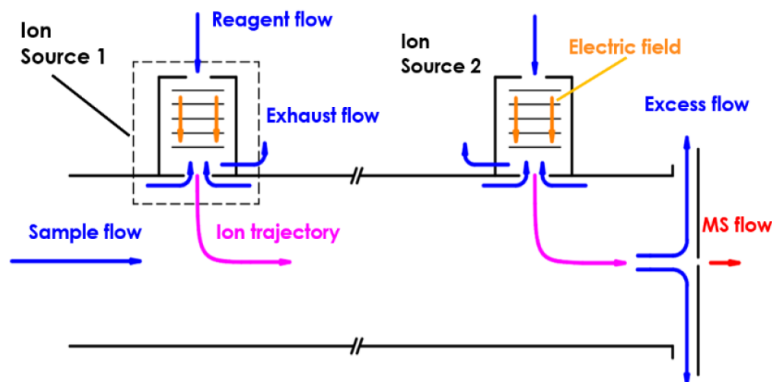


**Figure 8** Scheme of the gas flows and ion paths in the MION inlet (Rissanen et al., 2019)

In all of our experiments, we used a sample flow of  $10 \text{ L min}^{-1}$  from the reaction chamber. The sample tube is a stainless-steel tube with an inner diameter of 2.5 cm, leading to analyte reagent ion reaction times of 600 ms for ion source 1 and 60 ms for ion source 2. Before the addition of the reagent ions, a 50 cm long inlet tube is attached in front of ion source 1 to achieve a laminar flow regime, which minimizes wall losses of analyte and reagent ions.

We used nitrate as the reagent ion in ion source 1 and bromide as the reagent ion in ion source 2. As a reagent concentrated nitric acid (65 %  $\text{HNO}_3$ , Merck KGaA) is used for the nitrate ion source and dibromomethane ( $\text{CH}_2\text{Br}_2$ , purity 99 %, Sigma Aldrich) for the bromide ion source. The measuring mode was switched between nitrate and bromide mode every 10 minutes or 15 minutes depending on the experiment.

A special feature of the MION is that only the reagent ions are injected into the sample gas stream, while the reagent precursor gas stream is discarded to the exhaust. This is achieved by keeping the reagent flow into the ion source always smaller than the exhaust flow, so that no reagent can enter the sample flow and contaminate the instrument (Rissanen et al., 2019). For both ion sources, the exhaust flow was set to  $40 \text{ mL min}^{-1}$ . A reagent flow of  $3 \text{ mL min}^{-1}$  was used for the nitrate source. A reagent flow of  $15 \text{ mL min}^{-1}$  was used for the bromide source. A smaller flow was chosen for the nitric acid as no further optimization of reagent ion signal was observed at higher reagent flows and to minimize the concentration of corrosive  $\text{HNO}_3$  in the inlet.

Nitrate and bromide are well suited for alternating use as reagent ions due to their comparable adduct binding strength, as well as their similar molar masses, which leads to clusters with the analyte of similar m/Q ratios. These similarities ensure that analyte clusters with both reagent ions can be detected efficiently without changing the API-TOF settings.

### 3.1.3 General procedure for data analysis

Post processing of the raw data was performed with the software package "Tofware" (Version 3.2.3, Tofwerk AG) running in the Igor Pro environment (Version 7.08, Wavemetrics). Tofware provides a high resolution timeseries workflow for data analysis, of which the main steps are briefly described in this section. A broader description of the analysis software and its features can be found in Stark et al. (2015).

The raw data contained a mass spectrum every 2 s. Thus, for most experiment stages, the first processing step was to average 30 mass spectra to achieve a time resolution of 1 minute. For the determination of the wall loss rate of products in the reaction chamber, the original time resolution was used, as the wall loss rate is expected to be in the range of minutes.

After time averaging, the data set of one experiment was loaded into Tofware and the two measurement modes (nitrate and bromide) were separated into two timeseries sets. The two data sets for the two measurement modes were processed and analyzed separately.

A post measurement mass calibration was applied. Reagent ions, as well as the clusters of a perfluorinated compound were chosen as mass calibrants to cover a broader m/Q range. The ions were well isolated and had no interferences. The perfluorinated acid  $C_3F_5HO_2$  is a well-known contaminant in our instrument and could be observed as an anion and cluster in both reagent ion modes. Its source was most likely the perfluoralkoxy (PFA) tubing utilized in parts of the inlet.

In the next post processing step, a reference spectrum was chosen from the timeseries. The reference spectrum was used in the following steps to refine the baseline and determine peak width and shape. For each experiment stage, we chose around a period of 1 h of steady state with representative conditions.

This representative mass spectrum was then used to interpolate the baseline using a smoothing function. A filter was applied to remove noise before a moving average was made across the mass spectrum. The baseline in each step is represented by the lowest point. This procedure moves the baseline into the middle of the noise.

Peak width and shape were determined. The peak width of isolated peaks was determined as a function of the  $m/Q$  ratio. The software uses the full width at half maximum (FWHM) of each peak and calculates the peak width as a function of the  $m/Q$  ratio. To this end, the software fits a Gaussian peak at each integer  $m/Q$  and calculates the FWHM. Then an iterative process starts: A linear fit is calculated for the FWHM as a function of the  $m/Q$  ratio. It is also calculated how many peaks have FWHM above the fit line. The user chooses a tolerance value of how many peaks can have FWHM above the fit line. If the number is above the tolerance value, the peak with the largest width is removed from the fit curve and the steps are iterated. Once the tolerance value is achieved the process concludes. Tolerance values between 5 to 15 were used in our analysis.

In the next step, the peak shape function was determined. It is important to empirically describe the real observed peak shape as the peak shape function is used in the high-resolution peak fitting to determine the number of peaks at a unit mass and do peak assignment. For the peak shape determination, the 30 most intense peaks from the reference spectrum were used for visual inspection. For this the x-axis was normalized to Gaussian standard variations and peaks that deviated in shape were removed by the user. The average peak shape was calculated from the remaining peaks. The new custom peak shape was used to rerun the mass calibration. After all steps of the post-processing workflow, the high-resolution mass spectrum was used for peak assignment to build a peaklist of observed  $\alpha$ -pinene oxidation products.

The signal (in ions  $s^{-1}$ ) of the assigned compounds was extracted by peak integration. For integration a TOF duty cycle was applied. The TOF duty cycle accounts for the fact that from the continuous ion beam, arriving in the orthogonal extraction region in front of the TOF analyzer, only a certain percentage is pulsed into the TOF and accelerated. The ions arrive in the extraction region with different velocities. Under the assumption of a monoenergetic beam, smaller  $m/Q$  ratios have higher velocities, which leads to a systematic discrimination against low  $m/Q$  ions (Chernushevich et al., 2001). The TOF duty signal accounts for this by correcting the signal as shown in Eq. 3-1.

$$I_{corr} = I_{raw} * \sqrt{\frac{X}{m/Q}} \quad \text{Eq. 3-1}$$

$I_{corr}$  represents the corrected signal,  $I_{raw}$  the signal at one  $m/Q$  before correction and  $X$  a reference mass (Yuan et al., 2016). In our cases, the reference mass was chosen as the mass of the reagent ion (62  $m/Q$  for nitrate and 79  $m/Q$  for bromide). No transmission correction was

performed as previous measurements showed an approximately flat relative transmission curve in the mass region of interest.

#### **3.1.4 Determination of oxidized compounds and HO<sub>2</sub> with MION-CIMS**

The MION-NO<sub>3</sub>-CIMS was used to detect closed-shell HOMs, as well as HOM-RO<sub>2</sub>. Bianchi et al. (2019) suggested to define HOM as products stemming from autoxidation containing more than 6 oxygen. In our overall analysis, we decided to also include fragments and monomers containing 5 or in a few cases 4 oxygens (see peaklists in Appendix **Section A.6**) as we were interested to see if the importance of these less oxidized (but still detectable with NO<sub>3</sub>-CIMS) products change between the different chemical regimes. However, in all considerations regarding SOA formation, we furthermore set a molar weight threshold which automatically excluded any products with less than 6 oxygens.

In general, NO<sub>3</sub>-CIMS is a highly selective method since the analytes compete with nitric acid for cluster formation with NO<sub>3</sub><sup>-</sup>. Only few analytes have stronger gas phase acidities than nitric acid (Zhao, 2018). Proton transfer reactions are rarely observed and the main pathway for ionization is a ligand exchange from nitric acid to the analyte (Hytinen et al., 2018; Ehn et al., 2014). All analytes were detected as nitrate analyte clusters and were normalized with the reagent ion signal sum (sum of NO<sub>3</sub><sup>-</sup> and HNO<sub>3</sub>NO<sub>3</sub><sup>-</sup>).

The changes in the HOM product distributions were compared for the different experiment phases via the relative change in signal. For all detected products the same detection sensitivity is assumed. Hytinen et al. (2018) showed in quantum chemical calculations that HOMs containing 6 or more oxygen atoms have comparable sensitivity with the nitrate reagent ion. At this degree of oxidation, it can be expected that the HOMs already contain multiple hydroperoxyl and/or hydroxy functional groups (Bianchi et al., 2019) prior to the termination step, making it unlikely that the sensitivity is strongly influenced by the termination group. Thus, the signal strength reflects the correct ranking of the observations and relative comparisons do not require calibration. Pullinen et al. (2020) studied the mass balance between condensable HOMs and formed particle mass and were able to find closure within a factor of 2.

The MION-Br-CIMS was used to detect the HO<sub>2</sub> radical. The detection of HO<sub>2</sub> via Br-CIMS has been previously reported by Albrecht et al. (2019) and Sanchez et al. (2016). It should also be mentioned that the Br-CIMS can also be used to detect earlier stage, lower oxidized oxidation products than NO<sub>3</sub>-CIMS as shown by Rissanen et al. (2019), but this was not pursued further in this work.

The HO<sub>2</sub> radical was detected as a bromide cluster and its signal was normalized with the reagent ion signal sum (sum of Br<sup>-</sup> and BrH<sub>2</sub>O). Since no direct HO<sub>2</sub> calibration was available, the HO<sub>2</sub> signal in the Br-MION-CIMS was used to compare the levels of HO<sub>2</sub> relative to each other in the different phases of the experiment. Furthermore, the measured HO<sub>2</sub> signal was compared to modeled HO<sub>2</sub> concentrations, details of the modeling are explained in **Section 3.2.5**.

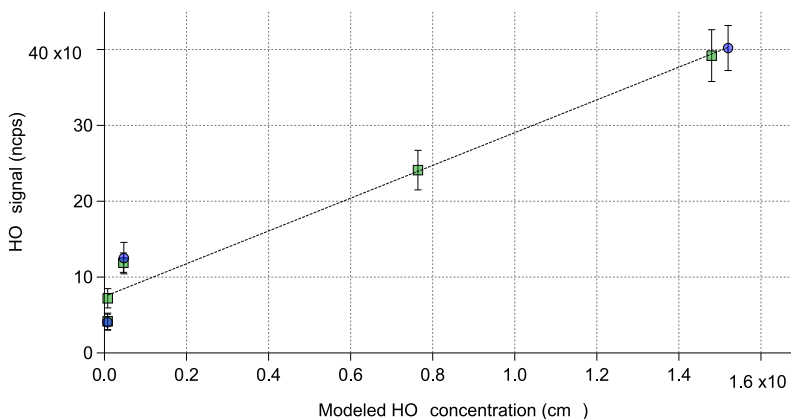


**Figure 9** Modeled HO<sub>2</sub> concentration vs. normalized HO<sub>2</sub> signal for each steady state of experiment *apinCO\_2*. HO<sub>2</sub> was measured as the BrHO<sub>2</sub> cluster and was normalized with the sum of the reagent ion Br<sup>-</sup> and its water cluster. The dotted line shows the linear fit to all (unseeded and seeded) measurement points.

**Figure 9** illustrates this for the example of an experiment (*apinCO\_2*) spanning a wide range of HO<sub>2</sub> concentration due to CO addition. We see a good linear relation between the model predictions and observations. However, a background signal of around  $\sim 1 \cdot 10^{-5}$  was observed as soon as VOC and ozone were present in the reactor. The background HO<sub>2</sub> signal was not observed when only O<sub>3</sub> or only VOC were in the system. As shown by the modeling results, HO<sub>2</sub> production of this strength is not expected in the  $\alpha$ -pinene ozonolysis phase but this background phenomenon was observed before (Albrecht et al., 2019) and is not fully understood.

### 3.1.5 Derivation of condensable HOM mass proxy in the gas-phase from CIMS-measurement

A simple proxy for the condensable mass from HOM products can be calculated from the steady-state HOM signals measured by the NO<sub>3</sub>-CIMS, assuming condensation for all low volatility HOM compounds and no back evaporation into the gas phase.

To this end, a threshold has to be determined to only take low volatility HOM compounds into account. For the threshold a lower-limit molar mass was defined to only include significantly condensing products in the calculation of the proxy. To determine the lower-limit molar mass of significantly condensing products, we used the comparison between experiment stages without particles (unseeded experiment phases) and experiments with particles providing surface for condensation (seeded experiment phases). The product signal in the seeded experiment phase was compared with the unseeded experiment phase, yielding the product's fraction remaining in presence of seed. We defined the criteria of usable signals as no significant background signal and standard deviation of the average steady-state signal < 30 %. The fraction remaining for each individual closed-shell oxidation product fulfilling the criteria was plotted against the product's molar mass. A trend curve was added to the data and the threshold was determined as the molar mass at which the trend expected a fraction remaining in the gas phase of 50 %. Therefore, only oxidation products with 50 % and more of the signal lost to condensation were considered as contributors for the condensable HOM mass proxy.

To calculate the condensable HOM mass proxy, all contributions were weighted by their molar mass, summed up, and normalized with the  $\alpha$ -pinene OH turnover ( $k_{OH} \cdot [OH]_{SS} \cdot [\alpha\text{-pinene}]_{SS}$ ) as shown in *Eq. 3-2*. Here  $S_i$  is the signal of compound  $i$  and  $M_i$  its molar mass. The normalization with the  $\alpha$ -pinene OH turnover mostly considers small experimental imperfections, but also allows better comparison between different chemical conditions, see **Section 3.2.2** for further explanation.

$$\text{mass weighted signal sum} = \frac{\sum_{i=0}^i S_i \cdot M_i}{k_{OH} \cdot [OH]_{SS} \cdot [\alpha\text{-pinene}]_{SS}} \quad \text{Eq. 3-2}$$

## 3.2 Atmospheric reaction chamber SAPHIR-STAR

The experiments were performed in the atmospheric reaction chamber SAPHIR-STAR. This reactor is part of the Forschungszentrum Jülich SAPHIR family of reactors with the name stemming from the original SAPHIR reactor: "Simulation of the Atmospheric PHotochemistry In a large Reaction Chamber". SAPHIR-STAR is a continuously stirred tank reactor (STR) and is the modernized successor of the Jülich plant atmosphere chamber (JPAC). More information about JPAC's set-up can be found in Mentel et al. (2009). SAPHIR-STAR was run as a steady-state reactor in all experiments.

A picture of the SAPHIR-STAR can be seen in **Figure 10**. The reactor body is a borosilicate glass cylinder ( $l=2.5$  m,  $d=1$  m) with a volume close to 2000 L. All equipment inside the chamber is either glass or glass coated steel (SilcoTek GmbH) to avoid wall effects.

The chamber inflow is split into two humidified air flows (Flow A and B in **Figure 10**). The synthetic air is mixed from  $N_2$  and  $O_2$  (both 6.0 purity grade). Flow A is used to add the oxidant, in our case  $O_3$ , and flow B is used to add all other trace gases, in our case  $\alpha$ -pinene, CO and/or NO in some experiment stages. The flow separation ensures that no reactions occur before the reactants enter the chamber. All experiments were performed with a total inflow of  $32$  L  $min^{-1}$  and at a relative humidity of 50 % and a temperature of  $20$  °C. Temperature stability is ensured by the climate-controlled surrounding of the chamber. The inflow of  $32$  L  $min^{-1}$  results in a residence time in the chamber of approximately 61 minutes with a fan ensuring mixing on a minute timescale. The mixing is conducted perpendicular to the cylinder axis.

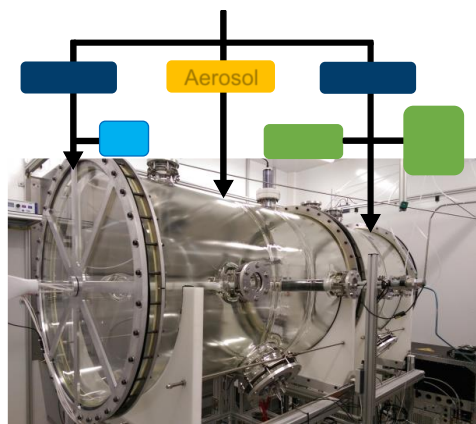


**Figure 10** Atmospheric reaction chamber SAPHIR-STAR with schematic flow set-up  $\alpha$ -Pinene ( $\geq 99$  % purity, Sigma-Aldrich Merck KGaA) was introduced via liquid injection with a syringe pump (Fusion 4000, CHEMYX Inc.) into a heated glass bulb and flushed by a stream of  $1$  L  $min^{-1}$  into the chamber. CO was added from a gas bottle (10% CO in  $N_2$ , Messer SE & Co. KGaA). NO was added from a gas bottle (100 ppmv NO in  $N_2$ , Linde Gas AG) as well. Ozone was directly produced photolytically before injection with a self-built ozone generator.

For photooxidation OH was produced via ozone photolysis using two UV-C lamps with a wavelength of 254 nm and subsequent reaction of  $O(^1D)$  with water vapor. The lamps are mounted in closed quartz cylinders in the middle of the chamber, vertically to the cylinder

axis and the light intensity can be varied with a movable shielding installed around the lamps. The shielding allows an exact percentage of the lamp to be covered, thus controlling the amount of OH produced in the chamber. The OH radical concentration was adjusted after each change in chemical regime via the O<sub>3</sub> inflow and the gap opening of the UV-C lamp.

The applied J(O<sup>1</sup>D) values in different phases were calculated to be in the range of  $0.8 \cdot 10^{-3} \text{ s}^{-1}$  to  $2.6 \cdot 10^{-3} \text{ s}^{-1}$ . In experiments with NO addition, additionally a UV-A lamp with a wavelength of 365 nm was turned on, to facilitate the photolysis from NO<sub>2</sub> back to NO and O<sub>3</sub>. The determined J(NO<sub>2</sub>) value was  $1.0 \cdot 10^{-3} \text{ s}^{-1}$ . The UV-A lamp was on for the full length of any experiments involving NO, including phases without NO and background measurements.

For targeted seeding ammonium sulfate particles ( $\geq 99\%$  purity, Merck KGaA) were added to the system to provide a surface for the condensation of organic material. The aerosol was produced with a modified TSI atomizer (Model 3076, TSI GmbH) and dried to 50% relative humidity.

### **3.2.1 Instrumentation**

VOC concentrations in the chamber were measured using proton-transfer-reaction mass spectrometry (PTR-TOF-MS; Ionicon GmbH). CO<sub>2</sub>, CO, H<sub>2</sub>O were measured with a cavity ring down spectrometer (G2401 Cavity Ringdown Spectrometer, Picarro Inc.). O<sub>3</sub> was monitored with a UV-photometer (O342e, Envea GmbH).

NO and NO<sub>x</sub> were measured via chemiluminescence (NCLD899, Eco Physics GmbH with a home-built photolytic converter). However, in two experiments (apinNO and apinCONO\_1) the measurement data required further correction, as the measurement of the NO concentration in the inflow was off compared to the expectation. Measurements of the NO inflow concentration from the same gas bottle with the same flow controllers and same flow settings were as expected in other experiments. Therefore, it was deduced that the measurement data for these experiments needed correction. The data was corrected by multiplication with a correction factor calculated from the expected NO concentration in the inflow divided by the NO concentration inflow measurement. A NO inflow concentration measurement was performed in every steady state and the correction factor was updated accordingly.

Particle size distribution and number concentration were measured with a condensation particle counter (CPC, Model 3788, TSI GmbH) and a scanning mobility particle sizer (SMPS; Model 3080, TSI GmbH) with a CPC (Model 3788, TSI GmbH). The aerosol composition was measured with a high-resolution aerosol mass spectrometer (HR-TOF AMS; Aerodyne Inc.).

In all experiments, VOC, O<sub>3</sub>, NO, NO<sub>x</sub>, and SMPS+CPC sampling was switched between inlet and outlet of the chamber to measure the input concentrations as well as the concentrations in the reactor. The flow control system of the chamber adapts to these switches so that the inflow into the chamber remains constant.

Less oxidized organic species were measured by a second CI-API-TOF. It was configured with a CI inlet based on the design of Eisele and Tanner (1993) coupled to an HTOF (Resolution ~2700 for peaks at >200 m/Q) (Tofwerk AG) and was operated in positive-ion mode with propylamine as the reagent (C<sub>3</sub>H<sub>7</sub>NH<sub>2</sub>, Sigma-Aldrich, purity ≥99%). The instrument is able to detect early generation RO<sub>2</sub> and oxidation products (Berndt et al., 2018). The propylamine was purified and added as an amine-N<sub>2</sub> mixture (flow: 0.12 mL min<sup>-1</sup>) to the 30 L min<sup>-1</sup> sheath flow. Furthermore, the sheath flow air was humidified to optimize ionization. The instrument sampled 0.1 L min<sup>-1</sup> from the chamber, which was diluted with 9.9 L min<sup>-1</sup> for a sample flow of 10 L min<sup>-1</sup>. The dilution was necessary to reduce depletion of the primary ion (Hantschke, 2022). We will refer to selected observations from the amine-CIMS.

All parameters and data were recorded as a function of time over the whole experiment duration. The results discussed here were observed under steady-state conditions when all parameters were constant.

### 3.2.2 OH concentration and $\alpha$ -pinene OH turnover

For each steady state, the OH concentration was calculated from the decay of  $\alpha$ -pinene as described by Kiendler-Scharr et al. (2009). Eq. 3-3 is derived from the mass balance of  $\alpha$ -pinene at steady state. The steady state OH concentration [OH]<sub>ss</sub> depends on the amount of  $\alpha$ -pinene consumed by reaction with OH and the reaction with O<sub>3</sub>, as well as the flush out.

$$[OH]_{ss} = \frac{F}{V} * \frac{[VOC]_{in} - [VOC]_{ss} - k_{O_3} * [O_3]_{ss}}{k_{OH}} \quad \text{Eq. 3-3}$$

$F$  is the total flow and  $V$  the volume of the chamber. The subscript “SS” indicates steady-state concentrations, while  $[VOC]_{in}$  represents the  $\alpha$ -pinene concentration entering the chamber.  $k_{O_3}$  and  $k_{OH}$  represent the reaction rate coefficients of  $\alpha$ -pinene with the corresponding oxidant. We applied rate coefficients of  $k_{OH}=5.36 \cdot 10^{-11} \text{ cm}^3 \text{ s}^{-1}$  (Atkinson and Arey, 2003) and  $k_{O_3}=9.25 \cdot 10^{-17} \text{ cm}^3 \text{ s}^{-1}$  (Cox et al., 2020) at 20 °C. The uncertainty of the OH calculation was estimated as 20 % by Wildt et al. (2014).

McFiggans et al. (2019) described that one limiting factor in experiments with multiple OH reaction partners is oxidant scavenging: The products and their yields in mixed systems change, because there is less OH available to the individual VOC. One important methodical goal of this work was to compare the different chemical regimes at as constant as possible  $\alpha$ -pinene oxidation conditions.

The  $\alpha$ -pinene OH turnover is the best criterium to ensure the equality of oxidation conditions and is calculated as shown in *Eq. 3-4*. The same turnover guarantees the same production of the first generation RO<sub>2</sub>.

$$turnover_{\alpha\text{-pinene}+\text{OH}} = k_{\text{OH}} * [\alpha\text{-pinene}]_{\text{SS}} * [\text{OH}]_{\text{SS}} \quad \text{Eq. 3-4}$$

The turnover is defined by the steady-state concentrations of  $\alpha$ -pinene and OH, as well as the  $\alpha$ -pinene OH reaction rate coefficient  $k_{\text{OH}}$ . In our experiments, we added CO to increase the HO<sub>2</sub> concentration in the chamber via the reaction of CO and OH. Thus, after the CO addition, the OH production in the chamber was increased to compensate for the OH consumed by CO.

The same control of the OH production was applied after the NO additions, though smaller OH adjustment was necessary due to the influence of NO. NO reacts with O<sub>3</sub> forming NO<sub>2</sub>, affecting the oxidant level. In SAPHIR-STAR a UV-A lamp photolyzes NO<sub>2</sub>, reforming NO and O<sub>3</sub>. However, the J(NO<sub>2</sub>) rate achieved was at the lower end of expected atmospheric photolysis frequencies leading to higher NO<sub>2</sub> level. The J(NO<sub>2</sub>) rate in SAPHIR-STAR was  $1.0 \cdot 10^{-3} \text{ s}^{-1}$ , while for example a typical value for Germany in summer is  $J(\text{NO}_2) = 4.0 \cdot 10^{-3} \text{ s}^{-1}$  (Cho et al., 2023). Additionally, NO influences the HO<sub>x</sub> budget (see reactions (R2-9) and (R2-10)).

The  $\alpha$ -pinene OH turnover in the system before and after the CO and NO additions were approximately the same. Thus, the OH adjustment ensured that the primary  $\alpha$ -pinene chemistry was kept the same and enabled a better comparison. An overview of the OH concentrations and  $\alpha$ -pinene OH turnovers can be found in Appendix **Table A4**.

However, since experiments could only be performed at *about* the same OH levels, a normalization by the actual  $\alpha$ -pinene OH turnover was applied to the data. This compensates for slight experimental imperfections and enables better comparison of experiment series with different boundary conditions. This normalization eliminates differences due to changes in turnover and also directly shows the yield of certain oxidation products or product groups per  $\alpha$ -pinene consumed by OH.

### 3.2.3 Experimental conditions

**Table 1** contains an overview of the experiments performed for this work. All experiments had an  $\alpha$ -pinene inflow concentration of 10 ppbv and the  $\alpha$ -pinene sink was dominated by the reaction with OH. Three chemical regimes were compared to the typical simple laboratory settings, i.e.  $\alpha$ -pinene OH oxidation without further additions. For the first regime, 2.5 ppmv CO was added to the chamber to increase the HO<sub>2</sub> concentration and shift to higher HO<sub>2</sub>/RO<sub>2</sub> ratios, as such ratios are more realistic to the atmosphere (Schervish and Donahue, 2021). An overview with examples of HO<sub>2</sub>/RO<sub>2</sub> ratios and concentrations observed in the atmosphere can be found in Appendix **Table A11**. For the second regime NO was added. NO is an important anthropogenic trace gas and is found in varying concentrations nearly everywhere in the present-day atmosphere (Finlayson-Pitts and Pitts, 2000). Examples of atmospheric NO concentrations in different environments can be found in Appendix **Table A1**. For the third regime both additions were combined into a high HO<sub>2</sub> case with NO.

When adding NO, two different NO concentrations were investigated to vary the RO<sub>2</sub> sink from RO<sub>2</sub>+NO. NO inflow concentrations of 10 ppbv and 25 ppbv were utilized and are referred to in **Table 1** as “middle NO” and “high NO” respectively.

**Table 1** Overview of experimental conditions with corresponding experiments. For experiments with NO addition, the value in square brackets indicates the inflow NO concentration in ppbv. The “g” and “s” in parentheses refer to the particle phase information: “g” indicates unseeded, pure gas phase and “s” indicates seeded experiments. All information refers to steady-state conditions. HO<sub>2</sub>/RO<sub>2</sub> inferred from model calculations (see Section 3.2.5).

<u>Experimental conditions</u>	<u>Repetitions</u>	<u>Experiment names</u>	<u>HO<sub>2</sub>/RO<sub>2</sub> ratio</u>	<u>[NO]<sub>ss</sub></u>	<u>[NO]<sub>ss</sub></u>
<i>Base case</i>	Used for comparisons	apinCO_1 (g), apinCO_2 (g,s), apinCONO_1 [-] (s), apinCONO_2 [-] (g,s)	0.006 0.007 0.007 0.007	-	-
<i>High HO<sub>2</sub></i>	2	apinCO_1 (g), apinCO_2 (g,s), apinCONO_1 [-] (s)	0.6 1.0 1.0	-	-
<i>Middle NO</i>	1	apinNO [10] (g,s)	0.2	0.2 ppbv	3.3 ppbv
<i>High NO</i>	1	apinNO [25] (g,s)	0.4	0.5 ppbv	8.4 ppbv
<i>Middle NO, high HO<sub>2</sub></i>	1	apinCONO_1 [10] (g,s)	2.0	0.1 ppbv	4.8 ppbv
<i>High NO, high HO<sub>2</sub></i>	2	apinCONO_1 [25] (g,s), apinCONO_2 [25] (g,s)	2.4 2.7	0.4 ppbv 0.3 ppbv	11.2 ppbv 12.7 ppbv

As explained above, the base case for comparison was always the simple laboratory case with just  $\alpha$ -pinene photooxidation. This base case was either one stage of the experiment or was taken from another experiment for comparison. Information which experimental stages were

contained in each experiment can be found in the Appendix **Section A.3. Table A4** in the Appendix also contains the achieved OH concentrations and  $\alpha$ -pinene OH turnovers. **Table A12** gives an overview of important particle phase parameters like available particle surface and measured particle mass.

Another important comparison is the comparison of the seeded to the unseeded system (targeted seeding). As no significant nucleation was observed in any experiment, the unseeded phases represent pure gas phase conditions. Seed addition parameters were chosen, so that the available seed surface represented a competitive sink for HOM compounds compared to the wall loss. The typical lifetime for wall loss of HOM products in our chamber was 170 s. Typical lifetimes for loss on the particles (i.e. condensation) ranged from 28-50 s. The comparison between seeded and non-seeded systems, provides direct observation of the condensation behavior of the observed oxidation products. Seeded and unseeded stages of each condition were either achieved within one experiment or within different experiments at otherwise same conditions.

### **3.2.4 Experimental procedure**

All data presented represent comparisons of steady-state conditions. In general, experiments were run by setting the required boundary conditions, waiting for steady state to establish (transient period), and then measuring the steady state of this set of boundary conditions. At least 3 hours were allowed to reach steady state (three times the residence time in the chamber), normally 4 hours. The steady state itself lasted for at least 4 hours in each experiment stage to give all analytical instruments a long enough time for sufficient averaging. The steady-state times were also used to measure certain inflow parameters ( $\alpha$ -pinene, CO, NO and particle distribution) as mentioned in **Section 3.2.1** by switching the measurement instruments to the inlet of the chamber for a portion of the time.

As explained in **Section 3.2.2**, an important criterium is a similar, ideally constant,  $\alpha$ -pinene OH turnover to avoid effects of oxidant scavenging. To achieve the same  $\alpha$ -pinene OH turnover after a change in the chemical regime compared to the laboratory base case, the OH concentration in the chamber was adjusted. The OH concentration can be controlled via the gap opening of the UV-C light and if necessary, the O<sub>3</sub> inflow concentration.

An increase of OH concentration was especially critical in the high HO<sub>2</sub> experiments as the added CO consumed a significant portion of the available OH. An example of the OH adjustment after CO addition can be seen in **Figure 11**.

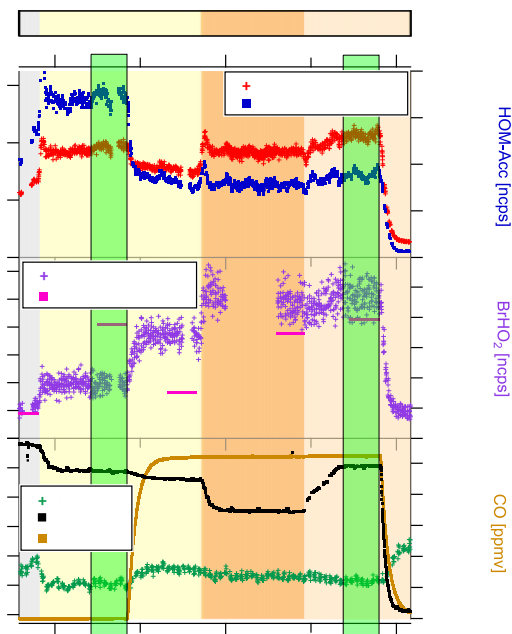


**Figure 11** Exemplary timeseries of high  $\text{HO}_2$  experiment (*apinCO\_1*) showing HOM-Mon and HOM-Acc product sum (top panel), calculated OH concentration and  $\text{BrHO}_2$  signal (middle panel), and  $\text{O}_3$ ,  $\alpha$ -pinene and CO concentrations (bottom panel). Background color represents light intensity (gap opening stated at the top of the graph). Highlighted in green are the base case steady state and the steady state at high  $\text{HO}_2$  (addition of CO and adjusted oxidant level).

After the photooxidation steady state as base case, CO was added to the system. In the displayed *apinCO\_1* experiment, the OH level was adjusted in three steps to approach the same concentration as before the CO addition. First the UV-C light opening was adjusted, then  $\text{O}_3$  was added, and the UV-C light opening was adjusted again. In some experiments the adjustment of the  $\alpha$ -pinene OH turnover via  $\text{O}_3$  concentration and UV-C light opening were made simultaneously with the CO addition. Highlighted in green are the steady states with the “same” OH concentration characterized by low and high  $\text{HO}_2$ , which were used for analysis and interpretation. The  $\text{BrHO}_2$  timeseries (purple plus markers in middle panel of **Figure 11**) show that, at a very comparable OH and  $\alpha$ -pinene level, a much higher  $\text{HO}_2$  level was achieved.

### 3.2.5 Box model calculations for RO<sub>2</sub> sink estimation

Modeling of the experiments was utilized for experiment planning and evaluation. As only sources, sinks and chemical reactions, but no transport processes have to be considered in SAPHIR-STAR, a zero-dimensional box model was used to represent the gas phase chemistry.

The box model applies the chemical mechanism of the “master chemical mechanism” (MCM) v3.3.1 (<https://mcm.york.ac.uk/MCM/>, see Jenkin et al. (1997), Saunders et al. (2003)) under the boundary conditions of the SAPHIR-STAR chamber. Utilized input parameters were temperature, relative humidity, chamber inflows and inflow concentrations of VOC, O<sub>3</sub>, NO, and CO, as well as the status of UV-C and UV-A lights. Reference photolysis frequencies *J* were available for the two lamp spectra. The photolysis frequencies used in the model were scaled to the observed *J*(O<sup>1</sup>D) and *J*(NO<sub>2</sub>), numerically switched on/off, and in the case of the UV-C light additionally scaled by the light gap opening.

Photolysis reaction rate coefficients were determined for *J*(O<sup>1</sup>D) and *J*(NO<sub>2</sub>) in separate experiments. For *J*(O<sup>1</sup>D) determination, O<sub>3</sub> was injected into the humidified chamber and *J*(O<sup>1</sup>D) was determined from the O<sub>3</sub> loss in the chamber as a function of the light gap opening. For *J*(NO<sub>2</sub>) determination, O<sub>3</sub> and NO were injected into the humidified chamber and *J*(NO<sub>2</sub>) was determined from the change in O<sub>3</sub> and NO concentration after turning the UV-A light on. Further necessary model parameters are OH background reactivity and radical wall loss rate coefficients. More information about these parameters can be found in Appendix **Section A.4.1**.

All calculations were performed with the institute software package EASY which uses FACSIMILE to solve the differential equations (EASY Version 5.69b). The model calculations reproduced the primary observables α-pinene, O<sub>3</sub>, CO, NO<sub>2</sub> and OH within the experimental uncertainties. For NO larger relative discrepancies were observed due to the low steady-state concentrations (below 1 ppbv) in the experiments. However, the absolute discrepancies were maximally 0.2 ppbv.

The box-model results were used to characterize the chemical reaction pool of the studied systems, i.e. the relative importance between reaction with NO, HO<sub>2</sub> and the pool of RO<sub>2</sub> for HOM-RO<sub>2</sub>. For the RO<sub>2</sub> pool and HO<sub>2</sub>, no direct measurement was available, however the observed signal of BrHO<sub>2</sub> follows the modeled HO<sub>2</sub> concentration (see example in **Figure 9**). To estimate the relative importance of the different reaction pathways, we applied generic rate coefficients  $k_{\text{RO}_2+\text{HO}_2}$ ,  $k_{\text{RO}_2+\text{NO}}$  and  $k_{\text{RO}_2+\text{RO}_2}$ .

For the reaction of  $\text{RO}_2+\text{HO}_2$  we used  $k_{\text{RO}_2+\text{HO}_2}=2.46\cdot 10^{-11} \text{ cm}^3 \text{ s}^{-1}$  and for the reaction of  $\text{RO}_2+\text{NO}$  we used  $k_{\text{RO}_2+\text{NO}}=9.2\cdot 10^{-12} \text{ cm}^3 \text{ s}^{-1}$  for reactions at 20 °C as specified in the MCM (Jenkin et al., 1997; Saunders et al., 2003)). The reaction rate coefficient for  $\text{RO}_2+\text{NO}$  represents the overall reaction rate with NO, including both termination to ON compounds and alkoxy radical formation.

We chose a  $k_{\text{RO}_2+\text{RO}_2}$  of  $5\cdot 10^{-12} \text{ cm}^3 \text{ s}^{-1}$  as the approximated reaction rate of the  $\text{RO}_2+\text{RO}_2$  reactions. This value applies to all possible reactions (accretion product, monomer, and alkoxy formation) and is in the range of  $k_{\text{RO}_2+\text{RO}_2}$  utilized by Roldin et al. (2019) in the PRAM model. As we cannot verify the  $\text{RO}_2$  and  $\text{HO}_2$  model results by measurements and can only apply generic reaction rate coefficients, the calculation results serve solely as indicators of changes in the system. We do not claim to have determined exact concentrations. The calculations help us to approximate the importance of the reactions of HOM- $\text{RO}_2$  with the  $\text{RO}_2$ -pool,  $\text{HO}_2$  and NO. With this information, we were able to develop a framework to understand the experimental observations.



## 4. Results and Discussion

### 4.1 Impact of high HO<sub>2</sub>

In order to understand the effect of the RO<sub>2</sub>+HO<sub>2</sub> reaction on the gas phase HOM product distribution compared to a RO<sub>2</sub>+RO<sub>2</sub> dominated system, we will present and compare two cases: The “laboratory” base case (RO<sub>2</sub>+RO<sub>2</sub> dominated) and the RO<sub>2</sub>+HO<sub>2</sub> dominated system (achieved via CO addition and OH adjustment by J(O<sup>1</sup>D) and O<sub>3</sub>), which in the following will be referred to as the “high HO<sub>2</sub> case”. For both the unseeded (gas-phase only) and seeded systems two experiments were performed providing one repetition. Thus, we report the average changes plus standard deviations. The repetitions showed good reproducibility with overall little variation in the results.

The box-model results of the HO<sub>2</sub> concentration and sum of RO<sub>2</sub> concentrations were used to determine the competition for reaction with HOM-RO<sub>2</sub> between HO<sub>2</sub> and RO<sub>2</sub>. Furthermore, we determined the HO<sub>2</sub>/RO<sub>2</sub> ratio as an indicator for atmospheric relevance.

The modeling results predicted HO<sub>2</sub>/RO<sub>2</sub> of about 1/1 for the high HO<sub>2</sub> case. In comparison, for the base case a HO<sub>2</sub>/RO<sub>2</sub> ratio of about 1/100 was predicted. The modeled concentrations can be found in Appendix **Section A.4.2**. HO<sub>2</sub>/RO<sub>2</sub> ratios of around 1 are highly relevant for atmospheric conditions with significant OH oxidation, though it should be kept in mind that in atmospheric conditions, the methyl peroxy radical and other small RO<sub>2</sub> contribute a significant portion to the total of peroxy radicals (Khan et al., 2015). Field studies reporting HO<sub>2</sub> and RO<sub>2</sub> measurements for different environments can be found in supplement Appendix **Section A.7**. These exemplary studies show that HO<sub>2</sub>/RO<sub>2</sub> ratios around 1 are relevant in remote to urban environments with different VOC sources and NO<sub>x</sub> levels.

Assuming correctly modeled [HO<sub>2</sub>] and [RO<sub>2</sub>], we calculated the competition between HO<sub>2</sub> and RO<sub>2</sub> reactions for each (observed) RO<sub>2</sub> expressed in form of pseudo first order rate coefficients of  $k_{RO_2+HO_2} \cdot [HO_2]$  or  $k_{RO_2+RO_2} \cdot [RO_2]$ . Herein [RO<sub>2</sub>] is the sum of all RO<sub>2</sub> species as defined in the MCM v3.3.1.

In the model [RO<sub>2</sub>] was reduced by about a factor of three, while [HO<sub>2</sub>] was increased by a factor of 30 for the high HO<sub>2</sub> case compared to the base case. Consequently, HO<sub>2</sub> reactions were almost negligible in the base case, while RO<sub>2</sub>+RO<sub>2</sub> reactions can still contribute in the high HO<sub>2</sub> case. **Figure 12 a)** shows the contribution of the reaction partners to the RO<sub>2</sub> chemical reaction pool within the triangle plot introduced in **Figure 1**. The **Figure 12 a)** shows an overview of all systems investigated in this study with the high HO<sub>2</sub> system highlighted in green and the base case highlighted in blue. For all experiments the results of our calculations indicate that the sink for HOM-RO<sub>2</sub> is dominated by

RO<sub>2</sub>+RO<sub>2</sub> reactions in the base case (~97 % contribution), while at high HO<sub>2</sub> RO<sub>2</sub>+HO<sub>2</sub> contributed ~80 %.

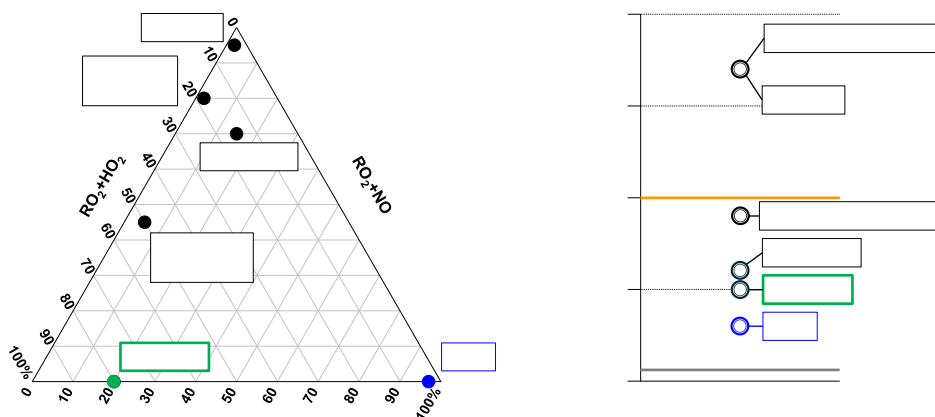


**Figure 12** Classification of the chemical regimes for the system with high HO<sub>2</sub> (highlighted in green):  
 a) Triangle plot showing the distribution of the chemical reaction pool for RO<sub>2</sub> with NO, HO<sub>2</sub> and RO<sub>2</sub>.  
 b) (Pseudo) first order chemical sink relative to average autoxidation rate and wall loss rate.

**Figure 12 b)** shows a comparison of the expected overall pseudo-first order chemical reaction rate coefficient in all investigated systems compared to the base case (again highlighted in blue). Also shown are the assumed average autoxidation rate and determined wall loss rate in the chamber (see Appendix **Section A.4.1**). The overall pseudo-first order (bimolecular) chemical reaction rate coefficient is the sum of the pseudo-first order reaction rate coefficients of RO<sub>2</sub>, HO<sub>2</sub>, and NO in the system. The comparison of the overall chemical reaction rate coefficients to the assumed average autoxidation rate coefficient indicates if significant interruption of the autoxidation chain compared to the base case can be expected due to the increased reactivity in the high HO<sub>2</sub> system. The chemical reaction rate coefficient in the high HO<sub>2</sub> case adds up to 0.05 s<sup>-1</sup>, compared to 0.03 s<sup>-1</sup> in the base case. Even though the chemical pseudo first order reaction rate is slightly higher, it is still significantly below the assumed average autoxidation rate coefficient of 0.1 s<sup>-1</sup>. The increase of [HO<sub>2</sub>] will likely not be able to interfere with autoxidation thus no systematic, significant decrease in HOM products due to early termination is expected.

An average autoxidation rate of 0.1 s<sup>-1</sup> was chosen due to the reported rate coefficients in the literature (Piletic and Kleindienst, 2022; Berndt, 2021; Xu et al., 2019; Vereecken et al., 2007). In general, rate coefficients for individual reactions are not well known and we have to rely on generic rate coefficients proposed in the literature. Since we cannot verify the modeling results for HO<sub>2</sub> and RO<sub>2</sub>, our calculations should be seen only as indications of the expected trends in the chemical system.

#### 4.1.1 Impact of HO<sub>2</sub> on overall HOM formation

The top panel in **Figure 11** shows the timeseries of HOM-Mon and HOM-Acc products in one of the high HO<sub>2</sub> experiments, so that the base case and high HO<sub>2</sub> case can be directly compared. The HOM-Mon signal recovered after the oxidant adjustment, while the HOM-Acc signal was significantly suppressed at high HO<sub>2</sub>. This indicates that the shift to the HO<sub>2</sub> dominated system substantially impacts the termination reactions, shifting formation from the HOM-Acc product channel (RO<sub>2</sub>+RO<sub>2</sub>) to the HOM-Mon channel.

An overview of the results for the product classes as defined in **Section 2.1** is shown in **Figure 13**. Plotted are the average ratios of signal in the NO<sub>3</sub>-CIMS in steady state in the high HO<sub>2</sub> case compared to the RO<sub>2</sub>+RO<sub>2</sub> dominated base case. All experiment phases were normalized to the actual  $\alpha$ -pinene OH turnover. The overall HOM signal was lower in the high HO<sub>2</sub> case showing a reduction of about 20 %. Most distinctive, the HOM-Acc were strongly reduced by about 60 %. A reduction of HOM-Acc by addition of CO was observed before by McFiggans et al. (2019), however there the OH concentration was not kept constant. The HOM-Frag (C<sub>5</sub>-C<sub>9</sub>) also show a reduction of about 20 %. In the high HO<sub>2</sub> case C<sub>10</sub>-HOM-RO<sub>2</sub> were also significantly reduced by about 40 %.

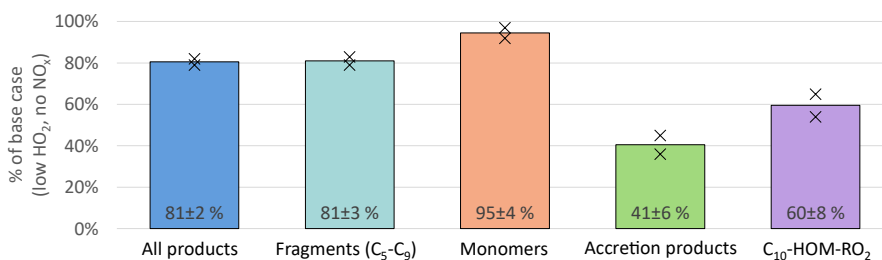


**Figure 13** Overview of average, relative change in product classes detected in NO<sub>3</sub>-CIMS between high HO<sub>2</sub> case and base case (both normalized to  $\alpha$ -pinene OH turnover) for unseeded experiments. Bars represent average of the two experiments, markers represent individual experiments.

The HOM-Mon signal remained about the same in the high HO<sub>2</sub> and base case. Without changes in the rates and contributions of the different termination reactions, the observed reduction in the HOM-RO<sub>2</sub> precursors should lead to nearly the same reduction in HOM-Mon. However, the decrease of accretion product formation and fragmentation should lead to an increase in HOM-Mon. The presence of HO<sub>2</sub> should reduce the alkoxy radical formation, and thus fragmentation of HOM-RO<sub>2</sub>. This missing sink could lead to an additional HOM-Mon source compared to the base case. However, the distribution of the product classes in both cases (**Figure 14**) shows that in the high HO<sub>2</sub> case the contributions were shifted from HOM-Acc to HOM-Mon, while the contribution of HOM-Frag remained constant. Each HOM-Acc is formed from one HOM-RO<sub>2</sub> (HOM-RO<sub>2</sub>+RO<sub>2</sub>) or potentially even two HOM-RO<sub>2</sub> (HOM-RO<sub>2</sub>+HOM-RO<sub>2</sub>) and therefore each HOM-Acc not formed will lead to at least one HOM-Mon.

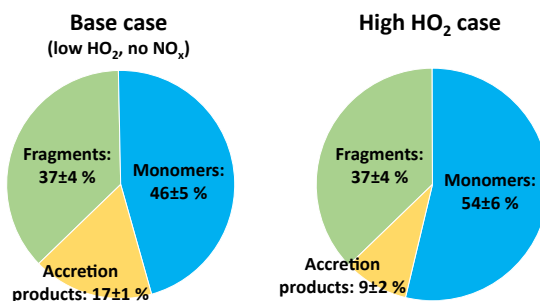


**Figure 14** Average contribution of the closed shell product classes to overall HOM product signal in the RO<sub>2</sub>+RO<sub>2</sub> dominated base case and the high HO<sub>2</sub> case (unseeded experiments)

Details of the changes in the product distribution become evident when considering the individual HOM-Mon families as shown in **Figure 15**. Due to their different formation pathways (see **Section 2.1.1**) the change in the HOM-Mon family distribution is a helpful tool to analyze the effect of the shifted importance of reaction of HOM-RO<sub>2</sub> with HO<sub>2</sub> compared to RO<sub>2</sub>. A decrease in the C<sub>10</sub>H<sub>14</sub>O<sub>z</sub> family and an increase of the C<sub>10</sub>H<sub>18</sub>O<sub>z</sub> family is expected with increasing HO<sub>2</sub> importance because of increasing termination by HO<sub>2</sub> (C<sub>10</sub>H<sub>17</sub>O<sub>x</sub> + HO<sub>2</sub> → C<sub>10</sub>H<sub>18</sub>O<sub>z</sub>) and decreasing termination by RO<sub>2</sub> (C<sub>10</sub>H<sub>15</sub>O<sub>x</sub> + RO<sub>2</sub> → C<sub>10</sub>H<sub>14</sub>O<sub>z</sub>). In the case of C<sub>10</sub>H<sub>18</sub>O<sub>z</sub> the increase of hydroperoxides is partially compensated by a decrease of the alcohol formation of RO<sub>2</sub>+RO<sub>2</sub>. For C<sub>10</sub>H<sub>16</sub>O<sub>z</sub> the situation is more complicated as it contains contributions from all termination pathways.

The C<sub>10</sub>H<sub>15</sub>O<sub>x</sub>-RO<sub>2</sub> family and the related C<sub>10</sub>H<sub>14</sub>O<sub>z</sub> family (carbonyl compounds) show the strongest suppression with a decrease of about 40 % at high HO<sub>2</sub>. For the C<sub>10</sub>H<sub>17</sub>O<sub>x</sub>-RO<sub>2</sub> family the suppression was less pronounced with an 18 % reduction. In contrast, the C<sub>10</sub>H<sub>16</sub>O<sub>z</sub> family remained about the same while the C<sub>10</sub>H<sub>18</sub>O<sub>z</sub> family showed a strong increase at high HO<sub>2</sub> compared to the base case.

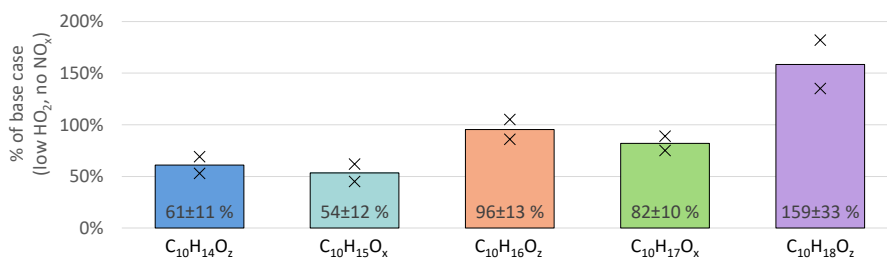


**Figure 15** Overview of average, relative change in monomer families detected in NO<sub>3</sub>-CIMS between high HO<sub>2</sub> case and base case (both normalized to α-pinene OH turnover) for unseeded experiments. Bars represent average of the two experiments, markers represent individual experiments.

The suppression of C<sub>10</sub>-HOM-RO<sub>2</sub> of only about 40 % compared to the reduction of overall [RO<sub>2</sub>] by ~70 % in the model calculations (for the modeled concentrations see Appendix **Section A.4.2**) shows that in many instances the autoxidation is too efficient to be out-competed by the RO<sub>2</sub>+HO<sub>2</sub> termination reaction, which is several times faster than RO<sub>2</sub>+RO<sub>2</sub> reactions.

Furthermore, the signal weighted O/C ratio of the monomer class did not change between base and high HO<sub>2</sub> case ( $0.70 \pm 0.01$ ). If the HO<sub>2</sub> termination would interrupt the autoxidation chain, a lower oxidation level would be expected at high HO<sub>2</sub>. The unchanged oxidation level and the suppression of HOM-Acc indicate that the average autoxidation rate must indeed be faster than  $k_{\text{HOM-RO}_2+\text{HO}_2}[\text{HO}_2]$ , while the average accretion rate for  $k_{\text{HOM-RO}_2+\text{RO}_2}[\text{RO}_2]$  must be slower. In conclusion, the change towards a RO<sub>2</sub>+HO<sub>2</sub> dominated system should essentially impact the distribution of the HOM-RO<sub>2</sub> termination products.

#### 4.1.2 Impact of HO<sub>2</sub> on the HOM-RO<sub>2</sub> concentration

C<sub>10</sub>-HOM-RO<sub>2</sub> are key to understand the changes in the HOM product distribution. Therefore, we will first discuss the changes in the HOM-RO<sub>2</sub> and then the changes in the closed-shell products.

The C<sub>10</sub> peroxy radical class consists of the C<sub>10</sub>H<sub>15</sub>O<sub>x</sub> and C<sub>10</sub>H<sub>17</sub>O<sub>x</sub> families which were reduced to 54 % and 82 %, respectively when comparing the high HO<sub>2</sub> case to the base case (**Figure 15**, light blue and green bars). The observed reduction in C<sub>10</sub>-HOM-RO<sub>2</sub> is significantly smaller than the overall RO<sub>2</sub> reduction predicted by the MCM model results (reduction to ~30 %). In the following paragraphs, we present a plausibility consideration to assess if these observed changes are consistent with our expectations from modeling results and generic reaction rates.

The change in the steady-state concentration of a compound is always defined by the changes in its sources and sinks. The source of a HOM-RO<sub>2</sub> is the autoxidation of a precursor RO<sub>2</sub>. Thus, the HOM-RO<sub>2</sub>'s source is reduced if the steady-state concentration of the precursor RO<sub>2</sub> is reduced. However, assuming the source term of the precursor RO<sub>2</sub> is the same in base case and high HO<sub>2</sub> case (due to the constant  $\alpha$ -pinene OH turnover) and the precursor RO<sub>2</sub>'s sink term is dominated by the fast autoxidation in both cases, then the RO<sub>2</sub>'s steady state concentration would not be significantly changed. This consideration is only applicable for RO<sub>2</sub> where autoxidation dominates the sink term in both conditions. However, **Figure 12 b**) shows that this is still a reasonable assumption for many autoxidation reactions.

As long as autoxidation source and sink are balanced, the change in steady-state concentration of the HOM-RO<sub>2</sub> will be determined by the changes in the termination. Owing to the faster reaction of RO<sub>2</sub>+HO<sub>2</sub> compared to RO<sub>2</sub>+RO<sub>2</sub>, the chemical sink for all RO<sub>2</sub> including HOM-RO<sub>2</sub> with slower autoxidation rates increased, which leads to a reduction in the steady-state concentration of RO<sub>2</sub> in general, despite keeping the primary RO<sub>2</sub> source term constant.

For steady-state conditions, we can estimate the expected effect on the RO<sub>2</sub> ratio between high HO<sub>2</sub> and base case for those HOM-RO<sub>2</sub> with production directly linked to the primary production ( $k_{\text{OH}}[\text{OH}][\alpha\text{-pinene}]$ ) with negligible further autoxidation. The necessary equations and assumptions can be found in Appendix **Section A.8**. We assume the same primary production in both cases and

that the reaction with HO<sub>2</sub>, the reaction with RO<sub>2</sub> and the wall loss are the only significant loss pathways. In the high HO<sub>2</sub> case compared to the base case, a reduction in concentration to 80 % is expected if the rate coefficient  $k_{\text{RO}_2+\text{HO}_2}$  (utilized value:  $2.46 \cdot 10^{-11} \text{ cm}^3 \text{ s}^{-1}$  at 20 °C (Jenkin et al., 1997; Saunders et al., 2003)) is 5 times faster than  $k_{\text{RO}_2+\text{RO}_2}$  (leading to  $k_{\text{RO}_2+\text{RO}_2} = 3.7 \cdot 10^{-12} \text{ cm}^3 \text{ s}^{-1}$ ). A reduction to 60 % is expected if  $k_{\text{RO}_2+\text{HO}_2}$  is 8 times faster than  $k_{\text{RO}_2+\text{RO}_2}$ . These reductions are in the range of observations for the C<sub>10</sub>-HOM-RO<sub>2</sub>. Note, that the approach of using generalized bulk rate coefficients is limited, but the resulting values for  $k_{\text{RO}_2+\text{RO}_2}$  were clearly within the range of rate coefficients expected for HOM-RO<sub>2</sub>+RO<sub>2</sub> reactions (Roldin et al., 2019), showing that the increased chemical sink is a plausible explanation for our observations.

The C<sub>10</sub>H<sub>15</sub>O<sub>x</sub> family was reduced by about 30 % more than the C<sub>10</sub>H<sub>17</sub>O<sub>x</sub> family (see **Figure 15**). C<sub>10</sub>H<sub>15</sub>O<sub>x</sub> peroxy radicals are either formed by sequential oxidation of  $\alpha$ -pinene, e.g. from oxidation products like pinonaldehyde, or directly from  $\alpha$ -pinene via the H-abstraction pathway (Shen et al., 2022). Formation of pinonaldehyde and, even more so HOM formation via the H-abstraction channel, involve alkoxy steps. However, alkoxy radicals should be reduced at high HO<sub>2</sub> since they are mainly formed by RO<sub>2</sub>+RO<sub>2</sub> reactions in the absence of NO<sub>x</sub>. Thus, missing source terms add to the increased chemical sink by HO<sub>2</sub> for C<sub>10</sub>H<sub>15</sub>O<sub>x</sub> peroxy radicals.

Amine-CIMS measurements enabled the detection of C<sub>10</sub>H<sub>16</sub>O<sub>2</sub> (e.g. formula composition of pinonaldehyde). The C<sub>10</sub>H<sub>16</sub>O<sub>2</sub> signal was reduced on average to 70±1 % at high HO<sub>2</sub> compared to the RO<sub>2</sub>+RO<sub>2</sub> dominated base case. This supports that a fraction of the C<sub>10</sub>H<sub>15</sub>O<sub>x</sub> radical decrease in the high HO<sub>2</sub> case arose from suppression of C<sub>10</sub>H<sub>16</sub>O<sub>2</sub> first generation products. In addition, a further suppression of HOM formation via the H-abstraction channel is likely. It should be noted that the reduction of C<sub>10</sub>H<sub>16</sub>O<sub>2</sub> is smaller than that expected by the MCM model results. Modeling results can be found in Appendix **Section A.4.2**. This might indicate that HO<sub>2</sub> can also enable alkoxy radical steps to a certain degree as summarized by Jenkin et al. (2019) and postulated by Eddingsaas et al. (2012) as a source of pinonaldehyde in HO<sub>2</sub> dominated systems.

According to the model calculations the pseudo first order rate coefficient  $k_{\text{RO}_2+\text{HO}_2} \cdot [\text{HO}_2]$  is expected to be about 0.04 s<sup>-1</sup> for the RO<sub>2</sub>+HO<sub>2</sub> reaction in the high HO<sub>2</sub> case. Consequently, only such HOM-RO<sub>2</sub> with autoxidation rates of  $\leq 0.04 \text{ s}^{-1}$  will be significantly lost by reaction with HO<sub>2</sub> at the higher HO<sub>2</sub> concentrations. However, typical isomerization rates of peroxy radicals in autoxidation are of the order of 0.1 s<sup>-1</sup> and many are faster (Piletic and Kleindienst, 2022; Berndt, 2021). Therefore, reduction in a HOM-RO<sub>2</sub> is only expected when the faster termination rate of  $k_{\text{RO}_2+\text{HO}_2} \cdot [\text{HO}_2]$  can compete with the autoxidation rate, i.e. when the autoxidation slows as the degree of oxidation increases on the specific HOM-RO<sub>2</sub>. This consideration shows that the smaller reduction in HOM-RO<sub>2</sub> compared to the

lowly oxidized RO<sub>2</sub> in the model is compatible due to fast autoxidation reactions that are missing in the MCM.

The increase in chemical sink strength by going from RO<sub>2</sub> termination to HO<sub>2</sub> termination is the main expected reason for the decrease in C<sub>10</sub>H<sub>17</sub>O<sub>x</sub>. As discussed, the C<sub>10</sub>H<sub>15</sub>O<sub>x</sub> family is subject to an additional decrease in the precursors due to the alkoxy steps necessary in the formation pathway. Since C<sub>10</sub>H<sub>15</sub>O<sub>x</sub> were the main contributors to the C<sub>10</sub>-HOM-RO<sub>2</sub> class their stronger reduction is reflected in the overall reduction of C<sub>10</sub>-HOM-RO<sub>2</sub>.

#### 4.1.3 C<sub>10</sub>-HOM-RO<sub>2</sub> chemistry: Importance of C<sub>10</sub>H<sub>15</sub>O<sub>x</sub> and C<sub>10</sub>H<sub>17</sub>O<sub>x</sub> families

In the unseeded, pure gas phase experiments, the contribution of the C<sub>10</sub>H<sub>17</sub>O<sub>x</sub> family to the C<sub>10</sub>-HOM-RO<sub>2</sub> class was 23±2 % on average in the base case. In the high HO<sub>2</sub> case the contribution increased to 31±4 % on average. As discussed above, the suggested pathways to C<sub>10</sub>H<sub>15</sub>O<sub>x</sub>-HOM-RO<sub>2</sub> may be additionally suppressed due to a decrease of alkoxy steps at high HO<sub>2</sub> reducing the entry channel into C<sub>10</sub>H<sub>15</sub>O<sub>x</sub>-HOM-RO<sub>2</sub>.

Nevertheless, the contribution of C<sub>10</sub>H<sub>15</sub>O<sub>x</sub> was substantial in both experiment stages. Kang (2021) and Shen et al. (2022) reported that, in the photooxidation of  $\alpha$ -pinene, the HOM-RO<sub>2</sub> detected by NO<sub>3</sub>-CIMS are dominated by the C<sub>10</sub>H<sub>15</sub>O<sub>x</sub> family, while C<sub>10</sub>H<sub>17</sub>O<sub>x</sub> formation is the main expected OH reaction pathway in the literature described for HOM formation (Berndt, 2021; Berndt et al., 2016; Xu et al., 2019) and in general (Atkinson and Arey, 2003; Jenkin et al., 1997; Saunders et al., 2003).

This hints towards an effective pathway to HOM via C<sub>10</sub>H<sub>15</sub>O<sub>x</sub>. A reason may be the fast opening of both carbon-rings in the bicyclic  $\alpha$ -pinene (Shen et al., 2022), or a four-ring opening in pinonaldehyde or similar compounds, for easy autoxidation. From our observations increasing the importance of RO<sub>2</sub>+HO<sub>2</sub> did increase the relative importance of the C<sub>10</sub>H<sub>17</sub>O<sub>x</sub> family, but the change was less than 10 % in contribution.

Contribution of the two peroxy radical families to the HOM formation is also reflected in the composition of C<sub>20</sub>-HOM-Acc. **Figure 16** shows the average contributions of the C<sub>20</sub>H<sub>30</sub>O<sub>z</sub>, C<sub>20</sub>H<sub>32</sub>O<sub>z</sub>, and C<sub>20</sub>H<sub>34</sub>O<sub>z</sub> families in the base and high HO<sub>2</sub> case. Although the absolute amount of HOM-Acc was suppressed by 60 % the family distribution was still similar, C<sub>20</sub>H<sub>32</sub>O<sub>z</sub> dominated, while C<sub>20</sub>H<sub>30</sub>O<sub>z</sub> was lowest. C<sub>20</sub>H<sub>30</sub>O<sub>z</sub> is formed from two members of the C<sub>10</sub>H<sub>15</sub>O<sub>x</sub> family, while C<sub>20</sub>H<sub>34</sub>O<sub>z</sub> is formed by two members of the C<sub>10</sub>H<sub>17</sub>O<sub>x</sub> family. C<sub>20</sub>H<sub>32</sub>O<sub>z</sub> is then a combination of a C<sub>10</sub>H<sub>15</sub>O<sub>x</sub>-RO<sub>2</sub> and C<sub>10</sub>H<sub>17</sub>O<sub>x</sub>-RO<sub>2</sub>.

Families that require one or two C<sub>10</sub>H<sub>17</sub>O<sub>x</sub> peroxy radicals for their formation have a higher contribution than the C<sub>10</sub>H<sub>17</sub>O<sub>x</sub> family's contribution to C<sub>10</sub>-HOM-RO<sub>2</sub>. Here, it is important to note that not only HOM-RO<sub>2</sub> can participate in HOM-Acc formation, but also traditional, less oxidized RO<sub>2</sub> radicals (Berndt et al., 2018; Pullinen et al., 2020; McFiggans et al., 2019), which are not detectable by

NO<sub>3</sub>-CIMS. However, higher oxidized peroxy radicals exhibit faster accretion rates (Berndt et al., 2018).

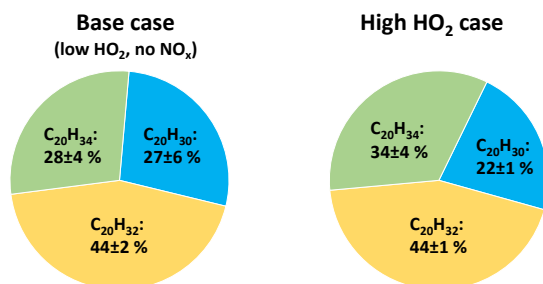


**Figure 16** Average contribution of the C<sub>20</sub>H<sub>30</sub>O<sub>z</sub>, C<sub>20</sub>H<sub>32</sub>O<sub>z</sub>, and C<sub>20</sub>H<sub>34</sub>O<sub>z</sub> family to the C<sub>20</sub> HOM-Acc group signal in the base case and high HO<sub>2</sub> case (unseeded experiments). Not pictured is C<sub>20</sub>H<sub>28</sub>O<sub>z</sub> due to its negligible signal (contribution ~1 %).

The large contributions of C<sub>20</sub>H<sub>32</sub>O<sub>z</sub> and C<sub>20</sub>H<sub>34</sub>O<sub>z</sub> thus clearly show the general importance of the C<sub>10</sub>H<sub>17</sub>O<sub>x</sub> peroxy radicals. The C<sub>20</sub>H<sub>32</sub>O<sub>z</sub> family contributing the largest section indicates the importance of HOM-C<sub>10</sub>H<sub>15</sub>O<sub>x</sub> and a high abundance of lower oxidized C<sub>10</sub>H<sub>17</sub>O<sub>x</sub> peroxy radicals. Lower oxidized C<sub>10</sub>H<sub>17</sub>O<sub>x</sub>-RO<sub>2</sub> were recently measured by Berndt (2021). The fraction of C<sub>20</sub>H<sub>34</sub>O<sub>z</sub> was smaller because their formation requires HOM-C<sub>10</sub>H<sub>17</sub>O<sub>x</sub> radicals which were less abundant compared to HOM-C<sub>10</sub>H<sub>15</sub>O<sub>x</sub>, while the small fraction of C<sub>20</sub>H<sub>30</sub>O<sub>z</sub> indicates that, despite the importance of HOM-C<sub>10</sub>H<sub>15</sub>O<sub>x</sub>, lower oxidized C<sub>10</sub>H<sub>15</sub>O<sub>x</sub> are less important.

These results indicate the importance of mixed HOM-Acc formation by cross reactions of HOM-RO<sub>2</sub> and a lower oxidized RO<sub>2</sub>. The importance of mixed HOM-Acc is supported by the relatively small fractions of HOM-Acc products with very high oxygen numbers, which more likely stem from HOM-RO<sub>2</sub>+HOM-RO<sub>2</sub>. For example, C<sub>20</sub>-HOM-Acc with 12 or more oxygen atoms contributed only around 30 % (base case: 26 ± 4 %, high HO<sub>2</sub> case: 31 ± 2 %) of the signal in the product group.

Although the effect is small, a tendency to higher C<sub>20</sub>H<sub>34</sub>O<sub>z</sub> contribution was observed at high HO<sub>2</sub>. This is consistent with the observation of a slightly higher C<sub>10</sub>H<sub>17</sub>O<sub>x</sub> contribution to the C<sub>10</sub>-HOM-RO<sub>2</sub>. The stronger suppression of the C<sub>10</sub>H<sub>15</sub>O<sub>x</sub> family at high HO<sub>2</sub> is the first indication for, and can be explained by, a reduction in the alkoxy radical formation.

#### 4.1.4 Impact of HO<sub>2</sub> on HOM alkoxy radical formation

Alkoxy radicals (RO) are the second important radical type in the oxidation chain of  $\alpha$ -pinene. RO cannot be detected directly as they are highly unstable and thus have very low concentrations. However, as introduced in Section 2.1.3 the parity change in the HOM-RO<sub>2</sub> families can be used as a diagnostic tool for the abundance of alkoxy steps (Kang, 2021). A second indicator for alkoxy steps is the abundance of HOM products with less than 10 C-atoms.

**Figure 17** shows the average contribution of C<sub>10</sub>H<sub>15</sub>O<sub>x</sub> and C<sub>10</sub>H<sub>17</sub>O<sub>x</sub> with an even and odd number of oxygens in both the base case and the high HO<sub>2</sub> case. C<sub>10</sub>H<sub>15</sub>O<sub>x</sub> radicals with an even number of oxygens contributed on average 32 % in the RO<sub>2</sub> dominated base case. For C<sub>10</sub>H<sub>15</sub>O<sub>x</sub>, the autoxidation chain is expected to start from an even number of oxygen either from C<sub>10</sub>H<sub>15</sub>O<sub>4</sub> (pinonaldehyde-like) (MCM v3.3.1 (Jenkin et al., 1997; Saunders et al., 2003)) or from C<sub>10</sub>H<sub>15</sub>O<sub>2</sub> (C<sub>10</sub>H<sub>16</sub> H-abstraction) (Berndt, 2021; Shen et al., 2022). Therefore, without the involvement of an alkoxy step, the parity of the oxygen number in the observed C<sub>10</sub>H<sub>15</sub>O<sub>x</sub>-HOM-RO<sub>2</sub> is expected to be even. Due to the average contribution of C<sub>10</sub>H<sub>15</sub>O<sub>odd</sub> of 69 % we conclude that in the base case at least one alkoxy step (or any odd number of alkoxy steps) must have taken place in most of the cases.

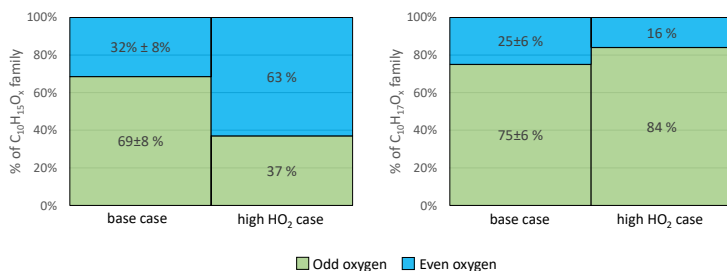


**Figure 17** Average contribution of O<sub>odd</sub> and O<sub>even</sub> to the HOM-RO<sub>2</sub> families C<sub>10</sub>H<sub>15</sub>O<sub>x</sub> (left) and C<sub>10</sub>H<sub>17</sub>O<sub>x</sub> (right) signal in the base case and high HO<sub>2</sub> case (unseeded experiments).

In the high HO<sub>2</sub> case C<sub>10</sub>H<sub>15</sub>O<sub>even</sub> contributed 63 % and the C<sub>10</sub>H<sub>15</sub>O<sub>odd</sub> contribution was reduced to 37 %. This demonstrates a change in the number of alkoxy steps along the formation pathway of the observed HOM-RO<sub>2</sub> radicals. The increased contribution of C<sub>10</sub>H<sub>15</sub>O<sub>even</sub> at high HO<sub>2</sub> lets us infer an even number of alkoxy steps as more common (0,2,4,...). In the simplest case 1 alkoxy step takes place in the base case due to HOM-RO formation from HOM-RO<sub>2</sub>+RO<sub>2</sub> reactions, while no alkoxy step takes place at high HO<sub>2</sub>, because HOM-RO<sub>2</sub>+HO<sub>2</sub> produces none or less HOM-RO than HOM-RO<sub>2</sub>+RO<sub>2</sub>.

For C<sub>10</sub>H<sub>17</sub>O<sub>x</sub> the entry channel into autoxidation is C<sub>10</sub>H<sub>17</sub>O<sub>3</sub> with an odd number of oxygen atoms. Therefore, in autoxidation without alkoxy steps, the oxygen parity is expected to be odd. In the base case, C<sub>10</sub>H<sub>17</sub>O<sub>odd</sub> species contributed 75 % to the total C<sub>10</sub>H<sub>17</sub>O<sub>x</sub> signal, indicating that either none or an even number (2,4,...) of alkoxy steps occurred. At high HO<sub>2</sub> the odd contribution increased to 84 % (see **Figure 17**). This result could indicate a low occurrence of alkoxy steps even in the base case, with a further decrease of alkoxy formation at high HO<sub>2</sub>. However, the observed shift was minor.

The different responses of the C<sub>10</sub>H<sub>15</sub>O<sub>x</sub> and C<sub>10</sub>H<sub>17</sub>O<sub>x</sub> families to the reduction of HOM-RO formation from HOM-RO<sub>2</sub>+RO<sub>2</sub> in the system dominated by HO<sub>2</sub> indicate that there could be fundamental differences in the autoxidation chains of C<sub>10</sub>H<sub>15</sub>O<sub>x</sub> and C<sub>10</sub>H<sub>17</sub>O<sub>x</sub> (or the limit of the parity analysis). The parity analysis indicates a decrease in alkoxy steps at high HO<sub>2</sub>, but it cannot be inferred with

certainty. However, decrease in alkoxy steps at high HO<sub>2</sub> is supported by the observation of changes in HOM-Frag products.

On average, the sum of all HOM-Frag products (detected compounds with  $5 \leq C < 10$  by NO<sub>3</sub>-CIMS) showed a reduction of around 20 % (unseeded experiments, see **Figure 13**). Further trends become recognizable when separating the species according to their carbon number. **Figure 18** shows the C<sub>5</sub>, C<sub>7</sub>, C<sub>8</sub>, and C<sub>9</sub> HOM-Frag groups at high HO<sub>2</sub> compared to the base case, normalized to the  $\alpha$ -pinene OH turnover. The C<sub>6</sub>-HOM-Frag group was not included, as it contributed less than 5 % of the fragment signal and contained few detected compounds.

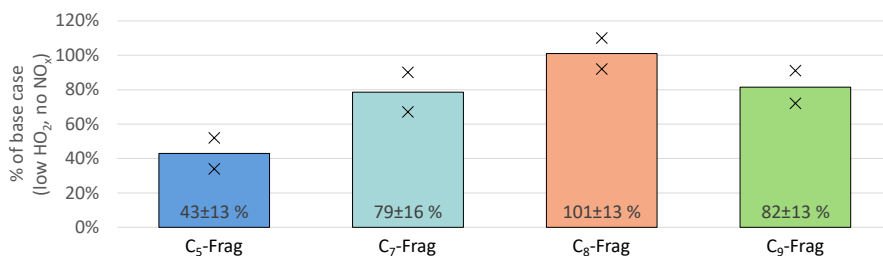


**Figure 18** Overview of average, relative change in C<sub>5</sub>, C<sub>7</sub>, C<sub>8</sub>, C<sub>9</sub> fragment groups detected in NO<sub>3</sub>-CIMS between high HO<sub>2</sub> case and base case (both normalized to  $\alpha$ -pinene OH turnover) for unseeded experiments. Bars represent average of the two experiments, markers represent individual experiments.

**Figure 18** shows the different behavior of the HOM-Frag groups: C<sub>8</sub>-HOM-Frag were the least affected, showing no reduction. This could indicate that an important formation pathway for C<sub>8</sub>-HOM-Frag is not dependent on alkoxy radical formation. However, HOM-Frag with shorter carbon chain length were significantly reduced at high HO<sub>2</sub>: C<sub>5</sub>-HOM-Frag were reduced by around 60 % compared to the base case. If we assume that the fragmentation of C<sub>10</sub> compounds happens in consecutive steps via scission of HOM-RO radicals (analogously to the MCM), this observation is in accordance with decreasing importance of alkoxy radical formation at high HO<sub>2</sub>.

Overall, all observations indicate strong involvement of RO in HOM formation as well as a reduced, but still significant, involvement of RO in the system with high HO<sub>2</sub>, when HO<sub>2</sub> chemistry dominates. This is supported by the change of the oxygen parity in C<sub>10</sub>-HOM-RO<sub>2</sub>, and the decrease of fragmentation products with lower carbon number, as well as the only moderate reduction in the observed C<sub>10</sub>H<sub>16</sub>O<sub>2</sub> product (pinonaldehyde) and the still substantial importance of the C<sub>10</sub>H<sub>15</sub>O<sub>x</sub>-HOM-RO<sub>2</sub> family in the high HO<sub>2</sub> case.

#### 4.1.5 Impact on carbonyl and hydroperoxide formation

Increased importance of RO<sub>2</sub>+HO<sub>2</sub> should shift the product distribution by reduction of alcohol and carbonyl compounds from the so-called molecular channel in the RO<sub>2</sub>+RO<sub>2</sub> reaction (see reaction (R2-3)), in favor of hydroperoxide formation from RO<sub>2</sub>+HO<sub>2</sub> termination (reaction (R2-1)). This effect can be best observed in the C<sub>10</sub>H<sub>18</sub>O<sub>z</sub> family, which contains the hydroperoxide and alcohol termination products arising from C<sub>10</sub>H<sub>17</sub>O<sub>x</sub>. C<sub>10</sub>H<sub>18</sub>O<sub>z</sub> significantly increased to on average 159 % (see Figure 15). This supports an increased hydroperoxide formation, however, with some uncertainty due to the alcohol termination products from C<sub>10</sub>H<sub>17</sub>O<sub>x</sub> (by reaction with RO<sub>2</sub>). To elucidate this further the contribution of individual species to the C<sub>10</sub>H<sub>18</sub>O<sub>z</sub> family was examined.

Formation of an alcohol from RO<sub>2</sub>+RO<sub>2</sub> (reaction (R2-3)) leads to the loss of one oxygen atom compared to the precursor C<sub>10</sub>H<sub>17</sub>O<sub>x</sub> radical, while in the hydroperoxide formation (reaction (R2-1)) the oxygen number remains the same. The most abundant member of the C<sub>10</sub>H<sub>17</sub>O<sub>x</sub> family was C<sub>10</sub>H<sub>17</sub>O<sub>7</sub> with a contribution of 72±6 % in the base case, and a contribution of 82±1 % in the high HO<sub>2</sub> case. C<sub>10</sub>H<sub>17</sub>O<sub>7</sub> terminates to C<sub>10</sub>H<sub>18</sub>O<sub>z</sub> products either as an alcohol with sum formula C<sub>10</sub>H<sub>18</sub>O<sub>6</sub>, or as a hydroperoxide with sum formula C<sub>10</sub>H<sub>18</sub>O<sub>7</sub>. These products have additional sources from C<sub>10</sub>H<sub>17</sub>O<sub>6</sub> and C<sub>10</sub>H<sub>17</sub>O<sub>8</sub> but due to the dominant contribution of C<sub>10</sub>H<sub>17</sub>O<sub>7</sub> to the C<sub>10</sub>H<sub>17</sub>O<sub>x</sub> family we expect any other production channels to be of minor importance.

Figure 19 shows the HOM product distribution within the C<sub>10</sub>H<sub>18</sub>O<sub>z</sub> family in the base and high HO<sub>2</sub> case. The sum of the O<sub>6</sub> and O<sub>7</sub> product did not change significantly in the two regimes (about 88 %), showing that these were the major products. This agrees well with the observation of C<sub>10</sub>H<sub>17</sub>O<sub>7</sub> as the major C<sub>10</sub>H<sub>17</sub>O<sub>x</sub>-HOM-RO<sub>2</sub>. In the RO<sub>2</sub>+RO<sub>2</sub> dominated base case the O<sub>6</sub> product has a larger contribution of 64±8 %, while at high HO<sub>2</sub> ~30 % of signal was shifted to the O<sub>7</sub> product. This shows that the increase in the C<sub>10</sub>H<sub>18</sub>O<sub>z</sub> was matched with an increase in hydroperoxide formation.

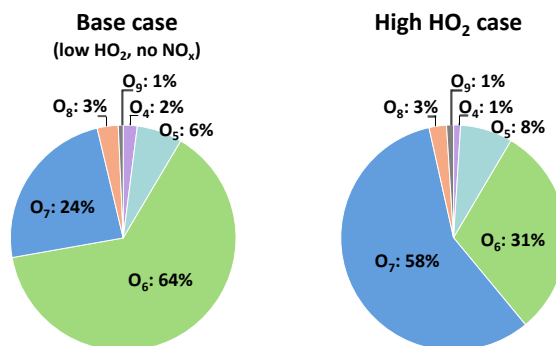
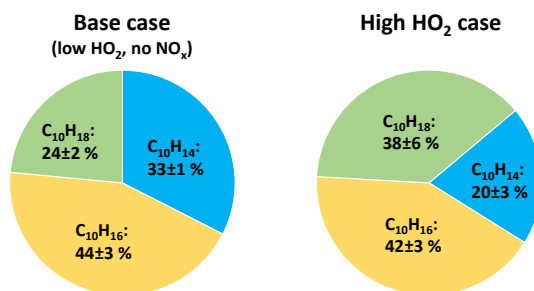


Figure 19 Average contribution of the individual compounds to the C<sub>10</sub>H<sub>18</sub>O<sub>z</sub> family signal in the base case and high HO<sub>2</sub> case (unseeded experiments).

An indicator for carbonyl formation is the C<sub>10</sub>H<sub>14</sub>O<sub>z</sub> family as it only contains the carbonyl products arising from C<sub>10</sub>H<sub>15</sub>O<sub>x</sub>-RO<sub>2</sub>. The C<sub>10</sub>H<sub>14</sub>O<sub>z</sub> family was reduced on average to 61 % at high HO<sub>2</sub>, however this decrease matched the decrease in the C<sub>10</sub>H<sub>15</sub>O<sub>x</sub> precursor family. If the reaction of a C<sub>10</sub>H<sub>15</sub>O<sub>x</sub>-HOM-RO<sub>2</sub> with a second RO<sub>2</sub> were the main formation pathway of C<sub>10</sub>H<sub>14</sub>O<sub>z</sub>, a stronger reduction should be expected as both precursor species were decreased significantly. Instead, it appears that C<sub>10</sub>H<sub>14</sub>O<sub>z</sub> was mainly impacted by the decrease in C<sub>10</sub>H<sub>15</sub>O<sub>x</sub> as their reductions are similar. This points to internal termination as a major reaction pathway for C<sub>10</sub>H<sub>15</sub>O<sub>x</sub>-HOM-RO<sub>2</sub> resulting in C<sub>10</sub>H<sub>14</sub>O<sub>z</sub>-carbonyls. Internal termination of the autoxidation chain has been discussed in the literature for different VOCs (Shen et al., 2021; Guo et al., 2022), Rissanen et al. (2014) discussed the possible importance of the internal termination via an H-shift, followed by formation of a carbonyl functional group and OH loss in the autoxidation chain of cyclohexene (see **Figure 3** in **Section 2.1**). Piletic and Kleindienst (2022) calculated fast reaction rate coefficients in the range of 1-30 s<sup>-1</sup> for such internal termination reactions to carbonyls for some C<sub>10</sub>H<sub>17</sub>O<sub>5</sub> in the α-pinene photooxidation, indicating that this pathway could also be significant for C<sub>10</sub>H<sub>15</sub>O<sub>x</sub>.

The contributions of the C<sub>10</sub>H<sub>14</sub>O<sub>z</sub>, C<sub>10</sub>H<sub>16</sub>O<sub>z</sub>, and C<sub>10</sub>H<sub>18</sub>O<sub>z</sub> families to the HOM-Mon class shifted in the high HO<sub>2</sub> case as shown in **Figure 20**.



**Figure 20** Average contribution of the C<sub>10</sub>H<sub>14</sub>O<sub>z</sub>, C<sub>10</sub>H<sub>16</sub>O<sub>z</sub>, and C<sub>10</sub>H<sub>18</sub>O<sub>z</sub> family to the HOM-Mon class in the base case and high HO<sub>2</sub> case (unseeded experiments).

The contribution of C<sub>10</sub>H<sub>16</sub>O<sub>z</sub> was the largest and remained similar in both cases, matching the already shown unchanged signal level in **Figure 15**. This is the case because the C<sub>10</sub>H<sub>16</sub>O<sub>z</sub> family contains the alcohols from C<sub>10</sub>H<sub>15</sub>O<sub>x</sub>+RO<sub>2</sub>, carbonyls from C<sub>10</sub>H<sub>17</sub>O<sub>x</sub>+RO<sub>2</sub> and hydroperoxides from C<sub>10</sub>H<sub>15</sub>O<sub>x</sub>+HO<sub>2</sub> (see **Figure 4**). A separation of the effects of enhanced HO<sub>2</sub> on this monomer family is difficult, as the loss of carbonyls and alcohols is partially compensated by the gain of hydroperoxides. A strong gain in hydroperoxides is clearly reflected in the strong increase of C<sub>10</sub>H<sub>18</sub>O<sub>z</sub> at high HO<sub>2</sub>.

Inspection of the C<sub>10</sub>H<sub>14</sub>O<sub>z</sub> and C<sub>10</sub>H<sub>18</sub>O<sub>z</sub> families shows that ~13 % of the contribution by C<sub>10</sub>H<sub>14</sub>O<sub>z</sub> were lost (carbonyls, 33 % in the base case) and were present instead as C<sub>10</sub>H<sub>18</sub>O<sub>z</sub> (hydroperoxides), giving C<sub>10</sub>H<sub>18</sub>O<sub>z</sub> a contribution of 38 % in the high HO<sub>2</sub> case.

#### 4.1.6 Impact of HO<sub>2</sub> on condensable organic mass

In the previous sections, we demonstrated a shift of the product distribution by the shift from the RO<sub>2</sub>+RO<sub>2</sub> dominated “laboratory” base case to the RO<sub>2</sub>+HO<sub>2</sub> dominated high HO<sub>2</sub> case. We also showed that the changes could be rationalized by generic mechanistic considerations. We added (NH<sub>4</sub>)<sub>2</sub>SO<sub>4</sub> seed aerosol in two experiments to determine how the shift in the product distribution affects the condensable organic mass by determining the fraction which remained in the gas-phase after seeding.

**Figure 21** shows the fraction remaining in the gas phase after seed addition for the sum of all products, as well as for the individual product classes for the base and the high HO<sub>2</sub> case. In both cases a significant reduction of products in the gas phase was observed with seed present. Overall, the sum of all products was reduced by about 60 %, with a somewhat higher reduction in the base case. This can be attributed to the larger importance of HOM-Acc in the base case, as well as to a 10 % lower reduction of the HOM-Frag in the high HO<sub>2</sub> case. In both cases a reduction of the HOM-RO<sub>2</sub> was observed, which indicates that the presence of seed particles could have affected HOM formation chemistry, e.g. by loss of HOM-RO<sub>2</sub> onto particles, however only moderately.

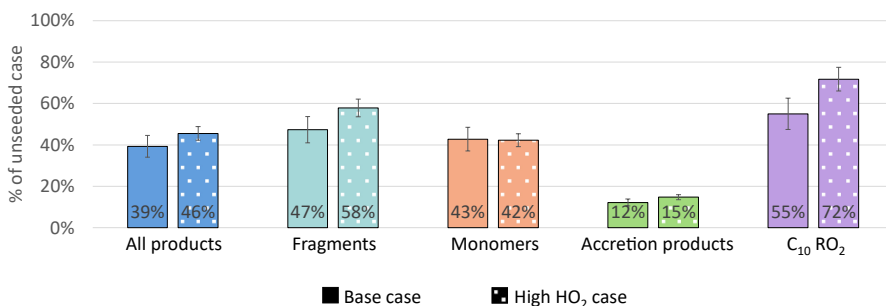


**Figure 21** Overview of average, relative change in product class signals between unseeded and seeded system.

Solid colored bars show the base case, dotted colored bars the high HO<sub>2</sub> case. (All data from apinCO<sub>2</sub> experiment, normalized to  $\alpha$ -pinene OH turnover. Error bars via error propagation, for more information see Appendix Section A.5)

The total organic particulate mass, determined by AMS measurements, was 3.4  $\mu\text{g m}^{-3}$  and 2.0  $\mu\text{g m}^{-3}$  in the base case and high HO<sub>2</sub> case in the experiment (apinCO<sub>2</sub>) displayed in **Figure 21**. A reduction of condensed organic mass to 73 $\pm$ 2 % in the system with high HO<sub>2</sub> (orange bar in **Figure 23**) was observed on average. Since unseeded and seeded experiments were conducted at otherwise the same conditions and we did not observe significant new particle formation, the gas-phase compositions can be directly compared. Therefore, we conclude that the shift in the product distribution led to a reduction of condensable material at the same  $\alpha$ -pinene turnover with OH (and O<sub>3</sub>).

We calculated the SOA yields with the wall-loss corrected SOA mass. The detailed results and calculation method can be found in Appendix **Section A.9**. The resulting SOA yields were between

9.0 % and 5.3 %. When comparing high HO<sub>2</sub> conditions to the base case, the SOA yields show an absolute reduction of ~3 % (relative a reduction of about 30 %). A reduction of the SOA yield of  $\alpha$ -pinene by addition of CO was described before by McFiggans et al. (2019), however, there the  $\alpha$ -pinene OH turnover was not held constant.

The change from the RO<sub>2</sub>+RO<sub>2</sub> to the RO<sub>2</sub>+HO<sub>2</sub> dominated regime favored termination reactions to protic termination groups, as we observed less carbonyl compounds and more hydroperoxides. This could shift the product distribution to products with lower vapor pressures and favor SOA formation, since protic groups can act as hydrogen bond donors as well as hydrogen bond acceptors. (As exemplified by the comparison of ethanol (boiling point (b.p) 78 °C) and ethane hydroperoxide (b.p. 93-97 °C) with acetaldehyde (b.p. 20 °C) (Richter et al., 1955)). However, the effect of the termination group should be small for HOM as they likely contain multiple hydroperoxide groups (compare Pullinen et al. (2020)). The reduction in HOM-Acc is expected to decrease the condensable mass, since the HOM-Acc scavenge non-HOM-RO<sub>2</sub>, that would otherwise not partition into the particle phase.

Which of the measured compounds contribute significantly to the organic particle mass can be inferred by comparing their signal from the pure gas phase, unseeded cases to their signal with seed in the system. Under the assumptions that, for most HOM compounds re-evaporation to the gas phase is negligible and that the precursor chemistry is not substantially disturbed by seed addition, the fraction of signal remaining with seed in the system reflects to which degree the compound is condensing. **Figure 22** shows the fraction remaining with seed in the system plotted against the molar mass of each individual compound. The plot includes all closed-shell products that were measured with a relative standard deviation of less than 30 % for all measurement phases and depicts the results for both the base and the high HO<sub>2</sub> case.

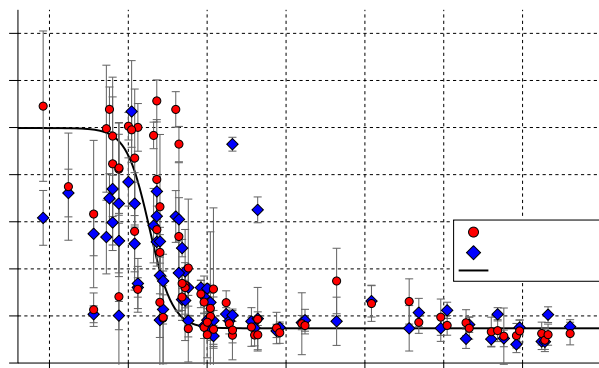


**Figure 22** Gas-phase fraction remaining in presence of seed for the base case (blue) and high HO<sub>2</sub> case (red) (normalization of all data with  $\alpha$ -pinene OH turnover). Displayed points represent all closed-shell compounds that were detected with relative standard deviation <30 % in all four experiment phases. Error bars represent result of error propagation (see Appendix Section A.5)

Overall, in both cases we observed the same trend. Lighter compounds were not affected by the presence of seed particles, but with increasing molar mass the fraction remaining in the gas phase was reduced. A difference between the base case and the high HO<sub>2</sub> case can be observed in the low molar mass range: In the high HO<sub>2</sub> case many fragmentation products show a higher gas-phase fraction remaining up to 1. In some cases, values larger than 1 were observed, however within the error limits. For the error estimation see Appendix **Section A.5**. Fractions remaining larger than 1 beyond error could be an indication that such products have a particle-phase production source.

**Figure 22** also shows a critical SVOC/LVOC region for molar masses between 175 g mol<sup>-1</sup> and 250 g mol<sup>-1</sup> where neither a fraction remaining of 1 nor complete condensation was observed. The position of this region on the molar mass scale depends on the available particulate organic mass concentration (see **Section 2.2**). The large variation of the fraction remaining in this small range of molar masses shows that the partitioning coefficients are dependent on the detailed structure of the compounds and not simply on their molar mass. The semi-volatile and low volatility products represent mainly higher oxidized fragments and HOM-Mon with less than 8 oxygen.

For compounds with a molar mass larger than 250 g mol<sup>-1</sup> a constant fraction remaining was reached in steady state, which is due to the ongoing production of the compounds. From the condensation behavior shown in **Figure 22**, we conclude that the compounds with molar masses larger than 230 g mol<sup>-1</sup> are expected to be of sufficiently low volatility to be mainly found in the particle phase for the organic mass present in the system and therefore contribute significantly to the SOA mass formation. Our finding agrees with the threshold used for low volatility HOM products in Pullinen et al. (2020).

Therefore, the signal of all compounds with a molar mass heavier than 230 g mol<sup>-1</sup> was weighted with their molar mass and summed (see *Eq. 3-2*). The ratio of this weighted signal sum in the high HO<sub>2</sub> case compared to the base case is then a measure of expected SOA mass loss at high HO<sub>2</sub>. The calculation resulted in an expected reduction to 72 % (blue bar, **Figure 23**). This simple approach shows good agreement with the AMS measurements and can thus explain the reduced particulate organic mass by changes in the HOM product distribution within the errors.

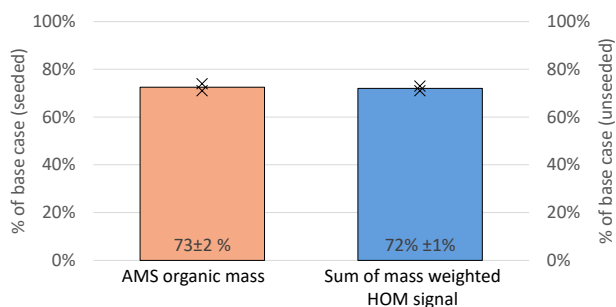


**Figure 23** Overview of the average, relative change in organic mass observed in the AMS (left y-axis, seeded experiments) and the mass weighted HOM signal that is supposed to condense as observed by NO<sub>3</sub>-CIMS (right y-axis, unseeded experiments) between the high HO<sub>2</sub> and base case (both normalized to  $\alpha$ -pinene OH turnover).

#### 4.1.7 Summary: Impact of HO<sub>2</sub>

The shift from a RO<sub>2</sub>+RO<sub>2</sub> dominated reaction system (our base case with strong laboratory bias) to a RO<sub>2</sub>+HO<sub>2</sub> dominated system led to significant changes in the HOM gas-phase product distribution. The HOM-Acc formation from RO<sub>2</sub>+RO<sub>2</sub> was significantly suppressed as HO<sub>2</sub> shifted the system to HOM-Mon production. Furthermore, within the HOM-Mon class a shift from the formation of carbonyl to hydroperoxide termination groups was observed as expected from RO<sub>2</sub>+HO<sub>2</sub> termination. A reduction of alkoxy radical formation in the system with high HO<sub>2</sub> could be seen in the oxygen parity of C<sub>10</sub>-HOM-RO<sub>2</sub> and the reduction of HOM-Frag with small carbon numbers compared to the base case.

We propose that the suppression of alkoxy radical formation also led to a reduction in the formation of C<sub>10</sub>H<sub>15</sub>O<sub>x</sub>-HOM-RO<sub>2</sub> as its suggested formation pathways are dependent on the involvement of alkoxy steps. Even though the overall pseudo-first order rate coefficient of the chemical sink was still significantly lower than the assumed average autoxidation rate (0.1 s<sup>-1</sup>), we observed a decrease in both C<sub>10</sub>-HOM-RO<sub>2</sub> and overall HOM products at high HO<sub>2</sub>. This observation is consistent with HO<sub>2</sub> being able to interfere in a crucial HOM formation step: the alkoxy radical formation which is needed for C<sub>10</sub>H<sub>15</sub>O<sub>x</sub> formation. Thus, enhanced HO<sub>2</sub> leads to the observed reduction in HOM, rather by reducing the precursor RO<sub>2</sub> levels than by impeding the autoxidation itself.

We investigated the effect of the changes in the HOM product distribution on the SOA formation potential of the  $\alpha$ -pinene OH oxidation system and could show that moving towards atmospheric HO<sub>2</sub>/RO<sub>2</sub> ratios affected the SOA formation potential. The observed organic mass was reduced at high HO<sub>2</sub>. This is in support of the potential bias towards high SOA yields in chamber studies at low HO<sub>2</sub>/RO<sub>2</sub> (i.e. our base case) as discussed by Schervish and Donahue (2021). Besides the overall decrease in HOM products, one major factor for the reduced SOA formation was the suppression of HOM-Acc formation due to the reduction in RO<sub>2</sub>+RO<sub>2</sub> cross reactions. This prevented contribution to

SOA by less oxidized RO<sub>2</sub> which were scavenged in the HOM-Acc in the RO<sub>2</sub>+RO<sub>2</sub> dominated base case.

By the comparison of the seeded to the unseeded system, we determined which products were contributing to the SOA formation and showed that their volatility is a function of molar mass and detailed molecular structure. This revealed a critical mass region in which compounds have significant fractions in gas and particulate phase. Based on absorptive partitioning theory the volatilities at which this critical region is found should depend on the organic mass present in the system.

We successfully determined a molar mass threshold from the fraction remaining with seed to classify a product's condensation behavior. The good agreement between particle phase measurement and HOM mass proxy calculated from the gas-phase observations shows that we understand the processes governing the SOA formation in our experiments.

## 4.2 Impact of NO

As for the high HO<sub>2</sub> case the impact of NO on the HOM product distribution was investigated via the comparison of the system with NO to the “classical laboratory” base case with  $\alpha$ -pinene and OH as the only major reactants.

The box model results and the generic bulk rate coefficients (see **Section 3.2.5**) were used to determine which percentage of the chemical sink was expected to be from RO<sub>2</sub>+NO, as well as to determine the change in the overall size of the chemical reaction pool. The results can be seen in **Figure 24**. Two levels of NO were investigated. At the lower NO level, 70 % of RO<sub>2</sub> were expected to be terminated with NO. The remaining 30 % were equally divided between RO<sub>2</sub>+HO<sub>2</sub> and RO<sub>2</sub>+RO<sub>2</sub>. At the higher NO level, the reaction of RO<sub>2</sub>+NO was expected to dominate 95 % of the termination reactions. Since reaction with NO dominates the chemical sink at the higher NO level, this case is dubbed the “high NO case”. A steady-state concentration of 0.5 ppbv NO was measured in this case. Even at the lower NO concentration, NO was still the major expected reaction partner for RO<sub>2</sub> and thus the case is dubbed the “middle NO case”. At middle NO a steady-state NO concentration of 0.2 ppbv was measured.

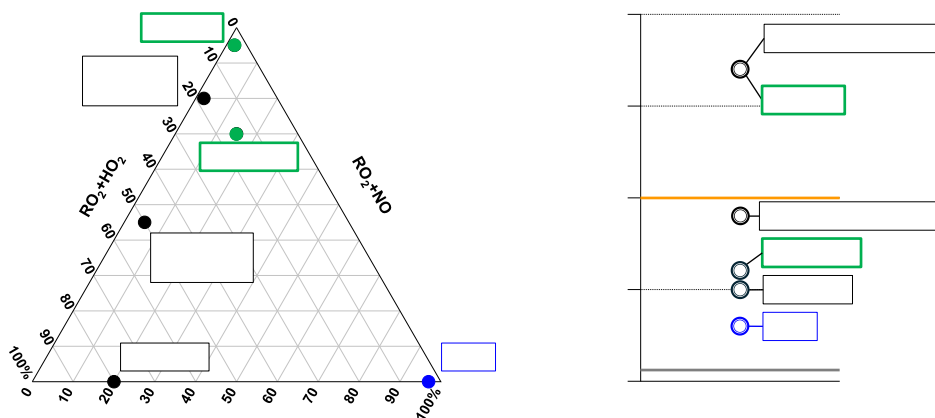


**Figure 24** Classification of the chemical regimes for the system with NO addition (highlighted in green):

- Triangle plot showing the distribution of the chemical reaction pool for RO<sub>2</sub> with NO, HO<sub>2</sub> and RO<sub>2</sub>.
- (Pseudo) first order chemical sink relative to average autoxidation rate and wall loss rate.

**Figure 24 b)** shows the pseudo-first order reaction rate of the chemical reaction pool compared to the other investigated systems, as well as the average assumed autoxidation rate and wall loss rate (for more information on the assumptions see **Section 4.1**). The total chemical sink was calculated as 0.06 s<sup>-1</sup> for the middle NO case and as 0.17 s<sup>-1</sup> for the high NO case. The chemical RO<sub>2</sub> sink is in competition to autoxidation and wall loss of the RO<sub>2</sub>. In the NO<sub>x</sub>-free base case the chemical sink was calculated as 0.03 s<sup>-1</sup>, so the larger chemical sink will lead to more product formation compared to wall loss and potentially to an interference in the autoxidation chain. With the assumption of an average

autoxidation rate of  $0.1 \text{ s}^{-1}$  at middle NO the bimolecular reaction rate was still expected to be slower than many autoxidation rates, while at high NO the pseudo-first order reaction rate of  $k_{\text{RO}_2+\text{NO}}[\text{NO}]$  was faster than the average expected autoxidation rate. However, it has to be kept in mind, that the model results and assumed reaction rate coefficients cannot describe the system fully and have high uncertainties. Thus, these calculations and comparisons of bulk average reaction rate coefficients can always only serve as trend indicators.

#### 4.2.1 Impact on overall HOM formation

An overview of the changes in the different product classes at the two NO levels compared to the  $\text{NO}_x$ -free,  $\text{RO}_2+\text{RO}_2$  dominated base case can be found in **Figure 25**. All compared conditions were normalized with the  $\alpha$ -pinene OH turnover to ensure direct comparability. At the lower NO level there was no change in the overall HOM product sum, while at high NO a reduction in products of about 20 % was observed.

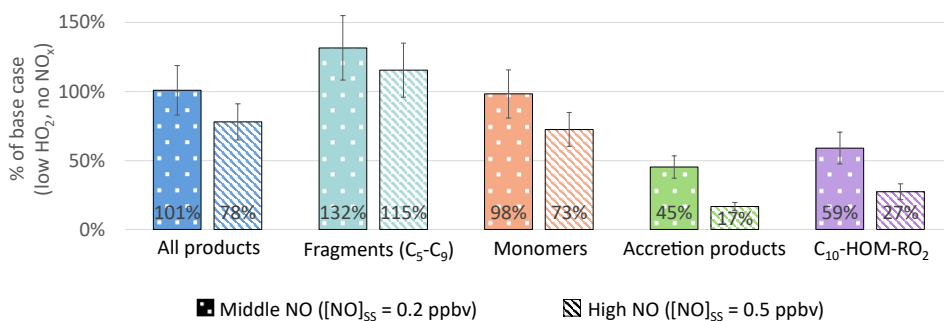


**Figure 25** Overview of relative change in product classes detected in  $\text{NO}_3$ -CIMS at the two NO levels compared to base case in unseeded system (All normalized to  $\alpha$ -pinene OH turnover, base case from experiment *apinCO\_2*. Error bars via error propagation, for more information see Appendix Section A.5)

In the high NO case, the comparison of the assumed average autoxidation rate to the pseudo-first order reaction rate of the chemical sink indicates that the termination can potentially interfere with the autoxidation chain. Such interference will lead to a decrease in all observed HOM product classes, making a comparison to the base case more complicated as two different factors will contribute to the changes in the product distribution. The reduction of the entry channel due to scavenging of  $\text{RO}_2$  by NO and the shift of the product distribution due to reaction with NO overlap, making an interpretation of the observed mixed effect difficult. Moreover, a part of the reaction of  $\text{RO}_2$  with NO leads to alkoxy radicals, which may either continue the radical chain, keeping the carbon backbone intact, or undergo fragmentation.

Most significantly, in both cases the HOM-Acc products were significantly reduced. The high NO case had only around 20 % of the HOM-Acc signal of the base case showing that as expected termination by  $\text{RO}_2+\text{RO}_2$  was strongly suppressed.

HOM-Mon, as well as HOM-Frag, contained a new product class compared to the high HO<sub>2</sub> and base case, as the termination with NO forms ON species (see **Section 2.1.2**). At middle NO, no significant change in the overall HOM-Mon signal was observed, indicating that the change was only a shift between the different HOM-Mon termination groups (ON, hydroperoxides, carbonyls and alcohols). At high NO a reduction of HOM-Mon by around 30 % was observed.

The HOM-Frag class showed a significant increase of around 30 % in the middle NO case and even in the high NO case still an increase in HOM-Frag was visible. This increase clearly highlights the increased importance of alkoxy radical formation in the reaction of RO<sub>2</sub> and NO, as fragmentation is one of the main reaction pathways for alkoxy radicals.

The importance of the HOM-Frag formation with NO in the system is also visible in **Figure 26**, where the distribution between the HOM-product classes is shown for the base case and the two NO levels. While the contribution of HOM-Mon stayed approximately constant in all cases, a shift from HOM-Acc to HOM-Frag contribution was observed with increasing NO.

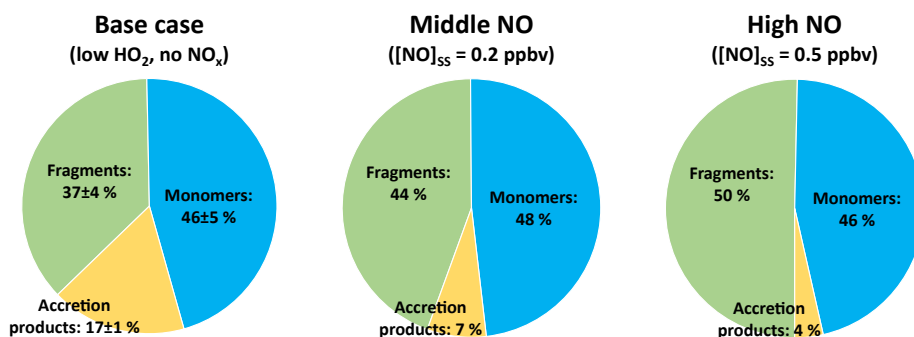


**Figure 26** Contribution of the closed shell product classes to overall HOM-product signal in the base case and at the two NO levels (unseeded experiments).

If we compare the NO<sub>x</sub>-free base case to the high NO case, the contribution of HOM-Frag increased by 13 %, while the contribution of HOM-Acc decreased by the same amount. This shift in contribution clearly shows the shift from RO<sub>2</sub>+RO<sub>2</sub> to RO<sub>2</sub>+NO. RO<sub>2</sub>+NO can form ON-HOM-Mon and from our findings in the high HO<sub>2</sub> case (**Section 4.1.1**) we know that suppression of HOM-Acc can act as a source of HOM-Mon. However, in the NO case we instead observed a shift in contribution to HOM-Frag, highlighting the importance of the alkoxy pathway in the reaction with NO.

#### 4.2.2 Impact of NO on the HOM-RO<sub>2</sub> concentration

HOM-RO<sub>2</sub> were reduced by 40% at middle NO while at high NO the reduction was about 70 % (see **Figure 25**). As discussed for the HO<sub>2</sub> case (see **Section 4.1.2**) it is unfortunately not possible to attribute directly if and to which parts the reduction is due to a decrease in the HOM-RO<sub>2</sub> source compared to an increase in the chemical sink. In **Section 4.1.2** we introduced a calculation for the expected

HOM-RO<sub>2</sub> ratio for RO<sub>2</sub> directly connected to the primary production ( $k_{OH}[OH][\alpha\text{-pinene}]$ ) and without significant further autoxidation, between the high HO<sub>2</sub> and the base case. The same approach was applied to the middle NO case (equation can be found in **Appendix Section A.8.2**), since for the middle NO case the assumption of unchanged HOM-RO<sub>2</sub> primary production is still reasonable for many RO<sub>2</sub>. This assumption is likely not valid for the high NO case as shown by the large pseudo-first order rate coefficient of the chemical sink provided by NO compared to the average autoxidation rate (see **Figure 24 b**). In the middle NO case, the calculation yielded a reduction to 66 % with our standard assumed bulk reaction rate coefficients  $k_{RO_2+HO_2}=2.46\cdot 10^{-11}$  cm<sup>3</sup> s<sup>-1</sup>,  $k_{RO_2+NO}=9.2\cdot 10^{-12}$  cm<sup>3</sup> s<sup>-1</sup> at 20 °C (Jenkin et al., 1997; Saunders et al., 2003) and  $k_{RO_2+RO_2}=5.0\cdot 10^{-12}$  cm<sup>3</sup> s<sup>-1</sup>. The calculated reduction is close to the observed reduction, showing that the reduction is explainable by just an increase in the chemical sink. However, the limitation of applying bulk reaction rate coefficients has to be kept in mind.

In the high HO<sub>2</sub> case, the discussion detailed changes observed within the HOM-RO<sub>2</sub> class as RO<sub>2</sub> are the central species to understand the changes observed in the product distribution. Unfortunately, in the system with NO the HOM-RO<sub>2</sub> observation was more uncertain. Two factors were responsible for the increase in uncertainty. Firstly, in the mass spectrum the peaks of the HOM-RO<sub>2</sub> compounds can be found at the same nominal m/Q ratios as the peaks of different ON products. Both are found at odd m/Q ratios, which in the base and high HO<sub>2</sub> case had little contribution besides HOM-RO<sub>2</sub> (only <sup>13</sup>C-isotope peaks of closed-shell products). The resolution of the mass spectrum was not sufficient to fully separate the ON species and the HOM-RO<sub>2</sub> as shown on the example in **Figure 27**.

Secondly, the strong reduction in the HOM-RO<sub>2</sub> signal led to low signal levels, in some cases even close or below the detection level. The low signals were an issue especially in the C<sub>10</sub>H<sub>17</sub>O<sub>x</sub> family, which already had low signals in the base case. The combination of small signals with assignment on the shoulder of an often much larger product peak led to high uncertainties in the determined HOM-RO<sub>2</sub> levels. Owing to this large uncertainty we will focus on the changes observed in the closed-shell families to draw conclusions for the changes of HOM-RO<sub>2</sub> with NO.

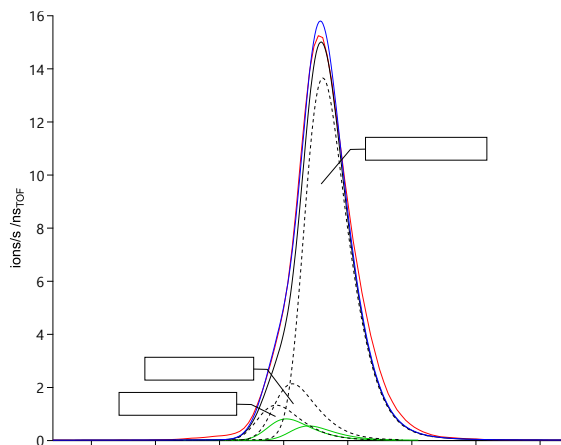


**Figure 27** Peak assignment of  $C_{10}H_{15}O_9$  between organic nitrate compounds at middle NO level. Red line shows peak shape. Dashed lines show calculated individual compound peaks, black line is fit of assigned compounds. Green lines are  $^{13}C$  isotope peaks, blue line is fit of assigned compounds including  $^{13}C$  isotopes.

#### 4.2.3 $C_{10}$ -HOM-RO<sub>2</sub> chemistry: Importance of $C_{10}H_{15}O_x$ and $C_{10}H_{17}O_x$ families

**Figure 28** shows the contribution of the different HOM-Mon families to the non-ON HOM-Mon product sum. As  $C_{10}H_{18}O_z$  can only be formed from  $C_{10}H_{17}O_x$ -HOM-RO<sub>2</sub> and  $C_{10}H_{14}O_z$  can only be formed from  $C_{10}H_{15}O_x$ -HOM-RO<sub>2</sub> the contributions of these families give us an indication of the importance of their radical precursor families. It should be kept in mind however, that both  $C_{10}$ -HOM-RO<sub>2</sub> precursor families will also form  $C_{10}H_{16}O_z$  products, and that the HOM-Mon family contributions are not a good indicator, if a precursor family has a specific fast pathway into  $C_{10}H_{16}O_z$  in the case with NO, that was not important in the base case.

The contribution of  $C_{10}H_{16}O_z$  did not significantly change, while a clear decrease in contribution by  $C_{10}H_{18}O_z$  and increase in contribution by  $C_{10}H_{14}O_z$  was observed with increasing NO. At high NO, the contribution of  $C_{10}H_{18}O_z$  decreased to under 10 %, while  $C_{10}H_{14}O_z$  contributed around 50 %. In comparison, in the NO<sub>x</sub>-free base case  $C_{10}H_{14}O_z$  contributed about 30 %.

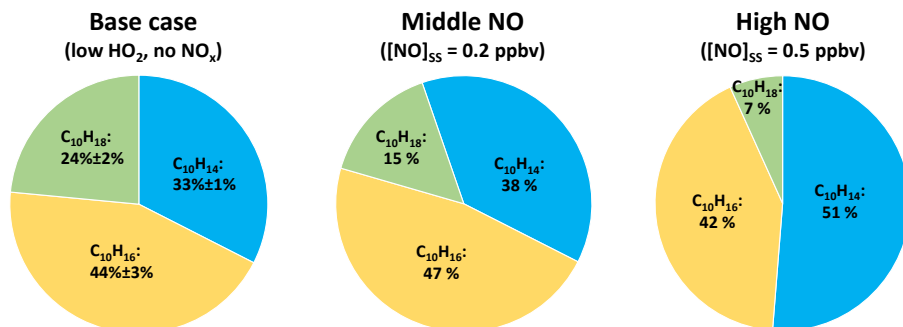


**Figure 28** Contribution of the  $C_{10}H_{14}O_z$ ,  $C_{10}H_{16}O_z$  and  $C_{10}H_{18}O_z$  families to the non-ON HOM-Mon in the base case and at the two NO levels (unseeded experiments).

This clear shift towards  $C_{10}H_{14}O_z$  indicates a growing importance of the  $C_{10}H_{15}O_x$ -HOM-RO<sub>2</sub> in the non-ON products. This indication is corroborated by the observations in the  $C_{20}$ -HOM-Acc products (Figure 29). Here, we see a similar trend: the contribution of  $C_{20}H_{30}O_z$ -HOM-Acc, which are formed from two  $C_{10}H_{15}O_x$ -RO<sub>2</sub>, increased with NO availability, while the contribution of  $C_{20}H_{34}O_z$ -HOM-Acc, which are formed from two  $C_{10}H_{17}O_x$ -RO<sub>2</sub>, decreased. The  $C_{20}H_{32}O_z$ -HOM-Acc, which are formed from both radical families, remained about the same.

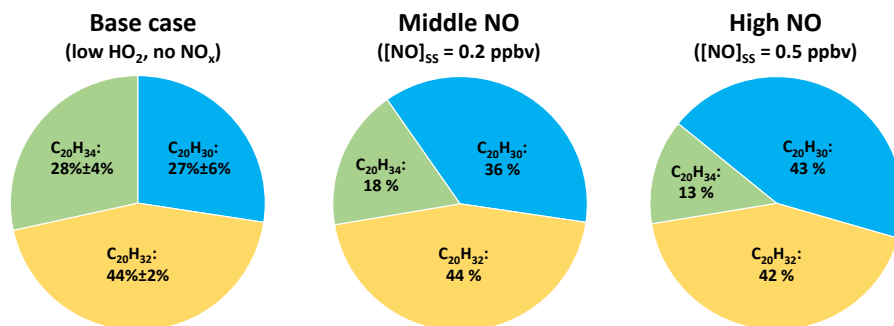


**Figure 29** Contribution of the  $C_{20}H_{30}O_z$ ,  $C_{20}H_{32}O_z$  and  $C_{20}H_{34}O_z$  families to the  $C_{20}$ -HOM-Acc in the base case and at the two NO levels (unseeded experiments).

The increased importance of  $C_{10}H_{15}O_x$  products compared to  $C_{10}H_{17}O_x$  products in the non-ON HOM products could be due to two reasons. One reason could be that the  $C_{10}H_{17}O_x$ -HOM-RO<sub>2</sub> have a specific fast pathway into ON formation and therefore contribute less to the non-ON products. The second reason could be that the importance of  $C_{10}H_{15}O_x$ -HOM-RO<sub>2</sub> increased in general.

To further investigate which reason is more likely, we compared the behavior of products that can be clearly assigned to either  $C_{10}H_{15}O_x$  or  $C_{10}H_{17}O_x$ . The monomer products directly assignable to one radical precursor family are  $C_{10}H_{14}O_z$  and the ON family  $C_{10}H_{15}NO_z$  for  $C_{10}H_{15}O_x$ -HOM-RO<sub>2</sub> and  $C_{10}H_{18}O_z$  and  $C_{10}H_{17}NO_z$  for  $C_{10}H_{17}O_x$ -HOM-RO<sub>2</sub>.

This comparison has to be applied with caution as it cannot capture pathways of the HOM-RO<sub>2</sub> families into  $C_{10}H_{16}O_z$ . Thus, for  $C_{10}H_{15}O_x$  only the RO<sub>2</sub>+RO<sub>2</sub> and internal termination pathway into carbonyl formation are included, with the other reaction products from RO<sub>2</sub> and HO<sub>2</sub> missing. For  $C_{10}H_{17}O_x$  the carbonyl formation is missing, which includes the potentially fast carbonyl formation from internal termination. The alcohol (RO<sub>2</sub>+RO<sub>2</sub>) and hydroperoxide (RO<sub>2</sub>+HO<sub>2</sub>) formation of  $C_{10}H_{17}O_x$  are included. The termination via RO<sub>2</sub> and HO<sub>2</sub> were expected to both contribute only around 15% at middle NO and less than 5% each at high NO (see Figure 24), showing that the missing bimolecular pathways should have minor effects, but the missing internal termination pathway of  $C_{10}H_{17}O_x$  into  $C_{10}H_{16}O_z$  should be kept in mind. The results of the comparison can be found in Figure 30 a).

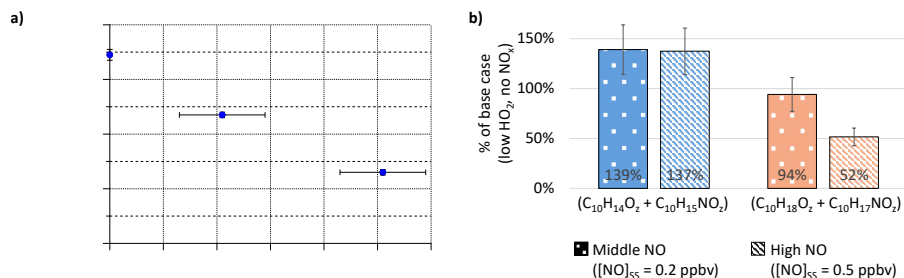


**Figure 30** Behavior of clearly assignable HOM-Mon products from  $C_{10}H_{15}O_x$  and  $C_{10}H_{17}O_x$  in the base case and at the two NO levels **a)** Ratio of  $(C_{10}H_{18}O_2 + C_{10}H_{17}NO_2)$  to  $(C_{10}H_{14}O_2 + C_{10}H_{15}NO_2)$  in  $NO_x$ -free base case and with increasing NO **b)** Relative change in clearly assignable HOM-Mon products from  $C_{10}H_{15}O_x$  and  $C_{10}H_{17}O_x$  at the two NO levels compared to base case in the unseeded system. (Data for b) normalized to  $\alpha$ -pinene OH turnover, base case from Experiment apinCO\_2)

In the  $NO_x$ -free base case, the ratio of  $C_{10}H_{18}O_2$  to  $C_{10}H_{14}O_2$  was close to 0.7. With increasing NO, even taking the formed ON products into account, the ratio decreased significantly. This trend indicates that the higher importance of  $C_{10}H_{15}O_x$  products in the non-ON HOM-Mon and HOM-Acc is not due to a fast formation pathway for  $C_{10}H_{17}O_x$  to ON products. **Figure 30 b)** shows the relative change of the HOM-Mon products clearly assignable to  $C_{10}H_{15}O_x$  termination (blue columns) and  $C_{10}H_{17}O_x$  termination (orange columns) at the two NO levels compared to the base case: The sum of  $C_{10}H_{17}O_x$  termination products was comparable to the base case at middle NO and reduced to around 50 % at high NO, while the sum of  $C_{10}H_{15}O_x$  termination products increased in the system with NO to around 140 % of the base case and showed no reduction at high NO.

The increase in  $C_{10}H_{15}O_x$  HOM-Mon products supports the hypothesis of an increase in importance of the  $C_{10}H_{15}O_x$  peroxy radical precursors. However, this observation is not reflected by observations in the radical families themselves as here no higher contribution by  $C_{10}H_{15}O_x$  to the overall  $C_{10}$ -HOM-RO<sub>2</sub> sum was observed. Instead, the contributions at both NO levels showed no significant shift compared to the base case with contributions by  $C_{10}H_{17}O_x$  close to 25 % within the uncertainties. The detailed result can be found in Appendix **Section A.10.1**. Note, that the contributions are based on steady-state concentrations, and it cannot be distinguished if the change in a compound's steady-state concentration is due to changes in its sources, sinks or both. Therefore, it is plausible that no increase of the  $C_{10}H_{15}O_x$  sum could be observed, because NO not only facilitates additional formation of  $C_{10}H_{15}O_x$  but also leads to an increase of the chemical sink into product formation. Thus, the increase is only observable in the products, not the radical family itself.

The  $C_{10}H_{14}O_2$  signal sum did not decrease as much as expected from the observed decrease in the  $C_{10}H_{15}O_x$  family with addition of NO. In steady state, it would be expected that the relative decrease in  $C_{10}H_{14}O_2$  is at least as much as in its precursor family. The reduction should be even larger if the  $C_{10}H_{14}O_2$  are formed in a bimolecular reaction in which both reactants were reduced compared to the

base case, as is expected for the RO<sub>2</sub>+RO<sub>2</sub> formation pathway: From our observation the C<sub>10</sub>H<sub>15</sub>O<sub>x</sub>-HOM-RO<sub>2</sub> were reduced to around 50 % and 30 % of the base case at middle and high NO and a strong reduction in the overall RO<sub>2</sub> pool was expected from the modeling results (relatively around 30 % and 10 % of the base case). Still the C<sub>10</sub>H<sub>14</sub>O<sub>z</sub> family was only decreased to 80 % and 50 % of the base case at middle and high NO. A bar chart showing the relative changes in the HOM-Mon can be found in Appendix **Section A.10.2**.

A smaller than expected decrease of C<sub>10</sub>H<sub>14</sub>O<sub>z</sub> was also observed in the system with high HO<sub>2</sub> (see **Section 4.1.5**), but there the decrease in the C<sub>10</sub>H<sub>14</sub>O<sub>z</sub> family and its C<sub>10</sub>H<sub>15</sub>O<sub>x</sub> precursor family were similar, indicating that internal termination could be an important pathway for C<sub>10</sub>H<sub>14</sub>O<sub>z</sub> formation. However, in the system with NO the C<sub>10</sub>H<sub>14</sub>O<sub>z</sub> family showed a significantly smaller reduction than the C<sub>10</sub>H<sub>15</sub>O<sub>x</sub> family. A possible explanation for this could be that the C<sub>10</sub>H<sub>14</sub>O<sub>z</sub> are formed from C<sub>10</sub>H<sub>15</sub>O<sub>x-1</sub> alkoxy radicals. Such alkoxy radicals are too reactive to be directly measured and represent a sink of the C<sub>10</sub>H<sub>15</sub>O<sub>x</sub> peroxy radicals. A C<sub>10</sub>H<sub>15</sub>O<sub>x-1</sub> alkoxy radical could undergo internal termination analogous to the mechanism proposed by Rissanen et al. (2014) for RO<sub>2</sub>. An intramolecular H-shift forming an alcohol group from the alkoxy radical, would be followed by carbonyl formation from the formed alkyl radical attached to the hydroperoxide group and OH would be lost from the molecule. Another source of C<sub>10</sub>H<sub>14</sub>O<sub>z</sub> could be hydrolysis and loss of HNO<sub>3</sub> from C<sub>10</sub>H<sub>15</sub>NO<sub>z</sub>, as discussed for the particle phase (Takeuchi and Ng, 2019), however such reactions may not be likely in the gas phase. Though formation through alkoxy radicals offers a possible explanation, further investigations are necessary to clarify the reason for the unexpected behavior of the C<sub>10</sub>H<sub>14</sub>O<sub>z</sub> family.

In general, an increase in formation of C<sub>10</sub>H<sub>15</sub>O<sub>x</sub>-HOM-RO<sub>2</sub> agrees well with the increased importance of alkoxy radical formation in presence of increasing NO. As discussed in the HO<sub>2</sub> case (**Section 4.1.2**) the formation of C<sub>10</sub>H<sub>15</sub>O<sub>x</sub> is expected to rely on the involvement of alkoxy steps. Alkoxy radical formation is necessary in the  $\alpha$ -pinene H-abstraction pathway presented by Shen et al. (2022), as well as in the formation of first-generation  $\alpha$ -pinene oxidation products like pinonaldehyde (MCM mechanism, (Jenkin et al., 1997; Saunders et al., 2003)). Such compounds are expected to be an important source of second-generation C<sub>10</sub>H<sub>15</sub>O<sub>x</sub>-HOM-RO<sub>2</sub> oxidation products.

The formula composition of pinonaldehyde (C<sub>10</sub>H<sub>16</sub>O<sub>2</sub>) was detected by amine-CIMS. However, no increase in the signal was observed in the system with NO. At middle NO, no significant change was observed (97 % of signal compared to base case), and at high NO even a slight reduction to around 90 % of the base case was observed. This observation is unexpected as model results predicted a strong increase (by around factor 3) in pinonaldehyde with the addition of NO. However, in the system dominated by HO<sub>2</sub> only a moderate decrease of pinonaldehyde was observed, while the model predicted a strong decrease (see **Section 4.1.2**). This general mismatch could indicate that the

formation pathway of pinonaldehyde (and like compounds) is not fully reflected in the model, as its formation is not impacted as predicted by the availability of RO<sub>2</sub> or NO for alkoxy formation.

Our observations cannot link the increased importance of C<sub>10</sub>H<sub>15</sub>O<sub>x</sub>-HOM-RO<sub>2</sub> to an increase of the precursor pinonaldehyde and subsequent secondary oxidation. This could be an indication, that the formation of C<sub>10</sub>H<sub>15</sub>O<sub>x</sub>-HOM-RO<sub>2</sub> starts directly from  $\alpha$ -pinene (H-abstraction). However, also here further investigation is necessary.

#### 4.2.4 Importance of HOM alkoxy chemistry in the system with NO

The alkoxy radical formation can be related to multiple major changes in the product distribution. In the last section the C<sub>10</sub>-HOM-Mon class (ON and non-ON products), as well as the C<sub>20</sub>-HOM-Acc showed clear indications that alkoxy radical formation is responsible for an increased importance of C<sub>10</sub>H<sub>15</sub>O<sub>x</sub> compared to C<sub>10</sub>H<sub>17</sub>O<sub>x</sub> chemistry. Another clear indication of increased alkoxy radical formation is the increase in concentration and contribution of HOM-Frag products (see **Figure 25** and **Figure 26**). As explained in **Section 2.1.3** alkoxy radicals are highly unstable, thus fragmentation, leading to oxidation products with carbon numbers smaller than 10, is one of their major expected reaction pathways. A more detailed breakdown of the changes in the HOM-Frag grouped by carbon number (non-ON and ON HOM-Frag) can be found in **Figure 31 a**). The graph shows that fragments with smaller carbon numbers (C<sub>5</sub>-C<sub>7</sub>) increased in the presence of NO. As discussed before in the HO<sub>2</sub> case (see **Section 4.1.4**), this fits well to a stepwise fragmentation process as implemented in the MCM chemistry (Jenkin et al., 1997; Saunders et al., 2003).

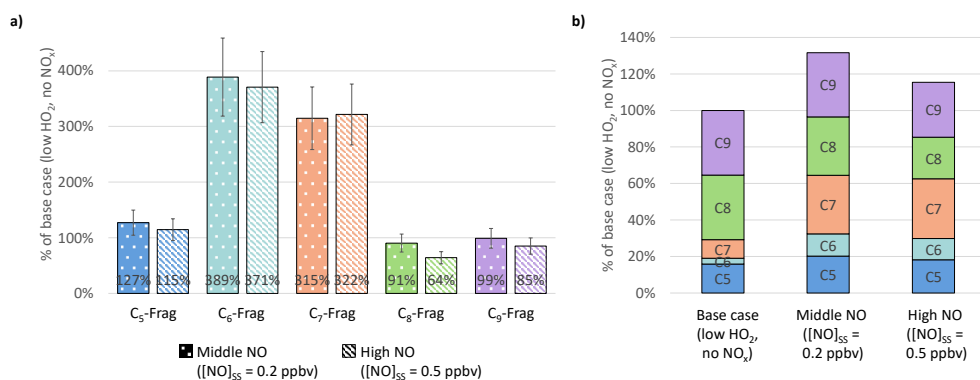


**Figure 31** Behavior of HOM-Frag groups in system with NO **a)** Overview of relative change in HOM-Frag groups detected in NO<sub>3</sub>-CIMS at the two NO levels compared to NO<sub>x</sub>-free case in unseeded system **b)** Contribution of each HOM-Frag group in relation to the base case (contribution of each group multiplied with overall relative change compared to base case.) Base case from Experiment apinCO<sub>2</sub>, all data normalized to  $\alpha$ -pinene OH turnover.

The C<sub>8</sub>- and C<sub>9</sub>-HOM-Frag groups decreased with increasing NO. Besides the C<sub>7</sub>-HOM-Frag group, all groups slightly decreased at high NO compared to middle NO. The C<sub>6</sub>- and C<sub>7</sub>-HOM-Frag groups had the largest increase with NO, though the large relative increase in C<sub>6</sub>-HOM-Frag has to be judged in

context of the small contribution of C<sub>6</sub>-HOM-Frag in general. **Figure 31 b)** visualizes the importance of the different HOM-Frag groups in a stacked bar chart, showing that even though the C<sub>6</sub>-HOM-Frag group had the largest relative increase compared to the base case, its importance was still minor.

The contribution of C<sub>6</sub> was only around 3 % in the base case and increased to around 10 % with NO in the system. The contribution of each group to the HOM-Frag class for the three experimental conditions can be found in Appendix **Section A.10.3**. **Figure 31 b)** also shows that the most significant shift in contribution was the increase in importance of C<sub>7</sub>-HOM-Frag.

Different reaction pathways can lead to the formation of C<sub>7</sub>-HOM-Frag. One pathway we would like to highlight is the formation of C<sub>7</sub>-HOM-Frag via the elimination of acetone from a C<sub>10</sub>-precursor. The MCM chemistry contains a pathway from a C<sub>10</sub>H<sub>17</sub>O<sub>3</sub>-RO<sub>2</sub> to C<sub>7</sub>H<sub>11</sub>O<sub>3</sub> requiring only one bimolecular reaction as shown in **Figure 32** (Jenkin et al., 1997; Saunders et al., 2003). The essential prerequisite is the opening of the four-ring in  $\alpha$ -pinene. This pathway has been corroborated with quantum chemical calculations in the publications of Peeters et al. (2001) and Vereecken et al. (2007), due to the structure of the formed RO<sub>2</sub> we will call this path the “menthene pathway”.

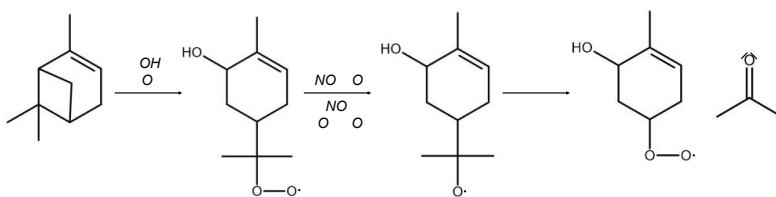


**Figure 32** Formation of C<sub>7</sub>H<sub>11</sub>O<sub>3</sub> peroxy radical and acetone via menthene pathway

Another possibility for C<sub>7</sub>-HOM-Frag formation in the MCM (Jenkin et al., 1997; Saunders et al., 2003) is the opening of the four-ring in first generation oxidation product pinonaldehyde and the subsequent elimination of acetone. Or similarly, formation via a breakdown from pinonaldehyde in multiple steps as proposed by Fantechi et al. (2002). The MCM also suggests pathways including a secondary attack on a first-generation oxidation ON-Mon-product. The details of the different formation paths can be found in the referenced sources and will not be discussed further here.

However, one interesting factor is that the different formation pathways will lead to C<sub>7</sub>-RO<sub>2</sub> with differing H-numbers: For example, the formation from the menthene pathway will lead to an C<sub>7</sub>H<sub>11</sub>O<sub>x</sub>, while formation via four-ring opening in the RO<sub>2</sub> formed from pinonaldehyde will lead to formation of an C<sub>7</sub>H<sub>9</sub>O<sub>x</sub>. Thus, the variety of hydrogen numbers in the detected C<sub>7</sub>-HOM-Frag gives an indication if one specific pathway is especially important or if a mixture of pathways lead to the observed products.

Overall, C<sub>7</sub>-species with hydrogen numbers between 6 and 12 were detected. C<sub>7</sub>-HOM-Frag with less than 10 hydrogen atoms contributed around 50 % at middle NO, and around 65 % at high NO (for a

detailed contribution overview see Appendix **Section A.10.3**). The broad distribution of contribution of different families shows that multiple of the described formation pathways contributed significantly to the observed C<sub>7</sub>-HOM-Frag.

As introduced in **Section 2.1.3** and utilized for the HO<sub>2</sub> case in **Section 4.1.4**, parity analysis of the oxygen number in HOM-RO<sub>2</sub> can be used as an indicator for a change in alkoxy radical formation. The parity between odd/even oxygen numbers in the C<sub>10</sub>-HOM-RO<sub>2</sub> was investigated, however no significant changes could be determined. This is probably at least partially due to the small radical signals and the described assignment issues leading to large uncertainties in the result. Note furthermore the limitations of parity analysis: The occurrence of two or any even number of alkoxy-peroxy steps will lead to the same parity as no alkoxy step. In the same way the occurrence of any uneven number of alkoxy steps will lead to the same parity as a single alkoxy step. Plots showing the contribution of odd and even oxygen numbers in the C<sub>10</sub>-HOM-RO<sub>2</sub> families with error estimation from error propagation can be found in the Appendix **Section A.10.1**.

Kang (2021) observed a higher oxidation degree of HOM products in the system with NO and proposed efficient alkoxy-peroxy steps extending the autoxidation chain length as the explanation. We detected only two higher oxidized compounds ( $x = 10,11$ ) in the C<sub>10</sub>H<sub>17</sub>O<sub>x</sub> family with NO. Furthermore, some of the closed-shell HOM-Mon families, as well as the HOM-Acc showed a slight increase in the weighted O/C ratio (for details see Appendix **Section A.10.4**). We suggest that Kang (2021) had more distinct findings due to somewhat higher NO concentrations (up to 3 ppbv) at higher  $\alpha$ -pinene turnover ( $1.2\text{-}1.6\cdot 10^8 \text{ cm}^3 \text{ s}^{-1}$ , OH:  $4\text{-}7\cdot 10^7 \text{ cm}^{-3}$ ) in their study.

Multiple observations point towards a clear increase in alkoxy radical formation with NO. The two major observed effects were the increased importance of C<sub>10</sub>H<sub>15</sub>O<sub>x</sub> products and the formation of HOM-Frag products, as well as the subsequent change in the HOM-Frag product distribution.

#### 4.2.5 Formation of HOM organic nitrates

The formation of ON is the major expected impact of NO addition next to fast alkoxy radical formation. The formation of nitrogen containing compounds was observed for the HOM-Frag and HOM-Mon product classes. We assume that the major reaction leading to the formation of the observed ON compounds is RO<sub>2</sub>+NO (see **(R2-6)** in **Section 2.1.2**) though we cannot fully exclude the reaction of acyl peroxy radicals with NO<sub>2</sub> (see **(R2-7)** in **Section 2.1.2**) forming PAN-like compounds.

We checked the importance of PAN-like ON compounds in our system by turning off the UV-A light during one experiment at middle NO in order to reduce the concentration of NO in the system (and increase the importance of NO<sub>2</sub>). At steady state this led to a decrease in NO concentration of about 40 %, while the sum of all detected ON compounds decreased by 30 %. The similar decrease in NO and ON indicate that indeed the major source of ON compounds in our system was RO<sub>2</sub>+NO

reactions, though the slightly smaller decrease in ON compounds indicates some formation from  $\text{RO}_2+\text{NO}_2$ . Stable PAN like compounds are expected from reactions of acyl peroxy radicals with  $\text{NO}_2$  while ON formed by reaction of other peroxy radicals with  $\text{NO}_2$  are thermally unstable and decompose into the reactants.

A small percentage of observed ON-HOM contained two nitrogen atoms, specifically within the HOM-Mon class ( $\text{C}_{10}\text{H}_{14}\text{N}_2\text{O}_z$ ,  $\text{C}_{10}\text{H}_{16}\text{N}_2\text{O}_z$ ,  $\text{C}_{10}\text{H}_{18}\text{N}_2\text{O}_z$ ). Such observations could be due to ON-HOM clustering with dimer reagent ions ( $\text{NO}_3\cdot\text{HNO}_3$ , for example  $(\text{C}_{10}\text{H}_{17}\text{NO}_{z-3}\cdot\text{HNO}_3\cdot\text{NO}_3)^-$  pretending  $(\text{C}_{10}\text{H}_{18}\text{N}_2\text{O}_z\cdot\text{NO}_3)^-$ ). No such clusters with reagent ion dimers were observed in the  $\text{NO}_x$ -free system, because only the  $\text{NO}_3^-$  ions are guided into the ion molecule reaction zone (IMR) of the inlet, but  $\text{HNO}_3$  becomes available in the IMR in  $\text{NO}_x$  experiments due to its production in the chamber. To exclude such CIMS measurement effects the timeseries of the ON-HOM with two nitrogen atoms were compared to the respective ON products with one nitrogen (comparison of  $\text{C}_{10}\text{H}_y\text{N}_2\text{O}_z$  to  $\text{C}_{10}\text{H}_{(y-1)}\text{NO}_{(z-3)}$ ). The 1-N and 2-N compounds showed clearly different temporal behavior during the experiment, leading to the conclusion that the observation of ON-HOM with two nitrogen atoms was not due to clustering of ON-HOM with dimer reagent ions ( $\text{NO}_3\cdot\text{HNO}_3$ ).

ON with 2 nitrogen containing groups contributed less than 10 % to the overall ON signal (6 % at middle NO and 8 % at high NO), but their presence indicates that in specific cases 1-N ON-HOM can undergo decay or a second OH attack and terminate a second time with NO. However, no nitrogen containing HOM-Acc products could be identified, which would be expected if nitrogen containing HOM- $\text{RO}_2$  are formed in significant concentrations. Either specific formation pathways led to the formation of the observed ON with two nitrogen atoms or the concentration of nitrogen containing HOM-Acc was too small to be detected. All identified nitrogen containing compounds can be found in the peaklist in Appendix **Section A.6.2**.

To study the development of the ON-HOM compounds signal, as well as their contribution to the overall product sum with increasing NO concentration, three different NO levels were compared. To this end, an extra experiment stage with lower NO concentration and  $\text{RO}_2+\text{NO}$  contribution was conducted ( $[\text{NO}]_{\text{ss}}=0.1$  ppbv,  $\text{RO}_2+\text{NO}$  termination expected to contribute about 20 %). This extra “low NO” stage was used to add another measurement point besides middle and high NO, as the  $\text{NO}_x$ -free base case cannot be used in the investigation of the behavior of ON compounds. Information about the low NO case can be found in Appendix **Section A.10.5**. **Figure 33** shows the contribution of all ON products to the overall product sum, as well as ON-Frag and ON-Mon to their respective product classes as a function of the measured steady-state NO concentration.

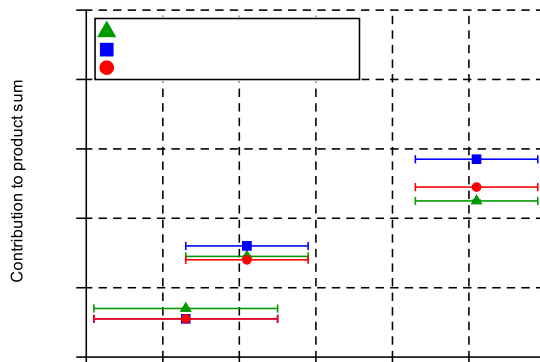


**Figure 33** Contribution of ON products to product sum as a function of measured steady-state NO concentration. Shown are the contribution of the overall ON-product sum (red circles), the ON-HOM-Mon sum (blue squares) and ON-HOM-Frag sum (green triangles) to their respective product class.

A strong increase in the contribution of ON products was observed between low and middle NO conditions, but from middle to high NO the slope seemed to decrease and the contribution of ON products seemed to level off. Considering the different termination pathways (see **Figure 24 a**), a saturation effect is expected. At high NO a contribution of  $\text{RO}_2+\text{NO}$  of close to 100 % was expected and thus no further increase in contribution of ON products is possible at a given branching ratio between ON and alkoxy radical formation. Indeed, assuming a given branching ratio into ON formation, the ON contribution should increase linearly with increasing contribution of  $\text{RO}_2+\text{NO}$  termination to the chemical sink.

In **Figure 34** the contribution of the ON products to the overall product sum is plotted against the calculated  $\text{RO}_2+\text{NO}$  contribution to the chemical sink. The  $\text{RO}_2+\text{NO}$  contribution should only be used as a guideline as it has large uncertainties due to the limited information available on the reaction rate coefficients, the application of generic bulk reaction rate coefficients and the high uncertainty from the modeled  $[\text{RO}_2]_{\text{ss}}$  sum and  $[\text{HO}_2]_{\text{ss}}$  concentrations. Nonetheless the linear trend in **Figure 34** is promising that our rough estimations have merit.

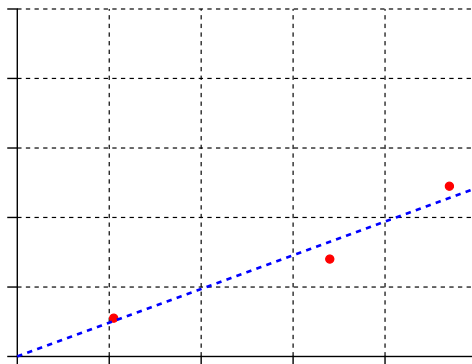


**Figure 34** Contribution of measured ON product sum to overall product sum as a function of the calculated RO<sub>2</sub>+NO contribution to the RO<sub>2</sub> chemical sink. Linear trend (blue dotted line) is constrained through the zero point. As the calculation of the RO<sub>2</sub>+NO contribution is based on general bulk calculations and modeling results large uncertainties apply.

For the high NO case, where the termination was dominated by the reaction with NO, ON-HOM contributed around 50 % of all observed HOM. Our results compare well to Pullinen et al. (2020), who reported a contribution of ON-HOM to the total observed HOM sum of about 50 % for  $\alpha$ -pinene photooxidation under high NO<sub>x</sub> conditions.

#### 4.2.6 Impact of NO on condensable organic mass

The previous subsections have shown that NO changes the gas-phase HOM product distribution significantly. How these changes affect the formed condensable organic mass and, thus SOA formation potential, was investigated via the addition of (NH<sub>4</sub>)<sub>2</sub>(SO<sub>4</sub>) seed aerosol. The comparison of the gas-phase signal without and with seed aerosol in the system shows how much of the HOM products condensed. The comparison to the NO<sub>x</sub>-free base case and between NO levels shows how the condensable product fraction changed with increasing NO.

An overview of the relative changes of the gas-phase product classes in the system with seed can be seen in **Figure 35**. A trend with increasing NO can be observed in the overall HOM product fraction remaining. A higher concentration of products remained in the gas phase with NO. At high NO the fraction remaining increased from 39 % to 56 % compared to the NO<sub>x</sub>-free base case. One reason for this is the higher abundance of very low volatile HOM-Acc products in the base case. However, the same trend was observed in the HOM-Frag class, where the gas-phase fraction remaining increased from 47 % in the base case to 65 % at high NO.

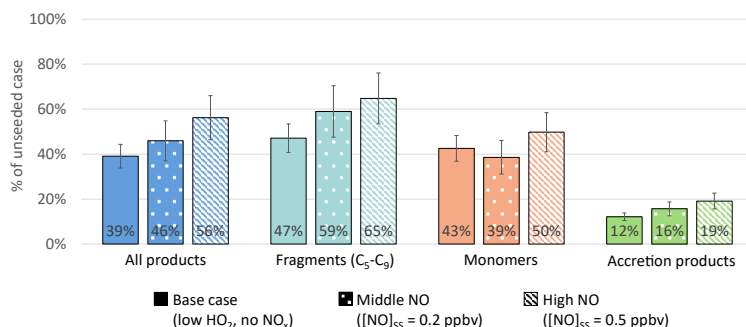


**Figure 35** Overview of relative change in signal in product classes between seeded and unseeded system. (All data normalized to  $\alpha$ -pinene OH turnover, base case from Experiment apinCO\_2. Error bars via error propagation, for more information see Appendix Section A.5)

The HOM-Mon fraction remaining didn't show a significant trend with increasing NO, though an increase from 39 % to 50 % could be observed going from middle to high NO. The gas-phase fraction remaining remained smallest for HOM-Acc, however slightly increased with increasing NO from 12 % to 19 %.

Formation of ON-HOM is another important reason for increasing fraction remaining with increasing NO, besides the suppression of HOM-Acc. **Figure 36** shows the fraction remaining after seed addition for just the ON products. In comparison to the NO<sub>x</sub>-free base case from **Figure 35**, where no ON products were present, the ON-HOM had about 25 % higher fractions remaining (39 % remaining of all products in base case compared to 65 % and 63 % of ON products in cases with NO respectively). The comparison of ON-HOM-Frag and ON-HOM-Mon to non-ON HOM-Frag and HOM-Mon in the base case revealed the same trend. A higher fraction remaining indicates a higher volatility of the ON products compared to the products in the base case.

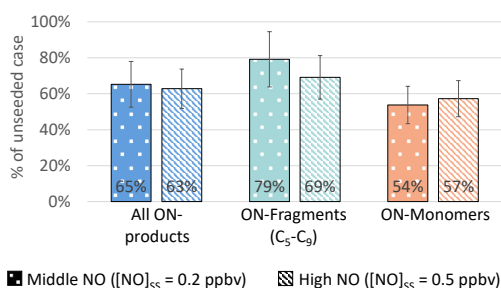


**Figure 36** Overview of relative change of ON product classes signal between seeded and unseeded system. (All data normalized to  $\alpha$ -pinene OH turnover. Error bars via error propagation, for more information see Appendix Section A.5)

Additionally, the increasing importance of (higher volatility) fragmentation products will overall increase the volatility of the product distribution, depending on size and oxidation degree of the fragments. Both, the contribution of ON products, as well as the contribution of fragments to the

HOM product sum, increased with increasing NO, and explain the trend of an increased fraction remaining for the overall product sum (**Figure 35**) and thus the product volatility.

Presence of NO can lead to two effects that reduce the formation of SOA mass: Firstly, reduction of HOM formation in NO dominated systems (see high NO case) and secondly production of HOM with higher fraction remaining, i.e. product distributions with higher volatility. The latter will cause a reduction in SOA mass even without reduction in overall HOM products observed in the gas phase (as seen in the middle NO case). Here the higher fraction remaining in the gas phase still indicated a decrease in condensation compared to the base case. However, it should be kept in mind that a condensing ON-HOM contributes more mass to the particle phase ( $30 \text{ g mol}^{-1}$  to  $46 \text{ g mol}^{-1}$  per ON-HOM) than a HOM product from the same precursor with a lighter termination group.

The organic mass concentration was measured with an AMS. The AMS measurement results, total particle surface from SMPS measurements, and the calculated wall loss corrected SOA yield can be found in **Table A12**. Organic mass concentrations of  $2.5 \mu\text{g m}^{-3}$  at middle NO and  $1.9 \mu\text{g m}^{-3}$  at high NO were measured. In the base case for comparison (Experiment apinCO\_2 (s)) an organic mass concentration of  $3.4 \mu\text{g m}^{-3}$  was measured. Thus, after normalization with the  $\alpha$ -pinene OH turnover, the observed organic mass concentration decreased to about 80 % in the middle NO and to 55 % in the high NO case compared to the base case (see also **Figure 38**). As suggested, we indeed observed a stronger decrease in the particle phase than in the gas-phase signal (overall product signal was not decreased at middle NO and decreased to about 80 % at high NO as shown in **Figure 25**).

To check whether the gas and particle-phase observations were still in agreement, the mass weighted HOM signal was calculated as a proxy for the condensable HOM mass found in the gas phase (see **Section 3.1.5**). For this the fraction remaining of the individual closed-shell oxidation products was plotted against their molar mass. The fraction remaining in the gas phase in the seeded system compared to the unseeded system is a direct indicator of the condensation behavior under the following assumptions: a) No significant disturbance of the products precursor chemistry, b) no particle phase production sources of the products and c) negligible re-evaporation of the HOM compounds into the gas phase. **Figure 37 a**) shows the result for the high NO case, plotting the fraction remaining in steady state with seed compared to the unseeded steady state against the molar mass of the HOM compounds.

**Figure 37 b**) shows just the non-ON HOM products. The sigmoidal trend from base and high HO<sub>2</sub> case (**Section 4.1.6**, **Figure 22**) is used here as well and fits well to the non-ON products in the NO case. This is expected if the same or similar non-ON products in the different cases are formed. We mainly expect the difference to be in the contribution of the different termination pathways, but do not expect the emergence of many completely new non-ON product species.

For the considerations regarding the condensation behavior, the contribution of the different product species is unimportant, as long as their concentration and consequentially their signal is sufficiently high. Thus, the ON product condensation behavior can be best seen in the high NO case, as here the ON products showed highest signals.

The same overview as in **Figure 37** for the middle NO case can be found in Appendix **Section A.10.6**. However, in the middle NO case higher fractions remaining than expected of ON-HOM were observed due to experimental imperfections. In the experiment the seeded middle NO case was studied last, which led to contaminations with ON compounds from previous experiment phases. Thus, for future experiments we recommend studying the seeded systems first and in order of increasing NO concentration to avoid such contamination effects.

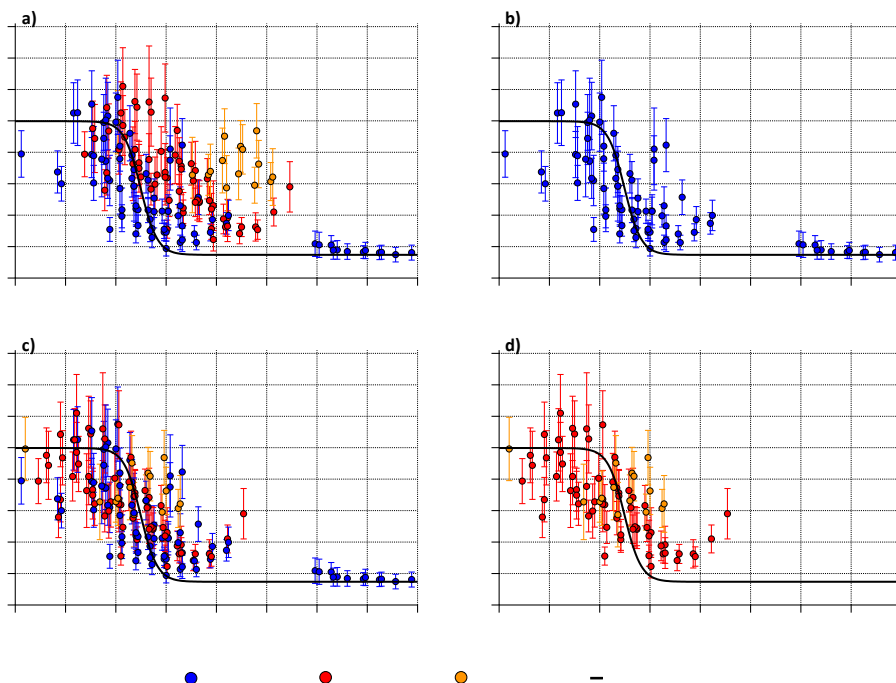


**Figure 37** Gas-phase fraction remaining in presence of seed for the high NO case.

- a)** all HOM compounds, **b)** just non nitrated HOM compounds, **c)** all HOM compounds with organic nitrate's molar mass being shifted by the nitrate termination group ( $\text{NO}_2$ ) to ( $M - 46 \text{ g mol}^{-1}$ ) for compounds containing one nitrogen (red markers) and to ( $M - 92 \text{ g mol}^{-1}$ ) for compounds containing two nitrogen (orange markers), **d)** just organic nitrates shifted by the nitrate termination groups.

All data is normalized with  $\alpha$ -pinene OH turnover. Points represent compounds that were detected with relative standard deviation  $<30\%$  in both experiment phases. Error bars represent result of error propagation (see Appendix Section A.5).

In **Figure 37 a)** the ON compounds (red and orange markers) show a different condensation behavior than the non-ON compounds. ON compounds had higher fractions remaining at the same molar mass compared to a non-ON compound. This observation matches the observation that the ON product classes overall show higher fractions remaining (see **Figure 36**). However, from the correlation of the

fraction remaining to the molar mass of single compounds, the effect in the ON-HOM becomes clearer: The nitrate termination group does not reduce the volatility by the same degree as the termination groups in non-ON compounds (carbonyl, alcohol, hydroperoxide). This smaller reduction in volatility leads to the effect that the volatility of the ON closed shell product is more comparable to a lighter non-ON product. In fact, **Figure 37 c)** shows that subtracting the weight of the nitrate termination group ( $M(\text{NO}_2) = 46 \text{ g mol}^{-1}$ ) from the ON compound's molar mass led to a much better fit with the correlation between molar mass and condensation behavior of non-ON compounds. To show this more clearly **Figure 37 d)** shows just ON compounds on the shifted molar mass axis together with the sigmoidal trend used for the non-ON compounds. In other words, the ON products have a higher molar mass threshold for condensing into the particle phase.

A similar conclusion was drawn by Pullinen et al. (2020), who compared effective uptake coefficients into the particle phase for non-ON and ON HOM products. Their results showed that there was no significant difference for a non-ON and ON product from the same HOM-RO<sub>2</sub>-precursor, even though the ON product is heavier and has a higher oxygen number. Furthermore, Presto et al. (2005) observed a higher volatility of nitrate containing products from  $\alpha$ -pinene ozonolysis. Recently, Graham et al. (2023) reported a higher volatility of  $\alpha$ -pinene + NO<sub>3</sub> derived SOA compared to SOA derived from  $\alpha$ -pinene ozonolysis.

The knowledge about the condensation behavior of the different HOM product species, gained from the inspection of the fractions remaining, was used to determine the molar mass threshold for the condensable HOM mass proxy from the gas-phase measurements (**Section 3.1.5**). For non-ON compounds a threshold of  $230 \text{ g mol}^{-1}$  was used, same as in the base and high HO<sub>2</sub> case (**Section 4.1.6**). For ON compounds two different thresholds were applied:  $276 \text{ g mol}^{-1}$  for compounds containing one nitrogen (non-ON threshold +  $M(\text{NO}_2)$ ) and  $322 \text{ g mol}^{-1}$  for compounds containing two nitrogen atoms (non-ON threshold +  $2 \cdot M(\text{NO}_2)$ ). These thresholds were chosen as such to only include HOM compounds with fractions remaining of 50 % and smaller into the proxy for the condensable HOM mass.

The result of the comparison of the condensable HOM mass proxy in the systems with NO in comparison to the base case system can be seen in **Figure 38** in direct comparison to the measured organic mass reduction by AMS. The results show a good agreement between organic mass measurement in the seeded system and the condensable HOM mass proxy from the unseeded system. The good agreement led to the following conclusions: Firstly, the particle-phase and gas-phase measurement were consistent with each other, showing that the organic mass formation was defined by HOM compounds in the investigated chemical regimes with NO. Secondly, in order to capture the change in the particle phase via the gas-phase observations the correct volatility assumptions are necessary. The necessary volatility distributions can be gained from the comparison of the gas-phase

measurement in the unseeded and seeded system, i.e. here determining the critical molar mass threshold for which species contribute to the condensable organic mass. The reason for the reduced organic mass was the production of higher volatility products with NO compared to the base case. These higher volatility products were organic nitrates, as well as fragments.

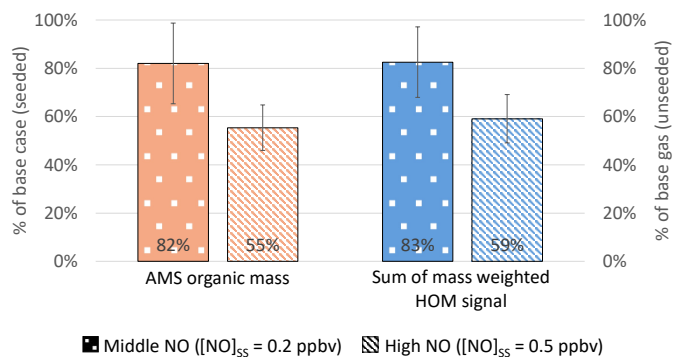


**Figure 38** Overview of the relative change in organic mass observed in the AMS (left y-axis, seeded experiments) and the mass weighted HOM signal that is supposed to condense as observed by NO<sub>3</sub>-CIMS (right y-axis, unseeded experiments) between the NO<sub>x</sub>-free base case and the two NO levels (all data normalized to  $\alpha$ -pinene OH turnover).

#### 4.2.7 Summary: Impact of NO

In summary, the addition of NO led to three major changes in the HOM product distribution: 1) The formation of ON-HOM created a new product class with different volatility. 2) The suppression of RO<sub>2</sub>+RO<sub>2</sub> termination caused a strong decrease in HOM-Acc products. 3) The increased importance of alkoxy radical formation from RO<sub>2</sub>+NO shifted the product distribution towards HOM-Frag products and increased the importance of the C<sub>10</sub>H<sub>15</sub>O<sub>x</sub>-HOM-RO<sub>2</sub> family and its closed-shell products.

Regarding the impact of these changes on the formed organic mass, the larger decrease in the measured organic mass compared to the decrease of the HOM products in the gas phase showed that higher volatility products were formed in the system with NO. This decrease of SOA formation potential is connected to both the decrease in HOM-Acc in favor of smaller, likely more volatile HOM-Frag, as well as to the formation of ON-HOM. The fraction remaining showed that ON-HOM have higher volatilities than non-ON HOM products of the same mass. The analysis of the SOA formation potential of HOM matched the direct observation of the SOA mass.

The high HO<sub>2</sub> case already showed the successful application of a molar mass threshold determined from the gas-phase fraction remaining with seed to classify a product's condensation behavior. The NO case furthermore showed that it is necessary to adapt the molar mass threshold depending on the product species.

### 4.3 Combination of NO and high HO<sub>2</sub>

In this chapter the  $\alpha$ -pinene photooxidation system with both HO<sub>2</sub> and NO as important reaction partners is discussed. In the previous chapters we separately studied the effects of HO<sub>2</sub> and NO on the HOM product distribution, here the mixed system will be investigated. The results are compared to the RO<sub>2</sub> dominated laboratory base case with just  $\alpha$ -pinene and OH available, as well as to the previously discussed HO<sub>2</sub> and NO dominated systems, where only one reactant was added. The purpose is to understand the potential bias in the laboratory base case compared to a more atmospherically relevant system, but also to highlight how the effects caused by HO<sub>2</sub> and NO are interacting in the mixed system.

Two mixed system cases with two different NO levels are discussed. The CO addition to produce HO<sub>2</sub> was kept the same. The lower NO level was only utilized in one experiment (apinCONO\_1 [10]), while the higher NO level was utilized in two experiments (apinCONO\_1 [25] and apinCONO\_2 [25]). Thus, the repetition shows the variability in the results for the high NO, high HO<sub>2</sub> case, while error propagation was used to estimate the errors in the middle NO, high HO<sub>2</sub> case.

An overview of the contribution of RO<sub>2</sub>, HO<sub>2</sub>, and NO to the reaction pool, as well as the pseudo-first order reaction rate of the overall chemical loss for the different regimes is shown in **Figure 39**.

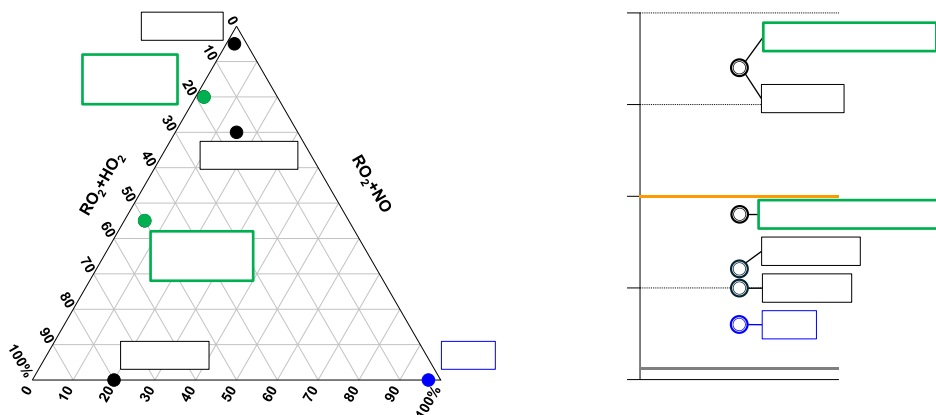


**Figure 39** Classification of the chemical regimes for the experiments with NO and HO<sub>2</sub> (highlighted in green):

- Triangle plot showing the distribution of the chemical reaction pool for RO<sub>2</sub> with NO, HO<sub>2</sub> and RO<sub>2</sub>.
- (Pseudo) first order chemical sink relative to average autoxidation rate and wall loss rate.

At the lower NO addition ( $[\text{NO}]_{\text{ss}} = 0.2$  ppbv), the overall pseudo-first order reaction rate coefficient of the chemical sink was  $0.09 \text{ s}^{-1}$ , which is close to the used generic average autoxidation rate of  $0.1 \text{ s}^{-1}$ . Thus, it can be expected that the chemical termination reduces the amount of observed autoxidation products. This middle NO, high HO<sub>2</sub> case is especially interesting, because the contribution to the chemical sink by RO<sub>2</sub>+HO<sub>2</sub> and RO<sub>2</sub>+NO was expected to be about equal (approximately 50 % by RO<sub>2</sub>+HO<sub>2</sub> and 45 % by RO<sub>2</sub>+NO, with the remaining 5 % by RO<sub>2</sub>+RO<sub>2</sub>). In the

high NO, high HO<sub>2</sub> case ([NO]<sub>ss</sub> = 0.4 ppbv), the termination was expected to be dominated by RO<sub>2</sub>+NO (80 %), with HO<sub>2</sub> contributing around 18 %. The total chemical sink was expected to be significantly larger with a pseudo-first order rate coefficient around 0.17 s<sup>-1</sup>.

All calculations are based on the box model results and generic bulk rate coefficients (see Section 3.2.5). The focus of the analysis will be on the middle NO, high HO<sub>2</sub> case as we use the nearly equal contribution of NO and HO<sub>2</sub> to the termination reactions to investigate if and what interactions the effects of the individual reaction partners have. The steady-state NO concentrations were very similar for both NO levels to the systems with only addition of NO (see Chapter 4.2), which allows direct comparison to see what changes were caused by the higher availability of HO<sub>2</sub>.

#### 4.3.1 Reduction of HOM formation in the system with NO and high HO<sub>2</sub>

Both the middle NO, high HO<sub>2</sub> and the high NO, high HO<sub>2</sub> case led to a reduction in the overall sum of observed HOM products of around 40 %. Interestingly, increasing NO from middle to high NO at high HO<sub>2</sub>, did not lead to a significant further decrease in the overall HOM products. An overview of the impact on the different product classes compared to the laboratory base case, which is characterized by low HO<sub>2</sub>, no NO<sub>x</sub>, and dominated by RO<sub>2</sub>+RO<sub>2</sub> reactions can be seen in Figure 40. Normalization with the  $\alpha$ -pinene OH turnover was applied to exclude effects by slight OH variations and to ensure direct comparability.

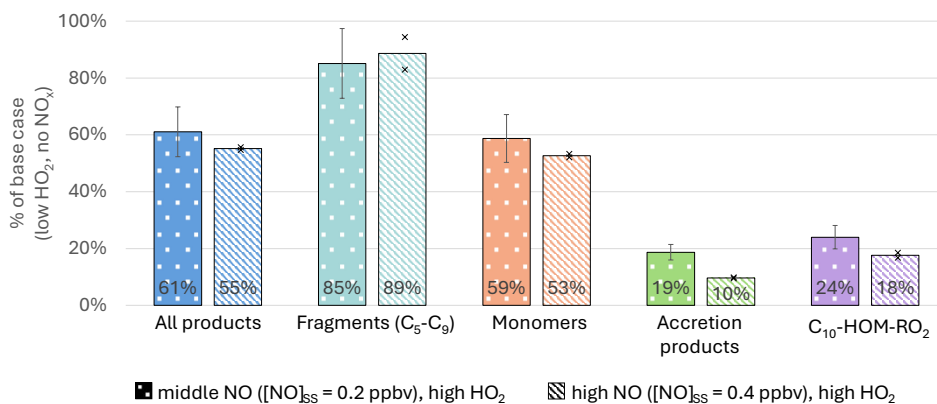


**Figure 40** Overview of relative change in product classes for the two NO, high HO<sub>2</sub> cases compared to the base case in unseeded systems (all data normalized to  $\alpha$ -pinene OH turnover). Data for the middle NO level were taken from the apinCONO\_1 [10] experiment and from the base case of Experiment apinCO\_2 and error bars were calculated by error propagation. For high NO level bars represent average relative change from apinCONO\_1 [25] (base case apinCO\_2), apinCONO\_2 [25] (base case within same experiment) and markers individual experiments.

In **Figure 40** the HOM-Mon showed about the same reduction as the overall HOM product sum. A reduction was observed for C<sub>10</sub>-HOM-RO<sub>2</sub> as a result of changes in their sources and sinks, as discussed before. However, low HOM-RO<sub>2</sub> signals in the mixed cases increased the uncertainty of the comparison. Strong reduction of HOM-Acc products indicated once more a successful suppression of the reaction of HOM-RO<sub>2</sub> with other RO<sub>2</sub> radicals. The HOM-Frag were the only product class that was not much reduced. In the middle NO, high HO<sub>2</sub> case a reduction by 15 % was observed, indicating that the HOM-Frag formation was impacted, but the reduction was still comparatively small to the reduction observed in the other product classes. As alkoxy radicals are a major source of fragmentation products, this indicates a persistent alkoxy radical formation from RO<sub>2</sub>+NO in presence of high HO<sub>2</sub>.

The large overall chemical sinks for HOM-RO<sub>2</sub> led to a reduction in the HOM source, making a comparison of the absolute changes difficult. It is not possible anymore to distinguish if changes are due to missing sources or due to shifts in the HOM product distribution by reactions of NO or HO<sub>2</sub> with HOM-RO<sub>2</sub>. Therefore, we will focus on the relative contribution of different product classes, groups, and families, as these comparisons do not depend on the overall concentration of HOM. The contribution of the different product classes in the middle NO, high HO<sub>2</sub> case can be seen in **Figure 41** (top row). The bottom row shows the distribution of product classes in the systems we want to compare to.

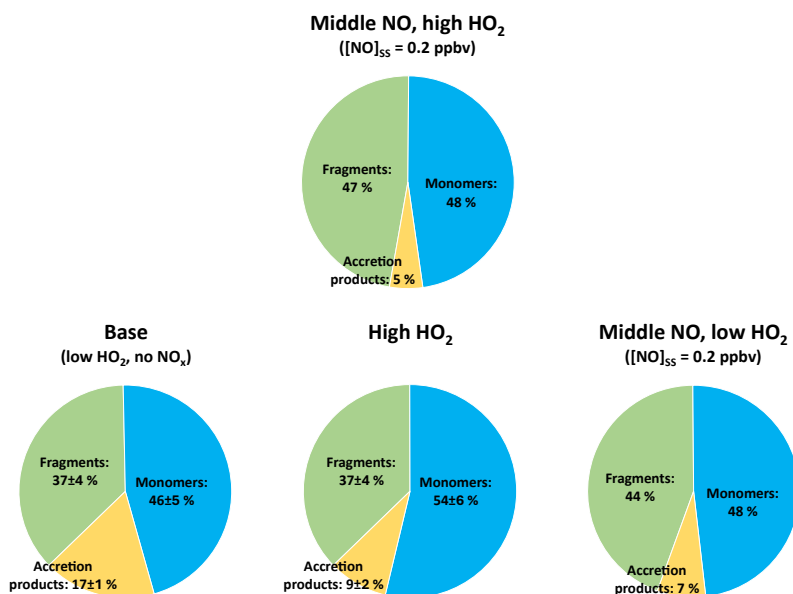


**Figure 41** Contribution of the closed-shell product classes to overall HOM product signal in the middle NO, high HO<sub>2</sub> case (top row) in comparison to the low HO<sub>2</sub>, NO<sub>x</sub>-free base case, the high HO<sub>2</sub> case and the middle NO, low HO<sub>2</sub> case (bottom row) (all experiments unseeded).

Compared to the base case (bottom left) we see a reduced importance of HOM-Acc, and an increased importance of HOM-Frag (shift of about 10 %). The high HO<sub>2</sub> system (bottom center) also showed a reduction in importance of HOM-Acc, however here, as expected from the termination of RO<sub>2</sub>+HO<sub>2</sub> the contribution shifted to HOM-Mon products. If we compare the middle NO, high HO<sub>2</sub> case (top row), to the middle NO case (bottom row, on the right), we see a very similar distribution in the contribution of the product classes.

**Figure 41** shows that the contribution by HOM-Frag was not reduced by the higher expected termination of HO<sub>2</sub> (50 %) in the middle NO, high HO<sub>2</sub> case compared to the middle NO case where HO<sub>2</sub> termination was expected to play a minor role (15 %). However, in the high HO<sub>2</sub> case compared to the base case no reduction in the contribution of overall HOM-Frag was observed either. Instead, the effect of HO<sub>2</sub> decreasing the alkoxy radical formation and subsequent fragmentation reactions could only be seen in the different HOM-Frag groups (C<sub>5</sub>-C<sub>9</sub>), for details see **Section 4.1.4**. The change in the HOM-Frag groups in the mixed system is discussed in **Section 4.3.5**. The contribution of product classes in the high NO, high HO<sub>2</sub> case can be found in Appendix **Table A15**.

#### 4.3.2 Impact of NO and high HO<sub>2</sub> on the HOM-RO<sub>2</sub> concentration

The direct analysis of the HOM-RO<sub>2</sub> radicals was already difficult in the system with NO due to ON-HOMs at the same nominal m/Q ratios and lower radical concentrations (for further explanation see **Section 4.2.2**). The large chemical sink in the system with both NO and HO<sub>2</sub> strongly reduced the steady-state concentration of HOM-RO<sub>2</sub>. Some HOM-RO<sub>2</sub> could no longer be assigned compared to the base case and the cases with just one dominant reactant. However, products of the missing HOM-RO<sub>2</sub> were detected with high signals, thus we conclude that the HOM-RO<sub>2</sub> were still important in the mixed system, but their steady-state concentrations were below the detection limit. For example, a significant product peak of C<sub>10</sub>H<sub>15</sub>NO<sub>10</sub> was detected, while C<sub>10</sub>H<sub>15</sub>O<sub>9</sub> itself was not assignable.

The significant product peaks support that an important reason for the low HOM-RO<sub>2</sub> concentration was the fast chemical termination to products. The comparison of the pseudo-first order chemical sink rate to the expected average autoxidation rate (**Figure 39 b**) shows that termination reactions with NO or HO<sub>2</sub> were expected to strongly compete with the autoxidation. In the middle NO, high HO<sub>2</sub> case this led to a reduction of C<sub>10</sub>-HOM-RO<sub>2</sub> to 24 %, while at high NO, high HO<sub>2</sub> only 18 % of the base case signal remained (**Figure 40**).

One way to find out if the observed reduction of C<sub>10</sub>-HOM-RO<sub>2</sub> is just due to a faster sink into products or due to a decrease in the HOM-RO<sub>2</sub> source is to calculate the HOM-RO<sub>2</sub> ratio between the case of interest and the base case. This calculation is only possible for HOM-RO<sub>2</sub> directly connected to the primary production ( $k_{OH} \cdot [OH] \cdot [\alpha\text{-pinene}]$ ) at the end of the autoxidation chain without significant further autoxidation). This approach was used in the high HO<sub>2</sub> (**Section 4.1.2**) and NO cases

(Section 4.2.2) and the equation can be found in Appendix Section A.8.2. The same approach was applied to the middle NO, high HO<sub>2</sub> case. The calculation yielded a reduction to around 40 % of HOM-RO<sub>2</sub> compared to the base case, while we observed a larger reduction to around 25 % (see Figure 40). The result is consistent with the reduction in steady-state HOM-RO<sub>2</sub> concentration due to both a fast sink into products and a reduction in the source. However, the result should be regarded with caution since the calculation directly links HOM-RO<sub>2</sub> to primary produced RO<sub>2</sub> and neglects possible interferences by fast chemical sinks of intermediate peroxy radicals.

### 4.3.3 C<sub>10</sub>-HOM-RO<sub>2</sub> chemistry: Importance of C<sub>10</sub>H<sub>15</sub>O<sub>x</sub> and C<sub>10</sub>H<sub>17</sub>O<sub>x</sub> families

Due to the low HOM-RO<sub>2</sub> signals, we will use changes in the closed-shell HOM products to derive the changes in the relative importance of the C<sub>10</sub>-HOM-RO<sub>2</sub> families (compare Section 4.2.3). One indicator is the contribution of different families in the non-ON HOM-Mon. However, in the mixed case the non-ON HOM-Mon family showed mainly an increase in the importance of the C<sub>10</sub>H<sub>16</sub>O<sub>z</sub> family, which can be formed from both C<sub>10</sub>H<sub>15</sub>O<sub>x</sub> and C<sub>10</sub>H<sub>17</sub>O<sub>x</sub>, and therefore does not directly give information about the contribution of C<sub>10</sub>H<sub>15</sub>O<sub>x</sub> and C<sub>10</sub>H<sub>17</sub>O<sub>x</sub> to the overall C<sub>10</sub>-HOM-RO<sub>2</sub>. The higher importance of C<sub>10</sub>H<sub>16</sub>O<sub>z</sub> in comparison to the base case and the high HO<sub>2</sub> and pure NO cases, however, indicates that a shift in the chemical system took place and its implications will be discussed in the following Section 4.3.4.

The C<sub>20</sub>-HOM-Acc families can also serve as an indicator for the contribution of C<sub>10</sub>H<sub>15</sub>O<sub>x</sub> and C<sub>10</sub>H<sub>17</sub>O<sub>x</sub>. Additionally, C<sub>20</sub>-HOM-Acc can only be formed via one pathway (RO<sub>2</sub>+RO<sub>2</sub>). C<sub>20</sub>H<sub>30</sub>O<sub>z</sub> and C<sub>20</sub>H<sub>34</sub>O<sub>z</sub> are clearly assignable to a single C<sub>10</sub>-HOM-RO<sub>2</sub> precursor (C<sub>10</sub>H<sub>15</sub>O<sub>x</sub> and C<sub>10</sub>H<sub>17</sub>O<sub>x</sub>, respectively). The contribution of the different C<sub>20</sub>-HOM-Acc families is shown in Figure 42, where the middle NO, high HO<sub>2</sub> case is shown in the top row, and the simpler cases for comparison are shown in the bottom row of the figure. The contributions of the different families to C<sub>20</sub>-HOM-Acc for the high NO, high HO<sub>2</sub> case can be found in Appendix Table A15.

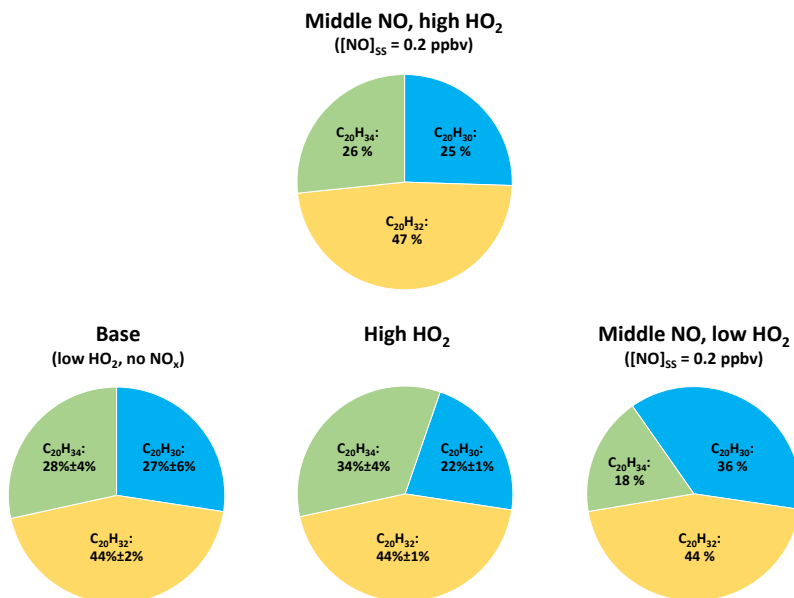


**Figure 42** Contribution of the C<sub>20</sub>H<sub>30</sub>O<sub>z</sub>, C<sub>20</sub>H<sub>32</sub>O<sub>z</sub>, and C<sub>20</sub>H<sub>34</sub>O<sub>z</sub> family to the C<sub>20</sub>-HOM-Acc signal in the middle NO, high HO<sub>2</sub> case (top row) in comparison to the low HO<sub>2</sub>, NO<sub>x</sub>-free base case, the high HO<sub>2</sub> case and the middle NO, low HO<sub>2</sub> case (bottom row) (all experiments unseeded).

The C<sub>20</sub>H<sub>30</sub>O<sub>z</sub> and C<sub>20</sub>H<sub>34</sub>O<sub>z</sub> family both contributed around 25 % to the C<sub>20</sub>-HOM-Acc in the middle NO, high HO<sub>2</sub> case. This is very similar to the base case (bottom row, left). The high HO<sub>2</sub> case (bottom row, center) showed a higher contribution of the C<sub>10</sub>H<sub>17</sub>O<sub>x</sub> produced HOM-Acc (C<sub>20</sub>H<sub>34</sub>O<sub>z</sub>), while the middle NO case (bottom row, right) had a higher contribution of the HOM-Acc produced by C<sub>10</sub>H<sub>15</sub>O<sub>x</sub> (C<sub>20</sub>H<sub>30</sub>O<sub>z</sub>). The system with NO and HO<sub>2</sub> showing a result closer to the base case indicates that the mixed effects of the two reactants compensate. The high importance of C<sub>10</sub>H<sub>15</sub>O<sub>x</sub> in the system with NO was attributed to RO<sub>2</sub>+NO facilitating the necessary alkoxy steps in the formation of C<sub>10</sub>H<sub>15</sub>O<sub>x</sub>-HOM-RO<sub>2</sub>, while its reduced importance in the system with HO<sub>2</sub> was attributed to the suppression of alkoxy formation from RO<sub>2</sub>+RO<sub>2</sub> by RO<sub>2</sub>+HO<sub>2</sub>.

The “in-between” behavior in the mixed system indicates that HO<sub>2</sub> is indeed able to compete with the alkoxy formation from RO<sub>2</sub>+NO in some cases, suppressing some C<sub>10</sub>H<sub>15</sub>O<sub>x</sub> formation and thus increasing the importance of the C<sub>10</sub>H<sub>17</sub>O<sub>x</sub> family. The increased importance of C<sub>10</sub>H<sub>17</sub>O<sub>x</sub> is supported by the ratio of products clearly assignable to one C<sub>10</sub>-HOM-RO<sub>2</sub> family. This measure was introduced in the pure NO system (Section 4.2.3) and Figure 30 showed that in the base case the ratio of (C<sub>10</sub>H<sub>18</sub>O<sub>z</sub> + C<sub>10</sub>H<sub>17</sub>NO<sub>z</sub>) to (C<sub>10</sub>H<sub>14</sub>O<sub>z</sub> + C<sub>10</sub>H<sub>15</sub>NO<sub>z</sub>) was 0.69±0.02 while it was significantly lower with NO present, dropping to 0.47±0.01 at [NO]<sub>ss</sub>=0.2 ppbv. In the middle NO, high HO<sub>2</sub> case the ratio was 0.73±0.02 at a very similar steady-state NO concentration. The results have to be interpreted carefully, keeping the importance of C<sub>10</sub>H<sub>16</sub>O<sub>z</sub> in the mixed system in mind. However, the observation of a high ratio of clear C<sub>10</sub>H<sub>17</sub>O<sub>x</sub> products to clear C<sub>10</sub>H<sub>15</sub>O<sub>x</sub> products, as well as the similarity to the ratio

measured in the base case, do support an increased importance of C<sub>10</sub>H<sub>17</sub>O<sub>x</sub> compared to the system with only NO and a compensation of the effects of HO<sub>2</sub> and NO in the mixed system.

An explanation for the changes in importance of the C<sub>10</sub>-HOM-RO<sub>2</sub> families could be the interference of HO<sub>2</sub> preventing the formation of crucial alkoxy radicals required in the formation pathway of C<sub>10</sub>H<sub>15</sub>O<sub>x</sub>-HOM-RO<sub>2</sub>. The application of generic reaction rate coefficients and the grouping into product classes, families etc. is too general to capture if HO<sub>2</sub> can compete with NO for the formation of a specific hydroperoxide instead of an alkoxy radical needed in the formation of C<sub>10</sub>H<sub>15</sub>O<sub>x</sub> (H-abstraction or pinonaldehyde-like pathway). This is the limit of a generalized chemistry approach. Here, an investigation of the specific intermediates expected in the C<sub>10</sub>H<sub>15</sub>O<sub>x</sub> formation pathway would be needed to gain further information.

Measurements with an amine-CIMS of C<sub>10</sub>H<sub>16</sub>O<sub>2</sub> (formula composition of pinonaldehyde) showed a reduction of about 25 % in the middle NO, high HO<sub>2</sub> case (for details see Appendix **Section A.11.3**). The similar reduction of C<sub>10</sub>H<sub>16</sub>O<sub>2</sub> in the high HO<sub>2</sub> case (**Section 4.1.2**) indicates that indeed this suppression effect by HO<sub>2</sub> could persist even with expected similar contribution to the chemical reaction pool by NO and HO<sub>2</sub>.

In summary, multiple observations point to a similar contribution of the C<sub>10</sub>-HOM-RO<sub>2</sub> families as were observed in the base case. Thereby, the C<sub>10</sub>H<sub>17</sub>O<sub>x</sub> family had a larger contribution than in the NO dominated case, but smaller than in the HO<sub>2</sub> dominated case. These changes are likely associated with the ability of the reactants to facilitate or suppress the alkoxy radical formation. Our observations indicate that HO<sub>2</sub> intervenes in the formation of C<sub>10</sub>H<sub>15</sub>O<sub>x</sub>, possibly by suppressing important C<sub>10</sub>H<sub>16</sub>O<sub>x</sub> precursors and thus HOMs formed by secondary oxidation. In a similar way also HOMs from the H-abstraction path (Shen et al., 2022) could be suppressed by presence of high HO<sub>2</sub>.

#### 4.3.4 Competition for termination group formation in the system with NO and high HO<sub>2</sub>

The availability of both NO and HO<sub>2</sub> for termination of the HOM-RO<sub>2</sub> resulted in a competition between the formation of the respective functional groups. Termination with NO will result in the formation of an organic nitrate group, while with HO<sub>2</sub> the formation of a hydroperoxide group is expected. Thus, the prevalence of these termination groups can be used to gain insight into the importance of the reaction partners and to investigate if our generic framework describes the competition appropriately.

In general, the same ON-HOM species as in the system with only NO added (**Section 4.2.5**) were observed and a list of all identified species can be found in Appendix **Section A.6.2**. ON compounds were observed in the HOM-Frag and HOM-Mon product classes. The contribution of ON-HOM can be directly compared to the expected contribution of NO to the chemical reaction pool as the formation of ON-HOM is uniquely connected to the reaction with NO. The expected linear

relationship between ON-HOM contribution to the HOM product sum and the contribution of NO to the chemical sink (assuming an unchanging branching ratio into alkoxy radical formation) was introduced in Section 4.2.5. Figure 43 shows the data from the system with NO and high HO<sub>2</sub> added to the results shown for the cases with only NO addition (Figure 34). For the system with NO and high HO<sub>2</sub>, besides to the middle NO and the two high NO cases, an additional steady state with an in-between NO concentration was utilized. The experimental details of this steady state can be found in Appendix Section A.11.2.

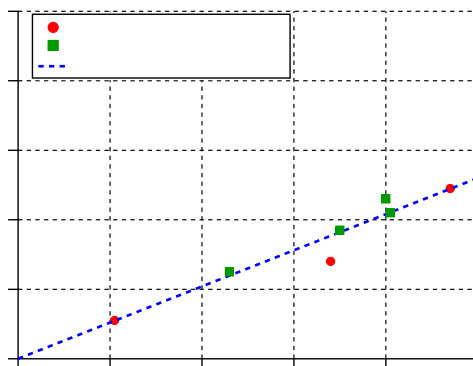


**Figure 43** Contribution of measured ON-HOM to the overall product sum as a function of the RO<sub>2</sub>+NO contribution to the RO<sub>2</sub> chemical sink. The linear fit is constrained through the zero point. Red circles represent data from the system with just NO addition. Green squares represent data from the system with NO and HO<sub>2</sub> addition. As the calculation of the RO<sub>2</sub>+NO contribution is based on general bulk reaction rate coefficients and modeling results, large absolute uncertainties apply.

In Figure 43 the contribution of ON-HOM to the overall HOM products shows a linear correlation with the expected contribution of RO<sub>2</sub>+NO to the overall chemical reaction pool. Furthermore, it fits well to the observations in the system with only NO addition. The results from the system with NO and high HO<sub>2</sub> minimally shifted the slope of the linear fit higher. The slope of the fit of 0.52 supports the previous conclusion of an ON-HOM yield of about 50 % in the reaction HOM-RO<sub>2</sub>+NO. This agrees with the molar yield reported by Pullinen et al. (2020) and compares to the regularly assumed branching ratio of 0.3 – 0.4 of RO<sub>2</sub>+NO into ON formation (see Section 2.1.2). The good correlation between ON-HOM contribution and expected RO<sub>2</sub>+NO termination shows that our generic chemical framework captures the actual termination to closed shell products (at least relative to each other) quite well.

The impact of termination with HO<sub>2</sub> (hydroperoxide termination group) was investigated via the contribution of the different non-ON HOM-Mon families to the overall non-ON HOM-Mon sum. Figure 44 shows the contribution in the middle NO, high HO<sub>2</sub> case (top row) as well as the

comparison cases (bottom row). The contribution of the non-ON HOM-Mon families to the non-ON HOM-Mon sum in the high NO, high HO<sub>2</sub> case can be found in Appendix Table A15.

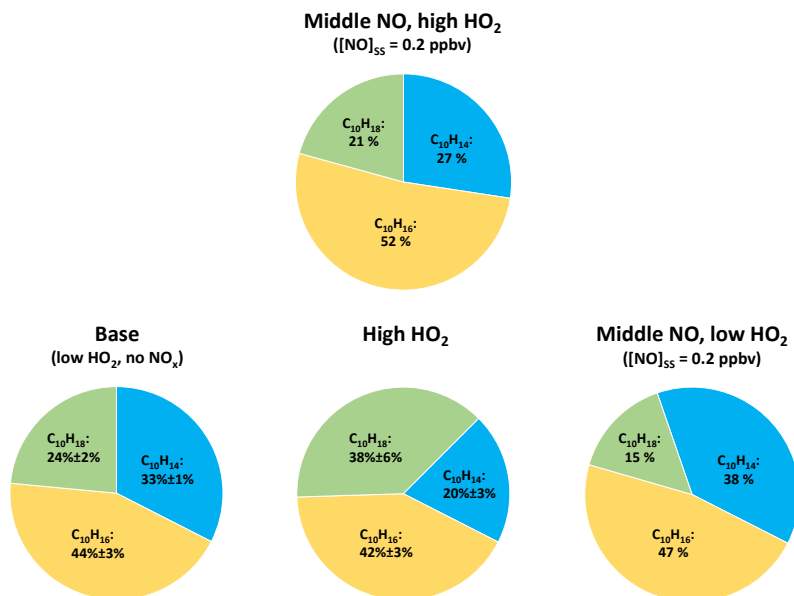


**Figure 44** Contribution of the C<sub>10</sub>H<sub>14</sub>O<sub>z</sub>, C<sub>10</sub>H<sub>16</sub>O<sub>z</sub>, and C<sub>10</sub>H<sub>18</sub>O<sub>z</sub> family to the non-ON HOM-Mon signal in the middle NO, high HO<sub>2</sub> case (top row) in comparison to the low HO<sub>2</sub>, NO<sub>x</sub>-free base case, the high HO<sub>2</sub> case and the middle NO, low HO<sub>2</sub> case (bottom row) (all experiments unseeded).

Compared to the base case (bottom row, left), the contribution by C<sub>10</sub>H<sub>14</sub>O<sub>z</sub> decreased, while the contribution of C<sub>10</sub>H<sub>16</sub>O<sub>z</sub> increased (by about 8 %). The decrease of contribution by C<sub>10</sub>H<sub>14</sub>O<sub>z</sub> (clear C<sub>10</sub>H<sub>15</sub>O<sub>x</sub> product) reflects the decrease of contribution by C<sub>10</sub>H<sub>15</sub>O<sub>x</sub> to the overall C<sub>10</sub>-HOM-RO<sub>2</sub> (see Section 4.3.3). However, with an expected 50 % contribution of RO<sub>2</sub>+HO<sub>2</sub> termination and the assumption of a similar C<sub>10</sub>H<sub>15</sub>O<sub>x</sub> to C<sub>10</sub>H<sub>17</sub>O<sub>x</sub> ratio as in the base case, a higher contribution of C<sub>10</sub>H<sub>18</sub>O<sub>z</sub> should be expected from the C<sub>10</sub>H<sub>17</sub>O<sub>x</sub>+HO<sub>2</sub> termination. The comparison to the high HO<sub>2</sub> case (bottom row, center) instead shows that in the middle NO, high HO<sub>2</sub> case, C<sub>10</sub>H<sub>18</sub>O<sub>z</sub> had a much lower contribution, while C<sub>10</sub>H<sub>16</sub>O<sub>z</sub> had an about 10 % higher contribution. The comparison to the middle NO case (bottom row, right) highlights again the higher importance of C<sub>10</sub>H<sub>15</sub>O<sub>x</sub> in the system with only NO addition, with an about 10 % lower contribution by C<sub>10</sub>H<sub>14</sub>O<sub>z</sub> in the system with NO and HO<sub>2</sub>. The middle NO case was also the only case with an even lower contribution of C<sub>10</sub>H<sub>18</sub>O<sub>z</sub>.

The unexpectedly low contribution of C<sub>10</sub>H<sub>18</sub>O<sub>z</sub> in the middle NO, high HO<sub>2</sub> case can be explained if another reaction contributes significantly to the sink of C<sub>10</sub>H<sub>17</sub>O<sub>x</sub>. One possibility that was already discussed for the system with only NO addition (Section 4.2.3) is a higher branching ratio into ON products. However, as detailed in Section 4.2.3, this would result in a higher-than-expected contribution of C<sub>10</sub>H<sub>17</sub>NO<sub>2</sub> to the product sum of clear C<sub>10</sub>H<sub>17</sub>O<sub>x</sub> products (C<sub>10</sub>H<sub>18</sub>O<sub>z</sub> + C<sub>10</sub>H<sub>17</sub>NO<sub>2</sub>).

Figure 45 shows the contribution of the C<sub>10</sub>H<sub>18</sub>O<sub>z</sub> HOM-Mon family to the sum of C<sub>10</sub>H<sub>18</sub>O<sub>z</sub> + C<sub>10</sub>H<sub>17</sub>NO<sub>z</sub>, plotted against the expected contribution of the RO<sub>2</sub>+HO<sub>2</sub> termination to the chemical reaction pool. The data points represent the mixed system cases with NO and high HO<sub>2</sub> (green square markers) as well as an extra data point for the high NO case from the pure NO system (red circle marker). As the termination of RO<sub>2</sub>+RO<sub>2</sub> also forms C<sub>10</sub>H<sub>18</sub>O<sub>z</sub>, in this comparison only cases were used, where the contribution of RO<sub>2</sub>+RO<sub>2</sub> termination was negligible.

We constraint the linear fit through the 1-to-1 point as in a hypothetical system with the RO<sub>2</sub>+HO<sub>2</sub> termination contributing 100%, C<sub>10</sub>H<sub>18</sub>O<sub>z</sub> is the only clear C<sub>10</sub>H<sub>17</sub>O<sub>x</sub> product and therefore would contribute 100 % to the C<sub>10</sub>H<sub>17</sub>O<sub>x</sub> product sum.

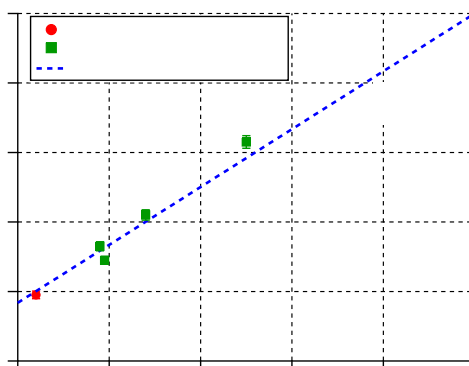


**Figure 45** Contribution of C<sub>10</sub>H<sub>18</sub>O<sub>z</sub> sum to clear C<sub>10</sub>H<sub>17</sub>O<sub>x</sub> product sum (C<sub>10</sub>H<sub>18</sub>O<sub>z</sub> + C<sub>10</sub>H<sub>17</sub>NO<sub>z</sub>) as a function of the calculated RO<sub>2</sub>+HO<sub>2</sub> contribution to the RO<sub>2</sub> chemical sink. Green squares represent data from system with NO and high HO<sub>2</sub> (middle NO, in-between NO and the two high NO cases). Red circle shows data of high NO case in pure NO system. Linear fit is constrained through 1-to-1 point. As the calculation of the RO<sub>2</sub>+HO<sub>2</sub> contribution is based on general bulk calculations and modeling results large uncertainties apply.

The correlation between the contribution of C<sub>10</sub>H<sub>18</sub>O<sub>z</sub> and the expected RO<sub>2</sub>+HO<sub>2</sub> termination contribution yielded a good linear fit. This result supports the conclusions from the system with just NO addition (Section 4.2.3) that C<sub>10</sub>H<sub>17</sub>O<sub>x</sub> does not have a higher-than-expected branching ratio into ON products. The good linear correlation with the expected contribution by the RO<sub>2</sub>+HO<sub>2</sub> termination reaction justifies once more the usefulness of the generic framework we developed to describe the chemical sinks.

The question remains why a higher-than-expected contribution by the C<sub>10</sub>H<sub>16</sub>O<sub>z</sub> HOM-Mon family to the non-ON HOM-Mon product sum was observed. The second possible reaction pathway for C<sub>10</sub>H<sub>17</sub>O<sub>x</sub> that should be considered is internal termination. Piletic and Kleindienst (2022) calculated fast reaction rate coefficients for specific C<sub>10</sub>H<sub>17</sub>O<sub>5</sub> internal termination pathways.

In Section 4.1.5 it was already discussed that internal termination is an important reaction path for C<sub>10</sub>H<sub>15</sub>O<sub>x</sub> in both the base case, as well as the system with high HO<sub>2</sub>. Furthermore, internal termination

of C<sub>10</sub>H<sub>15</sub>O<sub>x</sub> alkoxy radicals could play a role, as discussed in the system with NO addition (**Section 4.2.3**). In analogy, internal termination of C<sub>10</sub>H<sub>17</sub>O<sub>x</sub> will form a C<sub>10</sub>H<sub>16</sub>O<sub>x-1</sub> HOM-Mon (carbonyl termination) and OH.

Internal termination of C<sub>10</sub>H<sub>17</sub>O<sub>x</sub> would explain the larger than expected formation of C<sub>10</sub>H<sub>16</sub>O<sub>z</sub>-HOM compounds. In presence of NO, formation of C<sub>10</sub>H<sub>17</sub>O<sub>x</sub>-RO and subsequent internal termination may contribute to C<sub>10</sub>H<sub>16</sub>O<sub>z</sub>. This would explain why enhanced C<sub>10</sub>H<sub>16</sub>O<sub>z</sub> and reduced C<sub>10</sub>H<sub>18</sub>O<sub>z</sub> were especially visible in the system with NO and high HO<sub>2</sub>. NO facilitates alkoxy radical formation, and the missing C<sub>10</sub>H<sub>18</sub>O<sub>z</sub> products are especially noteworthy when a significant contribution of RO<sub>2</sub>+HO<sub>2</sub> termination is expected.

Overall, the ON-HOM production behaved as expected within our generic framework describing the HOM-RO<sub>2</sub> termination. The same was observed for the contribution of the C<sub>10</sub>H<sub>18</sub>O<sub>z</sub> HOM products as an indicator for the termination of RO<sub>2</sub>+HO<sub>2</sub>. Both results indicate that the competition between termination with NO and HO<sub>2</sub> is captured in the generic framework. However, the contribution of the non-ON HOM-Mon families revealed the importance of internal termination reactions for C<sub>10</sub>H<sub>17</sub>O<sub>x</sub>, as for C<sub>10</sub>H<sub>15</sub>O<sub>x</sub>, with possible contribution via HOM-alkoxy radicals. The middle NO, high HO<sub>2</sub> case, with its similar expected contribution of termination with NO and HO<sub>2</sub>, was especially helpful for these considerations.

#### 4.3.5 Changes in HOM alkoxy radical chemistry in the system with NO and high HO<sub>2</sub>

This section will further specify changes in the HOM-Frag product class as fragmentation is an important alkoxy radical reaction pathway. Afterwards the observed impacts of alkoxy radical formation in the mixed system with NO and HO<sub>2</sub> are summarized.

The contribution of the HOM-Frag product class in the mixed was very similar to the NO addition case (47 % compared to 44 %) and about 10 % higher than in the base or high HO<sub>2</sub> case (see **Figure 41**). As fragmentation is often facilitated by alkoxy radicals, a lower contribution in the presence of HO<sub>2</sub> should be expected. However, the HOM-Frag contribution also did not change significantly between base and high HO<sub>2</sub> case (see **Section 4.1.1** and **4.1.4**), with differences mainly in the different HOM-Frag product groups (C<sub>5-9</sub>). The changes in the HOM-Frag product groups in the middle NO, high HO<sub>2</sub> case compared to the base case are shown in **Figure 46** in the righthand bars. In comparison changes in the high HO<sub>2</sub> case (lefthand bars) and middle NO case (center bars) are also shown.

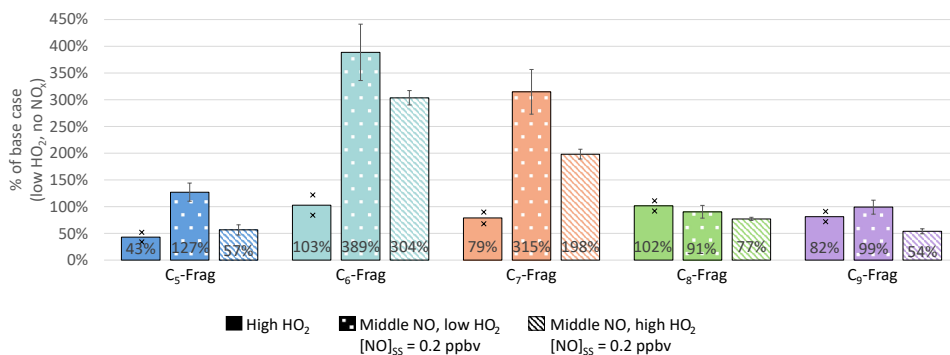


**Figure 46** Overview of relative change in HOM-Frag groups detected in NO<sub>3</sub>-CIMS in the high HO<sub>2</sub> system (lefthand bars), the middle NO, low HO<sub>2</sub> system (center bars) and the middle NO, high HO<sub>2</sub> system, (righthand bars), all in comparison to the low HO<sub>2</sub>, NO<sub>x</sub> free base case (unseeded experiments, all data normalized to  $\alpha$ -pinene OH turnover). Middle NO case from apinNO [10] experiment and middle NO, high HO<sub>2</sub> from apinCONO\_1 [10] experiment, for these two the base case is from experiment apinCO\_2 and error bars were determined via error propagation. For the high HO<sub>2</sub> case bars represent average relative change from apinCO\_1 and apinCO\_2 (base case within the experiments) and markers individual experiments.

The comparison shows that the mixed system yielded an overlap of the effects observed in the systems with one dominant reactant. The changes are in-between the one reactant systems for C<sub>5</sub>- to C<sub>7</sub>-HOM-Frag, which indicates competing effects of HO<sub>2</sub> and NO. In the C<sub>8</sub>-HOM-Frag and C<sub>9</sub>-HOM-Frag, the mixed system had stronger reductions than the systems with one dominant reactant. For the C<sub>8</sub>-HOM-Frag, the overall changes observed in both the high HO<sub>2</sub> and middle NO system were minor indicating that an important reaction path into this group is not disturbed by either reactant (also see **Section 4.1.3**). A reduction of about 20 % was observed in the mixed case. For C<sub>9</sub>-HOM-Frag, a significant reduction compared to both one dominant reactant systems was observed. A reason for this could be a reduction in the source term due to interference in the autoxidation chain, as the observed reduction in C<sub>9</sub>-HOM-Frag is similar to the reduction observed in HOM-Mon and the overall HOM reduction.

The contributions of the different product groups to the HOM-Frag class compared to the NO addition and HO<sub>2</sub> addition cases is shown in **Figure 47**. In the mixed system, the contribution of C<sub>5</sub> and C<sub>8</sub> were between the contributions of the one dominant reactant systems. This observation corroborates opposing effects of HO<sub>2</sub> and NO: NO and the increased alkoxy radical formation increased the importance of C<sub>5</sub>, but less than in the system with only NO due to the competition of reaction of RO<sub>2</sub> with HO<sub>2</sub>. C<sub>8</sub>-HOM-Frag were the most important contributor to the HOM-Frag class in the high HO<sub>2</sub> case (contribution of about 50 %) and were still more important in the middle NO, high HO<sub>2</sub> than in the middle NO case. The similar contribution from C<sub>6</sub> and C<sub>7</sub>-HOM-Frag as in the pure NO addition case indicates the existence of fast alkoxy radical pathways into these HOM-Frag groups.

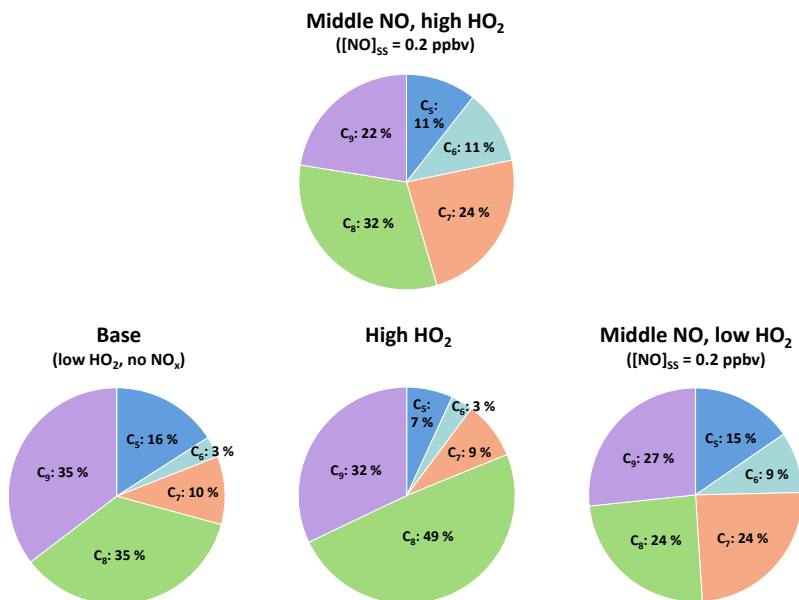


**Figure 47** Contribution of the C<sub>5</sub>- to C<sub>9</sub>-HOM Frag groups to the HOM-Frag signal in the middle NO, high HO<sub>2</sub> case (top row) in comparison to the low HO<sub>2</sub>, NO<sub>x</sub>-free base case, the high HO<sub>2</sub> case and the middle NO, low HO<sub>2</sub> case (bottom row) (all experiments unseeded).

The stronger reduction of C<sub>9</sub> than in either of the one reactant systems points towards a decrease in its specific sources. C<sub>5</sub> (60 % to 80 % of base case when going from middle to high NO at high HO<sub>2</sub>) and C<sub>9</sub> (60 % to 70 % of base case) were the only HOM-Frag groups showing an increase with increasing NO level in the mixed system. **Figure A7** in the Appendix shows the changes in the middle NO, high HO<sub>2</sub> and high NO, high HO<sub>2</sub> cases side by side. This indicates that the higher contribution of RO<sub>2</sub>+NO termination in the high NO, high HO<sub>2</sub> case (expected 80 %) results in more formation of these compounds even at the high overall chemical reaction rate coefficient. In contrast, the other HOM-Frag groups showed a decrease with increasing NO, probably due to the overall high chemical reaction rate coefficient reducing the entry channels into HOM production.

In summary it could be observed that the alkoxy formation from RO<sub>2</sub>+NO still played an important role in facilitating fragmentation in the mixed system. NO still increased the formation of C<sub>7</sub>-HOM-Frag (and C<sub>6</sub>-HOM-Frag). However, the reduction in the C<sub>5</sub>-HOM-Frag family indicates that RO<sub>2</sub>+HO<sub>2</sub> reactions can compete with the alkoxy radical formation in some cases. Still, a much higher influence of alkoxy radical formation than in the system dominated by HO<sub>2</sub> was observed.

For all systems, favoring alkoxy radical formation increases the importance of the C<sub>10</sub>H<sub>15</sub>O<sub>x</sub>-HOM-RO<sub>2</sub> family, probably due to alkoxy steps necessary in the formation of C<sub>10</sub>H<sub>15</sub>O<sub>x</sub>-HOM-RO<sub>2</sub>. The increased importance of C<sub>10</sub>H<sub>15</sub>O<sub>x</sub> was very pronounced in the system with only NO addition (see **Section 4.2.3**), while C<sub>10</sub>H<sub>15</sub>O<sub>x</sub> was suppressed in the high HO<sub>2</sub> system (see **Section 4.1.3**). In total this results in

compensating effects in the mixed system with contribution of C<sub>10</sub>H<sub>15</sub>O<sub>x</sub> and C<sub>10</sub>H<sub>17</sub>O<sub>x</sub>-HOM-RO<sub>2</sub> more similar to the base case. Furthermore, internal termination of HOM-RO, analogous to the internal termination of HOM-RO<sub>2</sub>, may contribute to HOMs as this could explain the high prevalence of carbonyl group termination products (C<sub>10</sub>H<sub>14</sub>O<sub>z</sub>, C<sub>10</sub>H<sub>16</sub>O<sub>z</sub>) compared to hydroperoxide group termination products from HO<sub>2</sub>. This would also fit the smaller reductions in the C<sub>10</sub>H<sub>14</sub>O<sub>z</sub> family's steady-state concentration compared to the observed decrease in the C<sub>10</sub>H<sub>15</sub>O<sub>x</sub> family's steady-state concentration. To our knowledge internal termination pathways of alkoxy radicals have not been described before and thus this hypothesis should receive some attention in future studies.

#### 4.3.6 Impact of combined NO and high HO<sub>2</sub> on condensable organic mass

The change in the gas-phase signal of the HOM product classes after seed addition can be seen in **Figure 48** for selected cases: In the figure the middle NO, high HO<sub>2</sub> case (righthand bars) is shown in comparison to the base case, as well as the high HO<sub>2</sub> case, and pure middle NO case.

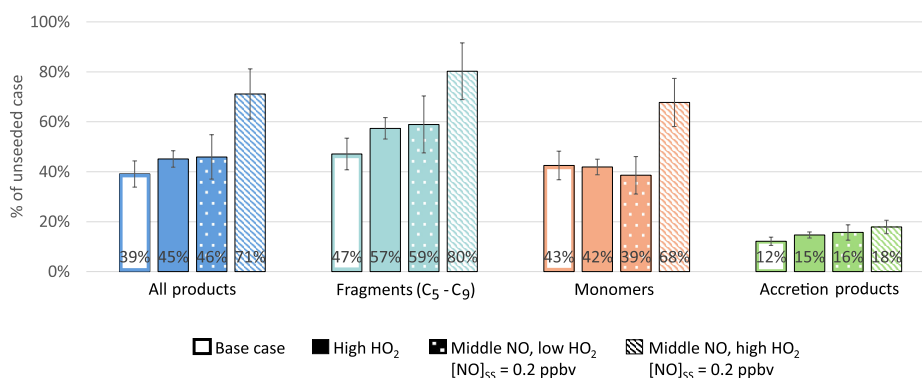


**Figure 48** Overview of relative change in signal in product classes between unseeded and seeded case in the middle NO, high HO<sub>2</sub> system. (Base case and high HO<sub>2</sub> case from experiment apinCO<sub>2</sub>, middle NO, low HO<sub>2</sub> case from apinNO [10].) All data normalized with  $\alpha$ -pinene OH turnover. Error bars via error propagation, for more information see Appendix Section A.5.

In the mixed system the overall signal, as well as the HOM-Frag and HOM-Mon class, had significantly larger signal remaining in the seeded system than was observed in the base case. Both the high HO<sub>2</sub> system and the system with only NO addition, showed already somewhat larger fractions remaining in the gas phase. However, the mixed middle NO, high HO<sub>2</sub> case showed an about 20% larger gas-phase fraction remaining with seed for overall products, HOM-Frag and HOM-Mon. The fraction remaining for HOM-Acc was similar for all systems, as expected for the low volatility HOM-Acc.

In the system with NO (see **Section 4.2.6**) the higher signal remaining in the gas phase was explained by the higher volatility of the ON compounds. However, in the middle NO, high HO<sub>2</sub> system also the non-ON compounds showed higher fractions remaining compared to the base case. The overall ON

compounds showed similar behavior as in the NO addition case ( $70 \pm 10\%$  compared to  $65 \pm 13\%$  signal remaining with seed), but here as well, some differences in the HOM-Frag and HOM-Mon product classes were observed (for details see Appendix Table A19).

Looking at the fraction remaining of the individual HOM compounds (Figure 49), the reason for the high overall fractions remaining in the middle NO, high HO<sub>2</sub> becomes clearer: Some non-ON HOM-Frag and non-ON HOM-Mon not only showed higher fractions remaining compared to the other cases, but also showed fractions remaining larger than 1. A fraction remaining larger 1 beyond the error estimation indicates heterogeneous production of these products. Weak indications of heterogenous production were also seen for a few HOM compounds in the high HO<sub>2</sub> system, although no fraction remaining larger 1 *beyond* the error estimation was observed (see Section 4.1.6).

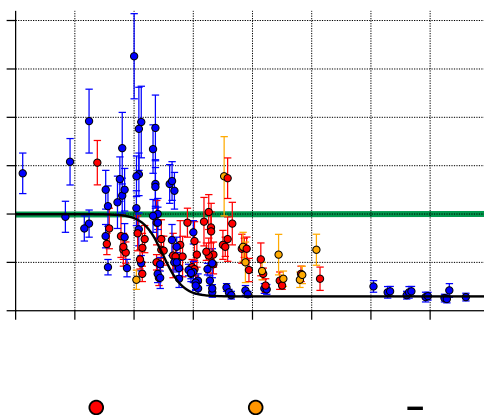


**Figure 49** Gas-phase fraction remaining in presence of seed for the middle NO, high HO<sub>2</sub> case (apinCONO\_1 [10] experiment). All data is normalized with  $\alpha$ -pinene OH turnover. Points represent compounds that were detected with relative standard deviation <30 % in both experiment phases. Error bars represent result of error propagation (see Appendix Section A.5).

Only in the middle NO, high HO<sub>2</sub> case a significant portion of products with fractions remaining larger than 1 were observed. In addition, the system showed further indications of ongoing chemical processes: In the steady state with seed the Br-CIMS measured an about 30 % higher HO<sub>2</sub> cluster signal compared to the unseeded state indicating an additional HO<sub>2</sub> production process.

A possibly important heterogenous reaction is the hydrolysis of ON-HOM compounds as this pathway is known to affect particulate organic nitrates (Zare et al., 2019). A simple general equation for such an ON hydrolysis reaction can be seen in (R4-1). If an ON-HOM undergoes hydrolysis depends on its specific structure. Additionally, the pH of the particulate aqueous phase may be important as acidic conditions can increase the hydrolysis rate (Zhao et al., 2023).



In reaction (**R4-1**) the former ON compound forms an alcohol group from the ON functional group and HNO<sub>3</sub> is lost from the molecule. If the formed alcohol is volatile enough it could evaporate, leading to a reduction in organic particulate mass and possibly explaining a fraction remaining larger 1. If the hydrolysis leads to the evaporation of small, oxidized VOCs that can produce HO<sub>2</sub>, this could also explain the higher HO<sub>2</sub> signal. Even only the evaporation of smaller products (and no evaporation of products observable in the NO<sub>3</sub>-CIMS with higher oxidation degree), could explain the observation if they contribute to HO<sub>2</sub>. In this case the chemical system is shifted, which could lead to fractions remaining larger 1 for HO<sub>2</sub> derived products.

Hydrolysis of ON, however, can only be part of the explanation as no increase in HO<sub>2</sub> signal or significant fractions larger than 1 were observed in the system with NO without high HO<sub>2</sub>. This raises the question of the impact of higher HO<sub>2</sub> concentration on the suspected heterogenous reactions. A possible factor could be the uptake of HO<sub>2</sub> in the aerosol (as discussed in the literature, see for example Dyson et al. (2023)), however no reduction in the HO<sub>2</sub> signal was observed with seed in the high HO<sub>2</sub> system (see **Figure 9**). In the mixed system more HO<sub>2</sub> was observed in the gas phase with seed in the system, which as mentioned above could be due to heterogeneous fragmentation as a source of small, oxidized VOCs, which increase HO<sub>2</sub> production.

No strong indications of heterogeneous production were observed in the high NO, high HO<sub>2</sub> case. The measured HO<sub>2</sub> concentration was increased, but not significantly. And while we still observed an about 10 % higher fraction remaining of non-ON HOM-Frag (see Appendix **Table A19**), no compounds with fractions remaining significantly larger than 1 (i.e. beyond the error estimation) were observed (**Figure 50**). If heterogeneous production is only of importance in the middle NO, high HO<sub>2</sub> case this could be an indication that the products from RO<sub>2</sub>+HO<sub>2</sub> play a crucial role, which are of less importance in the high NO cases.

The unusual behavior in the middle NO, high HO<sub>2</sub> system needs substantiation by repetitions, which unfortunately could not be done within the time frame of this work. Note that if the chemical system is substantially changed by the seed addition, a simple comparison of the seeded to unseeded case to investigate partitioning is in any case no longer possible.

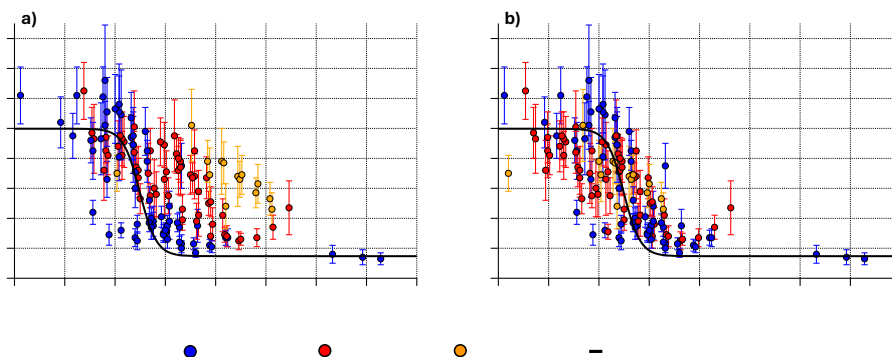


**Figure 50** Gas-phase fraction remaining in presence of seed for the high NO, high HO<sub>2</sub> case (apinCONO\_1 [25] experiment). **a)** all HOM-compounds, **b)** all HOM-compounds with organic nitrate's molar mass being shifted by the nitrate termination group (NO<sub>2</sub>) to ( $M - 46 \text{ g mol}^{-1}$ ) for compounds containing one nitrate group (red markers) and to ( $M - 92 \text{ g mol}^{-1}$ ) for compounds with two nitrate groups (orange markers).

All data normalized with  $\alpha$ -pinene OH turnover. Markers represent compounds that were detected with relative standard deviation <30 % in both experiment phases. Error bars represent result of error propagation (see Appendix Section A.3).

**Figure 50** shows the gas-phase fraction remaining of the individual products in the high NO, high HO<sub>2</sub> case. Here, a group of HOM-Frag and low oxidized HOM-Mon (blue markers below  $230 \text{ g mol}^{-1}$ ) with high fractions remaining can be observed. The high HO<sub>2</sub> case also already showed such a group with higher fractions remaining than in the base case. Thus, a possible explanation, besides heterogenous production, could be a higher importance of the products with high fractions remaining in the system with NO and HO<sub>2</sub>. A reason for this could be the formation of HOM-Frag-RO<sub>2</sub> via the alkoxy pathway facilitated by RO<sub>2</sub>+NO and the consecutive reaction with HO<sub>2</sub> to form the observed more volatile products.

If there are changes in the chemical system between unseeded and seeded case the product distribution in the unseeded case can no longer serve as reference for the seeded case. Nonetheless the comparison could help to understand the system further, e.g. to detect the influence of heterogenous processes. The reduction of organic mass observed in the AMS measurement, as well as the condensable HOM mass proxy calculated from the mass weighted HOM signal in the gas phase (see **Section 3.1.5**) are shown in **Table 2**. For the condensable HOM mass proxy the following molar mass thresholds for condensable compounds determined in the previous sections were applied:  $230 \text{ g mol}^{-1}$  for non-ON HOM (**Section 4.1.6**),  $276 \text{ g mol}^{-1}$  for 1 nitrogen containing ON-HOM and  $322 \text{ g mol}^{-1}$  for 2 nitrogen containing ON-HOM (**Section 4.2.6**). **Figure 50 a)** and **b)** corroborate that these thresholds fit in the mixed system as well.

However, two factors increased the uncertainty of the AMS measurement in the high NO, high HO<sub>2</sub> case: Due to instrument failure data were observed with two different AMS instruments (which could not be intercalibrated). Additionally, the seed concentration in the chamber increased during the

experiment (for the measured concentrations see Appendix Table A12), leading to an increase in the particle sink especially in the high NO, high HO<sub>2</sub> stage.

**Table 2** Overview of the relative change in organic mass observed in the AMS (seeded experiments) and the mass weighted HOM signal that is supposed to condense as observed by NO<sub>3</sub>-CIMS (unseeded experiments) for the system with NO and HO<sub>2</sub> in comparison to the base case. Base cases from within the experiment were used, besides for HOM mass proxy in apinCONO\_1, here the apinCO\_2 base case was used. All data normalized with  $\alpha$ -pinene OH turnover.

<u>Condition</u>	<u>Experiment</u>	<u>Organic mass measurement: % of base case</u>	<u>Condensable HOM mass proxy: % of base case</u>
Middle NO, high HO <sub>2</sub>	apinCONO_1 [10]	65 ± 12 %	47 ± 7 %
High NO, high HO <sub>2</sub>	apinCONO_1 [25]	68 ± 12 %	41 ± 6 %
	apinCONO_2 [25]	40 ± 19 %	38 ± 17 %

In all mixed cases, a reduction in the organic mass was measured. However, in the high NO, high HO<sub>2</sub> case where a repetition was performed, the organic mass reduction showed a discrepancy of around 30 %. Furthermore, for the apinCONO\_1 experiment the agreement between the expected condensable HOM mass from the CIMS measurement and the actual reduction in the organic mass was worse than observed in the previous chapters. The calculation of the condensable HOM mass proxy yielded 20-30 % stronger expected reductions than observed by AMS measurement. This could be either due to actual changes in the chemistry or due to instrumental or experimental effects. If compounds were produced heterogeneously in the particle phase and evaporated back to the gas phase, this could explain the mismatch. In that case, however, the expectation would be a larger-than-expected reduction in the organic mass as the re-evaporation of volatile compounds from the particle phase should reduce the organic mass further. Instead, a smaller than expected decrease in organic mass was measured.

The good agreement observed in the apinCONO\_2 experiment indicates that instrumental or experimental problems could be the reason for the discrepancy in the other two cases, but all in all the results are inconclusive. Repetitions, especially also of the middle NO, high HO<sub>2</sub> case, are necessary to determine if heterogenous production is of importance and to verify and investigate the observations described in this section.

In any case the reduction in organic mass and HOM gas-phase signal fits to the conclusions drawn for the gas phase: The overall HOM concentrations were reduced in both the middle NO, high HO<sub>2</sub> and high NO, high HO<sub>2</sub> case, with especially strong suppression of very low volatile HOM-Acc species. Furthermore, our observations indicate that the HOM, that were still formed, had higher volatility. Two factors mainly contributed to the formation of higher volatility HOM: 1) The formation of ON-HOM compounds who have higher volatility than a non-ON termination product from the same

precursor HOM-RO<sub>2</sub> (see Section 4.2.6). 2) The formation of HOM-Frag compounds. The importance of HOM-Frag increases with NO due to the alkoxy radical formation from RO<sub>2</sub>+NO. Furthermore, we saw indications that the additional availability of HO<sub>2</sub> could lead to the formation of higher volatility HOM-Frag. Overall, the unexpected observation of fractions remaining larger than 1 in the middle NO, high HO<sub>2</sub> case in combination with limited performance of the AMS, requires repetitions of the experiments with seed to reduce the uncertainty in the results.

#### 4.3.7 Summary: Impact of NO and high HO<sub>2</sub> in combination

In the system with both NO and HO<sub>2</sub> as important HOM-RO<sub>2</sub> reaction partners, we observed an overlap of the effects of the individual reactants. The contribution of reaction partner specific termination groups (ON formation for NO, hydroperoxide formation from C<sub>10</sub>H<sub>17</sub>O<sub>x</sub> for HO<sub>2</sub>) showed that the competition between NO and HO<sub>2</sub> fit the expectations of the calculated contribution of the reactants to the chemical sink. This indicates that the generic bulk reaction rates (and modeled reactant concentrations) used for the calculation of the competition were able to capture the distribution between the termination reactions. The applicability of the generalized chemistry scheme is still limited as can be seen in the results for individual reaction pathways.

One important investigation objective was the impact of NO and HO<sub>2</sub> on the alkoxy radical formation in the mixed system and its subsequent impact on the HOM product distribution. It was observed that even in the presence of NO, HO<sub>2</sub> still partially suppresses the importance of the C<sub>10</sub>H<sub>15</sub>O<sub>x</sub>-HOM-RO<sub>2</sub> family. Alkoxy radical formation is expected to be necessary for the formation pathway of C<sub>10</sub>H<sub>15</sub>O<sub>x</sub>-HOM-RO<sub>2</sub>. A decrease in the importance of this family was also observed in the high HO<sub>2</sub> case. In contrast, no significant reduction in the contribution of C<sub>7</sub>-HOM-Frag products to the HOM-Frag family could be determined. The similar contribution of C<sub>7</sub> products in the mixed case compared to the system with only NO addition indicates that here the alkoxy radical formation and subsequent fragmentation is too fast for HO<sub>2</sub> to compete.

Overall, in the mixed system a reduction in HOM products was observed and the suppression of HOM formation from C<sub>10</sub>H<sub>15</sub>O<sub>x</sub> by HO<sub>2</sub> may play an important role in the reduction. However, the large chemical sink for RO<sub>2</sub> in the mixed system can compete with autoxidation reaction rates leading to a reduction of the HOM product source in general.

The reduction in HOM products impacts the SOA formation potential of the system and a reduction in the measured organic mass was observed. However, due to some instrumental/experimental issues, as well as unexpected findings, repetitions of the experiments with seed are necessary. The middle NO, high HO<sub>2</sub> case showed indications of heterogenous production processes for higher volatility products. As this was only observed in one experiment the source of these products is an open

question and further experiments are needed to confirm or disprove the involvement of heterogenous processes.

Nonetheless our gas-phase investigations showed that the measured organic mass decreased not only due to the reduction of HOM product concentration, but also due to the higher volatility of the formed HOM. The molar mass thresholds determined in the one dominant reactant systems were applied in the mixed system to determine a condensable HOM mass proxy. The agreement between particle-phase measurement and the HOM mass proxy in the repetition of the high NO, high HO<sub>2</sub> experiment and more significantly the behavior of fractions remaining of the individual products with increasing molar mass, indicate that the thresholds determined in the one dominate reactant system are applicable to the mixed system as well.

## 5. Summary and Conclusion

In this work, we systematically varied the concentration of RO<sub>2</sub>, HO<sub>2</sub>, and NO in  $\alpha$ -pinene photooxidation experiments with the goal to elucidate their effect on the gas-phase HOM product distribution and thus the SOA formation potential of the system.

We performed a series of experiments in the reaction chamber SAPHIR-STAR and compared the steady states of the different chemical regimes. To assure comparability and to exclude effects by oxidant scavenging, we developed an experimental protocol to keep the primary  $\alpha$ -pinene oxidation conditions constant. We used generic bulk reaction rate coefficients together with model calculations to classify our experiments based on the expected contribution of RO<sub>2</sub>, HO<sub>2</sub> and NO to the overall HOM-RO<sub>2</sub> reactions. Herein, RO<sub>2</sub> denotes the sum of all peroxy radicals as defined in the MCMv.3.3.1 mechanism. We furthermore compared the reaction rate for the bimolecular reactions to an expected average autoxidation rate to assess if termination reactions interfere with the autoxidation chain. An interference in the autoxidation chain will result in lower HOM concentrations and a lower oxidation degree of the products, which in turn will reduce the SOA formation potential.

To understand the changes in gas and particle phase, our focus was the analysis of the gas-phase HOM product distribution. Here, we applied a generic  $\alpha$ -pinene HOM-RO<sub>2</sub> chemistry scheme to relate the observed changes to the shift in the chemical regime. To relate the changes in the HOM product distribution to their impact on the SOA formation potential, we applied targeted seed additions to directly probe the condensation of the HOM products, which is a measure of their volatility.

We chose the RO<sub>2</sub> dominated  $\alpha$ -pinene photooxidation system as a basis for comparison, as this “base case” represents a simple, typical laboratory set-up. We compared the base case to cases with high HO<sub>2</sub>, cases with different levels of NO, as well as cases with both high HO<sub>2</sub> and different levels of NO. Compared to the base case, the HOM concentration and SOA formation potential decreased to varying degrees in all systems. The investigation into the mechanistic reasons for the reduction led to a series of insights, which we relate to four general, important aspects impacting the SOA formation potential:

- 1) The ability of high bimolecular reaction rates to interfere with the autoxidation chain.
- 2) The ability of the reactants to intervene in a specific reaction step, that is crucial for HOM formation.
- 3) The ability of the reactants to facilitate or suppress alkoxy radical formation (which is in direct relation to point 2)).
- 4) The formation of products or termination groups, which impact the HOM product distribution’s volatility.

Our study highlights the importance of considering the different contributions to the HOM-RO<sub>2</sub> sink by HO<sub>2</sub>, RO<sub>2</sub>, and NO, in competition to autoxidation and wall losses, when designing experiments and transferring laboratory results to the real atmosphere. The following sections give a concise overview of the most important findings for the different systems, as the detailed results were summarized at the end of each chapter.

## 5.1 Impact of HO<sub>2</sub> and NO on HOM formation chemistry

Reactions of both HO<sub>2</sub> and NO strongly compete with the cross reactions of RO<sub>2</sub>, which leads to a strong suppression of HOM-Acc products. As expected from the generic chemistry scheme, HOM-RO<sub>2</sub>+HO<sub>2</sub> results in a shift in the formed termination groups from carbonyl, formed by RO<sub>2</sub> cross reactions, to hydroperoxide groups. HOM-RO<sub>2</sub>+NO termination results in the formation of ON-HOM containing nitrate groups. An ON-HOM contribution to all HOMs of around 50 % was observed when NO dominated the HOM-RO<sub>2</sub> termination. The findings in all systems also point towards significant importance of internal termination reactions of HOM-RO<sub>2</sub> forming a carbonyl group.

High HO<sub>2</sub> partially suppresses the alkoxy radical formation from RO<sub>2</sub>+RO<sub>2</sub>, which in the absence of NO can be detected by changes in the oxygen parity of the C<sub>10</sub>-HOM-RO<sub>2</sub> and the reduction of small (C<sub>5</sub>) fragmentation products. However, our observations still indicate significant involvement of alkoxy steps at high HO<sub>2</sub>. One indicator for this is the continued substantial importance of the C<sub>10</sub>H<sub>15</sub>O<sub>x</sub>-HOM-RO<sub>2</sub> family at high HO<sub>2</sub>. Alkoxy radical formation is expected to be crucial for C<sub>10</sub>H<sub>15</sub>O<sub>x</sub> formation independent of if C<sub>10</sub>H<sub>15</sub>O<sub>x</sub> is formed directly or by secondary oxidation (H-abstraction, pinonaldehyde-like pathway, respectively). However, C<sub>10</sub>H<sub>15</sub>O<sub>x</sub>-HOM-RO<sub>2</sub> did show a stronger reduction than expected from a simple increase in the chemical sink by HO<sub>2</sub>. This indicates that HO<sub>2</sub> intervenes in a crucial reaction for *some* HOM formation pathways. Interestingly, the same effect was observed in the system with both high HO<sub>2</sub> and NO, indicating that the specific HO<sub>2</sub> reaction is likely even fast enough to compete with the fast alkoxy radical formation by RO<sub>2</sub>+NO.

Alkoxy radical formation had a strong influence on the HOM product distribution in the system with NO, resulting in high importance of HOM-Frag (C<sub>5</sub>-C<sub>9</sub>), especially C<sub>7</sub>-HOM-Frag and high importance of the C<sub>10</sub>H<sub>15</sub>O<sub>x</sub>-HOM-RO<sub>2</sub> family and its closed-shell products. In the mixed system, an overlap of the individual effects of HO<sub>2</sub> and NO was observed: HO<sub>2</sub> continued to partially suppress the importance of C<sub>10</sub>H<sub>15</sub>O<sub>x</sub>. But the contribution of C<sub>7</sub>-HOM-Frag was similar to the system with just NO, indicating that for these reaction pathways alkoxy radical formation and subsequent fragmentation prevails. This is the limit of applying a generalized chemistry scheme and requires the consideration of individual formation pathways.

The distribution between the functional groups formed in termination (i.e. hydroperoxide or ON) agreed well with the contribution of RO<sub>2</sub>, HO<sub>2</sub> and NO determined via bulk reaction rate coefficients

and model results. The good agreement indicates that our framework captures the general (relative) importance of the three different reaction partners.

## 5.2 Impact of changed HOM formation chemistry on SOA formation

The targeted seeding allowed the direct comparison of HOM concentration lost from the gas phase to the formed organic particle mass concentration, at the same time reflecting the changes in the gas-phase product distribution of the condensing HOM.

All investigated chemical regimes showed a decrease in SOA formation potential compared to the base case. Besides the overall reduction of HOM products, the reduction of low volatility HOM-Acc was a key process for the SOA reduction. Here, the missing formation of HOM-Acc via HOM-RO<sub>2</sub> with lower oxidized RO<sub>2</sub> is crucial for the decrease in SOA formation, as it scavenges lower oxidized products that otherwise do not contribute to SOA. Missing HOM-Acc and the decrease in overall HOM formation were the reason for the decrease in SOA formation by around 30 % in the high HO<sub>2</sub> system.

In the system with NO, besides missing HOM-Acc, the formation of more volatile species reduced the SOA formation potential. The higher volatility products were HOM-Frag, as expected due to their smaller molar mass, but also ON-HOM. This shift in the product distribution resulted in a SOA reduction of around 20 % in the case without reduction of the HOM concentration (middle NO case). The reduction was around 40 % in the high NO case where the HOM concentration was decreased by about 20 %.

The mixed system showed a significant decrease in SOA formation potential which is in accordance with the fast chemical sink interfering with the autoxidation chain in this highly competitive system. However, our observations showed some indication of heterogenous production processes in the system with seed, which require further investigation.

The volatility of the HOMs was investigated via their fraction remaining in the gas phase in the seeded compared to the unseeded system. The gas-phase fraction remaining revealed the higher volatility of ON-HOM compared to a non-ON HOM of the same mass. The gas-phase fraction remaining as a function of the molar mass was used to determine a molar mass threshold for significant contribution of HOMs to condensation. We subsequently applied the molar mass threshold to calculate a HOM mass proxy for condensation from the gas-phase measurements in the unseeded cases. Owing to the higher volatility of ON-HOM, we determined separate molar mass thresholds for the ON species. The good agreement of the derived HOM mass proxy with the particle phase measurement in the systems with HO<sub>2</sub> and NO shows that we capture and understand the products and reactions governing the SOA formation in our experiments.



## 6. References

- Albrecht, S. R., Novelli, A., Hofzumahaus, A., Kang, S., Baker, Y., Mentel, T., Wahner, A., and Fuchs, H.: Measurements of hydroperoxy radicals (HO<sub>2</sub>) at atmospheric concentrations using bromide chemical ionisation mass spectrometry, *Atmos. Meas. Tech.*, 12, 891-902, <https://doi.org/10.5194/amt-12-891-2019>, 2019.
- Atkinson, R. and Arey, J.: Atmospheric degradation of volatile organic compounds, *Chem. Rev.*, 103, 4605-4638, <https://doi.org/10.1021/cr0206420>, 2003.
- Baker, Y., Kang, S., Wang, H., Wu, R., Xu, J., Zanders, A., He, Q., Hohaus, T., Ziehm, T., Geretti, V., Bannan, T. J., O'Meara, S. P., Voliotis, A., Hallquist, M., McFiggans, G., Zorn, S. R., Wahner, A., and Mentel, T.: Impact of HO<sub>2</sub>/RO<sub>2</sub> ratio on highly oxygenated  $\alpha$ -pinene photooxidation products and secondary organic aerosol formation potential, *EGUosphere*, 2023, 1-32, <https://doi.org/10.5194/egusphere-2023-2402>, 2023.
- Berndt, T.: Peroxy Radical Processes and Product Formation in the OH Radical-Initiated Oxidation of  $\alpha$ -Pinene for Near-Atmospheric Conditions, *J. Phys. Chem. A*, 125, 9151-9160, <https://doi.org/10.1021/acs.jpca.1c05576>, 2021.
- Berndt, T., Mentler, B., Scholz, W., Fischer, L., Herrmann, H., Kulmala, M., and Hansel, A.: Accretion product formation from ozonolysis and OH radical reaction of  $\alpha$ -pinene: mechanistic insight and the influence of isoprene and ethylene, *Environ. Sci. Technol.*, 52, 11069-11077, <https://doi.org/10.1021/acs.est.8b02210>, 2018.
- Berndt, T., Richters, S., Jokinen, T., Hyttinen, N., Kurtén, T., Otkjaer, R. V., Kjaergaard, H. G., Stratmann, F., Herrmann, H., Sipila, M., Kulmala, M., and Ehn, M.: Hydroxyl radical-induced formation of highly oxidized organic compounds, *Nat. Commun.*, 7, 13677, <https://doi.org/10.1038/ncomms13677>, 2016.
- Bianchi, F., Garmash, O., He, X. C., Yan, C., Iyer, S., Rosendahl, I., Xu, Z. N., Rissanen, M. P., Riva, M., Taipale, R., Sarnela, N., Petäjä, T., Worsnop, D. R., Kulmala, M., Ehn, M., and Junninen, H.: The role of highly oxygenated molecules (HOMs) in determining the composition of ambient ions in the boreal forest, *Atmos. Chem. Phys.*, 17, 13819-13831, <https://doi.org/10.5194/acp-17-13819-2017>, 2017.
- Bianchi, F., Kurtén, T., Riva, M., Mohr, C., Rissanen, M. P., Roldin, P., Berndt, T., Crouse, J. D., Wennberg, P. O., Mentel, T. F., Wildt, J., Junninen, H., Jokinen, T., Kulmala, M., Worsnop, D. R., Thornton, J. A., Donahue, N., Kjaergaard, H. G., and Ehn, M.: Highly Oxygenated Organic Molecules (HOM) from Gas-Phase Autoxidation Involving Peroxy Radicals: A Key Contributor to Atmospheric Aerosol, *Chem. Rev.*, 119, 3472-3509, <https://doi.org/10.1021/acs.chemrev.8b00395>, 2019.
- Bottorff, B., Lew, M. M., Woo, Y., Rickly, P., Rollings, M. D., Deming, B., Anderson, D. C., Wood, E., Alwe, H. D., Millet, D. B., Weinheimer, A., Tyndall, G. S., Ortega, J., Dusanter, S., Leonardis, T., Flynn, J., Erickson, M., Alvarez, S., Rivera-Rios, J. C., Shutter, J. D., Keutsch, F., Helmig, D., Wang, W., Allen, H. M., Slade, J. H., Shepson, P. B., Bertman, S., and Stevens, P.: OH, HO<sub>2</sub>, and RO<sub>2</sub> radical chemistry in a rural forest environment: measurements, model comparisons, and evidence of a missing radical sink, *Atmos. Chem. Phys.*, 23, 10287-10311, <https://doi.org/10.5194/acp-23-10287-2023>, 2023.
- Chernushevich, I. V., Loboda, A. V., and Thomson, B. A.: An introduction to quadrupole-time-of-flight mass spectrometry, *J. Mass Spectrom.*, 36, 849-865, <https://doi.org/10.1002/jms.207>, 2001.
- Cho, C., Fuchs, H., Hofzumahaus, A., Holland, F., Bloss, W. J., Bohn, B., Dorn, H. P., Glowania, M., Hohaus, T., Liu, L., Monks, P. S., Niether, D., Rohrer, F., Sommariva, R., Tan, Z., Tillmann, R., Kiendler-Scharr, A., Wahner, A., and Novelli, A.: Experimental chemical budgets of OH, HO<sub>2</sub>, and RO<sub>2</sub> radicals in rural air in western Germany during the JULIAC campaign 2019, *Atmos. Chem. Phys.*, 23, 2003-2033, <https://doi.org/10.5194/acp-23-2003-2023>, 2023.

- Cox, R. A., Ammann, M., Crowley, J. N., Herrmann, H., Jenkin, M. E., McNeill, V. F., Mellouki, A., Troe, J., and Wallington, T. J.: Evaluated kinetic and photochemical data for atmospheric chemistry: Volume VII – Criegee intermediates, *Atmos. Chem. Phys.*, 20, 13497-13519, <https://doi.org/10.5194/acp-20-13497-2020>, 2020.
- Crounse, J. D., Nielsen, L. B., Jørgensen, S., Kjaergaard, H. G., and Wennberg, P. O.: Autoxidation of organic compounds in the atmosphere, *J. Phys. Chem. Lett.*, 4, 3513-3520, <https://doi.org/10.1021/jz4019207>, 2013.
- Donahue, N. M., Epstein, S. A., Pandis, S. N., and Robinson, A. L.: A two-dimensional volatility basis set: 1. organic-aerosol mixing thermodynamics, *Atmos. Chem. Phys.*, 11, 3303-3318, <https://doi.org/10.5194/acp-11-3303-2011>, 2011.
- Donahue, N. M., Robinson, A., Stanier, C., and Pandis, S.: Coupled partitioning, dilution, and chemical aging of semivolatile organics, *Environ. Sci. Technol.*, 40, 2635-2643, <https://doi.org/10.1021/es052297c>, 2006.
- Dyson, J. E., Whalley, L. K., Slater, E. J., Woodward-Massey, R., Ye, C., Lee, J. D., Squires, F., Hopkins, J. R., Dunmore, R. E., Shaw, M., Hamilton, J. F., Lewis, A. C., Worrall, S. D., Bacak, A., Mehra, A., Bannan, T. J., Coe, H., Percival, C. J., Ouyang, B., Hewitt, C. N., Jones, R. L., Crilley, L. R., Kramer, L. J., Acton, W. J. F., Bloss, W. J., Saksakulkrai, S., Xu, J., Shi, Z., Harrison, R. M., Kotthaus, S., Grimmond, S., Sun, Y., Xu, W., Yue, S., Wei, L., Fu, P., Wang, X., Arnold, S. R., and Heard, D. E.: Impact of HO<sub>2</sub> aerosol uptake on radical levels and O<sub>3</sub> production during summertime in Beijing, *Atmos. Chem. Phys.*, 23, 5679-5697, <https://doi.org/10.5194/acp-23-5679-2023>, 2023.
- Eddingsaas, N., Loza, C., Yee, L., Seinfeld, J., and Wennberg, P.:  $\alpha$ -Pinene photooxidation under controlled chemical conditions – Part 1: Gas-phase composition in low- and high-NO<sub>x</sub> environments, *Atmos. Chem. Phys.*, 12, 6489-6504, <https://doi.org/10.5194/acp-12-6489-2012>, 2012.
- Ehn, M., Kleist, E., Junninen, H., Petäjä, T., Lönn, G., Schobesberger, S., Dal Maso, M., Trimborn, A., Kulmala, M., Worsnop, D., Wahner, A., Wildt, J., and Mentel, T. F.: Gas phase formation of extremely oxidized pinene reaction products in chamber and ambient air, *Atmos. Chem. Phys.*, 12, 5113-5127, <https://doi.org/10.5194/acp-12-5113-2012>, 2012.
- Ehn, M., Thornton, J. A., Kleist, E., Sipila, M., Junninen, H., Pullinen, I., Springer, M., Rubach, F., Tillmann, R., Lee, B., Lopez-Hilfiker, F., Andres, S., Acir, I. H., Rissanen, M., Jokinen, T., Schobesberger, S., Kangasluoma, J., Kontkanen, J., Nieminen, T., Kurtén, T., Nielsen, L. B., Jørgensen, S., Kjaergaard, H. G., Canagaratna, M., Maso, M. D., Berndt, T., Petaja, T., Wahner, A., Kerminen, V. M., Kulmala, M., Worsnop, D. R., Wildt, J., and Mentel, T. F.: A large source of low-volatility secondary organic aerosol, *Nature*, 506, 476-479, <https://doi.org/10.1038/nature13032>, 2014.
- Eisele, F. and Tanner, D.: Measurement of the gas phase concentration of H<sub>2</sub>SO<sub>4</sub> and methane sulfonic acid and estimates of H<sub>2</sub>SO<sub>4</sub> production and loss in the atmosphere, *J. Geophys. Res. Atmos.*, 98, 9001-9010, <https://doi.org/10.1029/93JD00031>, 1993.
- Fantechi, G., Vereecken, L., and Peeters, J.: The OH-initiated atmospheric oxidation of pinonaldehyde: Detailed theoretical study and mechanism construction, *Phys. Chem. Chem. Phys.*, 4, 5795-5805, <https://doi.org/10.1039/B205901K>, 2002.
- Finlayson-Pitts, B. J. and Pitts, J. N.: CHAPTER 1 - Overview of the Chemistry of Polluted and Remote Atmospheres, in: *Chemistry of the Upper and Lower Atmosphere*, edited by: Finlayson-Pitts, B. J., and Pitts, J. N., Academic Press, San Diego, USA, <https://doi.org/10.1016/B978-0-12-257060-5.X5000-X>, 2000.
- Fuchs, H., Tan, Z. F., Lu, K. D., Bohn, B., Broch, S., Brown, S. S., Dong, H. B., Gomm, S., Häsel, R., He, L. Y., Hofzumahaus, A., Holland, F., Li, X., Liu, Y., Lu, S. H., Min, K. E., Rohrer, F., Shao, M., Wang, B. L., Wang, M., Wu, Y. S., Zeng, L. M., Zhang, Y. S., Wahner, A., and Zhang, Y. H.: OH reactivity at a rural site (Wangdu) in the North China Plain: contributions from OH reactants and experimental OH budget, *Atmos. Chem. Phys.*, 17, 645-661, <https://doi.org/10.5194/acp-17-645-2017>, 2017.

- Fuller, E. N., Schettler, P. D., and Giddings, J. C.: New method for prediction of binary gas-phase diffusion coefficients, *Industrial & Engineering Chemistry*, 58, 18-27, <https://doi.org/10.1021/ie50677a007>, 1966.
- Graham, E. L., Wu, C., Bell, D. M., Bertrand, A., Haslett, S. L., Baltensperger, U., El Haddad, I., Krejci, R., Riipinen, I., and Mohr, C.: Volatility of aerosol particles from NO<sub>3</sub> oxidation of various biogenic organic precursors, *Atmos. Chem. Phys.*, 23, 7347-7362, <https://doi.org/10.5194/acp-23-7347-2023>, 2023.
- Gross, J. H.: *Mass spectrometry: a textbook*, Springer Science & Business Media, Heidelberg, 2011.
- Guo, Y., Shen, H., Pullinen, I., Luo, H., Kang, S., Vereecken, L., Fuchs, H., Hallquist, M., Acir, I. H., Tillmann, R., Rohrer, F., Wildt, J., Kiendler-Scharr, A., Wahner, A., Zhao, D. F., and Mentel, T. F.: Identification of highly oxygenated organic molecules and their role in aerosol formation in the reaction of limonene with nitrate radical, *Atmos. Chem. Phys.*, 22, 11323-11346, <https://doi.org/10.5194/acp-22-11323-2022>, 2022.
- Hallquist, M., Wenger, J. C., Baltensperger, U., Rudich, Y., Simpson, D., Claeys, M., Dommen, J., Donahue, N. M., George, C., Goldstein, A. H., Hamilton, J. F., Herrmann, H., Hoffmann, T., Iinuma, Y., Jang, M., Jenkin, M. E., Jimenez, J. L., Kiendler-Scharr, A., Maenhaut, W., McFiggans, G., Mentel, T. F., Monod, A., Prévôt, A. S. H., Seinfeld, J. H., Surratt, J. D., Szmigielski, R., and Wildt, J.: The formation, properties and impact of secondary organic aerosol: current and emerging issues, *Atmos. Chem. Phys.*, 9, 5155-5236, <https://doi.org/10.5194/acp-9-5155-2009>, 2009.
- Hantschke, L. L.: *Oxidation of monoterpenes studied in atmospheric simulation chambers*, Forschungszentrum Jülich GmbH, Zentralbibliothek, Verlag, 2022.
- Harrison, A. G.: *Chemical ionization mass spectrometry*, CRC press, Boca Raton, Florida, USA, 1992.
- Hasson, A. S., Kuwata, K. T., Arroyo, M. C., and Petersen, E. B.: Theoretical studies of the reaction of hydroperoxy radicals (HO<sub>2</sub>) with ethyl peroxy (CH<sub>3</sub>CH<sub>2</sub>O<sub>2</sub>), acetyl peroxy (CH<sub>3</sub>C(O)O<sub>2</sub>), and acetonyl peroxy (CH<sub>3</sub>C(O)CH<sub>2</sub>O<sub>2</sub>) radicals, *J. Photochem. Photobiol. A*, 176, 218-230, <https://doi.org/10.1016/j.jphotochem.2005.08.012>, 2005.
- Henry, K. M., Lohaus, T., and Donahue, N. M.: Organic aerosol yields from  $\alpha$ -pinene oxidation: bridging the gap between first-generation yields and aging chemistry, *Environ. Sci. Technol.*, 46, 12347-12354, <https://doi.org/10.1021/es302060y>, 2012.
- Hidy, G.: Atmospheric chemistry in a box or a bag, *Atmos.*, 10, 401, <https://doi.org/10.3390/atmos10070401>, 2019.
- Hyttinen, N., Otkjær, R. V., Iyer, S., Kjaergaard, H. G., Rissanen, M. P., Wennberg, P. O., and Kurtén, T.: Computational comparison of different reagent ions in the chemical ionization of oxidized multifunctional compounds, *J. Phys. Chem. A*, 122, 269-279, <https://doi.org/10.1021/acs.jpca.7b10015>, 2018.
- Iyer, S., Reiman, H., Møller, K. H., Rissanen, M. P., Kjaergaard, H. G., and Kurtén, T.: Computational investigation of RO<sub>2</sub><sup>+</sup> HO<sub>2</sub> and RO<sub>2</sub><sup>+</sup> RO<sub>2</sub> reactions of monoterpene derived first-generation peroxy radicals leading to radical recycling, *J. Phys. Chem. A*, 122, 9542-9552, <https://doi.org/10.1021/acs.jpca.8b09241>, 2018.
- Iyer, S., Rissanen, M. P., Valiev, R., Barua, S., Krechmer, J. E., Thornton, J., Ehn, M., and Kurtén, T.: Molecular mechanism for rapid autoxidation in  $\alpha$ -pinene ozonolysis, *Nat. Commun.*, 12, 878, <https://doi.org/10.1038/s41467-021-21172-w>, 2021.
- Jenkin, M. E., Saunders, S. M., and Pilling, M. J.: The tropospheric degradation of volatile organic compounds: a protocol for mechanism development, *Atmos. Environ.*, 31, 81-104, [https://doi.org/10.1016/S1352-2310\(96\)00105-7](https://doi.org/10.1016/S1352-2310(96)00105-7), 1997.
- Jenkin, M. E., Valorso, R., Aumont, B., and Rickard, A. R.: Estimation of rate coefficients and branching ratios for reactions of organic peroxy radicals for use in automated mechanism construction, *Atmos. Chem. Phys.*, 19, 7691-7717, <https://doi.org/10.5194/acp-19-7691-2019>, 2019.

- Johnson, D. and Marston, G.: The gas-phase ozonolysis of unsaturated volatile organic compounds in the troposphere, *Chem. Soc. Rev.*, 37, 699-716, <https://doi.org/10.1039/B704260B>, 2008.
- Junninen, H., Ehn, M., Petäjä, T., Luosujärvi, L., Kotiaho, T., Kostianen, R., Rohner, U., Gonin, M., Fuhrer, K., Kulmala, M., and Worsnop, D. R.: A high-resolution mass spectrometer to measure atmospheric ion composition, *Atmos. Meas. Tech.*, 3, 1039-1053, <https://doi.org/10.5194/amt-3-1039-2010>, 2010.
- Kang, S.: Formation of highly oxygenated organic molecules from  $\alpha$ -pinene photochemistry, Forschungszentrum Jülich GmbH, 2021.
- Khan, M., Cooke, M., Utembe, S., Archibald, A., Derwent, R., Jenkin, M. E., Morris, W., South, N., Hansen, J., Francisco, J., Percival, C. J., and Shallcross, D. E.: Global analysis of peroxy radicals and peroxy radical-water complexation using the STOCHEM-CRI global chemistry and transport model, *Atmos. Environ.*, 106, 278-287, <https://doi.org/10.1016/j.atmosenv.2015.02.020>, 2015.
- Kiendler-Scharr, A., Becker, K.-H., Doussin, J.-F., Fuchs, H., Seakins, P., Wenger, J., and Wiesen, P.: Introduction to Atmospheric Simulation Chambers and Their Applications, in: *A Practical Guide to Atmospheric Simulation Chambers*, 1 ed., edited by: Doussin, J.-F., Fuchs, H., Kiendler-Scharr, A., Seakins, P., and Wenger, J., Springer, Cham, Switzerland, <https://doi.org/10.1007/978-3-031-22277-1>, 2023.
- Kiendler-Scharr, A., Wildt, J., Maso, M. D., Hohaus, T., Kleist, E., Mentel, T. F., Tillmann, R., Uerlings, R., Schurr, U., and Wahner, A.: New particle formation in forests inhibited by isoprene emissions, *Nature*, 461, 381-384, <https://doi.org/10.1038/nature08292>, 2009.
- Lou, S., Holland, F., Rohrer, F., Lu, K., Bohn, B., Brauers, T., Chang, C. C., Fuchs, H., Häseler, R., Kita, K., Kondo, Y., Li, X., Shao, M., Zeng, L., Wahner, A., Zhang, Y., Wang, W., and Hofzumahaus, A.: Atmospheric OH reactivities in the Pearl River Delta - China in summer 2006: measurement and model results, *Atmos. Chem. Phys.*, 10, 11243-11260, <https://doi.org/10.5194/acp-10-11243-2010>, 2010.
- McDonald, B. C., de Gouw, J. A., Gilman, J. B., Jathar, S. H., Akherati, A., Cappa, C. D., Jimenez, J. L., Lee-Taylor, J., Hayes, P. L., McKeen, S. A., Cui, Y. Y., Kim, S.-W., Gentner, D. R., Isaacman-VanWertz, G., Goldstein, A. H., Harley, R. A., Frost, G. J., Roberts, J. M., Ryerson, T. B., and Trainer, M.: Volatile chemical products emerging as largest petrochemical source of urban organic emissions, *Science*, 359, 760-764, <https://doi.org/10.1126/science.aaq0524>, 2018.
- McFiggans, G., Mentel, T. F., Wildt, J., Pullinen, I., Kang, S., Kleist, E., Schmitt, S., Springer, M., Tillmann, R., Wu, C., Zhao, D., Hallquist, M., Faxon, C., Le Breton, M., Hallquist, A. M., Simpson, D., Bergstrom, R., Jenkin, M. E., Ehn, M., Thornton, J. A., Alfarra, M. R., Bannan, T. J., Percival, C. J., Priestley, M., Topping, D., and Kiendler-Scharr, A.: Secondary organic aerosol reduced by mixture of atmospheric vapours, *Nature*, 565, 587-593, <https://doi.org/10.1038/s41586-018-0871-y>, 2019.
- McVay, R. C., Zhang, X., Aumont, B., Valorso, R., Camredon, M., La, Y. S., Wennberg, P. O., and Seinfeld, J. H.: SOA formation from the photooxidation of  $\alpha$ -pinene: systematic exploration of the simulation of chamber data, *Atmos. Chem. Phys.*, 16, 2785-2802, <https://doi.org/10.5194/acp-16-2785-2016>, 2016.
- Mentel, T., Springer, M., Ehn, M., Kleist, E., Pullinen, I., Kurtén, T., Rissanen, M., Wahner, A., and Wildt, J.: Formation of highly oxidized multifunctional compounds: autoxidation of peroxy radicals formed in the ozonolysis of alkenes—deduced from structure–product relationships, *Atmos. Chem. Phys.*, 15, 6745-6765, <https://doi.org/10.5194/acp-15-6745-2015>, 2015.
- Mentel, T. F., Wildt, J., Kiendler-Scharr, A., Kleist, E., Tillmann, R., Dal Maso, M., Fisseha, R., Hohaus, T., Spahn, H., Uerlings, R., Wegener, R., Griffiths, P. T., Dinar, E., Rudich, Y., and Wahner, A.: Photochemical production of aerosols from real plant emissions, *Atmos. Chem. Phys.*, 9, 4387-4406, <https://doi.org/10.5194/acp-9-4387-2009>, 2009.

- Mihelcic, D., Holland, F., Hofzumahaus, A., Hoppe, L., Konrad, S., M $\ddot{u}$ sgen, P., P $\ddot{a}$ tz, H. W., Sch $\ddot{a}$ fer, H. J., Schmitz, T., Volz-Thomas, A., B $\ddot{a}$ chmann, K., Schlomski, S., Platt, U., Geyer, A., Alicke, B., and Moortgat, G. K.: Peroxy radicals during BERLIOZ at Pabstthum: Measurements, radical budgets and ozone production, *J. Geophys. Res. Atmos.*, 108, <https://doi.org/10.1029/2001JD001014>, 2003.
- Miyazaki, K.: Study of the nature and roles of peroxy radicals in the atmosphere towards the understanding of oxidant formation using laser-flash photolysis and LIF detection technique, Tokyo Metropolitan University; University of Lille, 2012.
- Mohr, C., Thornton, J. A., Heitto, A., Lopez-Hilfiker, F. D., Lutz, A., Riipinen, I., Hong, J., Donahue, N. M., Hallquist, M., Petaja, T., Kulmala, M., and Yli-Juuti, T.: Molecular identification of organic vapors driving atmospheric nanoparticle growth, *Nat. Commun.*, 10, 4442, <https://doi.org/10.1038/s41467-019-12473-2>, 2019.
- Nie, W., Yan, C., Yang, L., Roldin, P., Liu, Y., Vogel, A. L., Molteni, U., Stolzenburg, D., Finkenzeller, H., Amorim, A., Bianchi, F., Curtius, J., Dada, L., Draper, D. C., Duplissy, J., Hansel, A., He, X.-C., Hofbauer, V., Jokinen, T., Kim, C., Lehtipalo, K., Nichman, L., Mauldin, R. L., Makhmutov, V., Mentler, B., Mizelli-Ojdanic, A., Pet $\ddot{a}$ j $\ddot{a}$ , T., Qu $\acute{e}$ l $\acute{e}$ ver, L. L. J., Schallhart, S., Simon, M., Tauber, C., Tom $\acute{e}$ , A., Volkamer, R., Wagner, A. C., Wagner, R., Wang, M., Ye, P., Li, H., Huang, W., Qi, X., Lou, S., Liu, T., Chi, X., Dommen, J., Baltensperger, U., El Haddad, I., Kirkby, J., Worsnop, D., Kulmala, M., Donahue, N. M., Ehn, M., and Ding, A.: NO at low concentration can enhance the formation of highly oxygenated biogenic molecules in the atmosphere, *Nat. Commun.*, 14, 3347, <https://doi.org/10.1038/s41467-023-39066-4>, 2023.
- Noziere, B. and Barnes, I.: Evidence for formation of a PAN analogue of pinonic structure and investigation of its thermal stability, *J. Geophys. Res. Atmos.*, 103, 25587-25597, <https://doi.org/10.1029/98JD01677>, 1998.
- Otkjaer, R. V., Jakobsen, H. H., Tram, C. M., and Kjaergaard, H. G.: Calculated Hydrogen Shift Rate Constants in Substituted Alkyl Peroxy Radicals, *J. Phys. Chem. A*, 122, 8665-8673, <https://doi.org/10.1021/acs.jpca.8b06223>, 2018.
- Pankow, J. F.: An absorption model of the gas/aerosol partitioning involved in the formation of secondary organic aerosol, *Atmos. Environ.*, 28, 189-193, [https://doi.org/10.1016/1352-2310\(94\)90094-9](https://doi.org/10.1016/1352-2310(94)90094-9), 1994.
- Peeters, J., Vereecken, L., and Fantechi, G.: The detailed mechanism of the OH-initiated atmospheric oxidation of  $\alpha$ -pinene: a theoretical study, *Phys. Chem. Chem. Phys.*, 3, 5489-5504, <https://doi.org/10.1039/B106555F>, 2001.
- Peng, Z., Lee-Taylor, J., Orlando, J. J., Tyndall, G. S., and Jimenez, J. L.: Organic peroxy radical chemistry in oxidation flow reactors and environmental chambers and their atmospheric relevance, *Atmos. Chem. Phys.*, 19, 813-834, <https://doi.org/10.5194/acp-19-813-2019>, 2019.
- Piletic, I. R. and Kleindienst, T. E.: Rates and yields of unimolecular reactions producing highly oxidized peroxy radicals in the OH-induced autoxidation of  $\alpha$ -pinene,  $\beta$ -pinene, and limonene, *J. Phys. Chem. A*, 126, 88-100, <https://doi.org/10.1021/acs.jpca.1c07961>, 2022.
- Presto, A. A., Huff Hartz, K. E., and Donahue, N. M.: Secondary Organic Aerosol Production from Terpene Ozonolysis. 2. Effect of NO $_x$  concentration, *Environ. Sci. Technol.*, 39, 7046-7054, <https://doi.org/10.1021/es050400s>, 2005.
- Pullinen, I., Schmitt, S., Kang, S., Sarrafzadeh, M., Schlag, P., Andres, S., Kleist, E., Mentel, T. F., Rohrer, F., Springer, M., Tillmann, R., Wildt, J., Wu, C., Zhao, D., Wahner, A., and Kiendler-Scharr, A.: Impact of NO $_x$  on secondary organic aerosol (SOA) formation from  $\alpha$ -pinene and  $\beta$ -pinene photooxidation: the role of highly oxygenated organic nitrates, *Atmos. Chem. Phys.*, 20, 10125-10147, <https://doi.org/10.5194/acp-20-10125-2020>, 2020.
- Richter, F., Ostertag, R., Ammerlahn, G., Behrle, E., Baumann, M., and Kobel, M.: Beilstein's handbook of organic chemistry. Third supplement, covering the literature from 1930-1949, 1955.

- Rissanen, M. P., Mikkilä, J., Iyer, S., and Hakala, J.: Multi-scheme chemical ionization inlet (MION) for fast switching of reagent ion chemistry in atmospheric pressure chemical ionization mass spectrometry (CIMS) applications, *Atmos. Meas. Tech.*, 12, 6635-6646, <https://doi.org/10.5194/amt-12-6635-2019>, 2019.
- Rissanen, M. P., Kurtén, T., Sipila, M., Thornton, J. A., Kangasluoma, J., Sarnela, N., Junninen, H., Jorgensen, S., Schallhart, S., Kajos, M. K., Taipale, R., Springer, M., Mentel, T. F., Ruuskanen, T., Petaja, T., Worsnop, D. R., Kjaergaard, H. G., and Ehn, M.: The formation of highly oxidized multifunctional products in the ozonolysis of cyclohexene, *J. Am. Chem. Soc.*, 136, 15596-15606, <https://doi.org/10.1021/ja507146s>, 2014.
- Roldin, P., Ehn, M., Kurtén, T., Olenius, T., Rissanen, M. P., Sarnela, N., Elm, J., Rantala, P., Hao, L., Hyttinen, N., Heikkinen, L., Worsnop, D. R., Pichelstorfer, L., Xavier, C., Clusius, P., Öström, E., Petäjä, T., Kulmala, M., Vehkamäki, H., Virtanen, A., Riipinen, I., and Boy, M.: The role of highly oxygenated organic molecules in the Boreal aerosol-cloud-climate system, *Nat. Commun.*, 10, 4370, <https://doi.org/10.1038/s41467-019-12338-8>, 2019.
- Sanchez, J., Tanner, D. J., Chen, D., Huey, L. G., and Ng, N. L.: A new technique for the direct detection of HO<sub>2</sub> radicals using bromide chemical ionization mass spectrometry (Br-CIMS): initial characterization, *Atmos. Meas. Tech.*, 9, 3851-3861, <https://doi.org/10.5194/amt-9-3851-2016>, 2016.
- Sarrafzadeh, M., Wildt, J., Pullinen, I., Springer, M., Kleist, E., Tillmann, R., Schmitt, S. H., Wu, C., Mentel, T. F., Zhao, D., Hastie, D. R., and Kiendler-Scharr, A.: Impact of NO<sub>x</sub> and OH on secondary organic aerosol formation from  $\beta$ -pinene photooxidation, *Atmos. Chem. Phys.*, 16, 11237-11248, <https://doi.org/10.5194/acp-16-11237-2016>, 2016.
- Saunders, S. M., Jenkin, M. E., Derwent, R., and Pilling, M.: Protocol for the development of the Master Chemical Mechanism, MCM v3 (Part A): tropospheric degradation of non-aromatic volatile organic compounds, *Atmos. Chem. Phys.*, 3, 161-180, <https://doi.org/10.5194/acp-3-161-2003>, 2003.
- Schervish, M. and Donahue, N. M.: Peroxy radical kinetics and new particle formation, *Environ. Sci. Atmos.*, 1, 79-92, <https://doi.org/10.1039/d0ea00017e>, 2021.
- Seinfeld, J. H. and Pandis, S. N.: *Atmospheric Chemistry and Physics: from Air Pollution to Climate Change*, 3, John Wiley & Sons, Hoboken, New Jersey, USA, 2016.
- Shen, H., Vereecken, L., Kang, S., Pullinen, I., Fuchs, H., Zhao, D., and Mentel, T. F.: Unexpected significance of a minor reaction pathway in daytime formation of biogenic highly oxygenated organic compounds, *Sci. Adv.*, 8, eabp8702, <https://doi.org/10.1126/sciadv.abp8702>, 2022.
- Shen, H., Zhao, D., Pullinen, I., Kang, S., Vereecken, L., Fuchs, H., Acir, I. H., Tillmann, R., Rohrer, F., Wildt, J., Kiendler-Scharr, A., Wahner, A., and Mentel, T. F.: Highly Oxygenated Organic Nitrates Formed from NO(3) Radical-Initiated Oxidation of  $\beta$ -Pinene, *Environ. Sci. Technol.*, 55, 15658-15671, <https://doi.org/10.1021/acs.est.1c03978>, 2021.
- Shilling, J. E., Chen, Q., King, S. M., Rosenoern, T., Kroll, J. H., Worsnop, D. R., DeCarlo, P. F., Aiken, A. C., Sueper, D., Jimenez, J. L., and Martin, S. T.: Loading-dependent elemental composition of  $\alpha$ -pinene SOA particles, *Atmos. Chem. Phys.*, 9, 771-782, <https://doi.org/10.5194/acp-9-771-2009>, 2009.
- Sindelarova, K., Granier, C., Bouarar, I., Guenther, A., Tilmes, S., Stavroukou, T., Müller, J. F., Kuhn, U., Stefani, P., and Knorr, W.: Global data set of biogenic VOC emissions calculated by the MEGAN model over the last 30 years, *Atmos. Chem. Phys.*, 14, 9317-9341, <https://doi.org/10.5194/acp-14-9317-2014>, 2014.
- Stark, H., Yatavelli, R. L., Thompson, S. L., Kimmel, J. R., Cubison, M. J., Chhabra, P. S., Canagaratna, M. R., Jayne, J. T., Worsnop, D. R., and Jimenez, J. L.: Methods to extract molecular and bulk chemical information from series of complex mass spectra with limited mass resolution, *Int. J. Mass Spectrom.*, 389, 26-38, <https://doi.org/10.1016/j.ijms.2015.08.011>, 2015.

- Stevens, P., Mather, J., Brune, W. H., Eisele, F., Tanner, D., Jefferson, A., Cantrell, C., Shetter, R., Sewall, S., Fried, A., Henry, B., Williams, E., Baumann, K., Goldan, P., and Kuster, W.: HO<sub>2</sub>/OH and RO<sub>2</sub>/HO<sub>2</sub> ratios during the Tropospheric OH Photochemistry Experiment: Measurement and theory, *J. Geophys. Res. Atmos.*, 102, 6379-6391, <https://doi.org/10.1029/96JD01704>, 1997.
- Stolzenburg, D., Wang, M., Schervish, M., and Donahue, N. M.: Tutorial: Dynamic organic growth modeling with a volatility basis set, *J. Aerosol Sci.*, 166, 106063, <https://doi.org/10.1016/j.jaerosci.2022.106063>, 2022.
- Takeuchi, M. and Ng, N. L.: Chemical composition and hydrolysis of organic nitrate aerosol formed from hydroxyl and nitrate radical oxidation of  $\alpha$ -pinene and  $\beta$ -pinene, *Atmos. Chem. Phys.*, 19, 12749-12766, <https://doi.org/10.5194/acp-19-12749-2019>, 2019.
- Tan, Z., Lu, K., Hofzumahaus, A., Fuchs, H., Bohn, B., Holland, F., Liu, Y., Rohrer, F., Shao, M., Sun, K., Wu, Y., Zeng, L., Zhang, Y., Zou, Q., Kiendler-Scharr, A., Wahner, A., and Zhang, Y.: Experimental budgets of OH, HO<sub>2</sub>, and RO<sub>2</sub> radicals and implications for ozone formation in the Pearl River Delta in China 2014, *Atmos. Chem. Phys.*, 19, 7129-7150, <https://doi.org/10.5194/acp-19-7129-2019>, 2019.
- Tan, Z., Rohrer, F., Lu, K., Ma, X., Bohn, B., Broch, S., Dong, H., Fuchs, H., Gkatzelis, G. I., Hofzumahaus, A., Holland, F., Li, X., Liu, Y., Liu, Y., Novelli, A., Shao, M., Wang, H., Wu, Y., Zeng, L., Hu, M., Kiendler-Scharr, A., Wahner, A., and Zhang, Y.: Wintertime photochemistry in Beijing: observations of RO<sub>x</sub> radical concentrations in the North China Plain during the BEST-ONE campaign, *Atmos. Chem. Phys.*, 18, 12391-12411, <https://doi.org/10.5194/acp-18-12391-2018>, 2018.
- Tang, M., Shiraiwa, M., Pöschl, U., Cox, R., and Kalberer, M.: Compilation and evaluation of gas phase diffusion coefficients of reactive trace gases in the atmosphere: Volume 2. Diffusivities of organic compounds, pressure-normalised mean free paths, and average Knudsen numbers for gas uptake calculations, *Atmos. Chem. Phys.*, 15, 5585-5598, <https://doi.org/10.5194/acp-15-5585-2015>, 2015.
- Taylor, J.: Introduction to error analysis, the study of uncertainties in physical measurements, University Science Books, Sausalito, California, USA, 1997.
- Vereecken, L. and Nozière, B.: H migration in peroxy radicals under atmospheric conditions, *Atmos. Chem. Phys.*, 20, 7429-7458, <https://doi.org/10.5194/acp-20-7429-2020>, 2020.
- Vereecken, L. and Peeters, J.: A structure-activity relationship for the rate coefficient of H-migration in substituted alkoxy radicals, *Phys. Chem. Chem. Phys.*, 12, 12608-12620, <https://doi.org/10.1039/C0CP00387E>, 2010.
- Vereecken, L., Müller, J.-F., and Peeters, J.: Low-volatility poly-oxygenates in the OH-initiated atmospheric oxidation of  $\alpha$ -pinene: impact of non-traditional peroxy radical chemistry, *Phys. Chem. Chem. Phys.*, 9, 5241-5248, <https://doi.org/10.1039/b708023a>, 2007.
- Wildt, J., Mentel, T. F., Kiendler-Scharr, A., Hoffmann, T., Andres, S., Ehn, M., Kleist, E., Müssgen, P., Rohrer, F., Rudich, Y., Springer, M., Tillmann, R., and Wahner, A.: Suppression of new particle formation from monoterpene oxidation by NO<sub>x</sub>, *Atmos. Chem. Phys.*, 14, 2789-2804, <https://doi.org/10.5194/acp-14-2789-2014>, 2014.
- Xu, L., Møller, K. H., Crouse, J. D., Otkjær, R. V., Kjaergaard, H. G., and Wennberg, P. O.: Unimolecular reactions of peroxy radicals formed in the oxidation of  $\alpha$ -pinene and  $\beta$ -pinene by hydroxyl radicals, *J. Phys. Chem. A*, 123, 1661-1674, <https://doi.org/10.1021/acs.jpca.8b11726>, 2019.
- Yuan, B., Koss, A., Warneke, C., Gilman, J. B., Lerner, B. M., Stark, H., and de Gouw, J. A.: A high-resolution time-of-flight chemical ionization mass spectrometer utilizing hydronium ions (H<sub>3</sub>O<sup>+</sup> ToF-CIMS) for measurements of volatile organic compounds in the atmosphere, *Atmos. Meas. Tech.*, 9, 2735-2752, <https://doi.org/10.5194/amt-9-2735-2016>, 2016.
- Zare, A., Fahey, K. M., Sarwar, G., Cohen, R. C., and Pye, H. O. T.: Vapor-Pressure Pathways Initiate but Hydrolysis Products Dominate the Aerosol Estimated from Organic Nitrates, *ACS Earth Space Chem.*, 3, 1426-1437, <https://doi.org/10.1021/acsearthspacechem.9b00067>, 2019.

Zhao, Q., Xie, H.-B., Ma, F., Nie, W., Yan, C., Huang, D., Elm, J., and Chen, J.: Mechanism-based structure-activity relationship investigation on hydrolysis kinetics of atmospheric organic nitrates, *npj Clim. Atmos. Sci.*, 6, 192, <https://doi.org/10.1038/s41612-023-00517-w>, 2023.

Zhao, R.: The Recent Development and Application of Chemical Ionization Mass Spectrometry in Atmospheric Chemistry, in: *Encyclopedia of Analytical Chemistry*, John Wiley & Sons, 1-33, <https://doi.org/10.1002/9780470027318.a9655>, 2018.

Ziemann, P. J. and Atkinson, R.: Kinetics, products, and mechanisms of secondary organic aerosol formation, *Chem. Soc. Rev.*, 41, 6582-6605, <https://doi.org/10.1039/C2CS35122F>, 2012.

## A. Appendix

### A.1 Exemplary RO<sub>2</sub> sink distributions in the atmosphere

The data is shown in **Figure 1** in **Section 1.1**. The RO<sub>2</sub>, HO<sub>2</sub> and NO concentrations were taken from Peng et al. (2019) and are listed in **Table A1**. The contributions of the individual reaction partners were calculated with the same general bulk reaction rate coefficients which we used for our analysis and which are listed in **Table A2**.

**Table A1** Concentrations RO<sub>2</sub>, HO<sub>2</sub>, NO in exemplary atmospheric conditions. Data from Peng et al. (2019). OHR stands for OH reactivity. In cases without RO<sub>2</sub> measurement the “RO<sub>2</sub> fate estimator” provided for download by the authors and the OH reactivity were used for the contribution calculation. For NO the concentration is given additionally as a mixing ratio in parentheses.

	<u>Conditions</u>	<u>OHR</u>	<u>OH [cm<sup>-3</sup>]</u>	<u>RO<sub>2</sub> [cm<sup>-3</sup>]</u>	<u>HO<sub>2</sub> [cm<sup>-3</sup>]</u>	<u>NO [cm<sup>-3</sup>]</u>
<b>P1</b>	Pristine (Pacific Ocean, high RO <sub>2</sub> )	1.9	9.75E+06	from OHR	2.75E+08	4.75E+07 (2 pptv)
<b>P2</b>	Pristine (Pacific Ocean, typical)	1	6.25E+06	from OHR	6.25E+08	7.50E+07 (3 pptv)
<b>F1</b>	Forested (Rocky Mountains)	-	2.50E+07	1.25E+09	2.50E+09	1.50E+09 (60 pptv)
<b>F2</b>	Forested (Amazon, wet season)	9.6	1.20E+06	from OHR	5.10E+08	9.25E+08 (37 pptv)
<b>U</b>	Urban (Los Angeles)	25	1.50E+06	from OHR	1.50E+08	3.75E+10 (1500 pptv)

**Table A2** Overview of utilized bulk reaction rate coefficients

<u>Reaction</u>	<u>Assumed bulk reaction rate coefficient</u>	<u>Reference</u>
RO <sub>2</sub> +RO <sub>2</sub>	5.0E-12 cm <sup>3</sup> ·s <sup>-1</sup>	(Roldin et al., 2019)
RO <sub>2</sub> +HO <sub>2</sub>	2.46E-11 cm <sup>3</sup> ·s <sup>-1</sup>	MCM v3.3.1 at 20°C (Jenkin et al., 1997; Saunders et al., 2003)
RO <sub>2</sub> +NO	9.2E-12 cm <sup>3</sup> ·s <sup>-1</sup>	MCM v3.3.1 at 20°C (Jenkin et al., 1997; Saunders et al., 2003)

## A.2 Voltage and flow settings of MION-APi-TOF

**Table A3** Applied TOF power supply (TPS) settings (optimized)

<b><u>Interface: SSQ RF</u></b>	
SSQ mode	med mass
SSQ Freq.	2 460 000 Hz
SSQ Amp.	200.0 V
<b><u>Interface: SSQ Low voltages</u></b>	
Nozzle	0.0 V
SSQ EP	0.0 V
SSQ Front	8.0 V
SSQ Back	-4.0 V
Lens skimmer	-10.0 V
<b><u>Interface: BSQ RF</u></b>	
BSQ mode	low mass
BSQ Freq.	4 110 000 Hz
BSQ Amp.	350.0 V
<b><u>Interface: BSQ Low voltages</u></b>	
Skimmer	7.0 V
Q2 Front	9.2 V
Q2 Back	9.2 V
Skimmer 2	14.2 V
Reference (bias)	66.7 V
Ions-Lens 2	130.0 V
Deflector Flange	40.0 V
Deflector	43.0 V

Table continuous on next page.

<b><u>TOF: Extraction Pulser</u></b>	
TOF Pulse	1000.0 V
TOF Ref	21.5 V
TOF Extr. 1	40.0 V
TOF Extr.2	1000.0 V
<b><u>TOF: TOF High voltages</u></b>	
Lens	1600.0 V
Drift	5700.0 V
RG	1469.2 V
RB	1000.0 V
MCP	2075.0 V
PA	5400.0 V
HVB3 (unused)	0.0 V
HV-Source (Accelerator voltage MION)	-2750.0 V
HVB0 (Deflector voltage IS1 MION)	If instrument is in IS1 mode: -150.0 V Otherwise: 0.0 V
HVB1 (Deflector voltage IS2 MION)	If instrument is in IS2 mode: -200.0 V Otherwise: 0.0 V
<b><u>MION flows</u></b>	
Main inlet flow	10 L min <sup>-1</sup>
Carrier flow IS1	3.0 mL min <sup>-1</sup>
Exhaust flow IS1	40.0 mL min <sup>-1</sup>
Carrier flow IS2	15.0 mL min <sup>-1</sup>
Exhaust flow IS2	40.0 mL min <sup>-1</sup>

### A.3 Overview of experimental OH concentrations and $\alpha$ -pinene OH turnover

**Table A4** OH concentration and  $\alpha$ -pinene OH turnover in all experiments. The experiment phases are ordered chronologically. (g) marks unseeded experiment stages, (s) seeded.

<u>Experiment phase</u>	<u>OH concentration [cm<sup>-3</sup>]</u>	<u><math>\alpha</math>-Pinene OH turnover [cm<sup>-3</sup>·s<sup>-1</sup>]</u>
<u>Experiment: apinCO_1</u>		
<u>Photooxidation base case (g)</u>	4.8·10 <sup>6</sup>	3.5·10 <sup>7</sup>
<u>High HO<sub>2</sub> case (g)</u>	5.0·10 <sup>6</sup>	3.9·10 <sup>7</sup>
<u>Experiment: apinCO_2</u>		
<u>Photooxidation base case (s)</u>	1.1·10 <sup>7</sup>	5.2·10 <sup>7</sup>
<u>High HO<sub>2</sub> case (s)</u>	7.6·10 <sup>6</sup>	4.5·10 <sup>7</sup>
<u>High HO<sub>2</sub> case (g)</u>	9.1·10 <sup>6</sup>	5.0·10 <sup>7</sup>
<u>Photooxidation base case (g)</u>	1.5·10 <sup>7</sup>	5.7·10 <sup>7</sup>
<u>Experiment: apinNO</u>		
<u>Photooxidation base case (g)</u>	1.8·10 <sup>7</sup>	4.9·10 <sup>7</sup>
<u>(Additional: low NO case (g))</u>	2.0·10 <sup>7</sup>	5.1·10 <sup>7</sup>
<u>Middle NO case (g)</u>	2.2·10 <sup>7</sup>	5.0·10 <sup>7</sup>
<u>High NO case (g)</u>	2.9·10 <sup>7</sup>	5.3·10 <sup>7</sup>
<u>High NO case (s)</u>	2.6·10 <sup>7</sup>	5.4·10 <sup>7</sup>
<u>Middle NO case (s)</u>	1.9·10 <sup>7</sup>	4.8·10 <sup>7</sup>
<u>(Additional: low NO case (s))</u>	1.4·10 <sup>7</sup>	4.4·10 <sup>7</sup>
<u>Experiment: apinCONO_1</u>		
<u>Photooxidation base case (s)</u>	1.1·10 <sup>7</sup>	4.4·10 <sup>7</sup>
<u>High HO<sub>2</sub> case (s)</u>	7.2·10 <sup>6</sup>	3.7·10 <sup>7</sup>
<u>Middle NO, high HO<sub>2</sub> case (s)</u>	1.2·10 <sup>7</sup>	4.4·10 <sup>7</sup>
<u>(Additional: in-between NO, high HO<sub>2</sub> case (s))</u>	1.6·10 <sup>7</sup>	4.8·10 <sup>7</sup>
<u>High NO, high HO<sub>2</sub> case (s)</u>	1.5·10 <sup>7</sup>	4.7·10 <sup>7</sup>
<u>High NO, high HO<sub>2</sub> case (g)</u>	1.5·10 <sup>7</sup>	4.7·10 <sup>7</sup>
<u>(Additional: in-between NO, high HO<sub>2</sub> case (g))</u>	1.5·10 <sup>7</sup>	4.7·10 <sup>7</sup>
<u>Middle NO, high HO<sub>2</sub> case (g)</u>	1.2·10 <sup>7</sup>	4.4·10 <sup>7</sup>
<u>Experiment: apinCONO_2</u>		
<u>Photooxidation base case (s)</u>	4.7·10 <sup>6</sup>	1.7·10 <sup>7</sup>
<u>Photooxidation base case (g)</u>	5.7·10 <sup>6</sup>	2.0·10 <sup>7</sup>
<u>High NO, high HO<sub>2</sub> case (s)</u>	7.3·10 <sup>6</sup>	2.4·10 <sup>7</sup>
<u>High NO, high HO<sub>2</sub> case (g)</u>	7.6·10 <sup>6</sup>	2.1·10 <sup>7</sup>

## A.4 Modeling of experiments

### A.4.1 Box model input parameters: Wall loss and OH background reactivity

The OH background reactivity (loss of OH without VOC present) and the wall loss of the RO<sub>2</sub> and HO<sub>2</sub> species in the SAPHIR-STAR chamber are two important input parameters into the model. It is assumed that the product species in the MCM are too volatile to be lost on the walls, but that the radical species are lost upon wall collision. An OH background reactivity measurement (kOH instrument, see Lou et al. (2010), Fuchs et al. (2017)) for more detailed information) was performed in the empty, clean chamber at the same humidity as in the experiments and resulted in a reactivity of 3 s<sup>-1</sup>. The background reactivity was adapted in each experiment to represent the  $\alpha$ -pinene consumption in the photooxidation phase correctly, resulting in kOH<sub>Background</sub> between 2 s<sup>-1</sup> and 5 s<sup>-1</sup>. A possible reason for discrepancies is that the background reactivity determination was done only once, while during the experiment series small residual contaminations, resisting flushing over > 6 residence times, may have contributed to the background reactivity.

For the estimation of the maximum wall loss the following experiment was performed twice: In a gas phase  $\alpha$ -pinene photooxidation steady state the light was turned off and the decay of HOM product signals were observed in the NO<sub>3</sub>-MION-CIMS. This approach was used before by Ehn et al. (2014) and Sarrafzadeh et al. (2016) to determine the maximum loss in the JPAC chamber.

Only products showing a clear single exponential decay were considered and it is assumed that the chosen HOMs are no longer produced after light off and are lost on wall contact. Their timeseries is used to calculate an individual lifetime  $\tau$  by fitting the decay curve to the function shown in Eq. A-1. From the observation of the decay of C<sub>10</sub> products an average lifetime of  $\tau=171$  s is determined.

$$\ln(\text{normalized signal}) = -\frac{1}{\tau} * t + b \quad \text{Eq. A-1}$$

The derived wall loss rate for HOM was also applied to describe the wall loss of RO<sub>2</sub> radicals, and therefore, k<sub>RO<sub>2</sub> wall</sub> is set as 1/170 s<sup>-1</sup>. The wall loss rate is correlated to the transport through the diffusion layer of the chamber and thus should scale with the inverse of the square root of the molar mass (under the assumption of perfect mixing of the chamber core). It is therefore expected that the smaller HO<sub>2</sub> radical is lost faster due to its faster transport. Additionally, the removal efficiency for HO<sub>2</sub> and RO<sub>2</sub> radicals might differ further as RO<sub>2</sub> are not lost necessarily on every collision with the wall. The specific RO<sub>2</sub> removal efficiency depends on the radical's molecular structure (Miyazaki, 2012).

To estimate a value for the HO<sub>2</sub> wall loss, the expected diffusion constant for a HOM-Mon, HOM-Acc and HO<sub>2</sub> are calculated by the parametrization developed by Fuller et al. (1966) and recently reviewed by Tang et al. (2015). The results can be found in **Table A5**.

**Table A5** Calculated diffusion coefficients of an exemplary HOM-Mon, exemplary HOM-Acc and HO<sub>2</sub>

Compound	Diffusion constant at 1 bar (cm <sup>2</sup> s <sup>-1</sup> )
C <sub>10</sub> H <sub>15</sub> O <sub>6</sub> (HOM-Mon proxy)	0.053
C <sub>20</sub> H <sub>30</sub> O <sub>10</sub> (HOM-Acc proxy)	0.038
HO <sub>2</sub>	0.202

If the wall loss is only dependent on the diffusion to the wall (i.e. 100 % loss on wall contact), the lifetime should inversely scale with the diffusion speed. To verify this assumption, the ratio of the average lifetimes of HOM-Mon and HOM-Acc were compared to the ratio of their diffusion constants: The HOM-Acc proxy's diffusion constant is 0.71 of the monomer proxy's diffusion constant. The observed accretion products decay resulted in average lifetime of  $\tau=202$  s, leading to  $k_{HOM-Acc\ wall}/k_{HOM-Mon\ wall} = 0.85$ . Within the uncertainties of the diffusion constants calculation and the lifetime determination, the wall loss seems to depend indeed on the diffusion to the surface layer, thus on the diffusion constant. Therefore, considering the diffusion constant of HO<sub>2</sub>,  $k_{HO_2\ wall}=1/50$  s<sup>-1</sup> is chosen.

To study the sensitivity of the modeled HO<sub>2</sub>/RO<sub>2</sub> ratio to the assumed wall loss rates, a sensitivity study was performed by varying the rate coefficients for wall losses. The RO<sub>2</sub> wall loss was varied within 1 $\sigma$  of the determined HOM product wall loss. The HO<sub>2</sub> wall loss was varied in a wider range to cover the case that not all collision with the wall lead to loss of HO<sub>2</sub>. Therefore, the lifetime of HO<sub>2</sub> was either set as 50 s or to a maximum lifetime of 170 s as determined by HOM monomer loss. The resulting HO<sub>2</sub>/RO<sub>2</sub> ratios of the sensitivity study for the apinCO\_1 experiment are displayed in **Table A6** as an example.

**Table A6** Box model HO<sub>2</sub>/RO<sub>2</sub> ratio results at varying RO<sub>2</sub> and HO<sub>2</sub> wall loss at low HO<sub>2</sub>/RO<sub>2</sub> (left) and high HO<sub>2</sub>/RO<sub>2</sub> (right) in the apinCO\_1 experiment

$\tau(HO_2) \backslash \tau(RO_2)$	low HO <sub>2</sub> /RO <sub>2</sub>		high HO <sub>2</sub> /RO <sub>2</sub>	
	<u>50 s</u>	<u>170 s</u>	<u>50 s</u>	<u>170 s</u>
<u>145 s</u>	6.8E-3	7.5E-3	0.7	1.0
<u>170 s</u>	6.4E-3	7.0E-3	0.6	0.9
<u>195 s</u>	6.1E-3	6.7E-3	0.6	0.9

The sensitivity study shows that independent of the assumed wall loss rate the HO<sub>2</sub>/RO<sub>2</sub> ratio is around 0.007 and near one in the low and high HO<sub>2</sub>/RO<sub>2</sub> case, respectively. In any case, the modeling results are only used to qualify the change of chemical regime and not to yield absolute values.

A.4.2 Box model results: HO<sub>2</sub>, RO<sub>2</sub>, NO and pinonaldehyde

**Table A7** Modeling results for HO<sub>2</sub>, RO<sub>2</sub> sum, NO and pinonaldehyde. For NO the concentration is given additionally as a mixing ratio in parentheses. The experiment phases are ordered chronologically. (g) marks unseeded experiment stages, (s) seeded. These results only serve as indication of the expected trends as we cannot verify their results.

<u>Experiment phase</u>	<u>HO<sub>2</sub> [cm<sup>-3</sup>]</u>	<u>ΣRO<sub>2</sub> [cm<sup>-3</sup>]</u>	<u>NO [cm<sup>-3</sup>] (ppbv)</u>	<u>Pinonaldehyde [cm<sup>-3</sup>]</u>
<u>Experiment: apinCO_1</u>				
<u>Photooxidation base case (g)</u>	3.8·10 <sup>7</sup>	6.0·10 <sup>9</sup>	-	1.3·10 <sup>10</sup>
<u>High HO<sub>2</sub> case (g)</u>	1.2·10 <sup>9</sup>	1.9·10 <sup>9</sup>	-	4.8·10 <sup>9</sup>
<u>Experiment: apinCO_2</u>				
<u>Photooxidation base case (s)</u>	4.6·10 <sup>7</sup>	6.8·10 <sup>9</sup>	-	1.1·10 <sup>10</sup>
<u>High HO<sub>2</sub> case (s)</u>	1.5·10 <sup>9</sup>	2.0·10 <sup>9</sup>	-	3.7·10 <sup>9</sup>
<u>High HO<sub>2</sub> case (g)</u>	1.5·10 <sup>9</sup>	1.9·10 <sup>9</sup>	-	3.6·10 <sup>9</sup>
<u>Photooxidation base case (g)</u>	4.7·10 <sup>7</sup>	6.9·10 <sup>9</sup>	-	1.1·10 <sup>10</sup>
<u>Experiment: apinNO</u>				
<u>Photooxidation base case (g)</u>	5.7·10 <sup>7</sup>	7.5·10 <sup>9</sup>	-	6.3·10 <sup>9</sup>
<u>(Additional: low NO case (g) )</u>	1.7·10 <sup>8</sup>	4.6·10 <sup>9</sup>	7.6·10 <sup>8</sup> (0.03)	1.8·10 <sup>10</sup>
<u>Middle NO case (g)</u>	3.7·10 <sup>8</sup>	1.8·10 <sup>9</sup>	4.3·10 <sup>9</sup> (0.17)	2.8·10 <sup>10</sup>
<u>High NO case (g)</u>	2.7·10 <sup>8</sup>	6.7·10 <sup>8</sup>	1.8·10 <sup>10</sup> (0.71)	3.4·10 <sup>10</sup>
<u>High NO case (s)</u>	2.7·10 <sup>8</sup>	6.7·10 <sup>8</sup>	1.8·10 <sup>10</sup> (0.71)	3.4·10 <sup>10</sup>
<u>Middle NO case (s)</u>	3.6·10 <sup>8</sup>	1.7·10 <sup>9</sup>	4.6·10 <sup>9</sup> (0.18)	2.8·10 <sup>10</sup>
<u>(Additional: low NO case (s) )</u>	1.8·10 <sup>8</sup>	4.2·10 <sup>9</sup>	8.3·10 <sup>8</sup> (0.03)	1.8·10 <sup>10</sup>
<u>Experiment: apinCONO_1</u>				
<u>Photooxidation base case (s)</u>	4.4·10 <sup>7</sup>	6.3·10 <sup>9</sup>	-	9.8·10 <sup>9</sup>
<u>High HO<sub>2</sub> case (s)</u>	1.7·10 <sup>9</sup>	1.7·10 <sup>9</sup>	-	3.1·10 <sup>9</sup>
<u>Middle NO, high HO<sub>2</sub> case (s)</u>	1.9·10 <sup>9</sup>	1.0·10 <sup>9</sup>	4.5·10 <sup>9</sup> (0.18)	2.7·10 <sup>10</sup>
<u>(Additional: in-between NO, high HO<sub>2</sub> case (s) )</u>	1.6·10 <sup>9</sup>	6.9·10 <sup>8</sup>	1.1·10 <sup>10</sup> (0.42)	3.4·10 <sup>10</sup>
<u>High NO, high HO<sub>2</sub> case (s)</u>	1.3·10 <sup>9</sup>	5.6·10 <sup>8</sup>	1.6·10 <sup>10</sup> (0.62)	3.8·10 <sup>10</sup>
<u>High NO, high HO<sub>2</sub> case (g)</u>	1.3·10 <sup>9</sup>	5.2·10 <sup>8</sup>	1.6·10 <sup>10</sup> (0.63)	3.5·10 <sup>10</sup>
<u>(Additional: in-between NO, high HO<sub>2</sub> case (g) )</u>	1.6·10 <sup>9</sup>	6.5·10 <sup>8</sup>	1.1·10 <sup>10</sup> (0.43)	3.2·10 <sup>10</sup>
<u>Middle NO, high HO<sub>2</sub> case (g)</u>	1.9·10 <sup>9</sup>	8.9·10 <sup>8</sup>	4.8·10 <sup>9</sup> (0.19)	2.4·10 <sup>10</sup>
<u>Experiment: apinCONO_2</u>				
<u>Photooxidation base case (s)</u>	3.6·10 <sup>7</sup>	4.7·10 <sup>9</sup>	-	5.1·10 <sup>9</sup>
<u>Photooxidation base case (g)</u>	3.7·10 <sup>7</sup>	5.0·10 <sup>9</sup>	-	6.1·10 <sup>9</sup>
<u>High NO, high HO<sub>2</sub> case (s)</u>	1.2·10 <sup>9</sup>	4.9·10 <sup>8</sup>	1.4·10 <sup>10</sup> (0.55)	3.5·10 <sup>10</sup>
<u>High NO, high HO<sub>2</sub> case (g)</u>	1.2·10 <sup>9</sup>	4.2·10 <sup>8</sup>	1.4·10 <sup>10</sup> (0.57)	3.0·10 <sup>10</sup>

## A.5 Error propagation

Error propagation was utilized to estimate the error of derived parameters. For a parameter  $q$ , the error is defined by the errors of the variables  $x, \dots, z$  necessary to calculate  $q$ . The general equation to calculate the absolute uncertainty  $\delta q$  can be found in *Eq. A-2*. This equation is only valid if the uncertainties in  $x, \dots, z$  are independent and random. (Taylor, 1997)

$$\delta q = \sqrt{\left(\frac{\partial q}{\partial x} \delta x\right)^2 + \dots + \left(\frac{\partial q}{\partial z} \delta z\right)^2} \quad \text{Eq. A-2}$$

For all measured parameters the measured standard deviation in steady state was used as the absolute uncertainty. For parameters that cannot be measured directly their uncertainties were calculated with error propagation as shown in *Eq. A-2*. For the uncertainty of the diffusion coefficient, Tang et al. (2015) reviewed diffusion coefficient calculation and came to the result that the difference between measurement and estimation via the method of Fuller et al. (1966) are mostly below 10 %. Therefore, we assumed a 10 % uncertainty for the diffusion coefficient of each formula composition.

## A.6 Peaklists

### A.6.1 $\alpha$ -Pinene + OH in the base and high HO<sub>2</sub> case

**Table A8** Peaklist NO<sub>3</sub>-MION-CIMS for base and high HO<sub>2</sub> cases. All compounds were detected as clusters with (NO<sub>3</sub>). The table is sorted into fragments, monomers, and accretion products. Some compounds were just assignable in certain experiments, this is indicated by the superscript, no superscript indicated that the compound was assigned in all experiments. (1=apinCO\_1, 2=apinCO\_2, 3=apinCONO\_1 [-], 4= apinCONO\_2 [-])

Fragments		Monomers	Accretion products			
C <sub>5</sub> H <sub>6</sub> O <sub>4</sub> <sup>1</sup>	C <sub>8</sub> H <sub>10</sub> O <sub>6</sub>	C <sub>10</sub> H <sub>14</sub> O <sub>5</sub>	C <sub>14</sub> H <sub>20</sub> O <sub>9</sub>	C <sub>17</sub> H <sub>24</sub> O <sub>7</sub>	C <sub>19</sub> H <sub>26</sub> O <sub>8</sub> <sup>1,2,4</sup>	C <sub>20</sub> H <sub>28</sub> O <sub>9</sub>
C <sub>5</sub> H <sub>6</sub> O <sub>5</sub>	C <sub>8</sub> H <sub>10</sub> O <sub>7</sub>	C <sub>10</sub> H <sub>14</sub> O <sub>6</sub>	C <sub>14</sub> H <sub>22</sub> O <sub>10</sub>	C <sub>17</sub> H <sub>24</sub> O <sub>9</sub>	C <sub>19</sub> H <sub>28</sub> O <sub>7</sub>	C <sub>20</sub> H <sub>28</sub> O <sub>11</sub>
C <sub>5</sub> H <sub>6</sub> O <sub>6</sub>	C <sub>8</sub> H <sub>10</sub> O <sub>10</sub> <sup>1</sup>	C <sub>10</sub> H <sub>14</sub> O <sub>7</sub>	C <sub>14</sub> H <sub>22</sub> O <sub>11</sub> <sup>1,2,4</sup>	C <sub>17</sub> H <sub>24</sub> O <sub>10</sub> <sup>1,2,4</sup>	C <sub>19</sub> H <sub>28</sub> O <sub>8</sub>	C <sub>20</sub> H <sub>30</sub> O <sub>6</sub>
C <sub>5</sub> H <sub>6</sub> O <sub>7</sub>	C <sub>8</sub> H <sub>12</sub> O <sub>5</sub> <sup>1,2,4</sup>	C <sub>10</sub> H <sub>14</sub> O <sub>8</sub>	C <sub>14</sub> H <sub>26</sub> O <sub>11</sub>	C <sub>17</sub> H <sub>24</sub> O <sub>11</sub>	C <sub>19</sub> H <sub>28</sub> O <sub>9</sub>	C <sub>20</sub> H <sub>30</sub> O <sub>7</sub>
C <sub>5</sub> H <sub>6</sub> O <sub>8</sub> <sup>2,4</sup>	C <sub>8</sub> H <sub>12</sub> O <sub>6</sub>	C <sub>10</sub> H <sub>14</sub> O <sub>9</sub>		C <sub>17</sub> H <sub>24</sub> O <sub>13</sub> <sup>1,2,4</sup>	C <sub>19</sub> H <sub>28</sub> O <sub>10</sub>	C <sub>20</sub> H <sub>30</sub> O <sub>8</sub>
C <sub>5</sub> H <sub>7</sub> O <sub>8</sub>	C <sub>8</sub> H <sub>12</sub> O <sub>7</sub>	C <sub>10</sub> H <sub>14</sub> O <sub>10</sub>	C <sub>15</sub> H <sub>20</sub> O <sub>14</sub> <sup>1</sup>	C <sub>17</sub> H <sub>26</sub> O <sub>8</sub>	C <sub>19</sub> H <sub>28</sub> O <sub>11</sub>	C <sub>20</sub> H <sub>30</sub> O <sub>9</sub>
C <sub>5</sub> H <sub>8</sub> O <sub>7</sub>	C <sub>8</sub> H <sub>12</sub> O <sub>8</sub>	C <sub>10</sub> H <sub>14</sub> O <sub>11</sub>	C <sub>15</sub> H <sub>22</sub> O <sub>9</sub>	C <sub>17</sub> H <sub>26</sub> O <sub>9</sub>	C <sub>19</sub> H <sub>28</sub> O <sub>12</sub> <sup>1,2</sup>	C <sub>20</sub> H <sub>30</sub> O <sub>10</sub>
	C <sub>8</sub> H <sub>12</sub> O <sub>9</sub>		C <sub>15</sub> H <sub>22</sub> O <sub>10</sub>	C <sub>17</sub> H <sub>26</sub> O <sub>10</sub>	C <sub>19</sub> H <sub>28</sub> O <sub>13</sub> <sup>1,2,3</sup>	C <sub>20</sub> H <sub>30</sub> O <sub>11</sub>
C <sub>6</sub> H <sub>6</sub> O <sub>4</sub> <sup>1,3,4</sup>	C <sub>8</sub> H <sub>13</sub> O <sub>8</sub>	C <sub>10</sub> H <sub>15</sub> O <sub>5</sub>	C <sub>15</sub> H <sub>22</sub> O <sub>11</sub>	C <sub>17</sub> H <sub>26</sub> O <sub>11</sub>	C <sub>19</sub> H <sub>28</sub> O <sub>14</sub> <sup>1,2</sup>	C <sub>20</sub> H <sub>30</sub> O <sub>12</sub>
C <sub>6</sub> H <sub>10</sub> O <sub>5</sub>	C <sub>8</sub> H <sub>13</sub> O <sub>9</sub>	C <sub>10</sub> H <sub>15</sub> O <sub>6</sub>	C <sub>15</sub> H <sub>22</sub> O <sub>12</sub> <sup>1,2,4</sup>	C <sub>17</sub> H <sub>26</sub> O <sub>12</sub>	C <sub>19</sub> H <sub>28</sub> O <sub>15</sub> <sup>1</sup>	C <sub>20</sub> H <sub>30</sub> O <sub>13</sub>
C <sub>6</sub> H <sub>10</sub> O <sub>6</sub>	C <sub>8</sub> H <sub>14</sub> O <sub>5</sub>	C <sub>10</sub> H <sub>15</sub> O <sub>7</sub>	C <sub>15</sub> H <sub>22</sub> O <sub>13</sub> <sup>1</sup>	C <sub>17</sub> H <sub>26</sub> O <sub>13</sub> <sup>1,2</sup>	C <sub>19</sub> H <sub>28</sub> O <sub>16</sub> <sup>1,2</sup>	C <sub>20</sub> H <sub>30</sub> O <sub>14</sub>
C <sub>6</sub> H <sub>10</sub> O <sub>7</sub>	C <sub>8</sub> H <sub>14</sub> O <sub>6</sub>	C <sub>10</sub> H <sub>15</sub> O <sub>8</sub>	C <sub>15</sub> H <sub>22</sub> O <sub>14</sub> <sup>1</sup>	C <sub>17</sub> H <sub>26</sub> O <sub>14</sub> <sup>1,2,4</sup>	C <sub>19</sub> H <sub>30</sub> O <sub>6</sub>	C <sub>20</sub> H <sub>30</sub> O <sub>15</sub>
C <sub>6</sub> H <sub>12</sub> O <sub>6</sub> <sup>4</sup>	C <sub>8</sub> H <sub>14</sub> O <sub>7</sub>	C <sub>10</sub> H <sub>15</sub> O <sub>9</sub>	C <sub>15</sub> H <sub>24</sub> O <sub>13</sub> <sup>1,2,4</sup>	C <sub>17</sub> H <sub>28</sub> O <sub>8</sub>	C <sub>19</sub> H <sub>30</sub> O <sub>7</sub>	C <sub>20</sub> H <sub>30</sub> O <sub>16</sub>
	C <sub>8</sub> H <sub>14</sub> O <sub>8</sub>	C <sub>10</sub> H <sub>15</sub> O <sub>10</sub>	C <sub>15</sub> H <sub>26</sub> O <sub>10</sub> <sup>1,2,4</sup>	C <sub>17</sub> H <sub>28</sub> O <sub>9</sub>	C <sub>19</sub> H <sub>30</sub> O <sub>8</sub>	C <sub>20</sub> H <sub>30</sub> O <sub>17</sub> <sup>4</sup>
C <sub>7</sub> H <sub>8</sub> O <sub>5</sub> <sup>3,4</sup>	C <sub>8</sub> H <sub>14</sub> O <sub>9</sub>	C <sub>10</sub> H <sub>15</sub> O <sub>11</sub>		C <sub>17</sub> H <sub>28</sub> O <sub>10</sub>	C <sub>19</sub> H <sub>30</sub> O <sub>9</sub>	C <sub>20</sub> H <sub>30</sub> O <sub>18</sub>
C <sub>7</sub> H <sub>8</sub> O <sub>6</sub> <sup>3</sup>		C <sub>10</sub> H <sub>15</sub> O <sub>12</sub>	C <sub>16</sub> H <sub>22</sub> O <sub>9</sub> <sup>1,2,4</sup>	C <sub>17</sub> H <sub>28</sub> O <sub>11</sub>	C <sub>19</sub> H <sub>30</sub> O <sub>10</sub>	C <sub>20</sub> H <sub>32</sub> O <sub>6</sub>
C <sub>7</sub> H <sub>8</sub> O <sub>7</sub>	C <sub>9</sub> H <sub>12</sub> O <sub>4</sub> <sup>4</sup>		C <sub>16</sub> H <sub>24</sub> O <sub>9</sub>	C <sub>17</sub> H <sub>28</sub> O <sub>12</sub>	C <sub>19</sub> H <sub>30</sub> O <sub>11</sub>	C <sub>20</sub> H <sub>32</sub> O <sub>7</sub>
C <sub>7</sub> H <sub>8</sub> O <sub>8</sub>	C <sub>9</sub> H <sub>12</sub> O <sub>5</sub>	C <sub>10</sub> H <sub>16</sub> O <sub>3</sub> <sup>4</sup>	C <sub>16</sub> H <sub>24</sub> O <sub>10</sub>		C <sub>19</sub> H <sub>30</sub> O <sub>12</sub>	C <sub>20</sub> H <sub>32</sub> O <sub>8</sub>
C <sub>7</sub> H <sub>10</sub> O <sub>5</sub> <sup>1,3,4</sup>	C <sub>9</sub> H <sub>12</sub> O <sub>6</sub>	C <sub>10</sub> H <sub>16</sub> O <sub>4</sub>	C <sub>16</sub> H <sub>24</sub> O <sub>11</sub>	C <sub>18</sub> H <sub>26</sub> O <sub>9</sub>	C <sub>19</sub> H <sub>30</sub> O <sub>13</sub>	C <sub>20</sub> H <sub>32</sub> O <sub>9</sub>
C <sub>7</sub> H <sub>10</sub> O <sub>6</sub>	C <sub>9</sub> H <sub>12</sub> O <sub>7</sub>	C <sub>10</sub> H <sub>16</sub> O <sub>5</sub>	C <sub>16</sub> H <sub>24</sub> O <sub>12</sub> <sup>1,2,4</sup>	C <sub>18</sub> H <sub>26</sub> O <sub>10</sub>	C <sub>19</sub> H <sub>30</sub> O <sub>14</sub> <sup>1,2,4</sup>	C <sub>20</sub> H <sub>32</sub> O <sub>10</sub>
C <sub>7</sub> H <sub>10</sub> O <sub>7</sub>	C <sub>9</sub> H <sub>12</sub> O <sub>8</sub>	C <sub>10</sub> H <sub>16</sub> O <sub>6</sub>	C <sub>16</sub> H <sub>26</sub> O <sub>8</sub>	C <sub>18</sub> H <sub>26</sub> O <sub>11</sub>	C <sub>19</sub> H <sub>30</sub> O <sub>15</sub> <sup>1,2</sup>	C <sub>20</sub> H <sub>32</sub> O <sub>11</sub>
C <sub>7</sub> H <sub>10</sub> O <sub>8</sub>	C <sub>9</sub> H <sub>12</sub> O <sub>9</sub>	C <sub>10</sub> H <sub>16</sub> O <sub>7</sub>	C <sub>16</sub> H <sub>26</sub> O <sub>9</sub>	C <sub>18</sub> H <sub>26</sub> O <sub>15</sub> <sup>1</sup>	C <sub>19</sub> H <sub>30</sub> O <sub>16</sub> <sup>1,4</sup>	C <sub>20</sub> H <sub>32</sub> O <sub>12</sub>
C <sub>7</sub> H <sub>10</sub> O <sub>9</sub> <sup>1,2,4</sup>	C <sub>9</sub> H <sub>12</sub> O <sub>12</sub> <sup>2</sup>	C <sub>10</sub> H <sub>16</sub> O <sub>8</sub>	C <sub>16</sub> H <sub>26</sub> O <sub>10</sub>	C <sub>18</sub> H <sub>28</sub> O <sub>6</sub>	C <sub>19</sub> H <sub>32</sub> O <sub>7</sub>	C <sub>20</sub> H <sub>32</sub> O <sub>13</sub>
C <sub>7</sub> H <sub>10</sub> O <sub>10</sub>	C <sub>9</sub> H <sub>13</sub> O <sub>9</sub> <sup>1,2,3</sup>	C <sub>10</sub> H <sub>16</sub> O <sub>9</sub>	C <sub>16</sub> H <sub>26</sub> O <sub>11</sub>	C <sub>18</sub> H <sub>28</sub> O <sub>8</sub>	C <sub>19</sub> H <sub>32</sub> O <sub>8</sub>	C <sub>20</sub> H <sub>32</sub> O <sub>14</sub>
C <sub>7</sub> H <sub>14</sub> O <sub>5</sub> <sup>1,2,4</sup>	C <sub>9</sub> H <sub>13</sub> O <sub>10</sub>	C <sub>10</sub> H <sub>16</sub> O <sub>10</sub>	C <sub>16</sub> H <sub>26</sub> O <sub>12</sub>	C <sub>18</sub> H <sub>28</sub> O <sub>9</sub> <sup>1,4</sup>	C <sub>19</sub> H <sub>32</sub> O <sub>9</sub>	C <sub>20</sub> H <sub>32</sub> O <sub>15</sub>
C <sub>7</sub> H <sub>14</sub> O <sub>6</sub>	C <sub>9</sub> H <sub>14</sub> O <sub>4</sub>	C <sub>10</sub> H <sub>16</sub> O <sub>11</sub>	C <sub>16</sub> H <sub>26</sub> O <sub>13</sub> <sup>2,4</sup>	C <sub>18</sub> H <sub>28</sub> O <sub>10</sub>	C <sub>19</sub> H <sub>32</sub> O <sub>10</sub>	C <sub>20</sub> H <sub>34</sub> O <sub>6</sub>
	C <sub>9</sub> H <sub>14</sub> O <sub>5</sub>		C <sub>16</sub> H <sub>28</sub> O <sub>18</sub> <sup>1,2,4</sup>	C <sub>18</sub> H <sub>28</sub> O <sub>11</sub>	C <sub>19</sub> H <sub>32</sub> O <sub>11</sub>	C <sub>20</sub> H <sub>34</sub> O <sub>7</sub>
	C <sub>9</sub> H <sub>14</sub> O <sub>6</sub>	C <sub>10</sub> H <sub>17</sub> O <sub>6</sub>		C <sub>18</sub> H <sub>28</sub> O <sub>12</sub> <sup>1,2,4</sup>	C <sub>19</sub> H <sub>32</sub> O <sub>12</sub>	C <sub>20</sub> H <sub>34</sub> O <sub>8</sub>
	C <sub>9</sub> H <sub>14</sub> O <sub>7</sub>	C <sub>10</sub> H <sub>17</sub> O <sub>7</sub>		C <sub>18</sub> H <sub>28</sub> O <sub>13</sub>	C <sub>19</sub> H <sub>32</sub> O <sub>13</sub> <sup>1,4</sup>	C <sub>20</sub> H <sub>34</sub> O <sub>9</sub>
	C <sub>9</sub> H <sub>14</sub> O <sub>8</sub>	C <sub>10</sub> H <sub>17</sub> O <sub>8</sub>		C <sub>18</sub> H <sub>28</sub> O <sub>14</sub> <sup>1,3,4</sup>	C <sub>19</sub> H <sub>32</sub> O <sub>14</sub> <sup>1,2,4</sup>	C <sub>20</sub> H <sub>34</sub> O <sub>10</sub>
	C <sub>9</sub> H <sub>14</sub> O <sub>9</sub>	C <sub>10</sub> H <sub>17</sub> O <sub>9</sub>		C <sub>18</sub> H <sub>28</sub> O <sub>15</sub> <sup>1,4</sup>		C <sub>20</sub> H <sub>34</sub> O <sub>11</sub>
	C <sub>9</sub> H <sub>14</sub> O <sub>10</sub>	C <sub>10</sub> H <sub>17</sub> O <sub>10</sub> <sup>1,3</sup>		C <sub>18</sub> H <sub>28</sub> O <sub>16</sub> <sup>1,3,4</sup>		C <sub>20</sub> H <sub>34</sub> O <sub>12</sub>
	C <sub>9</sub> H <sub>16</sub> O <sub>5</sub>	C <sub>10</sub> H <sub>17</sub> O <sub>11</sub> <sup>3</sup>		C <sub>18</sub> H <sub>30</sub> O <sub>7</sub>		C <sub>20</sub> H <sub>34</sub> O <sub>13</sub>
	C <sub>9</sub> H <sub>16</sub> O <sub>6</sub>			C <sub>18</sub> H <sub>30</sub> O <sub>8</sub>		C <sub>20</sub> H <sub>34</sub> O <sub>14</sub> <sup>4</sup>
	C <sub>9</sub> H <sub>16</sub> O <sub>7</sub>	C <sub>10</sub> H <sub>18</sub> O <sub>4</sub>		C <sub>18</sub> H <sub>30</sub> O <sub>9</sub>		C <sub>20</sub> H <sub>34</sub> O <sub>16</sub> <sup>4</sup>
	C <sub>9</sub> H <sub>16</sub> O <sub>8</sub>	C <sub>10</sub> H <sub>18</sub> O <sub>5</sub>		C <sub>18</sub> H <sub>30</sub> O <sub>10</sub>		
		C <sub>10</sub> H <sub>18</sub> O <sub>6</sub>		C <sub>18</sub> H <sub>30</sub> O <sub>11</sub>		
		C <sub>10</sub> H <sub>18</sub> O <sub>7</sub>		C <sub>18</sub> H <sub>30</sub> O <sub>12</sub>		
		C <sub>10</sub> H <sub>18</sub> O <sub>8</sub>		C <sub>18</sub> H <sub>30</sub> O <sub>13</sub>		
		C <sub>10</sub> H <sub>18</sub> O <sub>9</sub>		C <sub>18</sub> H <sub>30</sub> O <sub>14</sub> <sup>1,4</sup>		

A.6.2  $\alpha$ -Pinene + OH at low and high HO<sub>2</sub> with NO in the system

**Table A9** Peaklist NO<sub>3</sub>-MION-CIMS for cases with NO (Fragments). All compounds were detected as clusters with (NO<sub>3</sub>). The table is sorted into fragments, monomers, and accretion products. Some compounds were just assignable in certain experiments, this is indicated by the superscript, no superscript indicated that the compound was assigned in all experiments. (5=apinNO, 6=apinCONO\_1 [with NO], 7= apinCONO\_2 [with NO])

Fragments				
C <sub>5</sub> H <sub>5</sub> NO <sub>7</sub>	C <sub>6</sub> H <sub>6</sub> N <sub>2</sub> O <sub>6</sub> <sup>5,6</sup>	C <sub>7</sub> H <sub>6</sub> O	C <sub>8</sub> H <sub>10</sub> O <sub>6</sub>	C <sub>9</sub> H <sub>12</sub> O <sub>4</sub> <sup>7</sup>
C <sub>5</sub> H <sub>5</sub> NO <sub>8</sub> <sup>5,6</sup>			C <sub>8</sub> H <sub>10</sub> O <sub>7</sub>	C <sub>9</sub> H <sub>12</sub> O <sub>5</sub>
C <sub>5</sub> H <sub>5</sub> NO <sub>9</sub>	C <sub>6</sub> H <sub>6</sub> O <sub>4</sub>	C <sub>7</sub> H <sub>7</sub> NO <sub>4</sub>	C <sub>8</sub> H <sub>10</sub> O <sub>10</sub>	C <sub>9</sub> H <sub>12</sub> O <sub>6</sub>
	C <sub>6</sub> H <sub>6</sub> O <sub>5</sub>	C <sub>7</sub> H <sub>7</sub> NO <sub>6</sub> <sup>7</sup>		C <sub>9</sub> H <sub>12</sub> O <sub>7</sub>
C <sub>5</sub> H <sub>6</sub> O <sub>5</sub>		C <sub>7</sub> H <sub>7</sub> NO <sub>8</sub>	C <sub>8</sub> H <sub>11</sub> NO <sub>6</sub> <sup>5</sup>	C <sub>9</sub> H <sub>12</sub> O <sub>8</sub>
C <sub>5</sub> H <sub>6</sub> O <sub>6</sub> <sup>6,7</sup>	C <sub>6</sub> H <sub>7</sub> NO <sub>6</sub>	C <sub>7</sub> H <sub>7</sub> NO <sub>9</sub>	C <sub>8</sub> H <sub>11</sub> NO <sub>7</sub> <sup>7</sup>	C <sub>9</sub> H <sub>12</sub> O <sub>9</sub>
C <sub>5</sub> H <sub>6</sub> O <sub>7</sub>	C <sub>6</sub> H <sub>7</sub> NO <sub>8</sub>		C <sub>8</sub> H <sub>11</sub> NO <sub>8</sub> <sup>5,6</sup>	
C <sub>5</sub> H <sub>6</sub> O <sub>8</sub> <sup>5,6</sup>		C <sub>7</sub> H <sub>8</sub> O <sub>6</sub>	C <sub>8</sub> H <sub>11</sub> NO <sub>9</sub>	C <sub>9</sub> H <sub>13</sub> NO <sub>8</sub>
	C <sub>6</sub> H <sub>8</sub> O <sub>6</sub>	C <sub>7</sub> H <sub>8</sub> O <sub>7</sub>	C <sub>8</sub> H <sub>11</sub> NO <sub>11</sub>	C <sub>9</sub> H <sub>13</sub> NO <sub>9</sub>
C <sub>5</sub> H <sub>7</sub> NO <sub>6</sub>	C <sub>6</sub> H <sub>8</sub> O <sub>7</sub>	C <sub>7</sub> H <sub>8</sub> O <sub>8</sub>		C <sub>9</sub> H <sub>13</sub> NO <sub>10</sub>
C <sub>5</sub> H <sub>7</sub> NO <sub>7</sub>			C <sub>8</sub> H <sub>12</sub> O <sub>5</sub> <sup>5,6</sup>	C <sub>9</sub> H <sub>13</sub> NO <sub>11</sub>
C <sub>5</sub> H <sub>7</sub> NO <sub>8</sub>	C <sub>6</sub> H <sub>9</sub> NO <sub>6</sub>	C <sub>7</sub> H <sub>9</sub> NO <sub>6</sub>	C <sub>8</sub> H <sub>12</sub> O <sub>6</sub>	
C <sub>5</sub> H <sub>7</sub> NO <sub>9</sub>	C <sub>6</sub> H <sub>9</sub> NO <sub>7</sub>	C <sub>7</sub> H <sub>9</sub> NO <sub>7</sub>	C <sub>8</sub> H <sub>12</sub> O <sub>7</sub>	C <sub>9</sub> H <sub>13</sub> O <sub>10</sub>
C <sub>5</sub> H <sub>7</sub> NO <sub>10</sub>	C <sub>6</sub> H <sub>9</sub> NO <sub>8</sub>	C <sub>7</sub> H <sub>9</sub> NO <sub>8</sub>	C <sub>8</sub> H <sub>12</sub> O <sub>8</sub>	
	C <sub>6</sub> H <sub>9</sub> NO <sub>9</sub>	C <sub>7</sub> H <sub>9</sub> NO <sub>9</sub>	C <sub>8</sub> H <sub>12</sub> O <sub>9</sub>	C <sub>9</sub> H <sub>14</sub> O <sub>4</sub>
C <sub>5</sub> H <sub>8</sub> O <sub>5</sub> <sup>7</sup>	C <sub>6</sub> H <sub>9</sub> NO <sub>10</sub>	C <sub>7</sub> H <sub>9</sub> NO <sub>10</sub>		C <sub>9</sub> H <sub>14</sub> O <sub>5</sub> <sup>6,7</sup>
C <sub>5</sub> H <sub>8</sub> O <sub>7</sub>		C <sub>7</sub> H <sub>9</sub> NO <sub>11</sub>	C <sub>8</sub> H <sub>13</sub> NO <sub>6</sub>	C <sub>9</sub> H <sub>14</sub> O <sub>6</sub>
	C <sub>6</sub> H <sub>10</sub> O <sub>5</sub>		C <sub>8</sub> H <sub>13</sub> NO <sub>7</sub>	C <sub>9</sub> H <sub>14</sub> O <sub>7</sub>
C <sub>5</sub> H <sub>9</sub> NO <sub>6</sub>	C <sub>6</sub> H <sub>10</sub> O <sub>6</sub>	C <sub>7</sub> H <sub>10</sub> O <sub>5</sub> <sup>7</sup>	C <sub>8</sub> H <sub>13</sub> NO <sub>8</sub>	C <sub>9</sub> H <sub>14</sub> O <sub>8</sub>
	C <sub>6</sub> H <sub>10</sub> O <sub>7</sub>	C <sub>7</sub> H <sub>10</sub> O <sub>6</sub>	C <sub>8</sub> H <sub>13</sub> NO <sub>9</sub>	C <sub>9</sub> H <sub>14</sub> O <sub>9</sub>
		C <sub>7</sub> H <sub>10</sub> O <sub>7</sub>	C <sub>8</sub> H <sub>13</sub> NO <sub>10</sub>	C <sub>9</sub> H <sub>14</sub> O <sub>10</sub>
	C <sub>6</sub> H <sub>11</sub> NO <sub>6</sub> <sup>7</sup>	C <sub>7</sub> H <sub>10</sub> O <sub>8</sub>	C <sub>8</sub> H <sub>13</sub> NO <sub>11</sub>	
	C <sub>6</sub> H <sub>11</sub> NO <sub>7</sub> <sup>7</sup>	C <sub>7</sub> H <sub>10</sub> O <sub>9</sub>		C <sub>9</sub> H <sub>15</sub> NO <sub>6</sub> <sup>5,7</sup>
	C <sub>6</sub> H <sub>11</sub> NO <sub>8</sub> <sup>7</sup>	C <sub>7</sub> H <sub>10</sub> O <sub>10</sub>	C <sub>8</sub> H <sub>13</sub> O <sub>8</sub>	C <sub>9</sub> H <sub>15</sub> NO <sub>7</sub> <sup>5,7</sup>
	C <sub>6</sub> H <sub>11</sub> NO <sub>9</sub> <sup>7</sup>			C <sub>9</sub> H <sub>15</sub> NO <sub>8</sub>
		C <sub>7</sub> H <sub>11</sub> NO <sub>6</sub>	C <sub>8</sub> H <sub>14</sub> O <sub>5</sub>	C <sub>9</sub> H <sub>15</sub> NO <sub>9</sub>
		C <sub>7</sub> H <sub>11</sub> NO <sub>7</sub> <sup>7</sup>	C <sub>8</sub> H <sub>14</sub> O <sub>6</sub>	C <sub>9</sub> H <sub>15</sub> NO <sub>10</sub>
		C <sub>7</sub> H <sub>11</sub> NO <sub>9</sub>	C <sub>8</sub> H <sub>14</sub> O <sub>7</sub>	
			C <sub>8</sub> H <sub>14</sub> O <sub>8</sub>	C <sub>9</sub> H <sub>16</sub> O <sub>5</sub>
		C <sub>7</sub> H <sub>12</sub> O <sub>5</sub>	C <sub>8</sub> H <sub>14</sub> O <sub>9</sub>	C <sub>9</sub> H <sub>16</sub> O <sub>6</sub>
		C <sub>7</sub> H <sub>12</sub> O <sub>5</sub>		C <sub>9</sub> H <sub>16</sub> O <sub>7</sub>
		C <sub>7</sub> H <sub>13</sub> NO <sub>7</sub> <sup>7</sup>		C <sub>9</sub> H <sub>16</sub> O <sub>8</sub>
		C <sub>7</sub> H <sub>14</sub> O <sub>6</sub> <sup>7</sup>		

**Table A10** Peaklist NO<sub>3</sub>-MION-CIMS for cases with NO (Monomers and Accretion products). All compounds were detected as clusters with (NO<sub>3</sub>)<sup>-</sup>. The table is sorted into fragments, monomers, and accretion products. Some compounds were just assignable in certain experiments, this is indicated by the superscript, no superscript indicated that the compound was assigned in all experiments. (5=apinNO, 6=apinCONO\_1 [with NO], 7=apinCONO\_2 [with NO])

Monomers		Accretion products		
C <sub>10</sub> H <sub>13</sub> NO <sub>7</sub>	C <sub>10</sub> H <sub>16</sub> O <sub>4</sub>	C <sub>14</sub> H <sub>22</sub> O <sub>10</sub>	C <sub>18</sub> H <sub>26</sub> O <sub>9</sub> <sup>7</sup>	C <sub>20</sub> H <sub>28</sub> O <sub>9</sub>
C <sub>10</sub> H <sub>13</sub> NO <sub>8</sub>	C <sub>10</sub> H <sub>16</sub> O <sub>5</sub>		C <sub>18</sub> H <sub>26</sub> O <sub>10</sub> <sup>7</sup>	C <sub>20</sub> H <sub>28</sub> O <sub>11</sub>
C <sub>10</sub> H <sub>13</sub> NO <sub>9</sub>	C <sub>10</sub> H <sub>16</sub> O <sub>6</sub>	C <sub>15</sub> H <sub>22</sub> O <sub>9</sub> <sup>7</sup>	C <sub>18</sub> H <sub>26</sub> O <sub>11</sub>	
C <sub>10</sub> H <sub>13</sub> NO <sub>10</sub>	C <sub>10</sub> H <sub>16</sub> O <sub>7</sub>	C <sub>15</sub> H <sub>22</sub> O <sub>10</sub>	C <sub>18</sub> H <sub>26</sub> O <sub>12</sub>	C <sub>20</sub> H <sub>30</sub> O <sub>6</sub> <sup>7</sup>
C <sub>10</sub> H <sub>13</sub> NO <sub>11</sub>	C <sub>10</sub> H <sub>16</sub> O <sub>8</sub>	C <sub>15</sub> H <sub>22</sub> O <sub>11</sub>		C <sub>20</sub> H <sub>30</sub> O <sub>7</sub>
C <sub>10</sub> H <sub>13</sub> NO <sub>12</sub>	C <sub>10</sub> H <sub>16</sub> O <sub>9</sub>	C <sub>15</sub> H <sub>22</sub> O <sub>12</sub>	C <sub>18</sub> H <sub>28</sub> O <sub>8</sub> <sup>6,7</sup>	C <sub>20</sub> H <sub>30</sub> O <sub>8</sub>
	C <sub>10</sub> H <sub>16</sub> O <sub>10</sub>	C <sub>15</sub> H <sub>22</sub> O <sub>13</sub> <sup>5,6</sup>	C <sub>18</sub> H <sub>28</sub> O <sub>9</sub>	C <sub>20</sub> H <sub>30</sub> O <sub>9</sub>
C <sub>10</sub> H <sub>14</sub> N <sub>2</sub> O <sub>9</sub>	C <sub>10</sub> H <sub>16</sub> O <sub>11</sub>		C <sub>18</sub> H <sub>28</sub> O <sub>10</sub>	C <sub>20</sub> H <sub>30</sub> O <sub>10</sub>
C <sub>10</sub> H <sub>14</sub> N <sub>2</sub> O <sub>10</sub>		C <sub>15</sub> H <sub>24</sub> O <sub>13</sub> <sup>5,6</sup>	C <sub>18</sub> H <sub>28</sub> O <sub>11</sub>	C <sub>20</sub> H <sub>30</sub> O <sub>11</sub>
C <sub>10</sub> H <sub>14</sub> N <sub>2</sub> O <sub>11</sub>	C <sub>10</sub> H <sub>17</sub> NO <sub>6</sub> <sup>7</sup>		C <sub>18</sub> H <sub>28</sub> O <sub>12</sub>	C <sub>20</sub> H <sub>30</sub> O <sub>12</sub>
C <sub>10</sub> H <sub>14</sub> N <sub>2</sub> O <sub>12</sub>	C <sub>10</sub> H <sub>17</sub> NO <sub>7</sub>	C <sub>16</sub> H <sub>24</sub> O <sub>11</sub> <sup>7</sup>	C <sub>18</sub> H <sub>28</sub> O <sub>13</sub>	C <sub>20</sub> H <sub>30</sub> O <sub>13</sub>
C <sub>10</sub> H <sub>14</sub> N <sub>2</sub> O <sub>13</sub>	C <sub>10</sub> H <sub>17</sub> NO <sub>8</sub>	C <sub>16</sub> H <sub>24</sub> O <sub>12</sub> <sup>7</sup>	C <sub>18</sub> H <sub>28</sub> O <sub>14</sub>	C <sub>20</sub> H <sub>30</sub> O <sub>14</sub>
	C <sub>10</sub> H <sub>17</sub> NO <sub>9</sub>			C <sub>20</sub> H <sub>30</sub> O <sub>15</sub>
C <sub>10</sub> H <sub>14</sub> O <sub>5</sub>	C <sub>10</sub> H <sub>17</sub> NO <sub>10</sub>	C <sub>16</sub> H <sub>26</sub> O <sub>8</sub>	C <sub>18</sub> H <sub>30</sub> O <sub>7</sub> <sup>7</sup>	C <sub>20</sub> H <sub>30</sub> O <sub>16</sub>
C <sub>10</sub> H <sub>14</sub> O <sub>6</sub>	C <sub>10</sub> H <sub>17</sub> NO <sub>11</sub>	C <sub>16</sub> H <sub>26</sub> O <sub>9</sub>	C <sub>18</sub> H <sub>30</sub> O <sub>8</sub> <sup>7</sup>	
C <sub>10</sub> H <sub>14</sub> O <sub>7</sub>		C <sub>16</sub> H <sub>26</sub> O <sub>10</sub>	C <sub>18</sub> H <sub>30</sub> O <sub>9</sub>	C <sub>20</sub> H <sub>32</sub> O <sub>6</sub> <sup>7</sup>
C <sub>10</sub> H <sub>14</sub> O <sub>8</sub>	(C <sub>10</sub> H <sub>17</sub> O <sub>5</sub> )	C <sub>16</sub> H <sub>26</sub> O <sub>11</sub>	C <sub>18</sub> H <sub>30</sub> O <sub>10</sub>	C <sub>20</sub> H <sub>32</sub> O <sub>7</sub>
C <sub>10</sub> H <sub>14</sub> O <sub>9</sub>	(C <sub>10</sub> H <sub>17</sub> O <sub>6</sub> )	C <sub>16</sub> H <sub>26</sub> O <sub>12</sub>	C <sub>18</sub> H <sub>30</sub> O <sub>11</sub>	C <sub>20</sub> H <sub>32</sub> O <sub>8</sub>
C <sub>10</sub> H <sub>14</sub> O <sub>10</sub>	(C <sub>10</sub> H <sub>17</sub> O <sub>7</sub> )	C <sub>16</sub> H <sub>26</sub> O <sub>13</sub> <sup>7</sup>	C <sub>18</sub> H <sub>30</sub> O <sub>12</sub>	C <sub>20</sub> H <sub>32</sub> O <sub>9</sub>
C <sub>10</sub> H <sub>14</sub> O <sub>11</sub>	(C <sub>10</sub> H <sub>17</sub> O <sub>8</sub> )		C <sub>18</sub> H <sub>30</sub> O <sub>13</sub>	C <sub>20</sub> H <sub>32</sub> O <sub>10</sub>
	(C <sub>10</sub> H <sub>17</sub> O <sub>9</sub> )			C <sub>20</sub> H <sub>32</sub> O <sub>11</sub>
C <sub>10</sub> H <sub>15</sub> NO <sub>6</sub>	(C <sub>10</sub> H <sub>17</sub> O <sub>10</sub> )	C <sub>17</sub> H <sub>24</sub> O <sub>9</sub>	C <sub>19</sub> H <sub>28</sub> O <sub>7</sub> <sup>7</sup>	C <sub>20</sub> H <sub>32</sub> O <sub>12</sub>
C <sub>10</sub> H <sub>15</sub> NO <sub>7</sub>	(C <sub>10</sub> H <sub>17</sub> O <sub>11</sub> )	C <sub>17</sub> H <sub>24</sub> O <sub>10</sub>	C <sub>19</sub> H <sub>28</sub> O <sub>8</sub>	C <sub>20</sub> H <sub>32</sub> O <sub>13</sub>
C <sub>10</sub> H <sub>15</sub> NO <sub>8</sub>		C <sub>17</sub> H <sub>24</sub> O <sub>11</sub> <sup>7</sup>	C <sub>19</sub> H <sub>28</sub> O <sub>9</sub>	C <sub>20</sub> H <sub>32</sub> O <sub>14</sub>
C <sub>10</sub> H <sub>15</sub> NO <sub>9</sub>	C <sub>10</sub> H <sub>18</sub> N <sub>2</sub> O <sub>8</sub>	C <sub>17</sub> H <sub>24</sub> O <sub>12</sub>	C <sub>19</sub> H <sub>28</sub> O <sub>10</sub>	C <sub>20</sub> H <sub>32</sub> O <sub>15</sub>
C <sub>10</sub> H <sub>15</sub> NO <sub>10</sub>	C <sub>10</sub> H <sub>18</sub> N <sub>2</sub> O <sub>9</sub>	C <sub>17</sub> H <sub>24</sub> O <sub>13</sub> <sup>7</sup>	C <sub>19</sub> H <sub>28</sub> O <sub>11</sub>	
C <sub>10</sub> H <sub>15</sub> NO <sub>11</sub>	C <sub>10</sub> H <sub>18</sub> N <sub>2</sub> O <sub>10</sub>			C <sub>20</sub> H <sub>34</sub> O <sub>6</sub> <sup>7</sup>
C <sub>10</sub> H <sub>15</sub> NO <sub>12</sub>	C <sub>10</sub> H <sub>18</sub> N <sub>2</sub> O <sub>11</sub>	C <sub>17</sub> H <sub>26</sub> O <sub>8</sub> <sup>7</sup>	C <sub>19</sub> H <sub>30</sub> O <sub>6</sub>	C <sub>20</sub> H <sub>34</sub> O <sub>7</sub> <sup>7</sup>
C <sub>10</sub> H <sub>15</sub> NO <sub>13</sub>		C <sub>17</sub> H <sub>26</sub> O <sub>9</sub>	C <sub>19</sub> H <sub>30</sub> O <sub>7</sub>	C <sub>20</sub> H <sub>34</sub> O <sub>8</sub>
C <sub>10</sub> H <sub>15</sub> NO <sub>14</sub>	C <sub>10</sub> H <sub>18</sub> O <sub>4</sub> <sup>6,7</sup>	C <sub>17</sub> H <sub>26</sub> O <sub>10</sub>	C <sub>19</sub> H <sub>30</sub> O <sub>8</sub>	C <sub>20</sub> H <sub>34</sub> O <sub>9</sub>
	C <sub>10</sub> H <sub>18</sub> O <sub>5</sub>	C <sub>17</sub> H <sub>26</sub> O <sub>11</sub>	C <sub>19</sub> H <sub>30</sub> O <sub>9</sub>	C <sub>20</sub> H <sub>34</sub> O <sub>10</sub>
C <sub>10</sub> H <sub>15</sub> O <sub>6</sub>	C <sub>10</sub> H <sub>18</sub> O <sub>6</sub>	C <sub>17</sub> H <sub>26</sub> O <sub>12</sub>	C <sub>19</sub> H <sub>30</sub> O <sub>10</sub>	C <sub>20</sub> H <sub>34</sub> O <sub>11</sub>
C <sub>10</sub> H <sub>15</sub> O <sub>7</sub>	C <sub>10</sub> H <sub>18</sub> O <sub>7</sub>	C <sub>17</sub> H <sub>26</sub> O <sub>14</sub>	C <sub>19</sub> H <sub>30</sub> O <sub>11</sub>	C <sub>20</sub> H <sub>34</sub> O <sub>12</sub>
C <sub>10</sub> H <sub>15</sub> O <sub>8</sub>	C <sub>10</sub> H <sub>18</sub> O <sub>8</sub>		C <sub>19</sub> H <sub>30</sub> O <sub>12</sub>	C <sub>20</sub> H <sub>34</sub> O <sub>13</sub> <sup>7</sup>
C <sub>10</sub> H <sub>15</sub> O <sub>10</sub>	C <sub>10</sub> H <sub>18</sub> O <sub>9</sub>	C <sub>17</sub> H <sub>28</sub> O <sub>9</sub> <sup>7</sup>	C <sub>19</sub> H <sub>30</sub> O <sub>13</sub>	
		C <sub>17</sub> H <sub>28</sub> O <sub>10</sub>	C <sub>19</sub> H <sub>30</sub> O <sub>14</sub>	
C <sub>10</sub> H <sub>16</sub> N <sub>2</sub> O <sub>7</sub>		C <sub>17</sub> H <sub>28</sub> O <sub>11</sub>	C <sub>19</sub> H <sub>30</sub> O <sub>15</sub> <sup>7</sup>	
C <sub>10</sub> H <sub>16</sub> N <sub>2</sub> O <sub>8</sub>		C <sub>17</sub> H <sub>28</sub> O <sub>12</sub> <sup>7</sup>		
C <sub>10</sub> H <sub>16</sub> N <sub>2</sub> O <sub>9</sub>			C <sub>19</sub> H <sub>32</sub> O <sub>7</sub> <sup>7</sup>	
C <sub>10</sub> H <sub>16</sub> N <sub>2</sub> O <sub>10</sub>			C <sub>19</sub> H <sub>32</sub> O <sub>8</sub> <sup>7</sup>	
C <sub>10</sub> H <sub>16</sub> N <sub>2</sub> O <sub>11</sub>			C <sub>19</sub> H <sub>32</sub> O <sub>9</sub>	
C <sub>10</sub> H <sub>16</sub> N <sub>2</sub> O <sub>12</sub>			C <sub>19</sub> H <sub>32</sub> O <sub>10</sub>	
C <sub>10</sub> H <sub>16</sub> N <sub>2</sub> O <sub>13</sub>			C <sub>19</sub> H <sub>32</sub> O <sub>11</sub>	
			C <sub>19</sub> H <sub>32</sub> O <sub>12</sub>	
			C <sub>19</sub> H <sub>32</sub> O <sub>13</sub> <sup>7</sup>	

## A.7 Exemplary reported HO<sub>2</sub>/RO<sub>2</sub> ratios from field studies

**Table A11** Measured HO<sub>2</sub> and RO<sub>2</sub> concentrations from field studies under different atmospheric conditions.

Conditions	HO <sub>2</sub> (10 <sup>8</sup> cm <sup>-3</sup> )	RO <sub>2</sub> (10 <sup>8</sup> cm <sup>-3</sup> )	HO <sub>2</sub> /RO <sub>2</sub>	Source
<u>Autumn, Pearl Riva Delta, China</u> (polluted) Morning (median) Afternoon (median)	0.8 2.5	0.3 1.7	2.7 1.5	(Tan et al., 2019)
<u>Winter, Beijing, China</u> (urban) Background (24 h average) Clean (24 h average) Polluted (24 h average)	1.04 ± 0.62 0.93 ± 0.72 0.52 ± 0.23	0.70 ± 0.34 0.76 ± 0.46 0.71 ± 0.41	1.5 1.2 0.7	(Tan et al., 2018)
<u>Jülich, Germany</u> (rural) Spring & Summer noon (median)	3.0	3.0	1.0	(Cho et al., 2023)
<u>Summer, Michigan, USA</u> (rural forest) Average diurnal maximum	3.5	4.0	1.1	(Bottorff et al., 2023)
<u>September, Colorado, USA</u> (remote) Single measurements: High NO <sub>x</sub> (1.9 ppbv) Low NO <sub>x</sub> (0.5 ppbv)	(Uncertainty factor of 2) 0.3 1	4.7 ± 2.0 4 ± 2	(Uncertainty factor of 2) 0.1 0.3	(Stevens et al., 1997)
Schauinsland/Pabsthum, Germany (rural)	-	-	Reported ratios around 1 for a range of NO concentrations (0.1 – 1.5 ppbv)	(Mihelcic et al., 2003)

## A.8 Estimation of change in peroxy radical steady state concentration between different chemical regimes

### A.8.1 Estimation for high HO<sub>2</sub> case in comparison to base case

Starting from the balance equation *Eq. A-3*, we derived an equation for the steady-state concentration (indicated by subscript SS) of a specific  $[RO_2]_i$  (*Eq. A-4*). The equation is only applicable for those HOM-RO<sub>2</sub> with production directly linked to the primary production ( $k_{OH\cdot}[OH]\cdot[\alpha\text{-pinene}]$ ) with negligible further autoxidation. The equations assume a primary production term  $Pri_i$  for  $[RO_2]_i$ , as well as only three significant loss pathways: The reaction with the pool of available  $[RO_2]$  with a bulk reaction rate coefficient  $k_{RO_2+RO_2}$ , the reaction with  $[HO_2]$  with a reaction rate of  $k_{RO_2+HO_2}=2.46\cdot 10^{-11} \text{ cm}^3 \text{ s}^{-1}$  at 20 °C as defined in the MCM (Jenkin et al., 1997; Saunders et al., 2003) and the wall loss. A wall loss rate coefficient of 1/170 s was used, as determined by our measurements for HOM products (see supplement section Appendix **Section A.4.1**). The rate coefficient  $k_{RO_2+RO_2}$  was varied in a range 1.0-5.0·10<sup>-12</sup> cm<sup>3</sup> s<sup>-1</sup>, typical values expected for substituted organic peroxy radicals (Jenkin et al., 2019), to determine what bulk rate coefficient would be reconcilable with our observations. To compare directly to the measured ratio of HOM-RO<sub>2</sub> signal, we calculated the RO<sub>2</sub> concentration ratio at high to low HO<sub>2</sub>/RO<sub>2</sub> applying *Eq. A-5*. In *Eq. A-5* the primary production term  $Pri_i$  could be eliminated as the primary production was same at high and low HO<sub>2</sub>/RO<sub>2</sub> in our experiments.

$$\frac{d[RO_2]_i}{dt} = Pri_i - k_{RO_2+RO_2}[RO_2][RO_2]_i - k_{RO_2+HO_2}[HO_2][RO_2]_i - k_{wall}[RO_2]_i \quad \text{Eq. A-3}$$

$$[RO_2]_{i,SS} = \frac{Pri_i}{k_{RO_2+RO_2}[RO_2] + k_{RO_2+HO_2}[HO_2] + k_{wall}} \quad \text{Eq. A-4}$$

$$\frac{[RO_2]_{i,SS,highHO_2}}{[RO_2]_{i,SS,lowHO_2}} = \frac{k_{RO_2+RO_2}[RO_2]_{SS,lowHO_2} + k_{RO_2+HO_2}[HO_2]_{SS,lowHO_2} + k_{wall}}{k_{RO_2+RO_2}[RO_2]_{SS,highHO_2} + k_{RO_2+HO_2}[HO_2]_{SS,highHO_2} + k_{wall}} \quad \text{Eq. A-5}$$

### A.8.2 Estimation for system with NO in comparison to base case

To estimate the expected change in RO<sub>2</sub> radical concentration the same approach as for the pure RO<sub>2</sub>, HO<sub>2</sub> system was used. The only necessary adaption is the addition of the loss of RO<sub>2</sub> with NO in the system with NO (not in the base case as this is NO<sub>x</sub> free), leading to equation *Eq. A-6* to estimate the RO<sub>2</sub> concentration ratio between base case and the case with NO.

$$\frac{[RO_2]_{i,SS,NO}}{[RO_2]_{i,SS,base}} = \frac{k_{RO_2+RO_2}[RO_2]_{SS,NOx\ free} + k_{RO_2+HO_2}[HO_2]_{SS,NOx\ free} + k_{wall}}{k_{RO_2+RO_2}[RO_2]_{SS,NO} + k_{RO_2+HO_2}[HO_2]_{SS,NO} + k_{RO_2+NO}[NO]_{SS,NO} + k_{wall}} \quad \text{Eq. A-6}$$

## A.9 Particular phase measurements and wall loss corrected SOA yield

**Table A12** Overview of important particle phase parameters. Total surface area was measured by SMPS, mass concentrations by AMS. SOA yield was wall-loss corrected, see Eq. A-7. In apinCONO\_2 experiment no absolute AMS measurement was available, due to instrument issues only a relative comparison between phases was possible.

<b>Experimental conditions</b>	<b>Experiment phase</b>	<b>Total surface area (m<sup>2</sup> m<sup>-3</sup>)</b>	<b>Median particle diameter of surface distribution (nm)</b>	<b>Organic mass (μg m<sup>-3</sup>)</b>	<b>Sulfate mass (μg m<sup>-3</sup>)</b>	<b>SOA yield</b>
<i>Base case</i>	apinCO_2 (s)	8.7E-04	84	3.4	10.2	9.0 %
	apinCONO_1 [-] (s)	6.8E-04	76	2.7	8.2	7.3 %
	apinCONO_2 [-] (s)	5.9E-04	79	-	-	-
<i>High HO<sub>2</sub></i>	apinCO_2 (s)	10.1E-04	89	2.0	13.6	5.9 %
	apinCONO_1 [-] (s)	6.9E-04	76	1.7	9.6	5.3 %
<i>Base case with middle NO</i>	apinNO [10] (s)	7.4E-04	81	2.5	8.0	6.7 %
<i>Base case with high NO</i>	apinNO [25] (s)	7.0E-04	80	1.9	7.1	4.9 %
<i>High HO<sub>2</sub> &amp; middle NO</i>	apinCONO_1 [10] (s)	7.3E-04	77	1.9	9.6	5.1 %
<i>High HO<sub>2</sub> &amp; high NO</i>	apinCONO_1 [25] (s)	8.6E-04	83	2.0	13.7	5.3 %
	apinCONO_2 [25] (s)	5.9E-04	81	-	-	-

For the SOA yield calculation, we calculate a corrected organic mass  $m_{SOA}$  from the organic mass  $m_{AMS}$  measured by aerosol mass spectrometry (AMS) and the fraction expected to be lost on the seed particles compared to the overall loss on particles and chamber wall as shown in Eq. A-7 (McFiggans et al., 2019).

$$m_{SOA} = m_{AMS} * \frac{k_{cond} + k_{wall}}{k_{cond}} \quad \text{Eq. A-7}$$

In Eq. A-7 we use the condensation rate coefficient  $k_{cond}$  calculated for one major HOM product (C<sub>10</sub>H<sub>16</sub>O<sub>7</sub>) and the average HOM-Mon wall loss rate  $k_{wall}$  which was determined by switching off the UV-C light and observing the decay of photooxidation products in the NO<sub>3</sub>-CIMS (also see Appendix Section A.4.1). The wall loss determination, as well as SOA mass correction were described before in Sarrafzadeh et al. (2016) and McFiggans et al. (2019). The SOA yield is then subsequently calculated from the corrected organic mass  $m_{SOA}$  and the consumed  $\alpha$ -pinene mass concentration (Eq. A-8). The consumed  $\alpha$ -pinene concentration is calculated from  $\alpha$ -pinene concentration entering the chamber  $[\alpha\text{-pinene}]_{in}$  and the  $\alpha$ -pinene concentration after reaction, which is the steady-state concentration  $[\alpha\text{-pinene}]_{SS}$ .

$$SOA \text{ yield} = \frac{m_{SOA}}{[\alpha\text{-pinene}]_{in} - [\alpha\text{-pinene}]_{SS}} \quad \text{Eq. A-8}$$

A difference in SOA yield between experiments can be observed even at experiments with the same experimental conditions (base case and high HO<sub>2</sub> case). These differences can be explained by the slightly different OH concentrations and subsequent difference in contribution by photooxidation (see **Table A4**). Overall, our yields are in the lower range in comparison with the SOA yields reported for example by McFiggans et al. (2019) for the  $\alpha$ -pinene photooxidation. However, our experiments were also performed at 5 °C higher temperature (20 °C) compared to 15 °C in McFiggans et al. (2019)).

## A.10 Supplemental information for experiments with NO addition

### A.10.1 C<sub>10</sub>-HOM-RO<sub>2</sub> family observations in experiments with NO addition

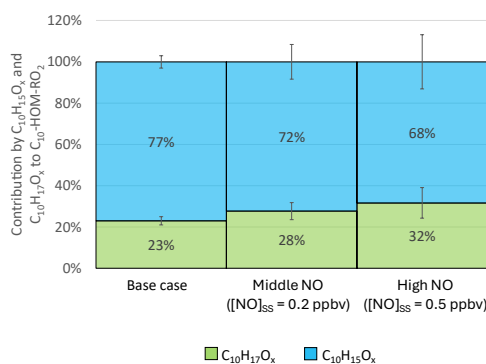


**Figure A1** Contribution of C<sub>10</sub>H<sub>15</sub>O<sub>x</sub> and C<sub>10</sub>H<sub>17</sub>O<sub>x</sub> to C<sub>10</sub>-HOM-RO<sub>2</sub> sum in base, middle NO and high NO case (unseeded). Higher uncertainty in the results due to difficulties in NO measurement as explained in **Section 4.2.2**. Error bars for base case are standard deviation from apinCO\_1 (g), apinCO\_2 (g). Error bars for NO cases determined via error propagation.

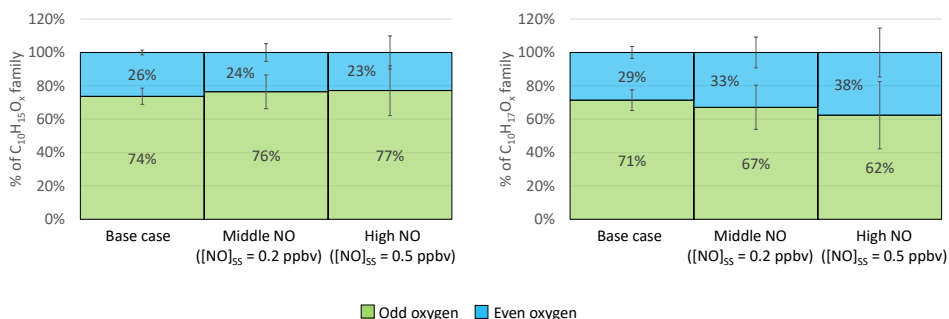


**Figure A2** Contribution of O<sub>odd</sub> and O<sub>even</sub> to the HOM-RO<sub>2</sub> families C<sub>10</sub>H<sub>15</sub>O<sub>x</sub> (left) and C<sub>10</sub>H<sub>17</sub>O<sub>x</sub> (right) signal in the base case (from apinCO\_2 experiment) and at the two NO levels (unseeded experiments). Error bars for NO cases determined via error propagation.

In **Figure A2** the C<sub>10</sub>H<sub>17</sub>O<sub>x</sub> family showed a slight increase in importance of O<sub>even</sub> family members with increasing NO, indicating in the simplest case the addition of one alkoxy-peroxy step to the autoxidation chain. The contribution at high NO increases only around 15 % compared to the NO<sub>x</sub>-

free base case however, making it insignificant within the expected errors. The parity of oxygen did not significantly change in the  $C_{10}H_{15}O_x$  family. As discussed, a possible explanation for this could be the occurrence of an even number of alkoxy-peroxy steps.

### A.10.2 Relative changes in the HOM-Mon families in experiments with NO addition

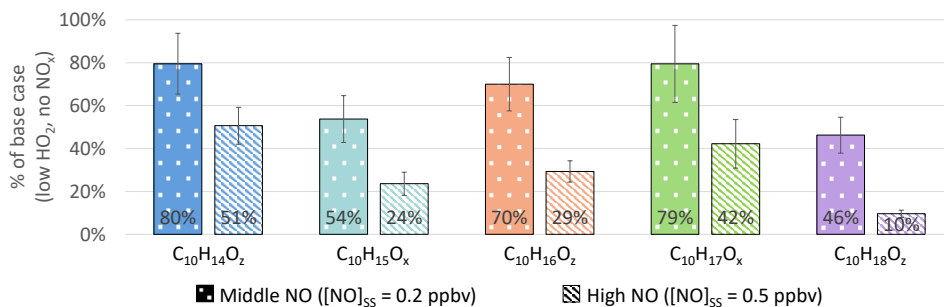


**Figure A3** Overview of relative change in monomer families detected in  $NO_3$ -CIMS at the two NO levels compared to base case in unseeded system (All data normalized to  $\alpha$ -pinene OH turnover, base case from experiment apinCO\_2. Error bars via error propagation, for more information see Appendix Section A.5)

### A.10.3 Contributions in the HOM-Frag product class in experiments with NO addition

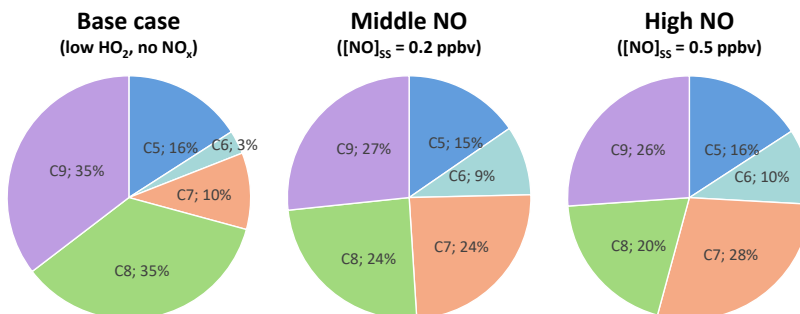


**Figure A4** Contribution of the  $C_5$  to  $C_9$  HOM-Frag groups to overall HOM-Frag signal in the NO free case (experiment apinCO\_2) and at the two NO levels in the pure NO cases (unseeded experiments).

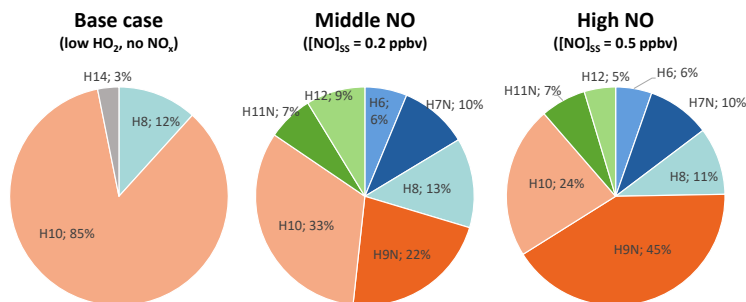


**Figure A5** Contribution of the different families to the C<sub>7</sub>-HOM-Frag group in the base case (experiment apinCO<sub>2</sub>) and at the two NO levels in the pure NO cases (unseeded experiments) including the ON-families (labelled H<sub>x</sub>N).

#### A.10.4 Investigation of oxidation degree in experiments with NO addition

The O/C ratio of the C<sub>10</sub>-HOM-RO<sub>2</sub> families as well as the O/C ratio of the closed shell monomer products were investigated as indicators if the increase in alkoxy formation led to an increase of oxidation degree.

The most direct indicators are the C<sub>10</sub>-HOM-RO<sub>2</sub> families themselves, but as explained in **Section 4.2.2** the data quality is not ideal. The C<sub>10</sub>H<sub>17</sub>O<sub>x</sub> family has a trend of increasing O/C ratio with increasing NO, as can be seen in **Table A13**, but the propagated errors are too large to confirm its significance. In the system with NO higher oxidized C<sub>10</sub>H<sub>17</sub>O<sub>x</sub> compounds (x=10, 11) could be assigned which was not possible in the NO<sub>x</sub>-free base case. The occurrence of higher oxidized species indicates an additional reaction pathway to higher oxidation levels in the system with NO.

**Table A13** Contribution weighted O/C ratio of the HOM-Mon families and HOM-Acc class in the base case and at the two NO levels.

Family	NO <sub>x</sub> -free base case	Middle NO case [NO] <sub>ss</sub> = 0.2 ppbv	High NO case [NO] <sub>ss</sub> = 0.5 ppbv
C <sub>10</sub> H <sub>15</sub> O <sub>x</sub>	0.75 ± 0.06	0.75 ± 0.18	0.75 ± 0.30
C <sub>10</sub> H <sub>14</sub> O <sub>z</sub>	0.77 ± 0.01	0.78 ± 0.02	0.81 ± 0.01
C <sub>10</sub> H <sub>15</sub> NO <sub>z</sub>	-	0.85 ± 0.02	0.87 ± 0.01
C <sub>10</sub> H <sub>16</sub> O <sub>z</sub>	0.66 ± 0.01	0.69 ± 0.01	0.72 ± 0.02
C <sub>10</sub> H <sub>17</sub> O <sub>x</sub>	0.69 ± 0.05	0.79 ± 0.11	0.83 ± 0.19
C <sub>10</sub> H <sub>17</sub> NO <sub>z</sub>	-	0.79 ± 0.03	0.79 ± 0.03
C <sub>10</sub> H <sub>18</sub> O <sub>z</sub>	0.66 ± 0.01	0.65 ± 0.02	0.67 ± 0.04
HOM-Acc	0.54 ± 0.01	0.55 ± 0.01	0.58 ± 0.01

In the C<sub>10</sub>H<sub>15</sub>O<sub>x</sub> family no such trend could be observed. However, **Table A13** also shows the expected large uncertainties. Additionally, the contribution of the RO<sub>2</sub> radicals is also influenced by the individual sink of each radical. Thus, the O/C ratio of closed shell products was investigated as well.

For the closed shell products similar sinks can be assumed. The focus was on  $C_{10}H_{14}O_z$ , due to the clear change in oxygen number in the termination reactions that form these family.  $C_{10}H_{14}O_z$  can only be formed via internal termination and the  $RO_2+RO_2$  termination and both lead to minus one oxygen compared to their precursor  $RO_2$ . The weighted O/C ratio of this family indicates a slight increase in oxidation degree with increasing NO, but of course other changes in formation pathways can also contribute to this. The weighted O/C ratio of additional HOM-Mon families are listed in **Table A13** and  $C_{10}H_{15}NO_z$  and  $C_{10}H_{16}O_z$  also show a slight increase in O/C ratio, however as these families can be formed by different termination pathways, it is not possible to draw direct conclusions.

In summary it can be said that there are some slight indications towards increasing oxidation degree in the system with NO due to efficient alkoxy-peroxy steps extending the autoxidation chain, but the evidence is very limited, and the effect is small.

#### A.10.5 Information about additional "low NO" steady state

**Table A14** Important experimental parameters for the additional "low NO" steady state utilized in **Figure 33** and **Figure 34** in the pure NO system.  $HO_2/RO_2$  ratio and contribution to the chemical sink from model calculations.

<u>OH concentration</u>	<u><math>\alpha</math>-Pinene OH turnover</u>	<u>[NO]<sub>ss</sub></u>	<u>[NO<sub>2</sub>]<sub>ss</sub></u>	<u>HO<sub>2</sub>/RO<sub>2</sub> ratio</u>	<u>Contribution to chemical sink</u>		
					<u>RO<sub>2</sub></u>	<u>HO<sub>2</sub></u>	<u>NO<sub>2</sub></u>
2.0·10 <sup>7</sup> cm <sup>-3</sup>	5.1·10 <sup>7</sup> cm <sup>-3</sup> s <sup>-1</sup>	0.1 ppbv	1.0 ppbv	0.04	67 %	12 %	21 %

## A.10.6 Gas-phase fraction remaining in presence of seed for the middle NO case

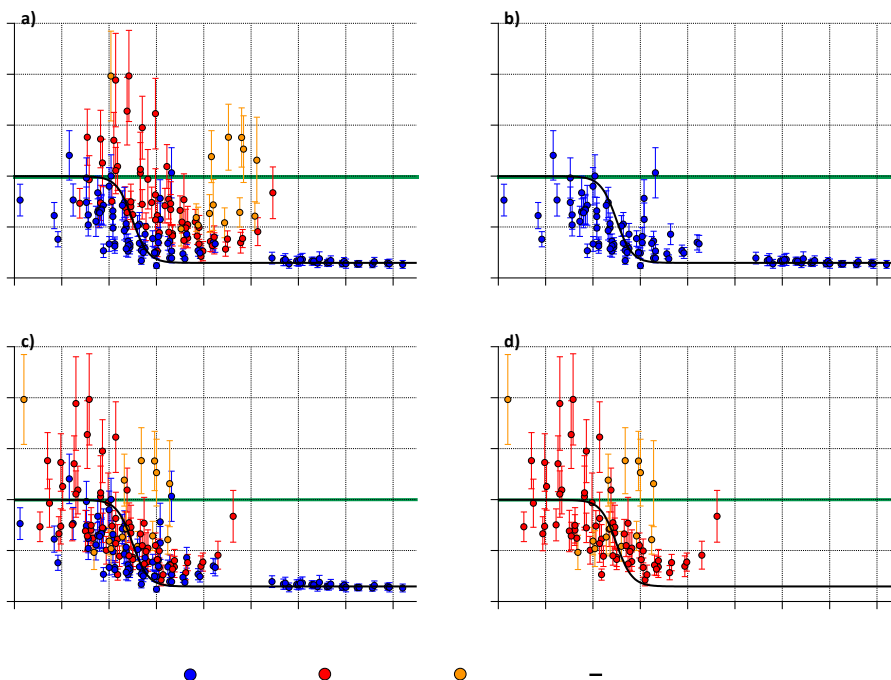


**Figure A6** Gas-phase fraction remaining in presence of seed for the middle NO case. All data is normalized with  $\alpha$ -pinene OH turnover. Points represent compounds that were detected with relative standard deviation  $<30\%$  in both experiment phases. Error bars represent result of error propagation (see Appendix Section A.3). The green line highlights a fraction remaining of 1.

**a)** all HOM-compounds, **b)** just non nitrated HOM-compounds, **c)** all HOM-compounds with organic nitrate's molar mass being shifted by the nitrate termination group ( $\text{NO}_2$ ) to  $(M - 46 \text{ g mol}^{-1})$  for compounds containing one nitrate group (red markers) and to  $(M - 92 \text{ g mol}^{-1})$  for compounds with two nitrate groups (orange markers), **d)** just organic nitrates shifted by the nitrate termination groups.

**Figure A6** shows the fraction remaining of individual HOM-compounds in the presence of seed. In comparison to **Figure 37**, which shows the same overview for the high NO case, in the middle NO case HOM compounds with a fraction remaining larger than 1 were observed. In total around 10 detected compounds had a fraction remaining significantly larger than 1 considering the uncertainty calculated via error propagation. **Figure A6 d)** shows that these compounds are all ON-products.

The most straightforward explanation for a fraction remaining larger than 1 is a heterogeneous production process of these products. However, if the ON products would be produced in the particle phase the same observation would be expected in the high NO case. Another possibility to consider are experimental imperfections and limitations: In this specific experiment the middle NO level with seed steady state was after the high NO level with seed. The previous high concentration of ON-products could have led to memory effects. Wall interactions of ON-products have been reported before (Pullinen et al., 2020) and should always be considered. In the simplest case the wall represents a reservoir for the ON-products, leading to re-evaporation into the chamber. Additionally, it is

possible that the compounds were heterogeneously produced on the wall, for example due to photolysis reactions.

## A.11 Supplemental information for experiments with NO and HO<sub>2</sub> addition

### A.11.1 Overview of contributions of product classes, groups, and families in the high NO, high HO<sub>2</sub> case

**Table A15** Contributions of product classes, groups and families in the high NO, high HO<sub>2</sub> case. Percentages present average of the two experiments (apinCONO\_1 [25], apinCONO\_2 [25]) followed by standard deviation.

Contributions are sorted into sections: a) Product classes b) C<sub>20</sub>-HOM-Acc c) non-ON HOM-Mon sum

a) <u>Contribution of product classes to HOM sum</u>	
<u>HOM-Frag</u>	49±2 %
<u>HOM-Mon</u>	47±1 %
<u>HOM-Acc</u>	3±1 %
b) <u>Contribution of families to C<sub>20</sub>-HOM-Acc sum</u>	
<u>C<sub>20</sub>H<sub>30</sub>O<sub>2</sub></u>	31±1 %
<u>C<sub>20</sub>H<sub>32</sub>O<sub>2</sub></u>	46±0 %
<u>C<sub>20</sub>H<sub>34</sub>O<sub>2</sub></u>	21±1 %
c) <u>Contribution of families to non-ON HOM-Mon sum</u>	
<u>C<sub>10</sub>H<sub>14</sub>O<sub>2</sub></u>	37±0 %
<u>C<sub>10</sub>H<sub>16</sub>O<sub>2</sub></u>	51±0 %
<u>C<sub>10</sub>H<sub>18</sub>O<sub>2</sub></u>	12±0 %

### A.11.2 Information about additional “in-between NO” steady state

**Table A16** Important experimental parameters for the additional “in-between NO, high HO<sub>2</sub>” steady state utilized in **Figure 43** in the mixed system. HO<sub>2</sub>/RO<sub>2</sub> ratio and contribution to the chemical sink from model calculations.

<u>OH concentration</u>	<u>α-Pinene OH turnover</u>	<u>[NO]<sub>ss</sub></u>	<u>[NO<sub>2</sub>]<sub>ss</sub></u>	<u>HO<sub>2</sub>/RO<sub>2</sub> ratio</u>	<u>Contribution to chemical sink</u>		
					<u>RO<sub>2</sub>:</u>	<u>HO<sub>2</sub>:</u>	<u>NO:</u>
1.5·10 <sup>7</sup> cm <sup>-3</sup>	4.7·10 <sup>7</sup> cm <sup>-3</sup> s <sup>-1</sup>	0.3 ppbv	8.9 ppbv	2.2	2 %	28 %	70 %

### A.11.3 C<sub>10</sub>H<sub>16</sub>O<sub>2</sub> (formula composition of pinonaldehyde) signal in the system with NO and HO<sub>2</sub> in comparison to the base case

**Table A17** Overview of change in C<sub>10</sub>H<sub>16</sub>O<sub>2</sub> (sum formula of pinonaldehyde) in amine-CIMS measurements compared to the no NO<sub>x</sub>, low HO<sub>2</sub> base case

<u>Experiment</u>	<u>Comment</u>	<u>% of base case</u>
<u>Middle NO, high HO<sub>2</sub> case</u> [NO] <sub>ss</sub> = 0.2 ppbv (apinCONO_1 [10] (s))	Caution, comparison of seeded base case to seeded experiment phase within the apinCONO_1 experiment.	74 %
<u>High NO, high HO<sub>2</sub> case</u> [NO] <sub>ss</sub> = 0.4 ppbv (apinCONO_1 [25] (s))	Caution, comparison of seeded base case to seeded experiment phase within the apinCONO_1 experiment.	84 %
<u>High NO, high HO<sub>2</sub> case</u> [NO] <sub>ss</sub> = 0.4 ppbv (apinCONO_2 [25] (g))	Only comparison of unseeded base to unseeded experiment phase.	85 %

### A.11.4 Investigation of oxidation degree in experiments with NO and HO<sub>2</sub> addition

**Table A18** Contribution weighted O/C ratio of the HOM-Mon families and HOM-Acc class in the base case and at the two NO levels at high HO<sub>2</sub> (apinCONO\_1 experiment).

<u>Family</u>	<u>NO<sub>x</sub>-free base case</u>	<u>Middle NO, high HO<sub>2</sub> case</u> [NO] <sub>ss</sub> = 0.2 ppbv	<u>High NO, high HO<sub>2</sub> case</u> [NO] <sub>ss</sub> = 0.4 ppbv
C <sub>10</sub> H <sub>15</sub> O <sub>x</sub>	0.75 ± 0.06	0.79 ± 0.09	0.75 ± 0.16
C <sub>10</sub> H <sub>14</sub> O <sub>z</sub>	0.77 ± 0.01	0.78 ± 0.01	0.80 ± 0.01
C <sub>10</sub> H <sub>15</sub> NO <sub>z</sub>	-	0.88 ± 0.02	0.89 ± 0.01
C <sub>10</sub> H <sub>16</sub> O <sub>z</sub>	0.66 ± 0.01	0.73 ± 0.01	0.73 ± 0.01
C <sub>10</sub> H <sub>17</sub> O <sub>x</sub>	0.69 ± 0.05	0.81 ± 0.16	0.83 ± 0.19
C <sub>10</sub> H <sub>17</sub> NO <sub>z</sub>	-	0.79 ± 0.03	0.79 ± 0.03
C <sub>10</sub> H <sub>18</sub> O <sub>z</sub>	0.66 ± 0.01	0.69 ± 0.02	0.70 ± 0.03
HOM-Acc	0.54 ± 0.01	0.56 ± 0.01	0.57 ± 0.01

### A.11.5 Relative change in HOM-Frag groups compared to base case for middle NO, high HO<sub>2</sub> and high NO, high HO<sub>2</sub> system

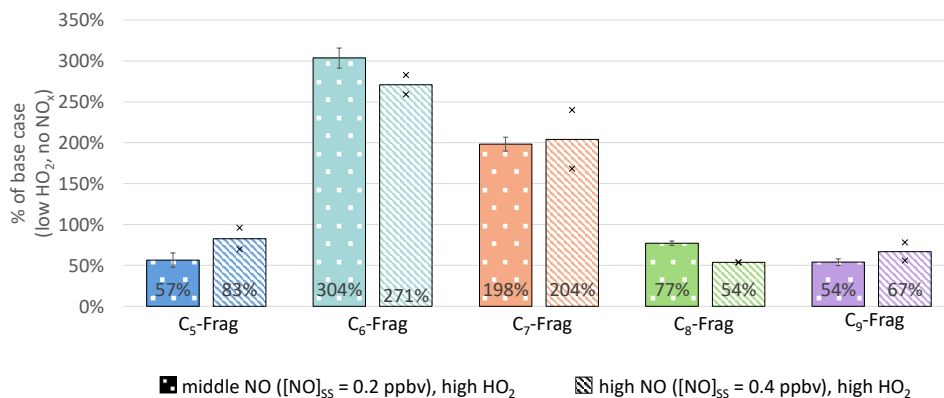


**Figure A7** Overview of relative change in HOM-fragment groups detected in NO<sub>3</sub>-CIMS in the middle NO, high HO<sub>2</sub> system (lefthand bars) and the high NO, high HO<sub>2</sub> case (righthand bars), both in comparison to the low HO<sub>2</sub>, NO<sub>x</sub> free base case (unseeded experiments, all normalized to  $\alpha$ -pinene OH turnover). For the apinCONO\_1 experiment the base case from Experiment apinCO\_2 was used. Middle NO, high HO<sub>2</sub> from apinCONO\_1 [10], error bars via error propagation. In the high NO, high HO<sub>2</sub> case bars represent average relative change from apinCONO\_1 [25] and apinCONO\_2 [25] (base case within the experiment) and markers individual experiments.

### A.11.6 Fraction remaining with seed in ON and non-ON product classes in system with just NO in comparison to system with NO and high HO<sub>2</sub>

**Table A19** Comparison of fraction of signal remaining in the presence of seed for system just with NO and system with NO and high HO<sub>2</sub>. All data normalized with  $\alpha$ -pinene OH turnover.

<b>Product class</b>	<b>Middle NO, low HO<sub>2</sub> case</b> [NO] <sub>ss</sub> = 0.2 ppbv	<b>High NO, low HO<sub>2</sub> case</b> [NO] <sub>ss</sub> = 0.5 ppbv	<b>Middle NO, high HO<sub>2</sub> case</b> [NO] <sub>ss</sub> = 0.2 ppbv	<b>High NO, high HO<sub>2</sub> case</b> [NO] <sub>ss</sub> = 0.4 ppbv
All ON-Products	65 ± 13 %	63 ± 11 %	70 ± 10 %	65 ± 9 %
ON-Fragments (C <sub>5</sub> -C <sub>9</sub> )	79 ± 15 %	69 ± 12 %	67 ± 10 %	70 ± 9 %
ON-Monomers	54 ± 10 %	57 ± 10 %	73 ± 10 %	61 ± 8 %
Non ON-Products	38 ± 7 %	50 ± 9 %	72 ± 10 %	58 ± 8 %
Non-ON Fragments (C <sub>5</sub> -C <sub>9</sub> )	51 ± 10 %	61 ± 11 %	85 ± 12 %	73 ± 10 %
Non-ON Monomers	31 ± 6 %	40 ± 7 %	66 ± 9 %	44 ± 6 %

Band / Volume 627

**Modeling orographic gravity waves from source to termination to improve parameterization schemes in climate models**

S. Rhode (2024), xii, ii, 138 pp

ISBN: 978-3-95806-750-9

Band / Volume 628

**Abscheidung kolumnarer Wärmedämmschichten mittels Suspensionsplasmaspritzen (SPS) und Plasma Spray – Physical Vapor Deposition (PS-PVD) Prozess**

J. Joeris (2024), vii, 133 pp

ISBN: 978-3-95806-752-3

Band / Volume 629

**Structure and properties of electrochemical interfaces from first principles simulations**

R. Tesch (2024), xvi, 161 pp

ISBN: 978-3-95806-753-0

Band / Volume 630

**Elucidation of Barocaloric Effect in Spin Crossover Compounds**

H. Shahed (2024), x, 261 pp

ISBN: 978-3-95806-758-5

Band / Volume 631

**Computational Investigation of Solvation Phenomena at Metal-Electrolyte Interfaces**

O. Cheong (2024), xvii, 142 pp

ISBN: 978-3-95806-759-2

Band / Volume 632

**Senkung zukünftiger Stickoxid- und Partikelemissionen in Nordrhein-Westfalen durch den Einsatz alternativer Energieträger und Antriebe**

J. L. Breuer (2024), vii, 339 pp

ISBN: 978-3-95806-760-8

Band / Volume 633

**Development of Model-Based Correction Methods for Temperature-Dependent Electromagnetic Induction (EMI) Measurement Errors in Soil Conductivity Estimations**

T. M. Tchantcho Amin (2024), xx, 100 pp

ISBN: 978-3-95806-761-5

Band / Volume 634

**Investigation and implementation of improved and degradation-tolerant fuel electrodes for solid oxide cells**

A. Schwiers (2024), VI, 163, XIII pp  
ISBN: 978-3-95806-762-2

Band / Volume 635

**In Situ Time Calibration for Stationary Multichannel GPR Monitoring Systems**

L. Steinbeck (2024), xvi, 98, xxxi pp  
ISBN: 978-3-95806-767-7

Band / Volume 636

**Erneuerbares Methanol als Ausgangsstoff für die Bereitstellung von flüssigen Kraftstoffen für den Transportsektor**

F. Schorn (2024), VI, 275 pp  
ISBN: 978-3-95806-769-1

Band / Volume 637

**Investigation of Lower Boundary Conditions of Brominated Very Short-lived Species (VLS)**

S. Zheng (2024), 2, iii, 160 pp  
ISBN: 978-3-95806-770-7

Band / Volume 638

**Modellgestützte Analyse zukünftigen Mobilitätsverhaltens**

J. P. Reul (2024), XVI, 291 pp  
ISBN: 978-3-95806-771-4

Band / Volume 639

**Insights into Mechanisms of Secondary Organic Aerosol Formation: Approaching Atmospherically Relevant Conditions in an Atmospheric Reaction Chamber**

Y. Baker (2024), XVII, 122 pp  
ISBN: 978-3-95806-776-9

Weitere **Schriften des Verlags im Forschungszentrum Jülich** unter  
<http://www.zb1.fz-juelich.de/verlagextern1/index.asp>



Energie & Umwelt / Energy & Environment  
Band / Volume 639  
ISBN 978-3-95806-776-9

Mitglied der Helmholtz-Gemeinschaft

